Preparation and Characterization of Novel Carbon Material Derived from Resorcinol-Formaldehyde Xerogels for CO_2 Capture

By

Mohamed A. M. Elsayed

A thesis submitted to the Department of Chemical and Process Engineering, University of Strathclyde, in part fulfilment of the regulations for the Degree of Doctor of Philosophy

(2007)

Copyright

Dedicated to

My wife Engy,

My sons Ahmad and Abd-elrahman,

And the rest of my supportive family.

Preface

The work presented in this thesis was preformed in The Department of Chemical & Process Engineering, University of Strathclyde under the supervision of Professor Peter J. Hall and Doctor Mark J. Heslop during the interval of January 2005-October 2007. Some of the work has been published as follows:

Journal publications:

- *"Preparation of New Carbons from Resorcinol-Formaldehyde Resin by CO_2 Activation"* submitted and accepted by *Adsorption*, Journal of the International Adsorption Society.
- *"High Surface Area and Porosity Carbons from Resorcinol-Formaldehyde Resin Catalyzed with Amine for CO_2 Capture and Separation"* submitted and under processing to *Adsorption*, Journal of the International Adsorption Society.

Conferences:

- Oral paper presentation:
  - *"Synthesis of New Nanoporous Carbon Materials from Resorcinol-Formaldehyde Resins Using Different Catalytic Species"* The International Conference on Carbon, Robert Gorden University, Aberdeen, Scotland, July 16 – 21, 2006.
  - *"Preparation and Structure Characterization of Carbons Prepared from Resorcinol-Formaldehyde Resin by CO_2 Activation"* 9th International Conference on Fundamental of Adsorption, Giardin Naxos, Sicily, Italy, May 20 – 25, 2007.
- Poster paper presentation:
  - *"Development of High Surface Area and Porosity Activated Carbon from Resorcinol-Formaldehyde Resin Catalyzed with Amine for CO_2 Capture and Separation"* 9th International Conference on Fundamental of Adsorption, Giardin Naxos, Sicily, Italy, May 20 – 25, 2007.

Acknowledgements

I am most grateful to my first supervisor Professor ***P.J.Hall*** *for his guidance, valuable comments and constant support. I wish to express my sincere gratitude to my second supervisor Doctor* ***M.J.Heslop*** *for his continuous support and advice through the period of this study.*

I also wish to thank Doctor ***Carl J Schaschke****, Head of the Chemical & Process Engineering Department and the staff of this department for the co-operation. My acknowledgements to Mr.* ***J. Murphy*** *and Mr.* ***J. Wilkie*** *for continuous help in the laboratory, without their help this study would not have been completed.*

I am grateful to my friends ***Ahmed Baraka,*** *members of Carbon Group and all the PhD researchers, Chemical Engineering Department, University of Strathclyde for their helpful discussions and* ***all Egyptian PhD students*** *in University of Strathclyde.*

I am thankful and grateful to ***Egyptian Government*** *for granting me in this study. My special thanks to Doctor* ***Ashraf Soltan*** *for his encouragement to achieve my PhD*

Last but not the least I present my warm thanks to my ***Mother, wife*** *and all members of the family for their support at all time during my study. Without the tremendous assistance and support of a great many other people, this research could not have been done. I offer sincere thanks to them all.*

Abstract

Reducing atmospheric CO_2, a main source of greenhouse gas, has been overemphasized recently. The primary sources of greenhouse gas emissions are the combustion of fossil fuels such as natural gas for the production of electricity purpose. The CO_2 capture step is accounted for approximately 70-80 % of the expense for the overall CO_2 capture and sequestration process. Since, the energy costs for CO_2 separation greatly depend on the performance of the adsorbents. Therefore, it is important to develop new adsorbents to reduce the energy for CO_2 separation. The principal aim of this work is to develop novel adsorbents derived from resorcinol formaldehyde xerogel that capable of operation at elevated temperature for more efficient CO_2 capture by adsorption.

In this work, resorcinol-formaldehyde (RF) carbon xerogels with high porosity and surface area have been synthesized via the sol-gel polycondensation reaction of resorcinol (R) with formaldehyde (F) in a slightly basic medium followed by drying and pyrolysis. The influences of selection the catalyst species and the catalyst ratios and other different parameters during synthesis have been investigated. The binary adsorption isotherms of the CO_2/N_2 system were measured using a modified gas chromatograph technique, the isotherm gradients are determined from the flow-rate and composition transient time, which are measured using a differential pressure transducer (DPT) and a thermal conductivity detector (TCD) respectively. The study demonstrates the potential of the surface chemistry of surface modified RF-carbon xerogels for the

generation of efficient CO_2 adsorbents, if their beneficial surface chemistry could be combined with advantageous pore structure.

The regeneration of the samples was studied using temperature programming desorption-mass spectrometry (TPD-MS) technique. The decrease in the CO_2 capture capacities upon regeneration was observed. The adsorptive capacity of regenerated carbon xerogel (after two cycles of regeneration) via CO_2 capture loses approximately 7% compared to the adsorptive capacity of fresh one. While the CO_2 capture capacities for the surface modified carbon xerogels RFC-MPDA30% (second regeneration cycle) and RFC-DPI30% (second regeneration cycle) lose about 12% and 8%.

Layout of the thesis

The main goal of this investigation is to make high surface area carbon xerogels with a controlled pore structure, new surface chemistry and high yield which could be regenerated and can be operated at high temperature for more efficient CO_2 separation by adsorption. Therefore, the bulk of the research has been related to investigating the influence of processing conditions on the pore structure and surface chemistry of the product material in moving from raw gel-type xerogel to pyrolytic carbon to activated carbon. The various chapters of this thesis are explained as follows:

The introduction, problems and main and detailed objectives of the major and specific field of study are described in *Chapter one*. *Chapter two* gives a review about the amount of CO_2 emitted by the industry and a brief about different methods and materials used for CO_2 capture and separations. *Chapter three* gives a brief review about: activated carbon properties and processing; activated carbon applicability for gas separation and storage; a broad review of phenolic resin derived carbons; an up-to-date and comprehensive overview of the growing literature on phenolic resin and carbon aerogels and xerogels. This review considered as a starting point of this research.

Chapter four deal with the most important theoretical aspects relevant to the experimental techniques. In addition to the equations and models which have been used for the analysis of the results obtained from these techniques are discussed. *Chapter five*

gives the experimental detail of the carbon xerogels preparations procedures. In addition to a description of the set of experiments that were conducted to quantify the factors that may affect the adsorption properties of the prepared carbons; the result of which are presented and discussed in *Chapter six*. The critical appraisal of the carbon xerogels preparation and applicability in CO_2 adsorption, in addition to the scope for further researches coming out of this project are outlined in *Chapter seven*. The conclusions drawn from this research are given in *Chapter eight. Chapter nine* and *Chapter ten* give the appendices and references respectively.

Chapter 1

Introduction, Problems and Objectives

The sun radiates vast quantities of radiant energy into earth every day, with a wide spectrum of wavelengths. Most of the radiant energy from the sun is concentrated in the visible and near-visible parts of the spectrum. The narrow band of visible light, between 400 and 700 nm, represents 43% of the total radiant energy emitted. Wavelengths shorter than the visible account for 7 to 8% of the total, but are extremely important because of their high energy per photon. The shorter the wavelength of light, the more energy it contains. Thus, ultraviolet light is very energetic (capable of breaking apart stable biological molecules and causing sunburn and skin cancers). The remaining 49 - 50% of the radiant energy is spread over the wavelengths longer than those of visible light. These lie in the near infrared range from 700 to 1000 nm; the thermal infrared, between 5 and 20 microns; and the far infrared regions. Various components of earth's atmosphere absorb ultraviolet and infrared solar radiation before it penetrates to the surface, but the atmosphere is quite transparent to visible light. Absorbed by land, oceans, and vegetation at the surface, the visible light is transformed into heat and re-radiates in the form of invisible infrared radiation. If that was all there was to the story, then during the day earth would heat up, but at night, all the accumulated energy would radiate back into space and the planet's surface temperature would fall far below zero very rapidly. The reason this doesn't happen is that earth's atmosphere contains molecules that absorb the heat and re-radiate the heat in all directions. This reduces the heat radiated out to space. These molecules called 'greenhouse gases' because they serve to hold heat in like the glass walls of a greenhouse; they are responsible for the fact that the earth enjoys temperatures suitable for our active and complex biosphere.

Carbon dioxide is one of the greenhouse gases. It consists of one carbon atom with an oxygen atom bonded to each side. When its atoms are bonded tightly together, the carbon dioxide molecule can absorb infrared radiation and the molecule starts to vibrate. Eventually, the vibrating molecule will emit the radiation again, and it will likely be absorbed by yet another greenhouse gas molecule. This absorption-emission-absorption cycle serves to keep the heat near the surface, effectively insulating the surface from the cold of space. Carbon dioxide, water vapor, methane, nitorus oxide (N_2O), and a few other gases are greenhouse gases. They all are molecules composed of more than two component atoms, bound loosely enough together to be able to vibrate with the absorption of heat. The major components of the atmosphere (nitrogen and oxygen) are two-atom molecules too tightly bound together to vibrate and thus they do not absorb heat and contribute to the greenhouse effect (Metz et al., 2001)

Since the industrial revolution and expansion of agriculture around 200 years ago, we have been pumping additional carbon dioxide gas into the atmosphere. Today, the concentration of this gas is approximately 30 per cent greater than in the 18th century. Levels of other greenhouse gases have also increased because of human activities. Higher concentrations of greenhouse gases in the earth's atmosphere will lead to increased trapping of infrared radiation. As a result, the lower atmosphere is likely to warm, changing weather and climate. The changes will add to the natural greenhouse effect, producing an enhanced greenhouse effect. (The enhanced greenhouse effect is often referred to as climate change or global warming). This

increase in the natural process of the greenhouse effect, brought about by human activities, whereby greenhouse gases are being released into the atmosphere at a far greater rate than would occur through natural processes and thus their concentrations are increasing.. (Schellnhuber, 2006).

The current available ways to reduce CO_2 emissions (the main responsible for the enhanced greenhouse effect) are divided into three categories (1) Use less energy to accomplish work economically. (2) Utilize energy sources that don't contain carbon, such as wind, solar, and nuclear, or reduced carbon energy sources, i.e., natural gas instead of coal. (3) Mitigate greenhouse gas by capturing carbon dioxide, which is the main focus of this study (Mathews, 2007).

Most of the increase in carbon dioxide comes from burning of fossil fuels such as oil, coal and natural gas, and from deforestation. Currently, about 7 billion tones of carbon (as carbon dioxide) are emitted each year during the combustion of fossil fuels and 1-2 billion tones per year from land clearing. Reducing atmospheric CO_2, a main source of greenhouse gas, has been accentuated recently. Capturing CO_2 from flue-gas streams is an essential parameter for the carbon management for sequestrating of CO_2 from our environment (Schellnhuber, 2006).

Pressure (and/or temperature) swing adsorption (P/TSA) have been proposed for separation and recovery of CO_2 emitted by thermal power stations, cement plants, and steel works. However, the energy costs for CO_2 separation from flue gases are

accounted for approximately 70-80 % of total cost for CO_2 sequestration. Therefore, it is important to develop new adsorbents to reduce the energy for CO_2 separation, because the energy costs for CO_2 separation greatly depend on the performance of the adsorbents.

Adsorption is one of the promising methods that could be used to separate CO_2 from gas mixtures, and numerous studies have been conducted on separation of CO_2 by adsorption in the last two decades. The two main reasons for this development are (a) the commercial availability of a large spectrum of microporous adsorbents (zeolites, activated carbons, aluminas, silica gels, polymeric adsorbents), with varying pore structures and surface properties, which can be used to selectively adsorb specific components of a fluid mixture, and (b) the possibility of designing many different process schemes under the generic category of pressure swing adsorption (PSA) and thermal swing adsorption (TSA), for a given separation need, using the available adsorbents. The technology has evolved to be extremely versatile and flexible, owing to the large choice of adsorbent materials and their use in the design of innovative separation processes.

Due to the highly developed porous structure, porous materials, like molecular sieve and zeolite, as well as activated carbons, are suitable candidates for CO_2 capture by adsorption (Xiaochun et al., 2003). Porous material developed from solid amines, metal oxides and ion exchange resins have limited application due to their high cost and intensive equipment requirement. Commercial available activated carbons, which derived from natural occurring materials, are used widely as an adsorbent in

many gas-phase applications; however its inherent problems encountered in their use in certain applications. In general, the application of such carbons as an adsorbent suffer from numerous drawbacks including significant levels of impurities, that inherent from the precursors (e.g. coconut shell, wood, coal, etc.), poor homogeneity and controllability pore size distribution, poor physical strength an a very limited rang of physical forms.

At lower temperatures (eg. room temperature), the zeolite-based adsorbents have generally been found to show higher adsorption capacity. Siriwardane et al. (2001) reported that the CO_2 adsorption capacity of zeolite 13X, zeolite 4A, and activated carbon was about 160, 135, and 110 mg/g-adsorbent, respectively, at 25°C and 1 atm CO_2 partial pressure. However, their adsorption capacities rapidly decline with increasing temperature. Moreover, Zeolite, which shows a good adsorption capacity for CO_2 cannot be used for CO_2 adsorption for a waste gas stream containing moisture (Harlick and Tezel, 2003). Also, due to high cost of production and regeneration of zeolite, an alternative and effective adsorbent for CO_2 , which is could be regenerated, operated at relatively high temperature up to ~ 100°C (typical value of power plant stack temperature) , is highly sought (Gray et al., 2004).

Pore structure (surface area and pore size distribution) and surface chemistry control the adsorption properties of any adsorbents in traditional applications like water filtration and air purification. Similarly, the CO_2 adsorption capacity of activated carbons is a function of their pore structure and surface chemistry properties. Moreover, since all the gases are physically adsorbed into/onto the different

adsorbent, the separation factors (such as CO_2/N_2 ratio) are low at low temperature. To operate at relatively high temperature and reach a high separation factor, chemical adsorption should be adopted. Ding et al. (2000) investigated the adsorption performance of hydrotalcite, and this material showed a CO_2 adsorption capacity of 22 mg/g-adsorbent at 400°C and 0.2 atm. CO_2 partial pressure. Xiaochun Xu et al. (2002) reported that MgO showed an adsorption capacity of 8.8 mg/g-adsorbent at 400°C. Both types adsorbents need high temperature operation and have a low adsorption capacity, thus they are not suitable for practical use for CO_2 separation.

Sometimes the original chemistry of the activated carbon surface is not sufficiently potent to enhance the specific adsorbate-adsorbent interactions. Therefore, different surface treatments have to be developed to improve the CO_2 adsorption capacity of activated carbons at high temperature. In the case of CO_2 adsorption, basic nitrogen functionalities are crucial for efficient CO_2 capture, which has led to efforts to maximize the number of nitrogen functional groups. Some of the most successful adsorbents for CO_2 have been developed via the alteration of the surface chemistry of porous substrates by impregnation with amine polymers. Another method is the modification of the surface chemistry of the carbon matrix by the incorporation of heteroatoms such as nitrogen to enhance the specific adsorbate–adsorbent interaction. Nitrogen within the carbon matrix can cause an increase in the number of basic groups and change the charge distribution in the grapheme layers and consecutively affect the CO_2 adsorption. There have been many attempts by a number of authors to enhance the adsorption of acidic pollutants by increasing basicity.

Alkaline activated carbons play a great role as catalyst in various chemical reactions (Huang and Teng, 2003). One popular method used for preparation of activated carbon with increased alkalinity is introducing nitrogen to the carbon structure. This can be done by preparing activated carbon from N-containing compound (Lopez et al., 2000), or treating activated carbon with ammonia. However, modification of activated carbon with aqueous ammonia (33 wt.%) either at 130°C for 9 h or at room temperature for 100 h did not result in a significant change in carbon surface chemistry (Severinin et al., 2002). Bagreev et al. (2004) have introduced nitrogen to bituminous coal-based activated carbon by impregnation with melamine and heat treatment at 850°C. Carbons prepared in such a way contained considerable percent of nitrogen however, their structural parameters (surface area and micropore volume) deteriorated by 25%, compared to unmodified carbon.

Activation is usually carried to increase the surface area and pore volume. In general, activation is commonly carried out in presence of a suitable oxidizing agent such as steam, CO_2, air and oxygen. The activation process together with the intrinsic nature of the precursors strongly determines the characteristics of the resulting activated carbons (Daud et al., 2002; Manocha, 2003). From the survey it was found that, the effect of activation temperature on the porosity of the activated carbon varies with the raw material used, and the experimental conditions to produce an activated carbon cannot be extrapolated from one given precursor material to another. So, it is very important, in the development of a new adsorbents process, to ascertain the effect of the different activation conditions on its pore structure and surface chemistry. Wigmans (1989) activated extruded peat semicoke and showed that

increasing the activation temperature from 860 to 1040°C has no significant effect on the total pore volume. However, above 900°C, the macropore volume decreased slightly with increasing burn-off. In another study, carbon produced from used tire and activated with H_2O-CO_2 mixture, the BET surface area of the produced carbons increase upon activation time reaching a maximum of 432 m^2/g after 150 min, at 970°C, at a burn-off level of 65 wt. % (Zabaniotou et al., 2004). Guo and Lua (2003), activated carbons prepared from oil-palm shell and showed that the increasing of activation temperature from 773 to 1173 K leads to progressively increase of the BET surface area, however the maximum surface area obtained was 1366 m^2/g. In another study on palm shell, Daud et al. (2002), found that; within the temperature range of 800 to 900°C, an increase in the activation temperatures has no remarkable effect on mesopore and macropore development.

The sol-gel process is a chemical synthesis method extensively applied to the preparation of numerous materials with different chemical structure and properties, such as glasses, ceramics, adsorbents, catalyst supports. The sol-gel process is quickly becoming one of the most promising material synthesis techniques because it readily allows for control of the texture, composition, homogeneity and structural properties of the resulting materials. Carbon materials derived from polycondensation of hydroxylated benzene (phenol, catechol, resorcinol, hydroquinone,...) and aldehyde (formaldehyde, furfural,....) in a solvent through a reaction mechanism similar to the sol-gel processing followed by drying and pyrolysis have been extensively studied and its importance are increasing more and more for their wide applicability as electrodes for supercapacitors and fuel cells. In

1989, organic aerogels syntheses were first introduced by Pekala et al. (1989 and 1991) patented using supercritical drying conditions. Since then, numerous articles have been published on the properties and potential uses of these organic gels and its pyrolized carbon version. The supercritical drying condition has many disadvantages and remains difficult to apply at an industrial scale. It needs high pressure, which is not good for both economical and safety reasons. When the gel is dried by simple evaporation, large capillary forces at the curved liqid-vapour interfaces often cause the material to shrink and crack, and the carbon obtained after pyrolysis is in most cases totally non-porous. This is the reason why complex drying methods which suppress the liquid-vapour interface or reduce the capillary forces have been developed. The increasing popularity of these materials is largely due to, their unique and controllable properties, which in turn are attributed to the reaction mechanism being akin to the sol-gel process, its fine structure, strength and relatively low price. The use of resorcinol-formaldehyde (RF) resins as precursors for adsorbent materials and its application for CO_2 adsorption is being under-exploited, probably due to the limited number of studies assessing the possible routes for their conversion into nitrogen enriched activated carbons and alter its surface chemistry. In addition, performance requirements are becoming increasingly more demanding, and there is a growing need for activated carbon with new and improved properties. In this thesis we tried to investigate a new route to produce activated carbon from resorcinol-formaldehyde resins with increasing surface basicity and control pore structure.

According to the preceding discussion, this study was conducted to further develop and modify resorcinol-formaldehyde sol-gel synthesis procedure to make high surface area nitrogen enriched carbon xerogel with a controlled pore structure,

surface chemistry and high yield, which could be regenerated and can be operated at high temperature for more efficient CO_2 separation by adsorption. The study also demonstrates, the potential of the surface chemistry of RF-carbon xerogels for the generation of efficient CO_2 adsorbents, if their beneficial surface chemistry could be combined with advantageous pore structure. Loading different substances during the RF-resin pyrolysis may produce a new material with different pore structure and surface chemistry. This may change the adsorption properties of the resulting carbon towards adsorption of gases, the new idea can be used to develop different types of high-selective, high adsorption capacity adsorbent. This work also shows that it is possible to synthesize still largely porous materials by simple vacuum drying of aqueous resorcinol-formaldehyde (RF) gels when the gel synthesis conditions are appropriate.

The research which has been conducted in this thesis is distinctive from the others by a number of ways. Various RF carbon xerogels are synthesized by using different catalysts species which have not been used before. Alkanolamine, monoethanolamine, diethanolamine, and methyldiethanolamine as well as the common basification agent potassium carbonate and sodium carbonate were used as a catalyst for the polycondensation reaction. The reason of using such basification agent is to alter the surface chemistry of the produced carbon to be more basic. Nnitrogen adsorption at 77 K was used to elucidate the influence of the new catalyst species, the catalyst ratio, amount of diluents and the initial pH of the RF solution on the surface area, pore volume and pore size distribution of the prepared RF carbon

xerogels. Infrared spectroscopy was employed to analyze the surface functional groups of the prepared RF gels and carbons.

In this study, we ascertain the effect of activation extent (time and temperature) on the porous structure, chemical properties and the yield of the prepared carbon. Optimization of the syntheses conditions is necessary to obtain good physical and chemical properties in addition to a high carbon yield. The nitrogen content was further increased in order to increase the basic functional group on the carbon surface for operation at high adsorption temperature. This done through impregnation of the resins with nitrogen containing compounds such as *m*-phenylenediamine, $C_6H_8N_2$, (MPDA) and diphenylenimine, $C_{12}H_9N$, (DPI), before the pyrolysis step. The binary adsorption isotherm of the CO_2/N_2 system was measured by a novel technique which has not been used before for the investigation of CO_2 adsorption and separation. The method has several advantages such as speed and the relative ease with which conditions can be changed. It depends on the flow rate and composition transient time measurements using perturbation gas chromatograph. Additionally, a study was made for the effect of the different preparations conditions of carbons as well as the effect of the adsorption temperature on the CO_2 adsorption capacity and CO_2/N_2 uptake ratio. The reversibility of the adsorption process and regeneration was studied by temperature programming desorption mass spectrometry (TPD-MS). To analyze the desorption data and calculating the desorption kinetics, the CO_2 spectra obtained from the TPD-MS measurements have been modelled using the assumption of a first order desorption process with a single activation energy for desorption (Readhead Eq.) equation.

Chapter 2

Carbon Dioxide Capture and Storage

2.1 Introduction.

In the 19th century, scientists realized that gases in the atmosphere cause a "greenhouse effect" which affects the earth's temperature. At the turn of the nineteenth century, Svante Arrhenius (1896) calculated that emissions from human industry might someday bring a global warming. It was deemed faulty by other scientists until the1950s. It was almost by chance that a few researchers discovered that global warming truly was possible. In the early 1960s, C.D. Keeling (1960) found that the level of carbon dioxide in the atmosphere was rising fast. Researchers began to focus on how the level of carbon dioxide had changed in the past, and how the level was influenced by chemical and biological forces. By now, it is well known that next to nitrogen, oxygen and argon, carbon dioxide is the most abundant gas in the earth's atmosphere. Next to water vapour, it is the most important greenhouse gas responsible for climate changes (Zeebe and Gladrow-Wolf, 2001).

In our environment, carbon is present in various forms. Carbon sinks include the following : (1) Intermediate and deep sea (excluding the surface layer), which includes 38,100 Gt of carbon as dissolved carbon, carbonates or bicarbonates; (2) Atmospheric gases with 750 Gt carbon; (3) Soil containing 1580 Gt; and (4) Vegetation and animals accounting for 610 Gt (Schnitzer, 2007).

2.2 Amount of CO_2 emitted by industry.

CO_2 is the by-product of combustion processes involving organic fuels, such as producing energy from fossil fuels, operating car engines or burning forests. The concentrations of CO_2 in the atmosphere has risen from 280 ppm to 360 ppm since

1900 (Robinson et al., 1998). Unchecked, it will pass 550 ppm this century. Scientists agree that increases above the 450 ppm level might result in massive disruptions of global climatic patterns. If nothing is done to reduce emissions, current climate models predict a global warming of about 2°C long-term. This will affect the climatic zones of the world, damage vulnerable ecosystems, raise mean sea level to risk flooding in low-lying areas. The Intergovernmental Panel on Climate Change (IPCC) has developed a widely cited energy scenario, IS92a, which predicts that the global CO_2 emission will increase form 7.4 billion tons of atmospheric carbon per year (GtC/yr) in 1994 to roughly 20 GtC/yr by 2100, as shown in Figure 2.1. According to the International Energy Agency in 1999, 33% of CO_2 emissions come from power plants, which generated the largest portion of the total CO_2 emissions, as shown in Figure 2.2 (Schellnhuber, 2006).

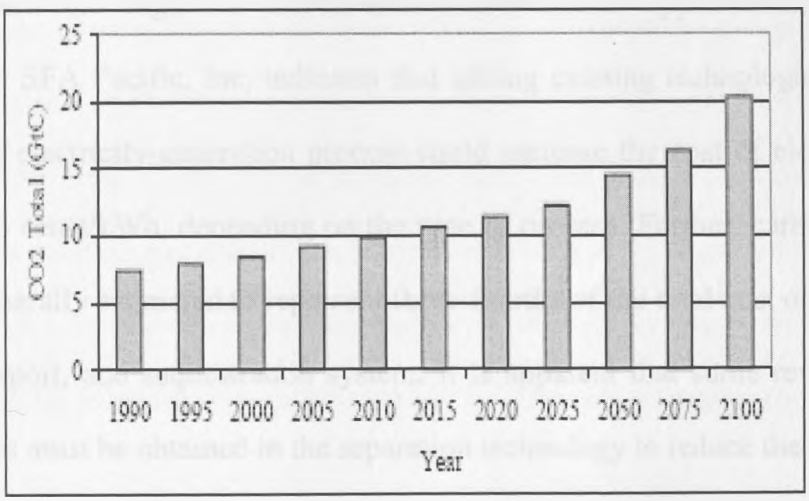

Figure 2.1. Global carbon dioxide emission (Schellnhuber, 2006).

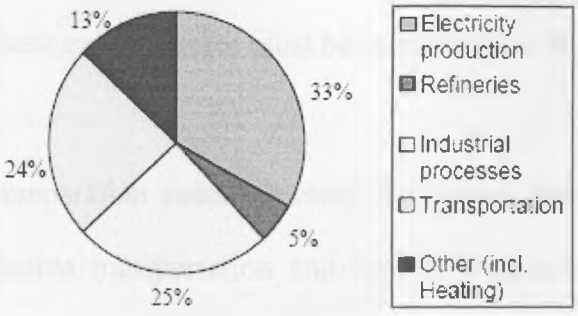

Figure 2.2 CO_2 emission statistics (Schellnhuber, 2006).

2.3 Means and cost of capturing industrial CO_2.

Sequestration entails the capture and storage of CO_2. Before CO_2 gas can be sequestered from power plants and other point sources, it must be captured as a relatively pure gas. The existing capture technologies are not cost-effective. The cost of CO_2 capture using current technology, however, is on the order of $150 per ton of carbon - much too high for carbon-emissions-reduction applications. Analysis performed by SFA Pacific, Inc. indicates that adding existing technologies for CO_2 capture to an electricity-generation process could increase the cost of electricity by 2.5 cents to 4 cents/kWh, depending on the type of process. Further, carbon dioxide capture is generally estimated to represent three-fourths of the total cost of a capture, storage, transport, and sequestration system. It is apparent that some revolutionary improvements must be obtained in the separation technology to reduce the cost.

Air combustion is the traditional process utilizing fossil fuels and most power plants adopt that process, but it produces CO_2 diluted with nitrogen. The gas from coal-fired power plants contains 10-12 percent CO_2 by volume, while flue gas from natural gas

combined cycle plants contain only 3-6 percent CO_2. For effective carbon sequestration, the CO_2 in these exhaust gases must be separated and concentrated.

In summary, CO_2 capture/separation costs represent the largest financial problem. Hence, efficient, cost-effective transportation and capture/separation technologies will need to be developed to allow large-scale use of geologic sinks. This is the new driving force for developing CO_2 separation technologies. The CO_2 separation markets are envisioned to be very large indeed. At the moment, there are three pathways for CO_2 separation: pre-combustion decarbonizations, O_2/CO_2 recycle combustion and post combustion CO_2 separation.

In pre-combustion decarbonization fuel is reacted with O_2 and/or steam to produce mainly carbon monoxide (CO) and hydrogen (H_2). The CO is reacted with steam in a catalytic reactor to give CO_2 and more H_2. The CO_2 is separated and the hydrogen can be used as fuel or in a hydrogen fuel cell. This process, in principle, is the same for coal, oil or natural gas. When coal is used, there are more stages of gas purification, to remove particles of ash, sulfur compounds and other compounds. Air or oxygen from a cryogenic air separation plant can be used to react with the fuel. In this way, the CO_2 concentration in the flue gas is increased improves the separation economics.

O_2/CO_2 recycle combustion uses a pure O_2/CO_2-enriched stream for combustion. This option effectively moves the separation (i.e. N_2 from air) upstream in front of the burner. By increasing the oxygen in the feed gas and eventually, by circulating

part of the flue gas, a CO_2 concentration of up to 98% by volume can be achieved. Coal combustion at a higher oxygen concentration is particularly attractive not only because it allows reducing the cost of CO_2 separation in the flue gas, but also because it reduces the volume of inert gas (i.e. N_2) in the furnace and thus increases the boiler thermal efficiency (Croiset et al., 1999).

For post combustion CO_2 separation from flue gas, which is the main focus of this study, there are four different approaches, namely (Wong and Bioletti, 2002):

1. Amine absorption. As the state-of-the-art technology for CO_2 capture, amine absorption has been commercially used for the removal of acid gas impurities (CO_2 and H_2S) from process gas streams.

2. Low temperature distillation (cryogenic separation). Low temperature distillation is a commercial process commonly used to liquefy and purify CO_2 from relatively high purity (>90%) sources. It cools the gases to a very low temperature in order to liquefy the CO_2 and then separate it.

3. Membranes. Based on different permeation of gases, membranes are used as a barrier to allow certain gases to pass through. For CO_2 separation, the membranes are normally made from polymers.

4. Solid physical adsorption - pressure swing and temperature swing adsorption.

2.3.1 Chemical and physical absorption.

2.3.1.1 Chemical absorption.

The chemical absorption process for separating CO_2 from flue gas is borrowed from the gas processing industry. Amine absorption has been commercially used for the removal of acid gas impurities (CO_2 and H_2S) from process gas streams. Alkanolamines remove CO_2 from the gas stream by the exothermic reaction of CO_2 with the amine functionality of the alkanolamine. Figure 2.3 proposed the reaction sequence for the capture of carbon dioxide by liquid amine-based systems. Different amines have different reaction rates with respect to the various acid gases. In addition, different amines vary in their equilibrium absorption characteristics for the various acid gases and have different sensitivities with respect to solvent stability and corrosions factors. Alkanolamines can be divided into three groups: (1) primary amines whose members include monoethanol amine (MEA), diglycolamine (DGA); (2) secondary amines whose members include diethanolamine (DEA), di-isopropylamine (DIPA); and (3) tertiary amines whose members include triethanolamine (TEA) and methyl-diethanolamine (MDEA).

In the amine gas processing operation, the gas stream and liquid amine solution are contacted by countercurrent flow in an absorption tower. Conventionally, the gas to be scrubbed enters the absorber at the bottom, flows up, and leaves at the top, whereas the solvent enters the top of the absorber, flows down (contacting the gas), and emerges at the bottom. Dilution of the circulating amine with water is done to reduce viscosity of the circulating fluid. The liquid amine solution containing the absorbed gas is then flowed to a regeneration unit where it is heated and the acid

gases liberated. The solvent regeneration can be carried out at low pressures to enhance desorption of CO_2 from the liquid. Some amine solution is typically carried over in the acid gas stream from the regeneration step and the amine solution is recovered using a condenser. The hot lean amine solution then flows through a heat exchanger where it is contacted with the rich amine solution from the contact tower and from there the lean amine solution is returned to the gas contact tower.

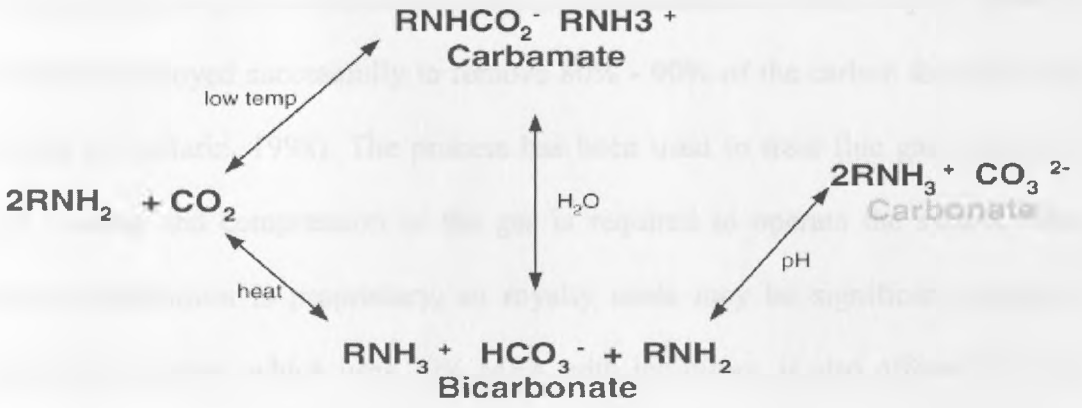

Figure 2.3 Proposed reaction sequence for the capture of carbon dioxide by liquid amine-based systems (Chung S, 2004)

Among the primary amines, MEA has been the traditional solvent of choice for carbon dioxide absorption and acid gas removal in general. MEA is the least expensive of the alkanolamines and has the lowest molecular weight, so it possesses the highest theoretical absorption capacity for CO_2. This theoretical upper absorption capacity of MEA is not realized in practice due to corrosion problems. In addition, MEA has the highest vapor pressure of any of the alkanolamines and high solvent carry-over can occur during carbon dioxide removal from the gas stream and in the regeneration step. To reduce solvent losses, a water wash of the purified gas stream

is usually required. In addition, MEA reacts irreversibly with minor impurities such as COS and CS_2 resulting in solvent degradation. Foaming of the absorbing liquid MEA due to the build-up of impurities can also be a concern.

There is considerable industrial experience with MEA and most systems at present use an aqueous solution with only 15-25 wt% MEA, mainly due to corrosion issues. Corrosion inhibitors may be added to MEA solution, and this result in an increase in solution strength. In a commercial process, concentrations of MEA up to 30-wt% have been employed successfully to remove 80% - 90% of the carbon dioxide from the feed gas (Mariz, 1998). The process has been used to treat flue gas, however, some cooling and compression of the gas is required to operate the system. The solvent composition is proprietary, so royalty costs may be significant. Another commercial process, which uses 20% MEA with inhibitors, is also offered for flue gas treatment (Barchas, 1992).

Limitations of amine-based processes: For the current MEA absorber systems, the adsorption and desorption rates are reasonably high. However, the column packing represents a significant cost, and its energy consumption is also significant for flue gas treatment. In addition, the stripping temperature should not be too high. Otherwise, dimerization of carbamate may take place, deteriorating the sorption capability of MEA. The greatest limitation for CO_2 recovery from flue gas is the low pressure of the flue gas. CO_2 is absorbed much more easily into solvents at high pressure. The oxygen content of the flue gas is an issue that must be addressed. Most solvents applicable for flue gas systems degrade to varying degrees in oxidizing

atmospheres, which lead to either high solvent losses or expensive reclaiming processes. Fly ash in the flue gas can cause foaming and degradation of the solvent and plugging and scaling of the process equipment. Flue gas entering the absorber at high temperature can lead to solvent degradation and decreased absorption efficiency. The flue gas must be cooled to a water dew point of 50°C (Mimura et al.; Veawab et al.; Aboudheir et al., 2001).

In summary, the recovery of CO_2 from combustion flue gas requires a significant amount of pre-treatment processing in order to avoid any foul-up in the solvent absorption step. Under flue gas conditions MEA has limited lifetime, MEA is highly corrosive, use of MEA requires heavy use of additives and regeneration stage is very energy intensive: can reduce power output by 20 %. This will add to the cost of CO_2 (Chapel et al., 1999).

2.3.1.2 Physical absorption.

For physical absorption, CO_2 is physically absorbed in a solvent according to Henry's Law, which means that they are temperature and pressure dependent with absorption occurring at high partial pressures of CO_2 and low temperatures. The solvents are then regenerated by either heating or pressure reduction. The advantage of this method is that it requires relatively little energy; but the CO_2 must be at high partial pressure. Hence, it is suitable for recovering CO_2 where the exhaust CO_2 would leave the gasifier at elevated pressures. Typical solvents are Selexol (dimethylether of polyethylene glycol) and Rectisol (cold methanol). Selexol has been used since 1969 to sweeten natural gas, both for bulk CO_2 removal and H_2S

removal. Absorption takes place at low temperature (0 - 5°C). Desorption of the rich Selexol solvent can be accomplished either by letting down the pressure (CO_2 removal) or by stripping with air, inert gas or steam. Hydrocarbons, COS, CS_2 and mercaptans are also removed by the solvent. Additionally, the low absorption temperature used requires that the lean solvent be returned to the absorber via a refrigeration unit.

2.3.2 Low temperature distillation (cryogenic separation).

Low temperature distillation is a commercial process commonly used to liquefy and purify CO_2 from relatively high purity (>90%) sources. It cools the gases to a very low temperature in order to liquefy the CO_2 and then separate it. Distillation generally has good economies of scale. This method is worth considering where there is a high concentration of CO_2 in the waste gas. The advantage is that it produces a liquid CO_2 ready for transportation by pipeline. The major disadvantages of this process are the amount of energy required to provide the refrigeration and the necessary removal of components that have freezing points above normal operating temperatures to avoid freezing and eventual blockage of process equipment. For post combustion flue gases, the waste streams contain water and other trace combustion by-products such as NO_x and SO_x several of which must be removed before the stream is introduced to the low temperature section. Moreover, these by-products are usually generated near atmospheric pressure. These tend to make cryogenic process less economical than others in separating CO_2 from flue gas. However, it is a serious contender for high-pressure gases such as in pre-combustion decarbonization processes.

2.3.3 Membranes.

Based on different permeation of gases, membranes are used as a barrier to allow certain gases to pass through. For CO_2 separation, the membranes are normally made from polymers. Membranes for gas separation are usually formed as hollow fibers arranged in a tube-and-shell configuration, or as flat sheets, which are typically packaged as spiral-wound modules. The membrane process has been widely used on the commercial scale for hydrogen recovery from purge gases in ammonia synthesis, refinery and natural gas dehydration, sour gas removal from natural gas, and nitrogen production from air. Compared to absorption separation, the advantages of the membrane process are:

1) It does not require a separating agent, thus no regeneration is required;

2) The systems are compact and lightweight, and can be positioned either horizontally or vertically, which is especially suitable for retrofitting applications;

3) Modular design allows optimization of process arrangement by using multi-stage operation; and

4) Low maintenance requirements because there are no moving parts in the membrane unit.

A number of solid polymer membranes are commercially available for the separation of CO_2 from gas streams, primarily for natural gas sweetening. These membranes selectively transmit CO_2 versus CH_4. The driving force for the separation is pressure differential across the membrane. As such, compression is required for the feed gas in order to provide the driving force for permeation, and the separated CO_2 is at low pressure and requires additional compression to meet pipeline pressure requirements.

The energy required for gas compression is significant when a very high pressure is required. The commercial membranes for CO_2 separation are mainly prepared from cellulose acetate, polysulfone, and polyimide. These membranes are primarily tailor-made for natural gas processing and not specifically developed for flue gas separation. The selectivity of CO_2/N_2 of these membranes is generally in the range of 20 ~ 40, depending on the operating temperature. Because of the specific characteristics of flue gas composition, and the specific features of the separation (i.e. large volumetric flow rate, low source pressure, high temperature, and the relatively low commodity value of CO_2), further development may be required for economically capturing CO_2 from flue gas on a large scale.

2.3.4 Physical adsorption.

An adsorption process consists of two major steps: adsorption and desorption. The technical feasibility of a process is dictated by the adsorption step, whereas the desorption step controls its economic viability. Strong affinity of an adsorbent for removing the undesired component from a gas mixture is essential for an effective adsorption step. The stronger the affinity, however, the more difficult it is to desorbs the gas impurity and the higher the energy consumed in regenerating the adsorbent for reuse in the next cycle. The desorption step, therefore, has to be very carefully balanced against the adsorption step for an adsorption step to be successful. The main advantage of physical adsorption over chemical or physical absorption is its simple and energy efficient operation and regeneration, which can be achieved with a pressure swing or temperature swing cycle. The primary adsorption material under consideration is zeolite. The concerns over this technology are scale up and the need

to develop CO_2 specific adsorbent materials.

Adsorption processes can be categorised as being one of the following,

1. Physical adsorption (Physisorption)
2. Chemical adsorption (chemisorption)

Physical adsorption (physisorption) is adsorption in which the forces involved are intermolecular forces (van der Waals forces) of the same kind as those responsible for the imperfection of real gases and the condensation of vapours, and which do not involve a significant change in the electronic orbital patterns of the species involved. The phenomenon is a general one and occurs in any solid/fluid system, although certain specific molecular interactions may occur, arising from particular geometrical or electronic properties of the adsorbent and/or adsorptive. In physical adsorption; the chemical nature of the fluid is not altered by adsorption and subsequent desorption, the energy of interaction between the molecules of adsorbate and the adsorbent is of the same order of magnitude as, but is usually greater than, the energy of condensation of the adsorptive. The forces bringing about physical adsorption always include "dispersion forces" and short-range repulsive forces. In addition there may be forces due to permanent dipoles within the adsorbed molecule. The dispersion forces originate through the rapidly changing electron density in one atom, which induces a corresponding electrical moment in a near neighbour and so leads to attraction between the two atoms. Dispersion forces between molecules are much weaker than the covalent bonds within molecules. It isn't possible to give any exact value, because the size of the attraction varies considerably with the size of the

molecule and its shape. Dispersion forces are always present between a solid and a molecule of adsorbate gas or vapour, and their dependence on distance is such that the first layer of adsorbed molecules will be strongly held, and higher layers more weakly so with an energy not much in excess of the latent heat of vaporization (Lowell, 1991).

Chemical adsorption (chemisorption) is adsorption in which the forces involved are valence forces of the same kind as those operating in the formation of chemical compounds. The phenomenon is characterized by chemical specificity. In chemisorption a transfer of electrons between the solid and the adsorbed molecule occurs; as a result a chemical compound is formed, but it is confined to a single layer of atoms or molecules on the surface of the solid. The energy of chemisorption is of the same order of magnitude as the energy change in a chemical reaction between a solid and a fluid: thus chemisorption, like chemical reactions in general, may be exothermic or endothermic and the magnitudes of the energy changes may range from very small to very large. The chemical nature of the adsorptive may be altered by surface dissociation or reaction in such a way that on desorption the original species cannot be recovered; in this sense chemisorption may not be reversible. Since the adsorbed molecules are linked to the surface by valence bonds, they will usually occupy certain adsorption sites on the surface and only one layer of chemisorbed molecules is formed

2.3.4.1 Pressure (and/or temperature) swing adsorption (P/TSA).

Separation by P/TSA adsorption is based on the selective accumulation of one or more components of a gas mixture on the surface of a microporous solid. When a gaseous mixture is exposed to an adsorbent for sufficient time, equilibrium is established between the adsorbed phase and the gas phase. The gas phase becomes richer in the less selectively adsorbed component. The attractive forces responsible for the adsorption are of the Van der Waals type. Desorption can be achieved by either increasing the temperature of the system or by reducing the adsorbate pressure. The desorption step also regenerates the adsorbent surface for reuse during the subsequent adsorption step. Thus, the adsorptive separation process consists of a cyclic sequence of adsorption and desorption steps. When desorption is achieved by increasing the system temperature, the process is called thermal swing adsorption. When desorption is achieved by decreasing the pressure, the process is called pressure swing adsorption. One of the components of a gas mixture is selectively adsorbed at higher partial pressure and desorbed subsequently by lowering the partial pressure. The change in partial pressure of the gas can be caused either by decreasing the total pressure, changing the composition of the gaseous mixture, or by a combination of both.

The major advantages of a PSA system over other separation techniques are low capital and maintenance costs; comparatively straight forward and automatic operation; high purity of the product, thus avoiding further purification steps; rapid shutdown and start-up characteristics; long lifetime of vessels; highest turndown flexibility at almost constant yields; lack of corrosion problems; absence of heat

requirements; and the absence of thermal insulation materials. However, the PSA process is limited by the size of the process vessel and the process pressure. The major operating cost associated with gas processing by adsorption-desorption techniques is the energy requirement for system heating (in TSA) and bed pressurization (in PSA). Applications of PSA gas separation systems have been described recently and include the separation of N_2 , and O_2 , from air, H_2 recovery from coke oven waste gases or steam reformer gas, CH_4 , recovery (and separation of CO_2) from natural gas wells, oil wells undergoing CO_2, flooding for enhanced oil recovery, and in industrial and municipal landfill gas separations.

The choice of adsorbent for PSA/TSA applications is governed by its adsorption capacity and selectivity for the desired gas to be separated. Ruthven (1984)has reported that for a PSA process to be economical, the minimum acceptable separation factor for the desired component is approximately 3. With separation factors of less than 2, it is difficult to design a satisfactory process. Moreover, increases in the separation factor beyond 445 have only minimal benefit. Three factors applied singly or in combination, may be used to achieve the desired selectivity: the difference in shape and size of the adsorbate molecules factor; equilibrium effects, i.e. when the adsorption isotherms of the components of the gas mixture differ appreciably; and kinetic effects. When the components have substantially different diffusion or adsorption rates.

2.3.4.2 Electrical swing adsorption.

Current PSA technology utilizes a vacuum or high-temperature gas to recover the adsorbed gas in the desorption stage. Therefore, it requires additional energy to concentrate the desorbed gas or increase gas purity. Compared with the indirect heating method, where the adsorbent is heated with hot inert gas (thermal swing adsorption (TSA)), electrical swing adsorption (ESA) offers the advantages of desorbing the adsorbed gas quickly and lower energy consumption. This is because the adsorbent is heated directly with electricity. In the electrical swing adsorption ESA, the adsorbed gas may be quickly and efficiently desorbed by the passage of an electric current, thereby allowing a low energy, electrical swing system. The electrical energy required for desorption is approximately equal to the heat of adsorption of the adsorbed gas. The electric swing adsorption process (ESA) conducted by Moon and Shim (2006), the temperature increase is not linearly proportionate to the power input, while the passage of higher electrical voltage (30 V) caused the activated carbon fiber ACF temperature to exceed 200°C within 30 s.

Burchell et al, 1997 and Judkins et al., 2001 used a novel carbon-bonded activated carbon fiber as the adsorption material for CO_2 capture. This material is called carbon fiber composite molecular sieve (CFCMS). This material is rigid and strong, resistant to attrition and dusting, and because of its continuous carbon skeletal structure, is electrically conductive. CFCMS regenerate electrically in the absence of a temperature increase. Potentially reducing swing cycle time and improving separation efficiency was observed. However, the technology is at an early stage of development.

2.4 Means and costs of sequestering industrial CO_2.

After separating CO_2 from the flue gas, the following step is sequestration. Sequestration is defined as the placement of CO_2 into a repository where it can be stored for hundreds of years. Sequestration technologies include geological sequestration, terrestrial sequestration and ocean sequestration.

2.4.1 Geological sequestration.

Geological sequestration stores CO_2 in a range of underground geologic formations, such as oil and gas reservoirs, unmineable coal seams, and saline formations. Although no one has adopted reservoir sequestration on a large scale, the oil companies have been injecting CO_2 into reservoirs for decades to extract more oil from wells by reducing its viscosity and surface tension. Norway's Statoil has launched a sequestration pilot project in the North Sea, sequestering the gas at a cost of about $15 per ton of CO_2. In unmineable coal seams too deep to be mined, the coals have methane adsorbed on pore surfaces. Such bed coal methane can be recovered by sweeping with CO_2, which preferentially adsorbs to the coal and displaces methane (Service, 2004).

Currently, studies are directed toward minimizing the negative effects of coal swelling, which lowers permeability for both CO_2 and recovered methane. Saline formations, which are layers of porous rock saturated with brine, could react with injected CO_2 to form solid carbonates as a permanent storage. Currently, less is known about this method.

2.4.2 Terrestrial sequestration.

Terrestrial sequestration increases CO_2 uptake by plants that grow on land or in freshwater. Importantly, it enhances carbon storage in soils where the CO_2 may remain more permanently stored. Vegetation and soils are widely recognized as carbon storage sinks. The global biosphere absorbs roughly 2 billion tons of carbon annually, an amount equal to roughly one third of all global carbon emissions from human activity.

Significant amounts of carbon remain stored in the roots of certain plants and in the soil. One fundamental approach to sequestering carbon in terrestrial ecosystems is to protect ecosystems that store carbon so sequestration can be maintained or increased. A second approach is to manipulate ecosystems to increase carbon sequestration beyond prevalent conditions. Current studies are focusing on enhancing the natural processes that remove CO_2 from the atmosphere, which is thought to be one of the most cost-effective means of reducing atmospheric levels of CO_2. The cost of this option for sequestration is around $10/ ton of avoided net costs.

2.4.3 Ocean sequestration.

CO_2 is soluble in ocean water, and through natural processes the oceans both absorb and emit huge amounts of CO_2 (90 GtC/yr.) into the atmosphere. In fact, the amount of carbon stored in the ocean (38,100 GtC) dwarfs the carbon stored in terrestrial ecosystems (610 GtC). It is widely believed that the oceans will eventually absorb 80-90 percent of the CO_2 in the atmosphere and transfer it to the deep ocean. However, the kinetics of ocean uptake is slow.

At present, two options for sequestering CO_2 in oceans are possible. One is to speed up the natural absorption processes by oceans, and the other is to inject CO_2 directly into the deep ocean. Most work now is focusing on understanding the mechanisms of CO_2 uptake in the ocean and assessing the environmental impacts of increased CO_2 ocean storage (Haefeli et al., 2004).

2.5 Common carbon dioxide sorbents.

2.5.1 Lithium hydroxide.

Lithium Hydroxide (LiOH) is the most commonly used CO_2 sorbent for use in expendible devices. Two types of LIOH canisters (one square and one round) played an important role during the Apollo 13 Mission. Expendible LIOH canisters were only recently replaced aboard the Shuttle Orbiter by a Vacuum Regenerable Solid Amine based system. LiOH is currently used in the EMU (Extravehicular Mobility Unit) life support back pack worn by astronauts (Boehm and Ouellette, 1995). The presence of water vapour is important to the functioning of LiOH beds. Chemisorption of CO_2 is thought to take place via a two step reaction in which lithium hydroxide monohydrate is first formed by the exothermic reaction.,

$$LiOH(s) + H_2O(g) \longrightarrow LiOH \cdot H_2O(s)$$

$$\Delta H^\circ = -14.5 \text{ kcal/mol LiOH}, \qquad (2.1)$$

followed by the endothermic formation of lithium carbonate, (ΔH° is the enthalpy change at 298K. ΔH value can be related to bond energy by ΔH = energy used in bond breaking – energy released in bond making products),

$$2\ LiOH \cdot H_2O(s) + CO_2(g) \longrightarrow Li_2CO_3(s) + 3\ H_2O(g)$$

$$\Delta H^\circ = +\ 3.8\ kcal/mol\ LiOH, \tag{2.2}$$

Significantly, water is required on both sides of these reaction equations. For the net reaction,

$$2\ LiOH + CO_2(g) \longrightarrow Li_2CO_3(s) + H_2O(s)$$

$$\Delta H^\circ = -10.7\ kcal/mol\ LiOH\ (-21.4\ kcal/mol\ CO_2) \tag{2.3}$$

two moles of water are liberated for each mole of CO_2 chemisorbed.

2.5.2 Solid phase amines

Primary and secondary alkanolamines react with dissolved CO_2 in a two step sequence: forming first a zwitterions Equation (2.4), which then transfers a proton to an un-ionized amine, then forming the corresponding carbamate Equation (2.5). The reaction of tertiary amines with CO_2 proceeds by the formation of a protonated amine and a bicarbonate anion Equation (2.6).

$$R_1R_2NH + CO_2\ (aq) \longleftrightarrow R_1R_2NH^+\ CO_2^- \tag{2.4}$$

$$R_1R_2NH + R_1R_2NH^+CO_2^- \longleftrightarrow R_1R_2NH^+ + R_1R_2NCO_2^- \tag{2.5}$$

$$R_1R_2R_3N + H_2O + CO_2\ (aq) \longleftrightarrow R_1R_2R_3NH^+ + HCO_3^- \tag{2.6}$$

The chemical structures of three common alkanolamine CO_2 sorbents, monoethanolamine (MEA), diethanolamine (DEA), and methyldiethanolamine (MDEA) are:

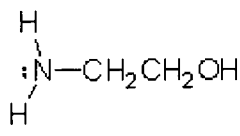

MEA

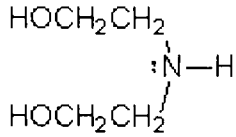

DEA

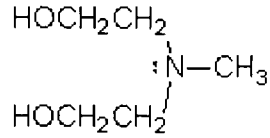

MDEA

The solid phase amine CO_2 sorbents work by analogous reactions between airborne CO_2, water vapor, and the amine bearing functional groups of the polymer. Early work in this area investigated the used of anion exchange resins bearing amine functional groups. Currently more specialized polymers are used. The thermally regenerable CO_2 removal system for the Shuttle Extended Duration Orbiter (EDO) uses Amberlite XAD-7 polystyrene-co-divinylbenzene beads coated with polyethyleneimine. Under heat and/or vacuum, the chemisorptions reactions are reversed and the polymeric sorbent is regenerated (Boehm et al., 1995).

2.5.3 Silver oxide.

Silver oxide reacts with carbon dioxide in the presence of water to yield silver carbonate.

$$Ag_2O + CO_2 \xrightarrow{H_2O} Ag_2CO_3 \qquad (2.7)$$

The chemisorption reaction can be reversed at elevated temperature,

$$Ag_2CO_3 \xrightarrow{\Delta,\,220^0C} Ag_2O + CO_2 \qquad (2.8)$$

those two reactions form the basis for the thermally regenerable CO_2 removal system which is currently in the final stages of development for use in the Portable Life Support Subsystem (PLSS).

Several metal oxides show potential for use as reversible CO_2 chemisorbents. Table 2.1 presents the densities, CO_2 capacities, and specific regeneration energies for various alkali metal, alkaline earth, and transition metal oxides.

Table 2.1 CO_2 capacities, densities and specific regeneration energies for various alkaline and transition metal oxides.

Metal Oxide	Density (g/cm^3)	CO_2 Capacity (g CO_2/g oxide)	Regeneration Energy(KJ/g CO_2)
Li_2O	2.01	1.471	5.146
Na_2O	2.27	0.709	7.309
K_2O	2.32	0.468	8.895
Rb_2O	3.72	0.235	9.172
Cs_2O	4.36	0.156	9.279
MgO	3.65	1.092	2.681
CaO	2.62	0.785	4.042
SrO	4.70	0.425	5.249
BaO	5.72	0.287	6.081
ZnO	5.47	0.540	1.616
Ag_2O	7.14	0.189	1.865

Inspection of Table 2.1 indicates that in addition to silver oxide, magnesium oxide and zinc oxide are also viable candidates for use as CO2 sorbents. However, neither of these oxides has been shown to load to theoretical capacity following thermal regeneration. A composite chemisorbent composed of a mixture of silver oxide and zinc oxide has shown promise

2.5.4 Molecular sieves.

The Molecular Sieves used for Carbon Dioxide Control are Zeolites, crystalline materials composed of silicon and aluminum. The crystal structure is based upon repeating units consisting of a silicon atom (+4 valence) surrounded by four oxygen

atoms (-2 valence) in a tetrahedral configuration. Each oxygen is shared by two Si atoms, giving the tetrahedra net valences of zero. When aluminum (with a valence of +3) is substituted in the tetrahedra a net charge defect of -1 occurs. Thus gives rise to the cation exchange properties of zeolites. Another interesting property of zeolites is their very uniform pore sizes which occur as a consequence of their unique crystal structures. Zeolites have both very high porosities and very well defined pore sizes, hence their use as Molecular Sieves. Both crystal and pore geometries are illustrated below for type A (Figures 2.4) and type X zeolites (Figures 2.5).

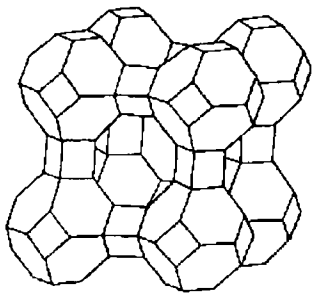

Figure 2.4 Type A zeolite

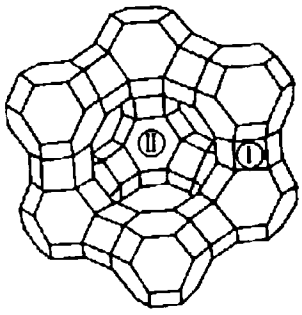

Figure 2.5 Type X zeolite

Chapter 3

Activated Carbon for Gas Separation and Storage

The objective of this chapter is to give a full understanding of the effect of carbon properties on its adsorption behavior which could help select the most suitable materials for adsorption. This knowledge can also be used to produce materials with optimum surface chemical and physical properties for selected application. Moreover, performance requirements are becoming increasingly more demanding, and there is a growing need for developing activated carbon with new and improved properties for CO_2 adsorption.

3.1 General.

Activated carbon is a commercial name define a group of materials with highly developed internal surface area and porosity and hence a large capacity for adsorbing chemicals from gases or liquid. Adsorption potential of active carbon is related to its surface area, pore size distribution and the chemical reactivity of the surface. Active carbons are widely used in waste water treatments, for chemical recovery and decolorizing. Active carbon is the material of choice in the air-pollution control operations, for use in gas storage, separation and clean-up applications. Activated carbons have been used for many years quite successfully for adsorptive removal of impurities from exhaust gas and waste water streams.

The strong market position held by the activated carbon due to its unique properties and low cost compared with that of possible competitive inorganic adsorbents like zeolites. Moreover, activated carbons characterize by a broad pore size distribution is usually obtained in sharp contrast to almost constant pore size in zeolites. This makes activated carbons more versatile adsorbing materials in different applications. More

than 30% of the carbon research is around activated carbons: newer precursors, methods of activation and applications. Theoretically, any carbonaceous material, natural or synthetic, can be converted into active carbon by an appropriate thermal treatment followed by a chemical or physical activation process. Cost is an important consideration when the active life of carbon is low and regeneration is not economical.

A number of technologies have been developed for active carbon production from new precursors. Different precursors, methods of carbonization and activation procedures have been used by many researchers to produce a large variety of activated carbons for gas separation applications. Activated carbons produced from coal, petroleum, vegetable and polymeric precursors have played a major role in the development of a major unit operation in the chemical and petrochemical industries for its role in separation and purification of gas mixtures by physical adsorption. However, for removal of certain impurities contained in gases (such as hydrogen sulfide, mercury and ammonia), the adsorption capacities and the removal rates must be improved by impregnation of the activated carbon by suitable chemicals. These chemicals are commonly deposited on the surface of the activated carbon. This leads to the change of the removal mechanism of that impurities. The impurities are no longer removed by adsorption but by chemisorptions (Raymundo-Pinero, 2000; Mangun et al., 2001).

3.2 Properties that affect activated carbon adsorption capacity and selectivity.

Activated carbon has unique properties. It has a porous structure which determines its adsorption capacity. It has a chemical structure which influences its interaction with the adsorbates. Activated carbon efficiency for removing a given pollutant depends on its physical characteristic (surface area, pore distribution) and its surface chemistry. Thus the adsorption behavior of an activated carbon cannot be interpreted on the basis of surface area and pore size distribution alone. Carbons having equal surface area but prepared by different methods or given different activation treatments show different adsorption characteristics. In general, activated carbon containing numerous pores in the size range of the pollutant is expected to be efficient due to the enhancement of the adsorption potential for such condition (Derbyshire et al., 1995). At the same time, significant progress has also been achieved on the understanding of the effect of carbon surface chemistry on adsorption.

3.2.1 Activated carbon pore structure.

The most important physical characteristics of activated carbon are surface area and pore size distribution. The adsorption capacity of activated carbon is also been proposed to be proportional to the amount of surface area within pores that is accessible to the adsorbate (Snoeyink and Summers, 1999). Subsequent research has shown more correlation to pore volume for many species (Nowack et al., 2004). Both surface area and porosity are usually characterized from information contained within the adsorption isotherm. The adsorption of nitrogen at 77K and its interpretation by the Brunauer, Emmett and Teller (BET) equation to give monolayer

coverage is often used as the preferred method to determine surface area of activated carbon.

The pores that give rise to this large surface area can be defined as spaces between irregularly arranged graphite-like platelets (Bansal et al., 1988). To classify pores according to size, the International Union of Pure and Applied Chemistry (IUPAC) differentiates between (1) micropores (<2 nm width), (2) mesopores (2 - 50 nm width), and (3) macropores (> 50 nm width) (Sing et al., 1990) as shown in Figure 3.1.

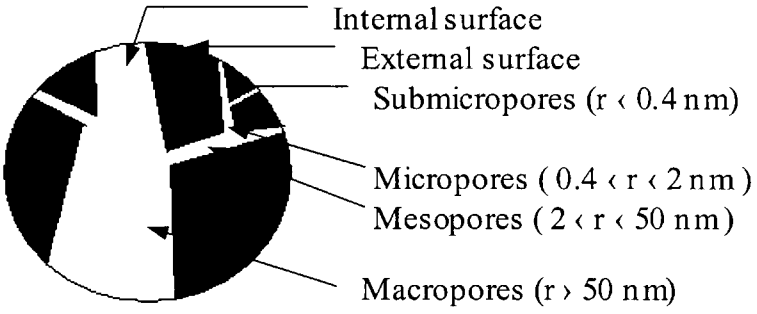

Figure 3.1 Porous structures of activated carbon schematically

The size of adsorbent pores affects the adsorption properties of activated carbon. This is due to the adsorption strength increases with decreasing pore size because the contact points between the adsorbate and the adsorbent surface increase (Newcombe et al., 1997). In addition, the adsorption potentials between opposing pore walls begin to overlap once the micropore width is less than twice the adsorbate diameter (Matsumoto et al., 1997). Different techniques have been used to determine pore size distribution in porous carbons. These are mercury porosimetry and gas adsorption isotherms and recently, the scanning tunneling microscopy (Bansal et al., 1988). Pore

size distribution is important because it determines the fraction of the total pore volume that can be accessed by an adsorbate of a given size.

3.2.2 Activated carbon surface chemistry.

The chemical nature of active carbons significantly influences their adsorptive, electrochemical, catalytic, acid-base, redox, hydrophilic-hydrophobic, and other properties. The precursor of activated carbon and its production procedure played an important role in surface chemistry. The great significance of this characteristic has mad it the subject of much research. However, many problems associated with the chemical nature of the surface are still not entirely explained. Both the growing variety of uses of active carbons and the development of new testing techniques provide the driving force for the continuous increase of research in testing the effect of activated carbon surface chemistry on its adsorption properties. Most of these researches focuses on illustrate comprehensively the chemical nature of the carbon surface. Detailed consideration of the state of the art in this field can be found in many papers (Barton et al. and Biniak et al., 1997).

Heteroatoms, which are the atoms other than carbon, are responsible for the chemical characteristics of activated carbon surfaces. Activated carbons generally contain appreciable amounts of various heteroatoms such as oxygen, hydrogen, nitrogen, phosphorous and sulfur, exist on the carbon surface. These heteroatoms are either derived from the starting material or from additional treatments. They can also be chemically bonded to the carbon surface during the treatment process. X-ray examination has shown that those heteroatoms are bonded to the carbon atoms at the

edges of the aromatic sheet of carbon structure (Pradhan and Sandle, 1999). These edges constitute the main adsorbing surface. The bonded oxygen and hydrogen have a great influence on the surface characteristics of carbons, such as surface acidity or basicity, ion exchange capacity and adsorption of polar and non-polar gases and vapor. The direct effect of these surface groups is that they give the carbon surface an acid-base character. In general, carbon surface can display both acidic and basic characters according to the functional groups presence on the surface. Acidic reactions have been associated with oxygenated surface functional groups. These oxygenated groups can arise from chemisorbed oxygen that can be found on all surfaces, which have been exposed to air or other oxidizing media. The existence of surface functional groups such as carboxyl, phenols, lactones, and acid anhydrides has been assumed as constituting the sources of surface acidity. The presence of basic oxygen-containing functionalities such as chromene- and pyrone type structures has also been assumed as constituting the sources of surface basicity.

Oxygen is an important heteroatom that commonly occurs in the form of carboxylic acid groups, phenolic or enolic hydroxyl groups, and quinone carbonyl groups Activated carbons assume an acidic character when exposed to oxygen between 200 and 700°C or to oxidants such as hydrogen peroxide, nitric acid, or nitric and sulfuric acid mixtures in aqueous solution . Oxygen surface compounds are usually divided into main types: functional groups of acidic nature (undergoing neutralization by bases) and basic groups which may be neutralized by acids. The increased activated carbon acidity is primarily explained by the formation of carboxylic acid and phenolic hydroxyl groups. X-ray photoelectron spectroscopy (XPS) data showed that

the above oxidation techniques increased the surface concentrations of acidic groups (carboxylic acid and phenolic hydroxyl groups)(Polovina et al. 1997, Mangun et al. 1999).

Increase in alkalinity can be achieved through various techniques. One of the most frequently used way to realize this is impregnation with proper chemicals (Lude and Miroslav, 2001). However, it should be noted that the introduction of these impregnant might result in some other negative effects. As reported elsewhere (Molina et al., 1994), dipping of activated carbon with a solution of chromium and copper salts caused blocking of pores in the structure of activated carbon. This lowers the adsorption capacity of activated carbon. Besides this disadvantage, the technique does not stabilize basic additives on the surface. Other techniques employed for modification of activated carbon could be found else where (Ahmadpour et al., 1996 Cheol and Katsumi 2001; Sarmeo et al., 2001; Lozano et al., 2001).

One of the popular ways used for preparation of activated carbon with increased basicity is introducing nitrogen to the carbon structure. This can be performed by preparing activated carbon from N-containing polymers (Stoeckli et al., 1996; Carrott et al., 2001) or treating activated carbon with ammonia. As was described by Mangun and co-workers (2001), modification of activated carbon fiber (ACF) with dry ammonia at several temperatures from 500 to 800°C for different periods of time results in the formation of new nitrogen-containing groups in the structure of the fiber. Modification of activated carbon with aqueous ammonia (33 wt.%) either at

130°C for less than 9 h or at room temperature for less than 100 h did not result in noticeable changes in the chemistry of activated carbon (Severini et al., 2002). However, as confirmed by XPS analyses, extension of the modification time caused the introduction of $-NH_2$ groups on the surface.

Attempts have been made to identify and estimate the surface functional groups using several physical, chemical and physicochemical techniques which include neutralization of bases, desorption of the oxide layer, potentiometric, thermometric, and radiometric titration, direct analysis by specific chemical reaction, polarography, infrared (IR) spectroscopy and X-ray photoelectron spectroscopy.

3.3 Activated carbon tailoring.

In general, the ability of activated carbon to adsorb pollutants is often estimated experimentally without anticipating a relationship between the chemical structure and adsorption capacity. Adsorption tests are commonly used to characterize a given activated carbon. However, knowledge of the activated carbon structure is necessary if we wish to adapt the product for adsorption of a specific pollutant. The nature of the surface functional groups can be modified through physical, chemical and electrochemical treatment. For example, carbon modification can be achieved by means of liquid phase treatments, using oxidizing agents such as HNO_3 or H_2O_2 at different temperatures, concentrations and/or contact. Modification can be also achieved by gas phase oxidation with O_2 or N_2O at different temperatures, pressures, concentrations and/or contact times. These procedures change the physicochemical structure of activated carbon, i.e. the specific surface area, porosity and surface

functional groups. With recent advances in surface chemistry and physics, many techniques are now available to identify the carbon properties that most strongly influence adsorbate-adsorbent interactions and to modify these properties. This is to maximize activated carbon performance (Radovic, 1999).

Ammonia tailored carbons have been studied on their adsorption for acidic gas (HCl), H_2S or SO_2 from flue gas, or their catalytic activities. Mangun et al. (2001) treated a series of activated carbons fibers (ACFs) with ammonia to yield basic surface. The adsorption of HCl gas was greatly enhanced by treating the fibers with ammonia to create a basic surface. Since HCL gas has a very low boiling point and not adsorbed well by untreated carbons, the adsorption of HCl was dominated by the amount of nitrogen present. In their efforts to elucidate the role of pore size, pore volume and surface chemistry on adsorption of SO_2, Mangun et al. (2001) also compared several ACFs and their ammonia-treated counterparts on their abilities to remove SO_2 from flue gas. ACFs were treated in ammonia for 10-60 min at 500 to 800°C. It was found that the SO_2 adsorption energy increased with the increase of nitrogen content. Before ammonia treatment, ACF with the highest microporosity shows the highest SO_2 adsorption due to its higher adsorption energy. Ammonia treatment results in a competition between increasing the chemical interaction (chemisorptions) from increased nitrogen versus decreasing the physical interaction (physical adsorption) because of the micropore blocking. The ACF with the right combination of nitrogen content and pore volume shows the best result.

Boudou et al. (2003) investigated how ammonia treatment of the surface can influence the activity of viscose-based activated carbon cloth (ACC) for the oxidative retention of H_2S and SO_2. The ACC was subjected to an ammonia/steam (28% NH_3 solution, carrying gas 100mL/min) treatment at 800°C or to two types of ammoxidation treatment with ammonia/air (NH_3, air 3.0l/h each) at 300°C. X-ray photoelectron spectroscopy showed nitrogen groups such as pyridine, pyrrole, quaternary nitrogen and nitrogen-oxide being introduced to carbon surface by ammonia treatment.

Bagreev et al. (2004) have introduced nitrogen to bituminous coal-based activated carbon by impregnation with melamine and heat treatment at 850°C. Carbons prepared in such a way contained considerable percent of nitrogen; however, the pore volume deteriorated by 25%, compared to unmodified carbon

3.4 Activated carbon processing and preparation.

To apply activated carbon more efficiently, many novel ways were proposed for obtaining different adsorption properties. Theoretically, almost any kind of carbonaceous material may be used as precursor for activated carbon; wood, nutshells, peat, coal (hard coal, soft coal, and bituminous coal), lignite, petroleum coke, etc. are usually used as raw material for activated carbon due to their high carbon content. Among these, bituminous coals have been one of the most extensive used raw materials because their hardness, abrasion resistance, relatively high density, and pore size distribution make them suitable to withstand operating conditions and to adsorb the small organic molecules often present in drinking water.

Amongst woods, pine is by far the precursor for the largest production of activated carbon and forms about 50% of precursor, while all other woods contribute about 40%. Regional bio wastes and woods have also been investigated and have been found to be promising precursors for porous carbons.

For the selection of an appropriate raw material for preparation of porous carbon, several factors are taken into consideration. Industrially, inexpensive material with high carbon and low inorganic (i.e. low ash) content is preferred as raw material for the production of activated carbon. High density of the precursor and sufficient volatile content are of considerable importance. Evolution of volatiles during pyrolysis results in porous char essential for making activated carbons, while high density contributes to enhanced structural strength of the carbon, essential to withstand excessive particle abrasion interaction during use.

The distribution of pores in activated carbons can vary significantly depending upon the precursor material. For example, anthracite and some bituminous coals yield carbons with a high proportion of micropores, lower rank bituminous coals give a broad PSD, while lignite and wood precursors produce mesoporous carbons (Blanco Lopez et al.,2000; Hu et al., 2001; Streat et al., 1995).

In the last two decades, extensive studies have been made on the selection and pyrolysis behavior of new synthetic precursors to develop active carbons with very high adsorption capacities and controlled pore size distributions for specific energy applications. These precursors are polymer-based fibrous materials. The examples

are viscose rayon, polyacrylonitrile, saran, phenolics polymer, PFA etc. (Jankowska ,1991).

Manufacturing activated carbons involves two steps: the carbonization (pyrolysis) of raw carbonaceous materials in an inert atmosphere and the activation of carbonized product. The pyrolysis of any carbonaceous material in absence of air involves decomposition of organic molecules, evolution of tarry and gaseous products, and finally a solid porous carbon mass. The porous carbons obtained after carbonization contain predominantly macropores and practically inactive materials with specific surface area of order of several square meters per gram (Bansal 1988). An adsorbent with a highly developed porosity and a correspondingly large surface area is obtained only by activating the carbonized material either by physical or chemical activation.

During carbonization, most of the non-carbon elements, hydrogen and oxygen are first removed in gaseous form by pyrolytic decomposition of the starting materials, and the free atoms of elementary carbon are grouped into organized crystallographic formations known as elementary graphite crystallites. The arrangement of the crystallite is irregular, so that free gap exists between them (called pores). Basically, carbons are described as graphitic or non-graphitic depending upon degree of crystallographic ordering. Graphitic carbons possess three-dimensional symmetry while non-graphitic carbons do not (Bansal, 1988). Carbonization involves thermal decomposition of carbonaceous material, eliminating non-carbon species producing a fixed carbon mass and rudimentary pore structure (Derbyshier et al 1995). The process is usually carried out at temperature below 800°C in a continuous stream of

an inert atmosphere. The important parameters that determine the quality and the yield of the carbonized product are: rate of heating, final temperature and soaking time. The carbonization process involves various important stages that markedly determine the properties of the final product to be obtained. The basic microstructure of the char with microporosity is formed around 500°C. Some of these pores are blocked by the tarry products evolved during pyrolysis and could be available only when further heat treatment to about 800°C is given. Further heat treatment to temperature of 1000°C and above normally lead to hardening of the carbon structure due to partial alignment of graphitic planes and decrease in porosity. As discussed above, during carbonization the free gap present in the carbon become filled or at least partially blocked by tarry substances. The resulting carbonized product has only a very small adsorption capacity. Such carbonized materials can be then activated by removing tarry products by heating in steam or under inert gas or by extraction with a suitable solvent or by chemical reaction.

Activation is carried out to enlarge the diameters of the pores which are created during the carbonization process and to create some new porosity. This results in the formation of a well-developed and readily accessible pore structure with very large internal surface area. Activation is carried out by two ways as in the following sections.

Physical activation; It is a process by which the carbonized product develops porous structure of molecular dimensions and extended surface area on heat treatment in the temperature range of 800–1000°C in presence of suitable oxidizing gases such as

steam, CO_2 and air. Gasification of the carbonized material with steam and carbon dioxide occurs by the following endothermic reactions:

$$C + H_2O \rightarrow CO + H_2 \text{ (29 kcal)}, \quad (3.1)$$

$$C + CO_2 \rightarrow 2CO \text{ (39 kcal)}, \quad (3.2)$$

$$CO + H_2O \rightarrow CO_2 + H_2 \text{ (10 kcal)}. \quad (3.3)$$

In case of activation with oxygen, both the following reactions take place

$$C + O_2 \rightarrow CO_2 + \text{(92.4 kcal), and} \quad (3.4)$$

$$2C + O_2 \rightarrow 2\,CO + \text{(53.96 kcal)}, \quad (3.5)$$

Since both reactions are exothermic, there is excessive burning and the reaction is difficult to control. Moreover, since there is always some local overheating, the product obtained is not uniform. As the reaction is very aggressive, burning is not restricted and also occurs on the surface of the grains, causing excessive weight loss.

The relative amounts of external and internal oxidation depends on how well-developed the pores are in the carbonized material. Activation of chars without development of significant pore structure only results in decrease in carbon granule size and mass reduction. Activation is associated with carbon loss and hence with decrease in weight of carbon mass. Weight loss increases linearly with activation temperature and time. Activation at lower temperature results in the development of mesopores. At higher activation temperature, the formation of pores which have no adsorption ability, i.e. macropores, increase

In the study by Ryu et al., (2002) steam, air, and KOH were used as activation agents to prepare PAN-based ACFs. For the steam activation series, with increasing degree of activation the BET surface area increase and the pores are gradually widened. The dominant pores change from micropore (activation at 750°C) to mesopore (860°C) and some macropore (1240°C) as the degree of activation goes up. For the air activation series, ultramicropores are the dominant pores. For the KOH activation series, a large fraction of mesopores is developed and the dominant pores can be though of as supermicropores. Similar results have been reported by other researchers (Martin-Gullon et al., 2001; Ryu et al., 2000). Micropores can be divided into ultramicropores (width less than 0.7 nm) and supermicropores (width from 0.7 nm to 2 nm) (Ryu et al., 2000; Sing et al., 1985). Activated carbons prepared from CO_2 activation exhibit a larger micropore volume and a narrower micropore size distribution than those prepared from steam activation (Huang et al., 2003; Molina-Sabio et al., 1996).

Park and Kim (2001) studied the influence of CO_2 activation temperature on adsorption characteristics of ACFs from carbon fabrics and phenolic resin. They found the evolution of pore size, pore volume, and specific surface area are with increase of activation temperature from 700-900°C. Daud et al. (2002) also reported that within the range of activation temperature 800-950°C, high burn-off products derived from high activation temperatures tend to have larger micropore development. However, the increase in the activation temperature has no remarkable effect on mesopore and macropore development. Higher activation temperature led to the decrease in the mechanical strength, in increase in the burn-off degree of the

surface, the reduction of micropores, and greatly broadening the PSD (Canizares et al., 2006; Yang & Yu, 1998). Moreover, when the temperature was less than 800°C, the surface developed acidic properties, but was basic when the temperature was greater than 900°C (Park & Kim, 2001).

Chemical activation is also a common method for active carbon production. In chemical activation, the raw material is impregnated with a concentrated solution of activating agents. It results in degradation of cellulosic material. Chemical-impregnated raw material is then pyrolyzed between 400 and 600°C in the absence of air. Pyrolyzed product is cooled and washed to remove activating agent, which is recycled. On calcinations, impregnated and chemically dehydrated raw material results in charring and aromatization, and creation of porous structure. Various types of activating agents are used. Some of them are: phosphoric acid, zinc chloride, H_2SO_4 ,K_2S, alkali metal hydroxide, and carbonate and chlorides of Ca^{+2} ,Mg^{+2} and Fe^{+3} (Bansal 1988; Derbyshier 1995). All activating agents are dehydrating agents which influence the pyrolytic decomposition and inhibit the formation of tar. They also decrease the formation of acetic acid, methanol etc. and enhance the yield of carbon. There are however, environmental concerns with the use of the activation agents, because they are considered hazardous chemicals in the pollution regulations. In addition, chemical activation poses problems such as lack of adequate control over porosity development.

3.5 Regeneration of the activated carbon.

Regeneration is the process used to recover the adsorptive capacity of the spent carbon. Among all the regeneration methods, the most common ways are: chemical to oxidize the adsorbed material, steam to drive off the adsorbed material, solvent extraction, and biological conversion process (Tchobanoglous et al., 2003). Typically, the adsorptive capacity of the activated carbon will lose about 4 – 10% in the regeneration process. The adsorbate properties and regeneration methods determine the percentage lose in adsorptive capacity.

Reactivation of spent activated carbon thermally involves essentially the same process used to create the activated carbon from the virgin material. Reactivation usually takes place in a furnace. Within the furnace, carbon is first heated to drive off the adsorbed adsorbate, followed by burning off the new compounds that were formed when the adsorbed material was burnt off. The conditions of regeneration and reactivation depend on the kind of active carbon involved and on the kind of substance to be removed. The optimal conditions of the regeneration or reactivation process should ensure minimal losses of the carbon. In general, there are three important factors playing a major role in regeneration process. These factors are: the temperature of the regeneration; the time of regeneration or reactivation and the degree of saturation of the carbon with the adsorbed substance.

3.6 Activated carbons from synthetic precursors.

The production of carbons based on polymeric precursors has been widely investigated over many years. The largest use of carbon derived from polymer is in the advanced composites fields, where carbon fiber is now extensively used for high-strength materials. Carbon/carbon composites are becoming more widely used for applications, such as aircraft brakes and rocket components where very severe operating temperatures and thermal shocks. The carbon fiber matrix is most commonly densified using carbon derived from the pyrolysis of polymers, such as phenolic resins combined with carbon deposited from the high-temperature cracking of gases such as methane. There has also been a wide interest over the years in the production of glassy carbons, by the carbonization of thermoset resins such as phenolic resins.

In general, numerous polymer systems have been investigated as the precursors to active carbons. The cost of such materials is related to the cost of the polymer precursor and the carbon yield during the carbonization and activation stages:

$$\text{Carbon cost} = \text{polymer cost} / (\text{carbon yield} \times \text{oxidation yield}). \qquad (3.6)$$

An acceptable cost for the carbon product will only be achieved if the yield on carbonization is high and the cost of the precursor polymer reasonable. It is also necessary that good surface areas and pore volumes are achieved at a minimum level of activation. It is worth stating that, the actual yield of activated carbon from conventional processes using naturally occurring precursors is only of the order of

approximately 10%, which is acceptable because of the low cost of the precursor's waste materials. Granular carbon material produced by the carbonization and activation of styrene divinyl benzene consider the currently commercially available polymer derived carbons . This material is only available as spherical particles with a maximum size of around 1 mm and a microstructure. The second to be available was an activated carbon cloth produced by the carbonization and activation of rayon fiber. These materials offer unique properties in terms of their physical form and the enhanced adsorption kinetics due to the fibrous structure.

Many other polymers have been investigated as active carbon precursors: including resins, such as phenolic and furfuryl resins and co-polymers of these systems; polvinylidene chloride (Tennison, 1998); polyamides and their derivatives (e.g. poly-p-phenylene terephthalamide, Nomex - poly m-phenylene isophthalamide, Novax) and cellulose based materials, etc. (Jankowska, 1991).

Performance requirements of the material to be used as an adsorbent are becoming increasingly more demanding, and there is a growing need for activated carbon with new and improved properties. So, in this thesis we tried to investigate a new rout to produce activated carbon from phenolic resins precursors with increasing basicity and control pore structure.

3.7 Activated carbons from phenolic resins.

Phenol-Formaldehyde resins (PF) were first discovered in 1872, it results from the polycondensation of phenols (e.g. phenol, cresol, xylenols, resorcinol, etc.) and aldehydes (e.g. formaldehyde, acetaldehyde, glyoxal, furfural, etc.). The most common is the simple resin produced from resorcinol and formaldehyde. PF resins have been of prime importance since the early 1900's, when they appeared as the first synthetically produced polymer. PF properties can be tailored for a Varity of applications, including foundry resins, adhesives, coating, molding compounds and wood-based composite binders (Megson, 1958).

Depending upon reagent ratios and catalyst type, two classes of resins have been developed. Resoles are produced from base catalyzed polymerization using excess formaldehyde. On the other hand, novolaks are obtained from acid catalyzed polymerization using excess phenol. Resoles and novolaks are inherently different: resoles heat curable while novolaks require addition of a crosslinking agent or hardener such as hexamethylenetetramine (HMTA) to cure. For most novolaks, this additional step results in slower cure rates and lower crosslinking than resoles. When novolaks heated to above melting point, the hexamine dissolves and decomposes by hydrolysis in the molten resin, evolving ammonia and forming α-ammino-alcohols and formaldehyde. Figure 3.2 shows the structure of the novolaks types. These are linear or slightly branched polymer with methylene bridges and molecular weights up to about 2000. They are generally solids with melting points up to about 120°C.

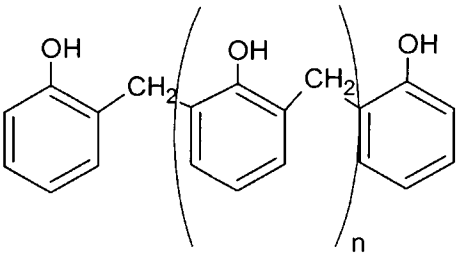

Figure 3.2 Structure of novolak type resin (Tennison, 1998).

Resoles are formed at molar excess of P: F ratios (1: 1-to-1: 3 are common) in alkaline medium. The resin precursors are mainly mono- or polymolecular hydroxymethyl phenols (HMP). Figure 3.3 shows the monomer structures in resole. These monomers are then transformed into three-dimensional, cross-linked polymers simply by heating or in few cases by the addition of acids. The resoles are typically formed in either aqueous or alcoholic solution. The chemistry of PF polymerization is very complex and thorough characterization of resole molecular structures is still under exploit. The process of curing of both the resoles and novolaks involve the cross-linking of mainly linear chains with the occurrence of gelation at some intermediate stage in the process.

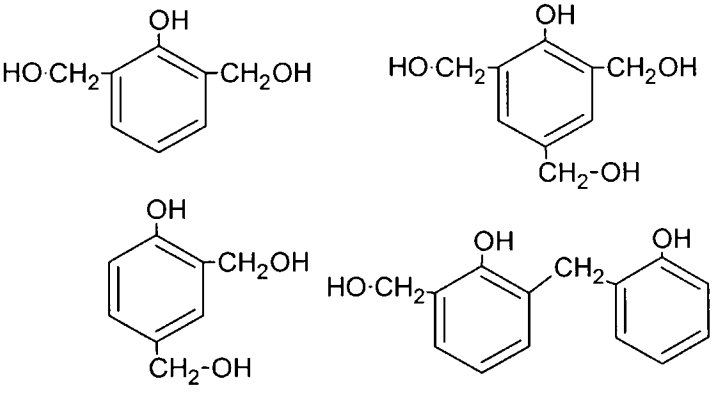

Figure 3.3 Monomer structures in resoles type resin

The resoles and novolaks structure described can be modified by usage a large variety of additives. Alkyl phenols could be successively used to introduce hydrocarbon chains into the structure. For example, the flexibility of the cured resin, which is generally very brittle, are frequently modified by adding naturally occurring alkyl phenols such as cashew-nut-shell liquid. Other modifications can include the production of mixed polymer systems, such as combinations of phenolic resins with polyamides,...etc.

Many routes have been investigated for the production of porous carbons from phenolic resins precursors. Carbon aerogels (Schaefer et al., 1995; Horikawa et al., 2004) and xerogels (Lin and Ritter, 2000) are produced by polymerization of resorcinol-formaldehyde rather than phenol-formaldehyde. These unusual materials are produced by a route that is analogy with the production of inorganic materials via sol-gel techniques. Linear polymer formation and cross-linking take place simultaneously to give the gel, in contrast to the two stage process for conventional phenolic resins. Aerogel are foam like materials with low densities due to the supercritical drying processes. By contrast, the xerogels are denser, where the contained water was removed by solvent extraction and conventional drying.

Rojas et al., (2004), prepared metal-carbons materials by polymerization of resorcinol with formaldehyde in the presence of metallic precursors for the aim of preparing catalysts. By this way, it is possible to combine the porous texture of the carbon with the basic properties of the oxides. The metallic precursors used were the

carbonate for Na and K and the nitrate for Mg. However, this results in carbon with low surface area.

3.7.1 RF carbon and activated carbon gels synthesis, processing, and properties.

Resorcinol-formaldehyde RF carbon and activated carbon gels could be produced with different variations of essentially the same recipe. The processing and synthesis procedures can be summarized as in Figure 3.4. The process starts with the organic gels preparation followed by drying, pyrolysis and activation. Each step has a significant effect on the final properties of the produced carbon material. Firstly, resorcinol (R) is added to formaldehyde (F) with appropriate molar ratio in the presence of a basic or acidic catalyst (Berthon et al., 2001). Then the solution is stirred to ensure the mixture homogeneity. Gelation and curing are carried out by heating the gel in a closed container to a predetermined temperature for a sufficient period of time to form a stable crosslinked structure. In a very few cases the mixing and curing steps have been carried out under inert atmosphere (e.g., in a glove box with a N_2 atmosphere). This is to avoid the possibility of change the pH of the solution due to the contamination with components in air such as CO_2 (Teng and Wang, 2000; Huang and Teng, 2003). The initial solution pH is most commonly adjusted by dilute acids (e.g., HNO_3 or HCL) or dilute bases (e.g. NH_4OH). The wet gel may then be subjected to a solvent exchange (or not) with a suitable organic solvent (acetone, cyclohexane, ..,etc) to exchange the aqueous solvent. Organic (phenolic resins structure) aerogels, xerogels or cryogels are then produced by drying the wet gel either supercritically with carbon dioxide, subcritically in air or nitrogen or freeze drying, respectively. Carbon aerogel, xerogel and cryogels are produced by

pyrolyzed the dried gel in inert atmosphere to form the highly porous carbons. The dried gel may also be activated, e.g., with CO_2 or steam either during or following carbonization. Other activation methods, e.g., chemical activation with KOH or K_2CO_3 may also be used however few have been tried with RF carbon aerogels and xerogels (Teng and Wang, 2000).

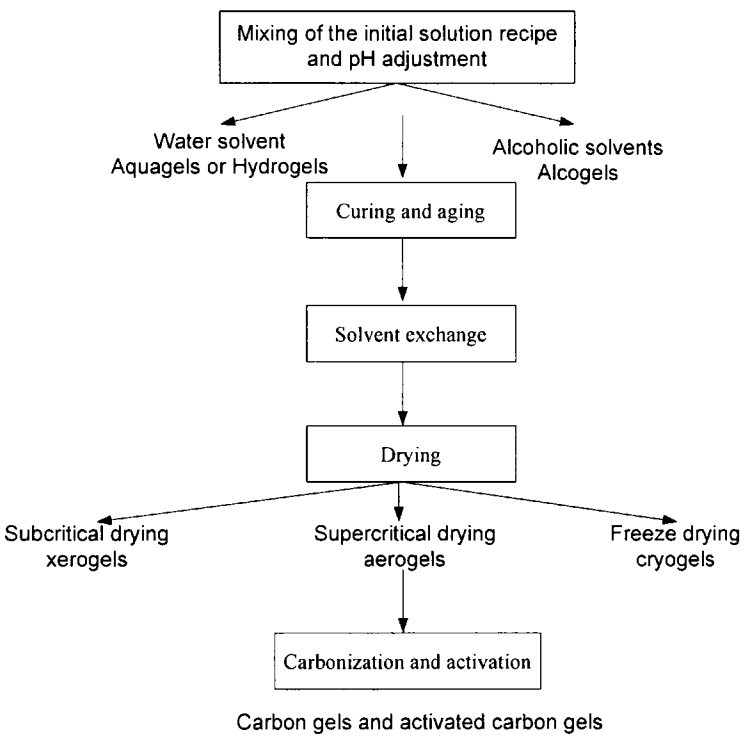

Figure 3.4 Carbon and activated carbon gels processing block diagram

3.7.1.1 The effect of starting reagents formulation on the final properties and pore structure of RF gel.

The resulting properties of the gels are depending on many factors. Varying the main reactants (resorcinol/formaldehyde) molar ratios has a significant effect on the resulting properties. The most commonly used R/F molar ratio in the literature is 1:2 (Yamamoto et al., 2001; Job et al., 2004). Using excess formaldehyde leads to a dilution of the reaction mixture. This increases the particle size near the gelation and consequently results in formation of crosslinked gels with large pore structure (Petricevic et al., 2001). Increasing the amount of solvent is another major factor that can result in this dilution effect. Distilled, deionised water (W) or organic solvents (e.g., acetone, methanol, ethanol, n-propanol, or isopropanol) have been used successively to dissolve resorcinol (Berthon et al., 2001). The final gels produced with water as the solvent are named hydrogels or aquagels. Whilst those produced with alcoholic solvents are called alcogels. The dilution of the reaction mixture could be either expressed by resorcinol to water R/W ratio or the dilution factor (D = water/(resorcinol + formaldehyde + catalyst) molar ratio) (Job et al., 2004).

The concentration of the reactants in the initial solution has also a considerable effect on the final density of the RF gel (Petricevic et al., 2001). Higher reactant concentrations result in a denser formation of the RF crosslinked clusters, while high dilution results in the formation of polymer suspension in the aqueous solvent. When the dilution ratio is high (D = 20), the mechanical resistance of the gel is low, and the sample break easily when manipulated (Job et al., 2005). The RF solution concentration has a more considerable effect on the properties of RF organic

(consequently carbon) xerogels than aerogels. Increasing the concentration of the reactants in the initial solution causes a decrease in the surface area of RF carbon xerogels, and either a decrease in their total pore volume at low pH. It also decreases the electrochemical double layer capacitance of RF carbon xerogels and aerogels (Saliger et al., 1998).

The level and nature of the catalyst influences the structure and particle morphology of the gel. Sodium carbonate (Na_2CO_3) and sodium hydroxide (NaOH) are the most commonly used alkaline catalyst, for the polymerization reaction of resorcinol with formaldehyde, in the literature. A resorcinol to catalyst (R/C) molar ratio ranging between 50 and 300 is the most common in the case of Na_2CO_3, however in some cases ratios as high as 1500 are used (Saliger et al., 1997). The primary role of this catalyst is the creation of ionized resorcinol by hydrogen abstraction from one of the OH group. This anion acts as sites for the growth of the monomer particles.

Loustalot et al., (1995) investigated the influence of the type of basic catalyst on the mechanisms and kinetics of phenol-formaldehyde reactions, in their research NaOH, KOH, LiOH, $Ba(OH)_2$ and $Mg(OH)_2$ have been used as a catalyst. The catalyst were classified into two families as a function of their behaviour: KOH, NaOH and LiOH, and $Ba(OH)_2$ and $Mg(OH)_2$. They found that the formation of methylene bridge (cross-liking) was slow in presence of KOH and NaOH, while the results obtained with $Ba(OH)_2$ and $Mg(OH)_2$ are very different, the methylene bridges formed much more rapidly. Maldonado et al.,(1999) used various metal salts (e.g., $[Pt(NH_3)_4]Cl_2$, $PdCl_2$, or $AgOOC\text{-}CH_3$) as a catalyst to incorporate certain transition metals (e.g., Pt,

Pd, or Ag) in the final RF carbon gels structure. The addition of these metals increases the meso- and macropore volumes.

Overall, the final structure and properties of the gels are mostly affected by the level of catalyst in the solution (Lu et al., 1995; Tamon et al., 1997; Merzbacher et al., 2001). Figure 3.5 shows that, using high R/C or low C/W ratio results in large polymer particles (16to 200 nm in diameter), produces lower density gels with large pore size. In contrast when low R/C or high C/W ratio has been used this results in small polymer particles (3-5 nm), produces higher density gels with small pore size.

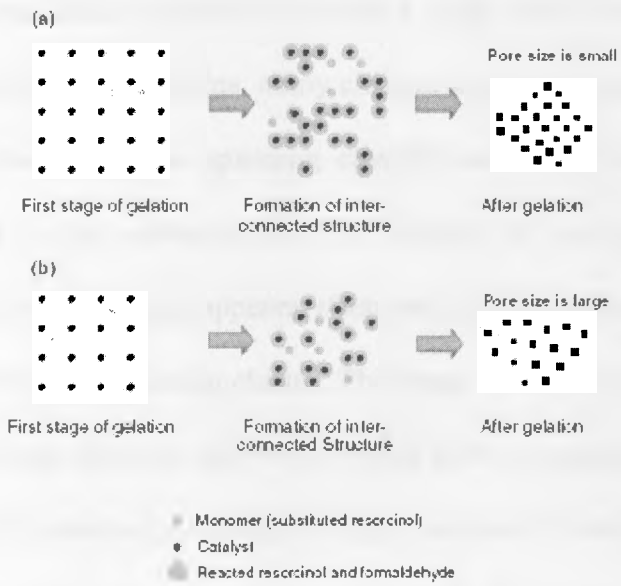

Figure 3.5 Mechanism of gelation progress with a) High and b) low C/W ratios (Yamatoto et al., 2001).

In addition to the basic catalysts, dilute acidic catalyst solutions (e.g., HNO_3) can be used. In few cases, the use of an acidic catalyst resulted in a reduction in the gelation time, which may indicate a change in the polymerization mechanism. When using an acidic catalyst solution with high RF concentrations, the fractal aggregates of gel

particles are not observed. This produces gels with very narrow pore size distributions. In contrast, when using low RF concentrations with an acidic catalyst, this produces small, smooth, fractal aggregates of gel particles with wide pore size distributions (PSDs) (Berthon et al., Merzbacher et al., 2001).

3.7.1.2 Gelation, curing and aging steps and their influence on the final properties of RF gels.

In general, gelation mechanism could be described as follows; the clusters grow by condensation of polymers or aggregations of particles until the clusters collide; then these clusters are crosslinked together to produce a single giant cluster that is called a gel. At the moment that the gel forms, many clusters will be present in the sol phase, adjacent but not attached to the spanning clusters; with time, they progressively become connected to the network and the stiffness of the gel will increase. According to this picture, the gel appears when the last link is formed between two large clusters to create the spanning cluster. This bond is similar to the others bonds that formed before and after the gel point, except that it is responsible for lose of elasticity of the gel by creating a continuous solid network. No latent heat is evolved at the gel point, but the viscosity rises significantly. The chemical reactions that cause gelation continue long after the gel point, producing strengthening, stiffening, and shrinking of the network. Figure 3.6 describes the previous mechanism, where the colloidal particles begin to aggregate and assemble into a stiff, interconnected structure locally resembling a string of pearls that fills the original volume of the aqueous solution.

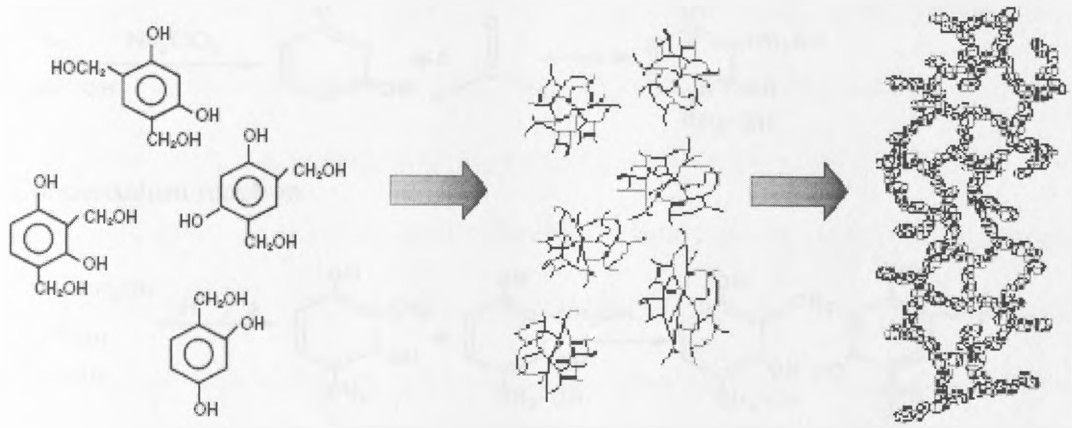

Figure 3.6 Cluster growths of resorcinol-formaldehyde monomers (Cook et al., 1997)

According to preceding scope, the structure and properties of the RF organic and carbon gels depend strongly on the gelation step and the conditions at which it proceeds. The gelation (the reaction between resorcinol and formaldehyde) process involves three reaction sequences as shown in Figure 3.7: (1) formaldehyde addition to phenol, (2) chain growth or prepolymer formation and, finally, (3) the cross-linking or curing reaction. The first step involves an addition reaction to form hydroxymethyl derivatives ($-CH_2OH$), and then a condensation reaction of the hydroxymethyl derivatives to form methylene ($-CH_2-$) and methylene ether ($-CH_2OCH_2-$) bridged compounds (Lin et al., 1997). This reaction could not be initialized (or proceed very slowly) without a catalyst. The presence of the catalyst results in the creation of ionized resorcinol (anions) by hydrogen abstraction from one of the OH group to form an O^-. These anions are much more active than the uncharged resorcinol towards the addition of formaldehyde to form the hydroxymethyl derivatives, which are essential for the proceeding of subsequent condensation reactions.

1- Addition reaction

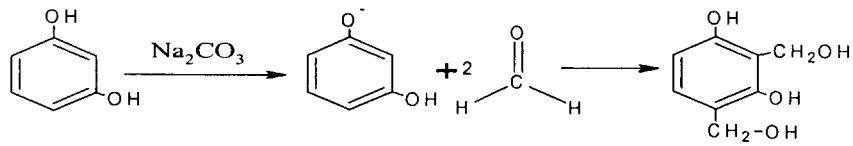

2- Condensation reaction

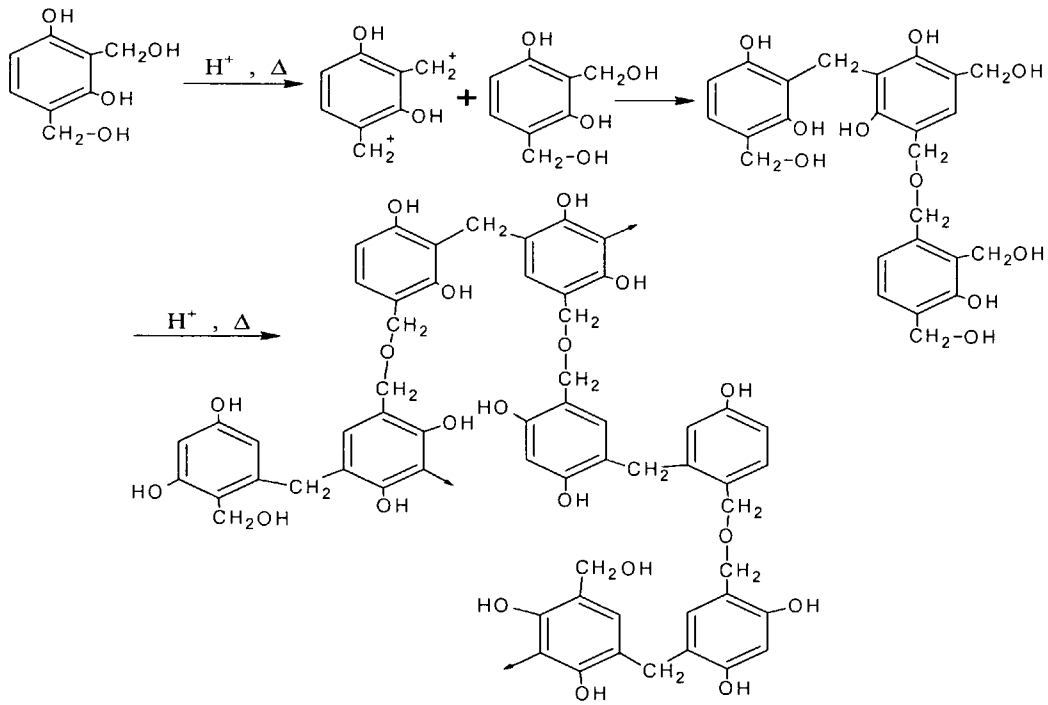

Figure 3.7 Gelation reaction mechanism of resorcinol with formaldehyde (Lin et al., 1997).

Depending on several factors, the curing time can vary from hours to days. During this time, monomers undergo further cross-linking to form nanometer-size clusters. Once a cluster is created, additional monomer groups attach themselves to the cluster. The result is that the cluster increases in size. The clusters continue to grow until all resorcinol is consumed. Highly crosslinked clusters (7 to 10 nm in diameter) are obtained as a result of this multi-step mechanism.

The gelation process depends mainly on many factors such as pH, reactant concentration, gelation temperature,...., etc. It can occur more rapidly with low R/C ratios, high reactants densities or high temperatures. The gelation time varies from several hours with low initial solution pH, to 24 hours for high initial solution pH (Lin et al., 1997). The initial cluster formation and particle growth reactions take only about one hour. Nevertheless, the stiffening of the gel, and the actual crosslinking of these particles, take place only after many hours and then progress very slowly. At gelation and curing step, heating is required to provide the required energy for the polymerization reaction to be completed. The common gelation temperature in the literature is 95°C. However, the gelation temperature can be lowered significantly to 40°C if acetone is used as the solvent instead of water (Berthon et al., 2001). The polymerization reaction could be carried out at low gelation temperatures as low as 30°C, but with far longer gelation times compared to using an elevated temperature.

Prolonged curing times may be necessary, because it allows the previously formed polymer particles to crosslink and make sure that the crosslinking reactions are sufficiently completed. This prevents swelling during the subsequent solvent exchange step. The direct placement of the sealed sample vial in an oven at the desired gelation temperature provides satisfactory results. However, in a few cases a temperature program sometimes applied during the curing, where the sample is kept at around room temperature for about 24 h, and then heated gradually for 24 more until it reaches the final temperature (90°C) and then dwelled at that temperature for several hours (Tamon et al., 2000).

At gelation point and before the complete hardening of the gels, the gels could be shaped easily, and a monolithic shape could be obtained, by pouring the solution into a mould (which can be made of glass, metal, or plastic) of the desired shape. Also, it is important to consider that the characteristics of the surface of the mould (especially when small moulds are used) may result in noticeable variations in the final structure of the gel (Petricevic et al., 2001).

Aging of the gels is an optional step carried out upon complete gelation and curing process. It carried out by soaking of the cured gel in a dilute acid (e.g., a 5 to 15% acetic acid solution) for several hours. This process is important to increase the crosslinking density by promoting the progress of the condensation reaction. However this sometimes results in a slight decrease in the surface area. This step also increases the mechanical strength of the gel. Overall, this step may be a very useful addition to the synthesis procedure, especially when it comes to handling the fragile aerogel monoliths without breaking them. In the production of RF resins a variety of additives are utilized to modify the application and cure properties. However, the addition of such additives influences the rate of gelation catalytically, causing a negative effect because of the deposition of the RF sol on the walls (Petricevic et al., 2001).

3.7.1.3 Drying conditions and its influence on the final properties of RF gels

The mechanism of the conventional drying process of a porous material can be divided into several stages. At first the body shrinks by an amount equal to the volume of liquid that evaporates, and the liquid-vapour interface remains at the

exterior surface of the body. The second stage begins when the body becomes too stiff to shrink and the liquid proceed into the interior, leaving air-filled pores near the surface. Even as air invades the pores, a continuous liquid film prevents the flow to the exterior. Eventually, the liquid becomes isolated into pocket and drying can proceed only by evaporation of the liquid within the body and diffusion of the vapour to the outside

Subcritical drying condition: This result in a dense gel structure called a xerogel. In general, when the gel is dried by simple evaporation, large capillary forces at the curved liquid–vapour interfaces often cause the material to shrink and crack, and the carbon obtained after pyrolysis is in most cases totally non-porous. However, if the mechanical strength of the gel is strong enough to withstand capillary pressures, the gel can be dried successively under subcritical conditions (sometimes at atmospheric pressure or under vacuum) without major changes to its structure. Large pore volume (up to 2.4 cm^3/g) and pore size are still could be obtained by evaporative drying of an aquagels without pre-treatment, despite the capillary forces exerted upon the pores during this process. Generally, evaporative drying is suitable when carbons with high density are required (Leonard et al.; Job et al., 2005).

Generally, the drying conditions play an important role in the shrinkage, the final pore structure and surface area of the gel. When hot air is used, the shrinkage depends on both the drying rate and the thickness of the sample, where the shrinkage increases with an increase in the thickness of the sample or an increase in the rate of drying (Tamon et al., 2000, Leonard et al., 2005). Accordingly, this drying method is

quicker, simpler and less expensive than the other drying procedures (Job et al., 2005).

Supercritical drying condition: The gels dried supercritically are named aerogels, and they are known to have outstanding characteristics (e.g., higher surface areas, total pore volumes and sometimes electrochemical double-layer capacitances) compared to carbon xerogels. However, the process is expensive and potentially unsafe due to use high pressure. In this method of drying, the solvent of the aquagel is exchanged with another solvent of lower surface tension (e.g., CO_2). This carried out by slowly exchange the air from a supercritical drying chamber (autoclave) with liquid CO_2. The temperature and pressure are then increases above the critical point (T_c =31°C, P_c = 7.4 MPa) of carbon dioxide (e.g., ~ 50°C and ~ 21 MPa), maintain at the supercritical condition for several hours (Pekala et al., 1998).

The gels prepared by this method are highly sensitive to the synthesis conditions for being tailored within very broad ranges of properties. Supercritical drying is most successful technique which better maintain the inherent pore texture of the wet gel. Moreover, monoliths are very easily to be produced and a large range of bulk densities and pore size can be obtained after drying (Job et al., 2005). Surprising, some shrinkage of the gel is also occur during supercritical drying although, theoretically it should not be occur. RF aerogels prepared with acetone as the solvent and an acidic catalyst do not fully maintain their structures during supercritical drying, possibly due to the polymer gel shrinking slightly during the exchange of acetone with CO_2(Petricevic et al., 1997).

Overall, the major disadvantages of supercritical drying are the high pressure conditions, which is not easily acceptable for both economical and security reasons and the long times (3 to 4 days) required for solvent exchange and drying. To avoid this problem, an alternative procedure to supercritical drying with CO_2 is developed. The supercritical drying with an organic solvent could be successively used instead of liquid CO_2 (e.g., acetone, $T_c = 235^{\circ}C$, $P_c = 4.7$ MPa). This results in shortening the corresponding process time significantly. However, the shrinkage and density of the RF aerogels prepare with supercritical drying with acetone are larger than those with CO_2. Sometimes partial decomposition or pyrolysis, due to the high temperatures required for shifting acetone to its supercritical state, occurred during that process. This results in preparation of aerogels with darker colour compared to those prepared with supercritical drying with CO_2 (Czakkel et al., 2005).

Freeze-Drying condition: This method of drying is widely used in food and pharmaceutical industries. It involves the elimination of the solidified solvents by low-pressure sublimation. When the solvent is removed by freeze drying the produced gels are named cryogels. In this method, the organic gels are frozen by immersion in liquid nitrogen and then dried in a freeze drier equipped with vacuum pump. During this process the solvent is frozen and then removed by sublimation thus avoiding the formation of a vapour-liquid interface. Overall, RF carbon cryogels are mostly mesoporous, the surface areas and mesopore volumes of the RF carbon cryogels smaller than those of RF carbon aerogels (Job et al., 2005). Monoliths are hardly to be obtained when using freeze-drying at high dilution ratio. This due to the cracking of the gel into small pieces because the solvent expansion during freezing,

and the existence of big channels due to ice crystal growth. Figure 3.8 shows the ice crystal growth mechanism at high dilution ratio which expected to occur during freeze drying.

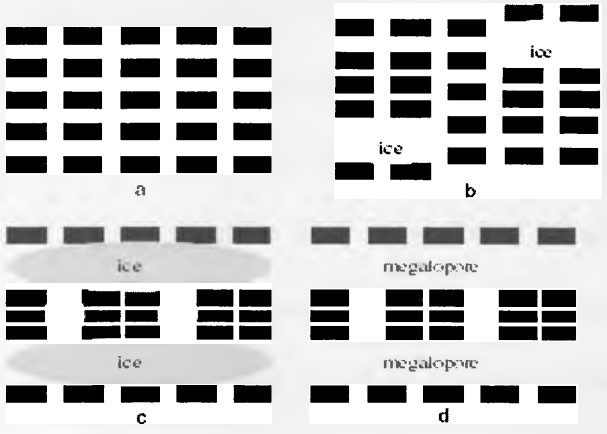

Figure 3.8 The proposed mechanism of the ice crystal growth mechanism during freeze drying at high dilution ratio; (a) the gel before freezing; (b) the gel during freezing which show the appearance of the ice crystal; (c) the ice crystal growth and restructure of the gel; (d) the gel after complete drying process in which a big channels and mega-pore are observed (Job et al., 2005).

Solvent exchange with an alternative liquid (e.g., tert-butanol, cyclohexane) that does not exhibit considerable changes in density upon freezing is an important step before freeze-drying the wet gel. This avoids the expansion of the aqueous solution upon freezing, which result in formation of very large pores and/or the destruction of the gel structure due to ice crystal growth. Moreover, the freeze-drying of the gel with tert-butanol leads to small density change and formation of more mesopores. The R/F molar ratio, R/C, C/W and time of curing also have significant effects on the final properties of the cryogels (Tamon et al., 1999, 2000; Yamamoto et al., 2001)

Czakkel et al (2005) studied the influence of the drying conditions on the morphology of resorcinol-formaldehyde-based carbon gel. The freeze dried gel (cryogel) in *t*-butanol shows the highest surface area (570 m^2/g), the supercritical dried gel (aerogel) shows an intermediate value of surface area (270 m^2/g), and while the gel dried in inert atmosphere (xerogel) shows the lowest surface area (110 m^2/g). Figure 3.9 shows the SEM images of the three gels after drying. The supercritical dried gel exhibits a compact structure and its structure is mainly consisting of microspheres which are interconnected together. The freeze dried gel exhibit a three-dimensional matrix structure consisting from very small microspheres (30 nm); however the network appears to be very fragile. Xerogel shows a compact structure consisting of more or less uniform microspheres of diameter about 0.1 μm.

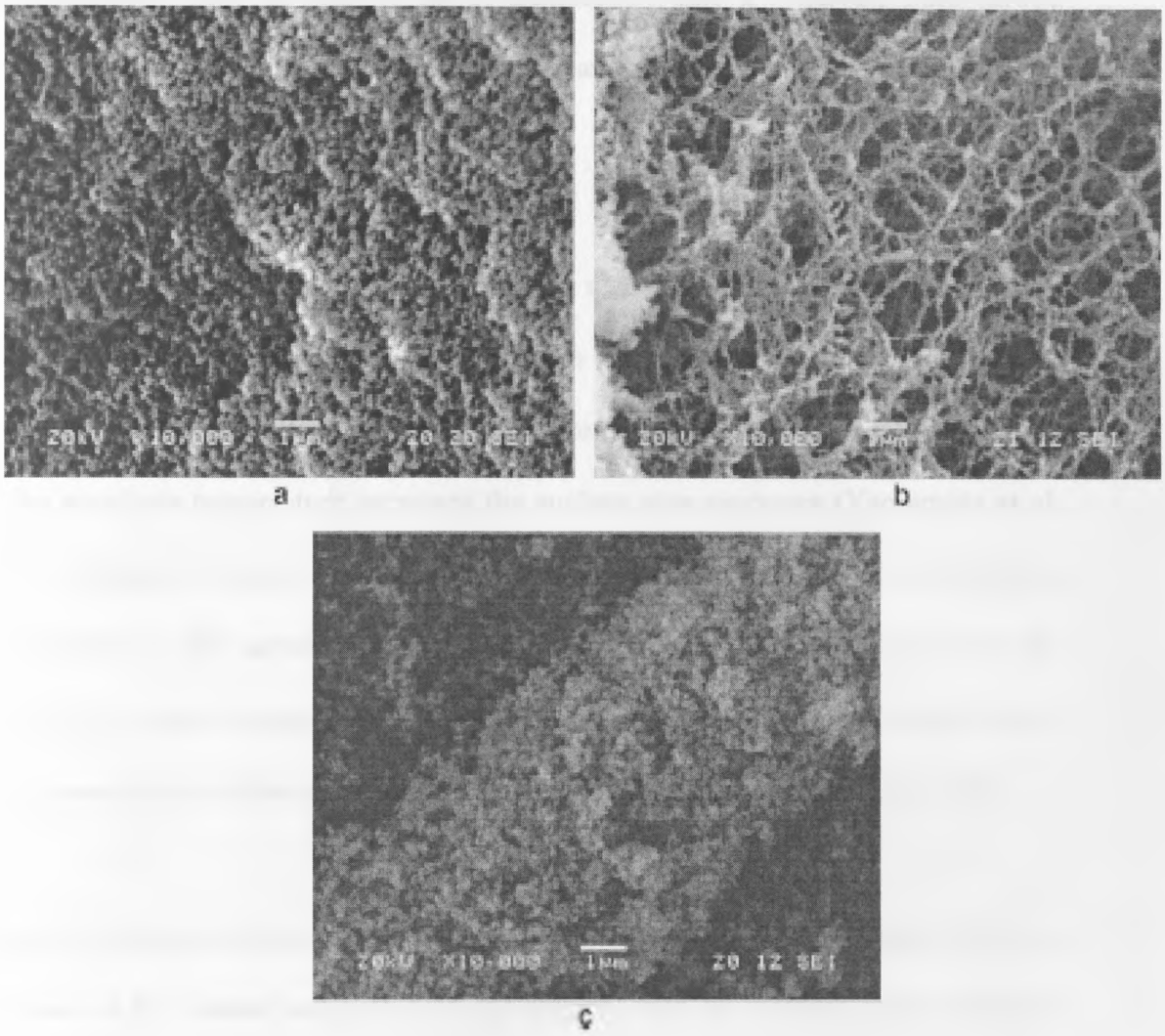

Figure 3.9 SEM images of the three gels dried at different drying conditions. (a) supercritical dried gel(aerogel), (b) freeze dried gel (cryogel), (c) gel dried in inert atmosphere (xerogel), scale-bar = 1 μm.

3.7.1.4 The effect of carbonization (pyrolysis) and activation conditions on the final properties of RF carbon gels.

Pyrolysis of RF gels is most commonly carried out in a tubular furnace under a constant, flow of inert gas, such as N_2, argon or He and at a fixed temperature ranging from 600 to 2100°C. The desired pyrolysis temperature is generally gradually increased using temperature programming. In general, at the pyrolysis

(carbonization) step the organic gel is transformed into a relatively pure carbon structure by removing any remaining oxide and hydrogen groups at an elevated temperature.

The properties of RF carbon gels are affected significantly by the variations of the pyrolysis conditions. Low surface areas of both RF carbon aerogels and xerogels are observed at higher pyrolysis temperatures above 600°C, while under that temperature as the pyrolysis temperature increases the surface area increases (Yamamoto et al. 2001). Higher pyrolysis temperatures also reduce the electrochemical double layer capacitance of RF carbon gels. However, RF carbon gels are not electrically conductive unless carbonized above 750°C. The electrochemical double layer capacitance also exhibits a maximum between 800 and 900°C (Pekala et al 1998).

Overall, pyrolysis produces almost the same PSD for RF carbon aerogels. The pore volumes of RF carbon xerogels decrease slightly with an increase in the pyrolysis temperature. Moreover, the weight loss of RF carbon xerogels due to pyrolysis is practically increases with increase the pyrolysis temperature up to750°C, after this it is almost constant at 50% which indicates the initiation of structural changes within the carbon gel without weight loss (Tamon et al., 1997). Graphitization of RF gels may occur at pyrolysis temperature exceed 2000°C; nevertheless, aerogels pyrolized at 1050°C contain separated graphitic structures. Partial graphitic character has also been reported by others based on XRD patterns (Lin and Ritter, 1997). At higher pyrolysis temperatures, some of the carbon particles will undergo a chemical reaction in which they shift from simple carbon particles to graphite. In regions where this

happens, the graphite particles will tend to attach themselves to adjacent graphite and carbon particles. The net effect is a reduction in the number of particles and a decrease in the overall surface area.

Usually, at the first endothermic reaction, which occurs during the first period of heating from room temperature to 250°C, the release of adsorbed water vapours are observed (as measured by the disappearance of the –OH group by FTIR). This step accompanied by a mass loss of 3%. The other endothermic reactions, which occur during the second period of heating, are attributed to breaking of the C-O and C-H bonds and the release of organic compounds and this step is accompanied by weight loss around 30-40%.

The pyrolysis step is accompanied by shrinkage and weight loss. While the micropores and mesopores volumes are increases, which leads to an increase in the surface area of RF carbon aerogels, especially at low pyrolysis temperatures. This may be attributed to the burnout of the organic groups, which leads to the creation of new pores or voids in the gel. Overall, shrinkage and mass reduction of 20 and 50%, respectively, can be expected due to pyrolysis of RF xerogels. Shrinkage and mass reduction due to pyrolysis decrease with increasing R/C ratio (Saliger et al., 1997). Moreover, there are several factors which could minimize shrinkage during pyrolysis, such as the gelation rate and pore structure of carbon xerogels. The addition of organic fibers to the gel solution may also minimize shrinkage during pyrolysis (Glora et al., 2001).

Activation is carried out to enlarge the diameters of the pores which are created

during the carbonization process and to create some new porosity. Theoretically, any activation method applied to activated carbons can in principal be applied to RF gels. RF organic aerogels and xerogels can be activated, either subsequent to or during pyrolysis. Activation process is most commonly carried out in presence of a suitable oxidizing agent such as steam, CO_2, air and oxygen. For steam and carbon dioxide activation, the temperature is generally in the region of 800 to 1000°C, while steam activation starts in the temperature region of 700 to 750°C. However, for oxygen activation, a lower temperature of 300 to 500°C is most commonly employed to avoid combustion. Overall, increasing the activation time with CO_2 increases the pore volume and the peak pore widths significantly, especially in the narrow pore size (micropore) range and, while this effect is small to a lesser extent, in the mesopore range. Activated RF carbon aerogels with a surface area of 2600 m^2/g can be obtained by activation with CO_2 for seven hours. However, the electrochemical double layer capacitance of RF carbon aerogels may exhibit a maximum after 3 h of activation with CO_2. Overall, the thermal activation step with CO_2 results in a 66 % increase in the electrochemical double-layer capacitance (Pekala et al., 1998). Activation is commonly accompanied with a weight losses, a three-hour activation of an RF carbon xerogel with CO_2 increases the total mass loss from 50 to 75%. Thermal activation with air also results in a comparable weight loss that depends on the activation time and temperature (Saliger et al., 1998).

Chemical activation can be carried out by placing the carbon gel in an acidic solution (e.g., 60 % HNO_3) for two days (Saliger et al., 1998) or KOH solution at 85°C for 3 h.(Teng and Wang, 2000). Figure 3.10 (a) and (b) shows the scanning electron

micrographs of the external surface of phenolic resins derived porous carbons prepared by chemical (using KOH as activating agent) and physical activation(using CO_2 as activating gas) respectively. The external structure of the carbon activated chemically is full of cavities, which results from the removal of the activating agents. In general, carbons with highly rugged surface are normally observed with this kind of activation. Unlike the chemical activation, the physical activated carbon has compact external structure, with a number of pits in the surface, indicating that most of the pores occur inside the carbon particles. Moreover, chemical activation produce carbons with high surface area and total pore volume compared to the physical activated one (Teng and Wang, 2000).

The chemical activation with HNO_3 increases the mass of the carbon gel by 10% and the oxygen content from 4 to 14%. This indicates the attachment of oxide functional groups to the surface of the carbon gel. In general, the carbon yield during chemical activation is higher than in case of physical activation. The chemically activated carbon gel exhibits a significant increase in both the electrochemical double-layer capacitance and the capacity for adsorbing CO_2 , with only a slight change of the surface area in comparison to thermal activation (Saliger et al., 1998).

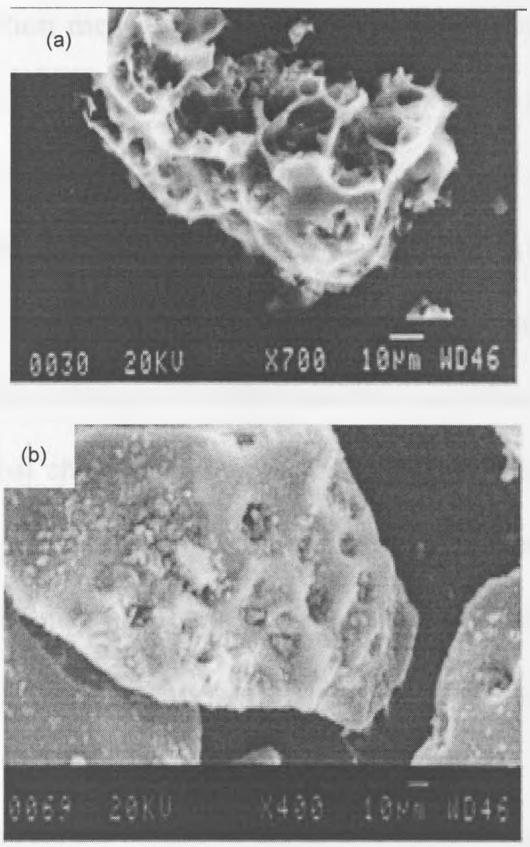

Figure 3.10 SEMs of the external surface of phenolic resins derived carbon prepared by (a) chemical activation with KOH; (b) physical activation with CO_2(Teng and Wang, 2000). Scale bar 10 = μm.

3.7.2 The objective of this research section and our approach.

The objective of this section is to give an up-to-date and comprehensive overview of the growing literature on phenolic resin and its carbon forms. This review is considered as a starting point of our work. It provides us with an insight on how to adjust the synthesis and processing conditions to tailor the structure of the produced carbon gels towards high CO_2 capture by adsorption.

From this review it was clear that, the unique and controllable properties of carbon and activated carbon derived from phenolic resin precursors, which in turn are

attributed to the reaction mechanism being akin to the sol-gel process, makes it a promising material for several investigations. However, the use of resorcinol-formaldehyde (RF) resins as a precursor for preparation of carbon which could be used in the adsorption field (especially CO_2 adsorption), is being under exploited. This is probably due to the limited number of studies assessing the possible routes for their conversion into nitrogen enriched carbons and alters its surface chemistry. In addition, the original chemistry of the carbon derived from phenolic resins is not sufficiently potent to enhance the specific adsorbate (CO_2)-adsorbent interactions at high temperature. Therefore, different surface treatments have to be developed to improve the CO_2 adsorption capacity of activated carbons gels at high temperature.

Accordingly, in this thesis we further developed and modify resorcinol formaldehyde sol-gel synthesis procedure to make high surface area RF carbon xerogels with a controlled pore structure and new surface functional groups for more efficiency CO_2 separation by adsorption. In addition, we altered the surface chemistry of the produced carbon xerogels by loading it with a nitrogen containing compounds during the pyrolysis process. Moreover, we studied the optimum co-pyrolysis conditions to derive carbons with high surface area, porosity and nitrogen content, which consequently affect its adsorption capacity.

Chapter 4

Theory of Experimental Techniques

This chapter deals with the most important theoretical aspects relevant to the experimental techniques used for the analysis of the organic and carbon xerogels samples. In addition, this section deals with the equations, models and assumption of experimental methods used.

4.1 Carbon characterization

Activated carbons are unique because of their extended surface area, porous structure, high adsorption capacity and high degree of surface reactivity. Both the porous structure and the chemical nature of the surface are significantly affect its adsorption potential. The porous structure determines its adsorption capacity by physical adsorption; however the chemical nature of the surface influences its interaction with different kinds of adsorbate molecules. Thus the adsorption behaviour of an active carbon cannot be interpreted on the basis of surface area and pore size distribution alone. Therefore, physical and chemical properties of activated carbons have to be determined to understand its adsorption behaviour and to know the cause of its deterioration due to repeated use. Carbons having equal surface area but prepared by different methods or given different activation treatments show markedly different adsorption characteristics. A proper way for the characterization of the adsorption behaviour of the adsorbents is one which takes into consideration both the chemical and the porous structure of the carbon.

4.1.1 Characterization by adsorption.

Adsorption could be defined as the formation of a gaseous or liquid layer by adsorbate molecules on the surface of an adsorbent by molecular attraction of the van der Waals type. This attraction is weak but long ranged. Atoms at the surface of adsorbent (like active carbons) have imbalanced forces compared to those within the bulk. Consequently, adsorbate molecules try to satisfy this imbalance get attracted to the surface. These adsorbate molecules form a monolayer on the surface of the adsorbent. Figure 4.1 describe the adsorption process showing transfer of adsorbate molecules through the bulk gas phase to the surface of the adsorbent and diffusion onto the internal surfaces of the pores in the adsorbent. The adsorption capacity of activated carbon depends on the type and number of pores and the total surface area available for adsorption. Activated carbons are characterized by their strong adsorption capacity, which occur mostly in cavities of approximately the same dimension of the gaseous molecule. These cavities called micropores. In general, a carbon containing numerous pores in the same size range of the adsorbate molecule is expected to be efficient due to enhancement of the adsorption potential at such condition. Adsorption is a dynamic process in which some adsorbate molecules are transferred from the fluid phase on to the solid surface while some are released again to the fluid state. These processes are functions of partial pressures. When the rates of two processes become equal, an adsorption equilibrium or so-called adsorption isotherm is obtained. This expresses the measurement of the amount of gas adsorbed over a range of partial pressure at constant temperature.

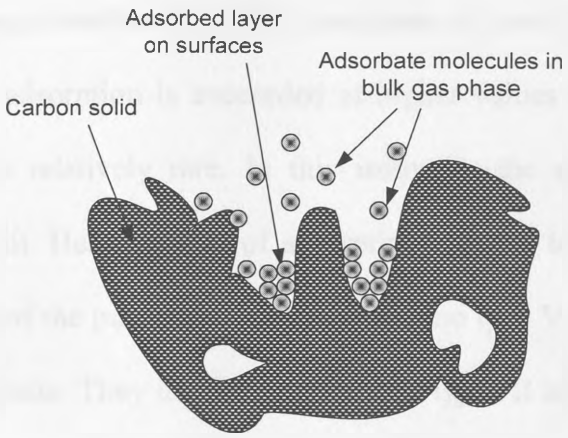

Figure 4.1 Adsorption processes in activated carbons, transfer of adsorbate molecules to the bulk of the adsorbent pores.

4.1.1.1 Adsorption isotherms.

Adsorption isotherms have been used to estimate surface area, pore volume and assessments of the surface chemistry of various porous materials for many years. It helps in fundamental the information on the efficiency of commercial carbon employed in separation/purification techniques. The first attempt to interpret adsorption isotherms for gas-solid equilibrium was carried out by Brunauer, Deming, and Teller (BDDT) in 1940 (Brunauer et al., 1940). The BDDT classification has then become the basis of the modern International Union of Pure and Applied Chemistry (IUPAC) classification of adsorption isotherms. According to IUPAC classification, six general types of isotherms have been introduced and the shapes of these characteristic isotherms are shown in Figure 4.2 (Sing et al., 1985). Type I isotherm is characterize microporous adsorbent where only monolayer adsorption occurs. In this isotherm, micropore filling occurs significantly at relatively low partial pressure less than $0.1\left(p/p_o\right)$. The adsorption process is being complete at approximately $0{\cdot}5\left(p/p_o\right)$(e.g. adsorption of nitrogen on microporous carbon at

77K). Type II isotherm describes physical adsorption of gases by nonporous solids. In which multilayer adsorption is succeeded at higher values of relative pressure. Type III isotherm is relatively rare. In this isotherm, the amount of adsorbate increases without limit. Here the heat of adsorption is equal to or smaller than the heat of condensation of the pure adsorbate. Type IV and type V represent adsorption isotherms with hysteresis. They differ from those of types II and III, in that at high relative pressure section they run parallel to the relative pressure axis. These isotherms are characteristic of weak gas-solid interaction. Type IV isotherms describe a multilayer adsorption process where complete filling of the smallest capillaries has occurred. Type IV isotherm originates from both non-porous and mesoporous solids, whilst type V isotherm originates from microporous or mesoporous solids. The type VI isotherm represents stepwise multilayers adsorptions on a uniform nonporous surface, in which the step depends on the system and the temperature. The step-height represents the monolayer capacity for each adsorbed layer and. In the simplest case, these steps are nearly constant for two or three adsorbed layers.

The understanding of adsorption isotherm is very important in solving many industrial problems. Many of these problems are of current research interest and investigations. The effective surface area, pore size distribution, micropore volume etc., calculation depend on the measured isotherm. Knowledge of the adsorption mechanism in different sizes of porosity is necessary to explain the isotherm shape. The adsorption process in micropores is more difficult to describe accurately. The adsorption process occurring within mesopores is more easily understood.

Macroporosity behaves in the same way as an open surface to adsorption, and accounts for less than 1% of the adsorption process within porous carbons (Rouquerol et al., 1999).

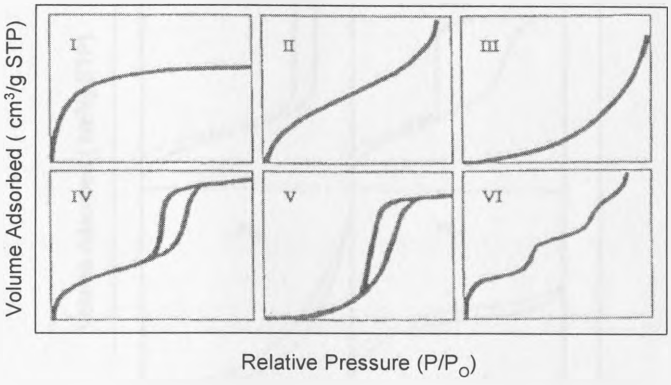

Figure 4.2 Classification of adsorption isotherms.

4.1.1.2 Hysteresis loops

Hysteresis loops, which appear in the multilayer range (relative pressure greater than approximately 0.5) of physisorption isotherms, are generally associated with capillary condensation. It is well known that most mesoporous adsorbents give distinctive hystersis loops (de Boer 1958; Sing et al., 1985). Many different forms of loop have been reported in the literature, but the major types are represented in the IUPAC classification (1985) given in Figure 4.3. This classification based on change of geometry during the adsorption desorption process. Types H1, H2 and H3 were included in the first classification introduced by de Boer (1958). Type H1 is a narrow steep loop with nearly parallel adsorption and desorption branches appear at high relative pressure. In contrast, the Type H2 loop is broad with a long and almost flat plateau and a steep desorption branch. Type H3 and H4 do not terminate in a plateau

at high relative pressure and the limiting desorption boundary curve is therefore more difficult to establish.

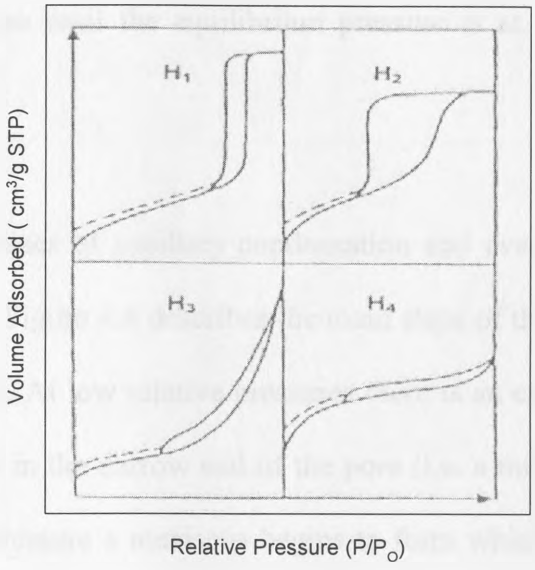

Figure 4.3 The IUPAC classification of hysteresis loops (Sing et al., 1985)

The characteristic features of some types of loop are associated with certain well defined pore structures. Thus, Type H1 loop is characterize adsorbent with a narrow distribution of uniform pores (eg. open-ended tubular pores). Type H2 loop corresponds to adsorbent with complex pore structure and tend to be made up of interconnected networks of pores of different size and shape, (eg. inorganic oxide gels). Type H3 loop is usually given by the aggregates of many particles plate or adsorbent containing slit-shaped pores. Hysteresis loop of type H4 is also given by slit-shaped pores, as in many activated carbons, but in this case the pore size distribution is mainly in the microporous range. A feature common to many loops that, the very steep region of the desorption branch joins the adsorption branch at a limiting relative pressure at a particular temperature. This lower limit of hysteresis is thus dependent on the adsorptive gas and the operational temperature, but not on the

adsorbent. In the case of nitrogen adsorption on porous carbon at 77K, the lower closure point is often located at around 0.42 relative pressures. H3 and H4 loops sometimes do not close until the equilibrium pressure is at, or very close to, the saturation pressure.

In principle, the processes of capillary condensation and evaporation should occur reversibly in the pore. Figure 4.4 describes the main steps of the successive filling of pore during adsorption. At low relative pressures there is an enhanced concentration of adsorbed molecules in the narrow end of the pore (i.e. a micropore filling effect). At a certain relative pressure a meniscus begins to form which with the increase of adsorbate partial pressure, moves steadily up towards the pore mouth. Evaporation proceeds in the reveres direction but involves the same steps (i.e. the meniscus configurations) and therefore the entire isotherm is reversible (Rouquerol et al., 1999).

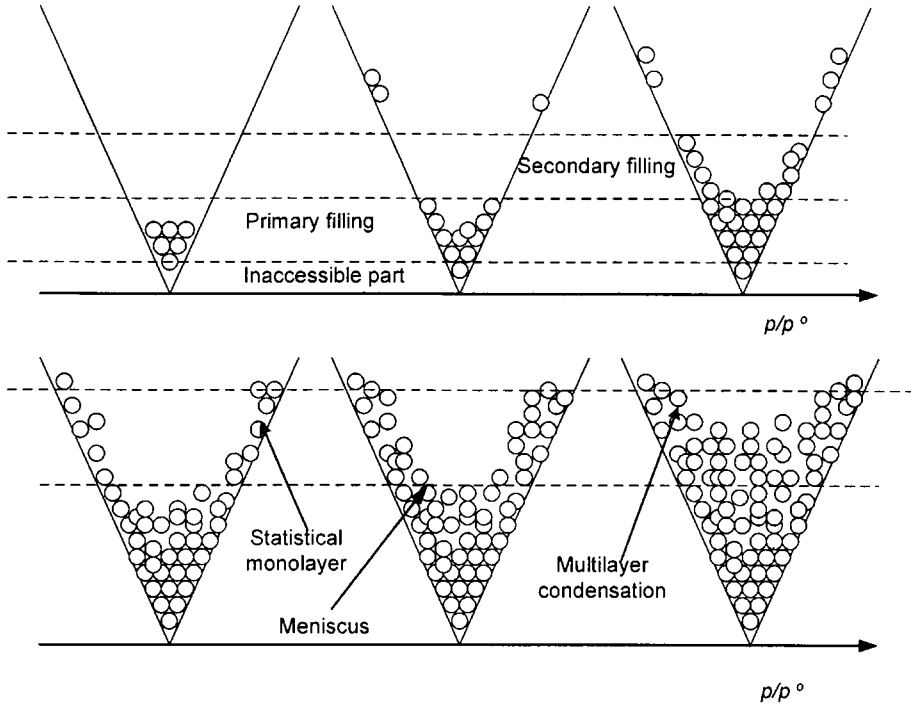

Figure 4.4 Main steps of the successive filling of micropores and mesopores during adsorption (Rouquerol et al., 1999).

4.1.1.3 Langmuir isotherm

20 year before the work on classification of isotherms was under taken, Langmuir (1918) proposed a kinetic theory for the description of what is now known as type I isotherm. The basic assumption that the theory was based on were; that at equilibrium, the rate of adsorption and desorption of gas molecules are equal, the atoms (or molecules) of the gas are adsorbed at given active sites of the adsorbent surface so that every such site can bind one and only one adsorbed atom, and that the energy of state of every adsorbed atom is independent of whether other atoms are adsorbed or not in the neighbourhood of the considered site. Thus the Langmuir theory deals with an ideally localised monomolecular layer with no intermolecular interactions. In the original kinetic approach it is assumed that the adsorbed layer is

in dynamic equilibrium with the gas phase. The number of molecules hitting unit surface area in unit time is given by the Equation 4.1,

$$N = \frac{\overline{N}\ P}{\left(2\pi\overline{M}RT\right)^{\frac{1}{2}}} \tag{4.1}$$

Where $\overline{N}, P, \overline{M}, R$ and T represent Avogadro's number, adsorbate pressure, adsorbate molecular weight, the gas constant and absolute temperature respectively. If θ_o is defined as the fraction of surface unoccupied, then the number of collision with uncovered surface per square centimetre per second is,

$$N = kP\theta_O \quad \text{where} \quad k = \frac{\overline{N}}{\left(2\pi\overline{M}RT\right)^{\frac{1}{2}}} \tag{4.2, 4.3}$$

The number of molecules thus striking and adhering to the surface, N_{ads}, is thus,

$$N_{ads} = kP\theta_o A_1 \tag{4.4}$$

where A_1 is a condensation coefficient representing the probability of a molecule being adsorbed upon collision with the surface. The number of molecules desorbing from the surface, N_{des} is therefore,

$$N_{des} = N_m\ \theta_1\ \nu_1 e^{\frac{-E}{RT}} \tag{4.5}$$

where N_m, θ_1, E and ν_1 represent the number of molecules in a completed monolayer, the fraction of the surface occupied by the adsorbed molecules , the energy of adsorption and the vibrational frequency of the adsorbate normal to the surface when adsorbed respectively.

At equilibrium the rates of adsorption and desorption are equal. Therefore by equating Equations 4.4 and 4.5.

$$kP\theta_o A_1 = N_m\ \theta_1\ \nu_1 e^{\frac{-E}{RT}} \tag{4.6}$$

Because θ_o is defined as shown in Equation 4.7

$$\theta_o = 1 - \theta_1 \tag{4.7}$$

Equation 4.6 can therefore be rearranged to yield,

$$N_m\ \theta_1\ \nu_1 e^{\frac{-E}{RT}} = kPA_1 - \theta_1 kPA_1 \tag{4.8}$$

Expressing Equation 4.8 to yield θ_1 gives Equation,

$$\theta_1 = \frac{kPA_1}{N_m\ \theta_1\ \nu_1 e^{\frac{-E}{RT}} + kPA_1} \tag{4.9}$$

If the following constant, K, is now defined,

$$K = \frac{kA_1}{N_m\ \theta_1\ \nu_1 e^{\frac{-E}{RT}}} \tag{4.10}$$

Equation 4.10 assumes that the adsorption energy is constant. This assumption imparts some weakness to the theory as such an assumption would require an energetically uniform surface which is rare.

Substitution of equation 4.10 into 4.9 equation yields Equation 4.11

$$\theta_1 = \frac{KP}{1 + KP} \tag{4.11}$$

For adsorption of up to and including one layer, the following is true,

$$\theta_1 = \frac{N}{N_m} = \frac{W}{W_m} \tag{4.12}$$

where N and N_m are the number of molecules in the incompleted and completed monolayers, respectively. W and W_m represent the mass adsorbed in the incompleted layer and the mass adsorbed in the completed monolayer, respectively.

Substitution of W/W_m into Equation 4.11 yields the Langmuir equation for Type I isotherm.

$$\frac{W}{W_m} = \frac{KP}{1 + KP} \tag{4.13}$$

The Langmuir theory is not sufficiently general to be applied to isotherms of the shape of Type II-V. The theory takes no account of the fact that multilayer adsorption may occur before the completion of the first monolayer. The Langmuir theory is thus applied only to Type I isotherm and to some chemisorption isotherm which is dominated in our adsorption at relatively high temperature study for CO_2 capture by surface modified and non-modified carbon xerogels. As chemisorption occurs on active sites, the area not included in these sites remains unknown. Also as the entire mass adsorbed is assumed to be contained in monolayer, where pore condensation or multilayer adsorption occurs, the Langmuir theory will over-estimate the surface area of the adsorbent.

4.1.1.4 The BET method for determination of surface area (S_{BET}).

In 1918, Langmuir tried to generalize the concept of an ideally localized monolayer adsorption so that it would include the formation of multi-molecular layers of adsorption. However, it was only in 1938 that an equation suitable for practical use was derived. The theory of multilayer adsorption developed by Brunauer, Emmett and Teller is commonly known as the BET theory (Brunauer et al., 1938). The understanding of this theory has played a dominant role in adsorption studies since it enables the specific surface area of the adsorbent and the approximate values of heats of adsorption to be calculated (Suzuki, 1990).

The theory was based on the assumption that the Langmuir isotherm can be applied to every adsorption layers. This generalization of the concept of an ideally localized monolayer is based on the assumption that every layer of adsorbed molecules constitutes a base for the adsorption of the molecules of the second layer which in turn acts as a base for the third layer, etc. Thus the concept of localization is maintained in all layers. Here, the theory based also on the assumption that the forces of interaction between the adsorbed molecules are neglected. With increasing pressure of the adsorbed vapours, i.e. as p approaches the saturated vapour pressure p_o, the number of unoccupied sites on the adsorbent surface is decrease. Single, double, triple, etc. adsorption complexes are formed. Figure 4.5 shows the multilayer adsorption proposed by BET model.

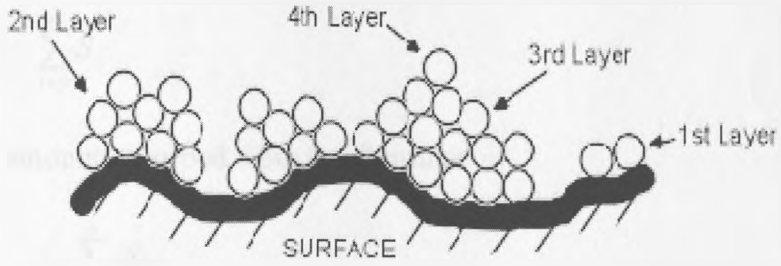

Figure 4.5 The BET model for adsorption, showing multilayer adsorption on adsorbent surface.

The BET adsorption isotherm may be derived in several ways; here the kinetic method is presented. Let S_0, S_1, S_2, S_3,……, S_i, ….,denote the surface areas covered by 0, 1, 2, 3,….., i-molecular layers of the adsorbate Figure 4.4. At equilibrium, the rate of condensation on surface area S_0 equals the rate of evaporation from surface area S_1 , hence we have

$$a_1 p S_0 = b_1 S_1 \exp\left(-\frac{\Delta E_1}{RT}\right), \tag{4.14}$$

where ΔE_1 is the heat of adsorption in the final layer, and a_1, b_1 are constant. Analogously the equilibrium between the first and the second adsorption layers can be written in the form:

$$a_2 p S_1 = b_2 S_2 \exp\left(-\frac{\Delta E_2}{RT}\right). \tag{4.15}$$

The general equation of equilibrium between i-1 and layer i is:

$$a_i p S_{i-1} = b_i S_i \exp\left(-\frac{\Delta E_i}{RT}\right). \tag{4.16}$$

The total surface area of the solid can be calculated from the equation:

$$S = \sum_{i=0}^{\infty} S_i \tag{4.17}$$

and the total amount adsorbed from the formula:

$$a = a_0 \sum_{i=0}^{\infty} i S_i \,, \tag{4.18}$$

where a_0 is the quantity of the adsorbed substance per unit surface area for complete coverage of that surface by a monolayer. Dividing Equation (4.18) by Equation (4.17) we obtain.

$$\frac{a}{a_0 S} = \frac{a}{a_m} = \frac{\sum_{i=0}^{\infty} i\, S_i}{\sum_{i=0}^{\infty} S_i} \,, \tag{4.19}$$

where a_m is the quantity of adsorbate necessary to cover unit mass of the adsorbent with a monomolecular layer, and has the same meaning as in the theory of the ideally localized monolayer. The BET equation can be derived after making some simplifying assumptions as follows:

$$\Delta E_2 = \Delta E_3 = ... = \Delta E_i = \Delta E_l \quad , \tag{4.20}$$

where ΔE_l heat of condensation of the liquid, and

$$\frac{b_2}{a_2} = \frac{b_3}{a_3} = ... = \frac{b_i}{a_i} \,, \tag{4.21}$$

It is assumed therefore that the processes of evaporation and condensation in the second and further layers proceed in the same way as on the surface of a liquid. Equation (4.14) can be transformed as follows:

$$S_1 = y S_0 \,, \tag{4.22}$$

where:

$$y = \frac{a_1}{b_1}\, p \exp\left(\frac{\Delta E_1}{RT}\right) \tag{4.23}$$

By using Equation (4.20) it is possible to transform in a similar way Equation (4.15)

$$S_2 = xS_1\,, \tag{4.24}$$

where

$$x = \frac{a_2}{b_2}\, p \exp\left(\frac{\Delta E_1}{RT}\right) \tag{4.25}$$

and in the general case , by making use of relationship (4.21) we obtain:

$$S_1 = xS_{i-1} = x^{i-1}\, S_i = yx^{i-1}\, S_0 = cx^i S_0\,, \tag{4.26}$$

where

$$c = \frac{y}{x} = \frac{a_1\, b_1}{a_2\, b_2} \exp\left(\frac{\Delta E_1 - \Delta E_2}{RT}\right). \tag{4.27}$$

Substituting Equation (4.26) into Equation (4.19) we obtain:

$$\frac{a}{a_m} = \frac{cS_0 \sum_{i=0}^{\infty} ix^i}{S_0 \left\{1 + c \sum_{i=0}^{\infty} x^i\right\}} \tag{4.28}$$

The sum in the denominator is that of an infinite geometric progression:

$$\sum_{i=1}^{\infty} x^i = \frac{x}{1-x}\,, \tag{4.29}$$

while the expression in the numerator can be transformed to :

$$\sum_{i=0}^{\infty} i\, x^i = x \frac{d}{dx} \sum_{i=0}^{\infty} x^i = \frac{x}{(1-x)^2}\,. \tag{4.30}$$

Substituting expressions (4.29) and (4.30) into Equation (4.28) we obtain:

$$\frac{a}{a_m} = \frac{cx}{(1-x)(1-x+cx)}. \tag{4.31}$$

The quantity of the substance adsorbed on the free surface at saturation is infinitely great. Thus for $p = p_0$, x in Equation (4.31) must be unity if a is tend to infinity. Thus from Equation (4.25) it follows that:

$$\frac{a_2}{b_2} p \exp\left(\frac{\Delta E_1}{RT}\right) = 1 \tag{4.32}$$

when

$$x = p/p_0. \tag{4.33}$$

Substituting Equation (4.33) into Equation (4.31) we obtain:

$$a = \frac{a_m c \frac{p}{p_0}}{\left(1-\frac{p}{p_0}\right)\left[1+(c-1)\frac{p}{p_0}\right]}. \tag{4.34}$$

This equation is the so-called normal BET adsorption isotherm. When Equation (4.34) is transformed to the expression:

$$\frac{\frac{p}{p_0}}{a\left(1-\frac{p}{p_0}\right)} = \frac{1}{a_m c} + \frac{c-1}{a_m c}\cdot\frac{p}{p_0} \tag{4.35}$$

one can easily see that the plot of $p/p_0/[a(1-p/p_0)]$ versus p/p_0 is a straight line whose slope is $(c-1)/(a_m c)$, and intercept is $1/(a_m c)$ Figure 4.6. If we assume that

$$\frac{a_1 b_1}{a_2 b_2} \approx 1, \tag{4.36}$$

then considering Equation 4.27 we can write:

$$c = \exp\left(\frac{\Delta E_1 - \Delta E_2}{RT}\right). \tag{4.37}$$

The term $\Delta E_1 - \Delta E_l$, i.e the difference between the heats of adsorption in the first layer and of condensation, is known as the pure heat of adsorption. If we know the value of a_m, i.e. the quantity of adsorbate (mmol g-1) covering the surface of the adsorbent with a monomolecular layer, we can calculate the specific surface area of the given adsorbent :

$$S_{BET} = a_m.N.\omega \tag{4.38}$$

where N is Avogadro's number.

According to the classical BET procedure the specific surface area of adsorbents is measured by low-temperature (77k) adsorption of nitrogen on the assumption that the surface area of one molecule is $\omega = 0.162$ nm2.

In reference (Hippe et al., 1979) a numerical program is proposed for calculating the specific surface area of adsorbents by the BET method. The program enables rejection of doubtful measurements and calculation of the maximum relative errors of approximation and is very useful for data processing. If, due to inadequate space in the capillaries, adsorption at saturation is limited to n layers, then the BET theory leads us to the following isotherm.

$$a = \frac{a_m cx\left[1 - (n+1)x^n + nx^{n+1}\right]}{(1-x)\left[1 + (c-1)x - cx^{n+1}\right]} \tag{4.39}$$

where x, c, and a_m have the same meaning as in Equation 4.34

Equation 4.39 is the most general form of the BET isotherm and it reduces to the Langmuir isotherm if $n = 1$ and the simple form of the BET equation, i.e to Equation 4.34 if $n = \infty$. Some authors (Bering et al., 1972) claim that the concept of specific surface area loses its physical meaning in the case of microporous adsorbents. The BET theory is specially criticised as regards the theory of volume filling of micropores. According to this theory it is believed that application of methods based on multilayer adsorption (BET, de Boer's t-method) for determination of the specific surface area of adsorbents leads to results that have no physical justification (Dubinin et al., 1981). However, some authors are of the opinion, based on experience and certain calculations (Choma,1983), that the values of the specific surface area obtained by the BET method, even for typical microporous adsorbents, are realistic and have a physical meaning. The results obtained have also confirmed that it is useful to use the BET specific surface area to characterize the porous structure of adsorbents denoted as mesoporous or having a mixed micro-and mesoporous structure. The BET analysis represents the standard method of evaluating and reporting the specific surface area of adsorbents. As a result, most modern adsorption apparatus perform the BET analysis automatically and return the results to the user.

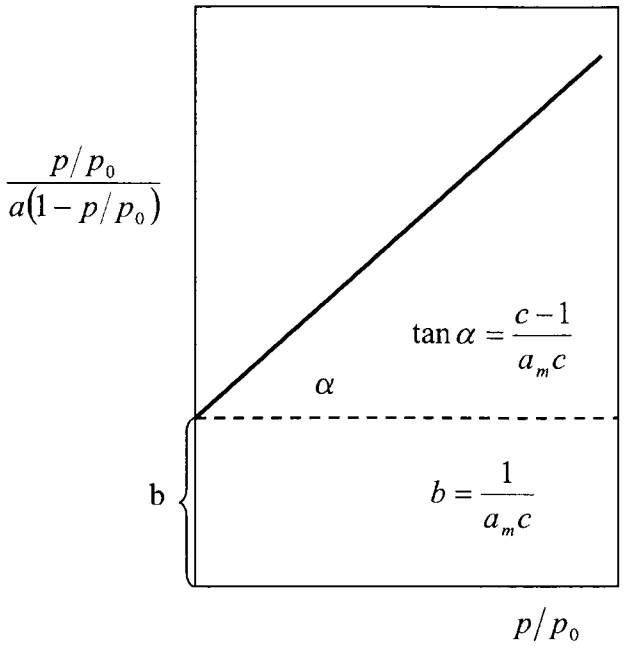

Figure 4.6 Determination of the constants in the BET isotherm for calculation of surface area.

4.1.1.5 The Barrett-Joyner-Haleda (BJH) theory

The BJH (Barrett et al., 1951) theory is the most common method of analysing and reporting the pore size – distribution of porous materials exhibiting capillary condensation in mesoporosity. The model was proposed by considering the adsorption process, when a stepwise reduction in relative pressure (from $(P/P_o)_1$ to $(P/P_o)_2$ to $(P/P_o)_3$ etc.), from cylindrical pores in which capillary condensation has occurred. The process is shown schematically in Figure (4.7)

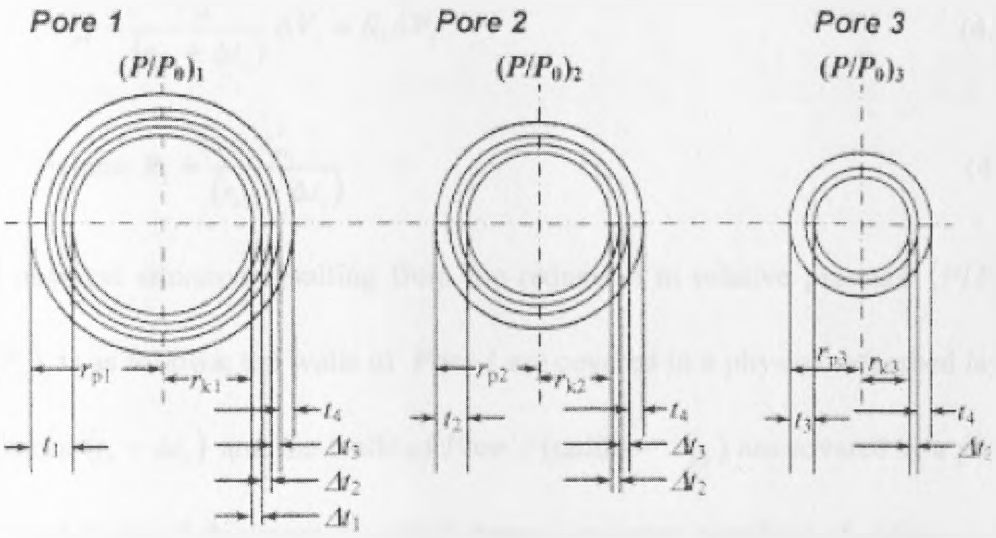

Figure 4.7 Diagrammatic representation of the BJH model for pore volume analysis in porous materials which exhibit capillary condensation

If it is assumed that the relative pressure $(P/P_o)_1$ is equal to unity, it follows that all the pores within the adsorbate are filled with liquid. On the wall of the largest pore, *Pore 1*, lies a physical adsorbed layer of thickness t_1. A capillary of radius r_{K1}, containing liquid adsorbate, is found within the bounds of the physical adsorbed layer. *Pore 1* has radius of r_{p1}. The thickness of the adsorbed layer and the radius of the inner capillary can be calculated using the Kelvin equation (Lowell, 1991). On decreasing the relative pressure to $(P/P_o)_2$, the liquid within the capillary in *Pore 1* evaporates and the physical adsorbed layer decreases in the thickness by a distance Δt_1. These two processes result in the desorption of a measurable volume of adsorbate, ΔV_1. The volume of *Pore 1* can be related to r_{p1}, r_{k1}, t_1 and ΔV_1 by the expression shown in Equation 4.40.

$$V_{p1} = \frac{r_{p1}^2}{(r_{k1} + \Delta t_1)} \Delta V_1 = R_1 \Delta V_1 \tag{4.40}$$

$$\text{where } R_1 = \frac{r_{p1}^2}{(r_{k1} + \Delta t_1)} \tag{4.41}$$

The physical situation resulting from the reduction in relative pressure $(P/P_o)_1$ to $(P/P_o)_2$ is as follows; the walls of *Pore 1* are covered in a physical adsorbed layer of thickness $(t_1 - \Delta t_1)$ and the walls of *Pore 2* (radius = r_{p2}) are covered in a physical adsorbed layer of thickness t_2 which houses an inner capillary of radius r_{k2} filled with liquid adsorbate in equilibrium with the vapour.

If the relative pressure is then decreased to $(P/P_o)_3$ a measurable volume of adsorbate, ΔV_2, is desorbed. This desorption is a result of two processes; evaporation of the inner capillary of liquid adsorbate in *Pore 2* followed by a thinning of the physical adsorbed layer in *Pore 2* by a distance Δt_2 and a second thinning of the physically adsorbed layer within *Pore 1* by a distance Δt_2.

The desorbed volume attributed to the second thinning of the physically adsorbed layer in *Pore 1* is given by Equation 4.42 where L_1 represent the length of *Pore 1*.

$$V_{\Delta t_2} = \pi L_1 (r_{k1} + \Delta t_1 + \Delta t_2)^2 - \pi L_1 (r_{k1} + \Delta t_1)^2 \tag{4.42}$$

ΔV_2 can thus be expressed as shown in Equation 4.43 where L_2 represent the length of *Pore 2*.

$$\Delta V_2 = \pi L_2 \left(r_{k2} + \Delta t_2\right)^2 + V_{\Delta t_2} \tag{4.43}$$

The volume of *Pore 2* can therefore be related to the adsorbed volume by the expression shown in Equation 4.44

$$V_{p2} = \frac{r_{p2}^2}{\left(r_{p2} + \Delta t_2\right)^2}\left(\Delta V_2 - V_{\Delta t2}\right) = R_2\left(\Delta V_2 - V_{\Delta t2}\right) \tag{4.44}$$

where $R_2 = \dfrac{r_{p2}^2}{\left(r_{p2} + \Delta t_2\right)^2}$

As the desorption proceeds, the expression for the volume desorbed due to thinning of the physically adsorbed layer, in pores which have been previously emptied of their liquid capillary, becomes larger and impractical to work with. An alternative method of considering the volume desorbed due to thinning of the physically adsorbed layer is to view the thinning as occurring from an average area. This yields the expression shown in Equation 4.45

$$V_{\Delta t2} = \Delta t_2 A c_1 \tag{4.45}$$

where Ac_1 is the average area from which the physically adsorbed gas is desorbed. Equation 4.45 can be generalized to consider any one of the steps a stepwise desorption process as shown in Equation 4.46

$$V_{\Delta t_n} = \Delta t_n \sum_{j=1}^{n-1} Ac_j \tag{4.46}$$

In a similar fashion, Equation 4.44 can be generalized and combined with Equation to yield the exact expression for the model, Equation 4.47

$$V_{pn} = R_n \Delta V_n - R_n \Delta t_n \sum_{j=1}^{n-1} Ac_j \tag{4.47}$$

Equation 4.47 is not suitable for computation because the average area, Ac, is a function of the relative pressure. The actual area of the pores from which desorption occurs, however, is constant. The following method was then proposed to relate the actual pore areas, A_p, to the average area from where the desorption occurs at each step. The method is shown schematically in Figure 4.8

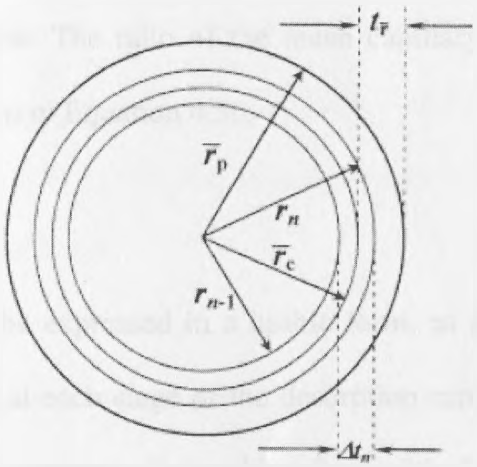

Figure 4.8 Relation of capillary area to actual pore area at nth step of desorption

It was assumed that all the pores which are emptied of their condensate during a relative pressure decrement have an average radius of $\bar{r}_p$. The change in thickness of the physically adsorbed layer due to desorption is referred to as Δt_n and the radii of the inner capillary before and after desorption are r_{n-1} and r_n respectively. The average diameter of the capillary is $\bar{r}_c$. As the capillary is assumed to be concentric with the pore, the average area, A_c, of the capillary during the desorption which produces Δt_n is given by Equation 4.48

$$A_c = A_p \frac{\bar{r}_c}{\bar{r}_p} \tag{4.48}$$

The average capillary radius during the desorption is given by Equation 4.49 as follows,

$$\bar{r}_c = \bar{r}_p - t_{\bar{r}} \tag{4.49}$$

where $t_{\bar{r}}$ is the thickness of the physically adsorbed layer at the mean relative pressure of the desorption. The ratio of the mean capillary and pore radii is thus abbreviated to c as shown in Equation 4.50,

$$c = \frac{\bar{r}_c}{\bar{r}_p} = \frac{\bar{r}_p - t_{\bar{r}}}{\bar{r}_p} \tag{4.50}$$

Equation 4.47 can thus be expressed in a usable form, as shown in Equation 4.51 where the capillary area at each stage of the desorption can be related to the actual pore area. Equation 4.51 represents the working form of the BJH equation.

$$V_{pn} = R_n \, \Delta V_n - R_n \Delta t_n \sum_{j=1}^{n-1} c_j A_{pj} \tag{4.51}$$

The use of the Kelvin equation to calculate the radius of the inner capillary precludes the use of the BJH equation for the analysis adsorption data at relative pressures less than around 0.3. Below relative pressure of 0.3 the Kelvin radius is less than 8 A^o ; the formation of menisci in pores of such small dimensions is considered to be unlikely making the use of the Kelvin equation inappropriate.

4.1.1.6 Horvath –Kawazoe (HK) model for analysis of microporosity

A novel method for determining the microspore size distribution was introduced by Horvath and Kawazoe in 1983. The model based on the progressive pore filling of microporous materials with an increase in adsorbate pressure, and that the relative pressure required for the filling of micropores of a given size and shape is directly related to the adsorbent – adsorbate interaction energy. The original HK model has been developed, depending on pore geometry of slit-shaped pores (Horvath and Kawazoe., 1983). Models for cylinder pores (Saito and Foly, 1991) and spherical pores (Baksh and Yang, 1997) have also been proposed. A brief description of the general HK concept is given next.

The molar integral change of free energy at a given temperature is given by

$$\Delta G^{ads} = \Delta H^{ads} - T\Delta S^{ads} \tag{4.52}$$

where ΔG^{ads}, ΔH^{ads}, and ΔS^{ads} are the free energy , molar enthalpy change and entropy change on adsorption at absolute temperate T,

The molar enthalpy change on adsorption can be shown to be given by

$$\Delta H^{ads} = -q^{diff} - RT + \left(\frac{T}{\theta}\right)\left(\frac{\partial \prod}{\partial T}\right) \tag{4.53}$$

where q^{diff} is the differential heat of adsorption , θ is the degree of void filling in the sorbent and $\prod$ is the spreading pressure.

Assuming that the change in the entropy on adsorption is negligible compared to the other terms in the equation , and noting that the free-energy change on adsorption ΔG^{ads} and q^{diff} can be respectively written as

$$\Delta G^{ads} = RT \ln\left(\frac{P}{P_0}\right) \tag{4.54}$$

and

$$-q^{diff} = U_0 + P_a - \Delta H^{vap} \tag{4.55}$$

where U_0 is sorbate-sorbent interaction energy, P_a is the sorbate –sorbate interaction energy and ΔH^{vap} is the molar enthalpy change on vaporization.

Combining Equations 4.52- 4.55 the following relation is obtained:

$$RT \ln\left(\frac{P}{P_0}\right) + \left[RT - \left(\frac{T}{\theta}\right)\left(\frac{\partial \Pi}{\partial T}\right)\right] = U_0 + P_a \tag{4.56}$$

Now assuming the adsorbed phase to be a two-dimensional ideal gas an assuming the adsorption occurs in the Henery's law region (linear isotherm) yield.

$$RT \ln\left(\frac{P}{P_0}\right) = U_0 + P_a \tag{4.57}$$

The previous equation is the basic framework for the different HK models, where the right –hand side is a function of the pore geometry and dimension, which is related to the relative pressure of the adsorbate. The calculation of the PSD is now relatively simple. By using different values of a pore dimension (pore width in the case of a slit pore, pore diameter in the case of pores with curvature), the threshold sorption relative pressure (P/P_0) at which the pore filling will occur can be obtained over the

expected pore-size range. From the adsorption measurements using a suitable sorbate such as N_2 (77K), the fraction adsorbed amount $(\theta = w/w_\infty)$ is obtained as a function (P/P_0). w and w_∞ represent the mass adsorbed in the incompleted layer and the mass adsorbed in the completed layer, respectively. From a combination of the above two functional relationships, the adsorbed amount w/w_∞ can be plotted as one-to-one function of pore dimension L, thus giving the cumulative PSD. A differential PSD can be further obtained by calculating the derivative $d(w/w_\infty)/dL$ as a function of L.

Limitation of HK models; The HK model seem to provide useful results for prediction of PSD with relative ease of computation. However, the simplifying assumption mad in order to keep the calculations to a minimum. It is a common observation that the predicted PSD seems to reflect the true PSD only for microspores sized lower than 1.3 nm. For larger –sized pores, The HK methods seem to greatly underestimate the pore size of a material. The reason for this drawback is attributed to an inaccurate relation between the adsorption potential and pore size in the HK models.

4.1.2 Characterization of surface chemical structure.

4.1.2.1 Infrared spectroscopy

Infrared (IR) spectroscopy is one of the most common spectroscopic techniques used by organic and inorganic chemists. Simply, it is the absorption measurement of different IR frequencies by a sample positioned in the path of an IR beam. The main

goal of IR spectroscopic analysis is to determine the chemical functional groups in the sample. Different functional groups absorb characteristic frequencies of IR radiation. This technique works almost exclusively on covalent bonds. Clear charts (or spectra) will be produced by samples with high levels of purity of one substance. Using various sampling accessories, IR spectrometers can accept a wide range of sample types such as gases, liquids, and solids. Thus, IR spectroscopy is an important and popular tool for structural elucidation and compound identification.

In order to measure a sample, a beam of infrared light at a specific frequency is passed through the sample. At temperatures above absolute zero, all the atoms in molecules are in continuous vibration with respect to each other. When the frequency of a specific vibration is equal to the frequency of the IR radiation directed on the molecule, the molecule absorbs the radiation. The frequency absorbed depends mainly on the masses of the atoms forming the bond and the geometry of the molecule. The amount of energy absorbed is recorded. By repeating this operation across a range of interest (usually no more than 4000-500cm^{-1}), a chart can be built up. It is generally presented in the form of a spectrum with wavelength or wave-number as the x-axis and absorption intensity or percent transmittance as the y-axis. When looking at a chart for a substance, an experienced user can identify the substance from the information on the chart. The common bond vibrations that are sensitive to IR radiation are stretching (change in bond length: symmetrical and asymmetrical) and bending (change in bond angle or respective position of a group to molecule) vibrations (Robinson et al., 2005).

Powdered potassium promide (KBr) can serve as a holder for the sample in the form of solid thin disc. A radiation source for IR spectroscopy has to fulfil continuity over wavelength range used, cover a wide wavelength range and be constant over long periods of time. Qualitative analysis is carried out by matching the wavelengths of the absorption bands in the spectrum of the sample with the wavelength of functional groups listed in tables. Tables of absorption bands and peaks are available for most organic groups which may show a slight shift due change in chemical structure from one compound to another.

4.1.2.2 CHN-O Elemental Analysis.

Elemental analysis is an experiment that determines the amount (typically a weight percent) of an element in a compound. Just as there are many different elements, there are many different experiments for determining elemental composition. The most common type of elemental analysis is for carbon, hydrogen, and nitrogen (CHN analysis). This type of analysis is especially useful for organic compounds (compounds containing carbon-carbon bonds).

The elemental analysis of a compound is particularly useful in determining the empirical formula of the compound. The empirical formula is the formula for a compound that contains the smallest set integer ratios for the elements in the compound that gives the correct elemental composition by mass. The technique of

analysis involves transformation of the compound elements into simple gaseous products. Typically the sample is weighed into a tin container, which gives the advantage of strong exothermic combustion ensuring complete sample oxidation at approximately 1000°C to yield carbon dioxide, water and nitrogen oxides:

$$\text{Organic material} \xrightarrow{O_2\ (1000^\circ C)} CO_2 + H_2O + NO_x \qquad (4.58)$$

The resulting combustion products pass through specialized oxidation reagents, to produce from the elemental carbon, hydrogen, and nitrogen, carbon dioxide (CO_2), water (H_2O), nitrogen (N_2) and N-oxides respectively. These gases are then passed over copper to remove excess oxygen and reduce the oxides of nitrogen to elemental nitrogen. Helium is used as the carrier gas. Other elements present are removed by the use of specialized combustion reagents.

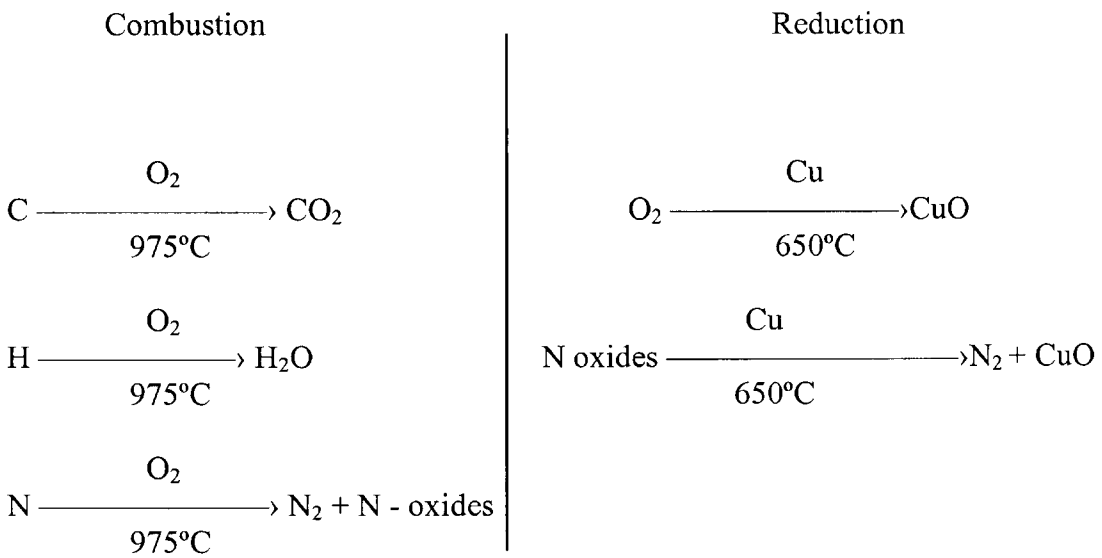

Figure 4.9 The combustion and reduction processes Note: The majority of Nitrogen is converted to N- oxides; some compounds will form N_2 directly.

The mixture of combustion products (CO_2, H_2O and N_2) is passed through a gas chromatographic column to separate the components resulting in a gas chromatogram of three peaks eluting in the order of N_2, CO_2, and H_2O. The subsequent signals are measured and referenced against compounds of known CHN content. According to the previous known weight of the sample, the percentages of carbon, hydrogen, and nitrogen are calculated. For a compound containing oxygen the percentage is calculated by subtraction (Ewing, 1997).

4.1.3 Characterization by scanning electron microscope (SEM):

Electron microscopy is a direct method of testing the porous structure of solids (including active carbons and other carbonaceous materials). It gives an image of the material under study in the nanometre scale which helps to understand its texture. The main advantage of this method over, e.g., adsorption methods, is the possibility of determining directly the shape and size of the pores (especially mesopores) which in turn allows us to estimate the usefulness and accuracy of other method. However, electron microscopy also has certain drawbacks. Among these the more important are (i) the poor reliability of results obtained for of adsorbents with a wide distribution of pore size and (ii) the painstaking preparation of the samples for testing.

Typically in the SEM instrument, beams of electrons are emitted from a tungsten or lanthanum hexaboride (LaB_6) cathode filament towards an anode in a vacuum. The electron beam (having an energy ranging from a few to 50 keV) is collected by two successive electromagnetic condensing lenses, focused by an objective lens into a

beam with a very fine spot size (~ 5 nm). The beam scans across the surface of the sample by electromagnetic deflection coils. Secondary electrons are emitted from the sample upon collision with the incident beam. The sample image is produced by collecting secondary electrons that are released by the sample. The secondary electrons are detected by a scintillation material that produces flashes of light. The flashes are then detected and amplified by a photomultiplier tube (Ewing, 1997).

4.2 CO_2 capture and separation measurements by modified gas chromatograph

In the design of pressure swing, or temperature swing, gas adsorption process, the fundamental design requirement is to know how much of the various components adsorb on the adsorbent under different conditions of pressure, temperature and composition; that is the binary adsorption isotherm. Because of the lack of available data a rapid technique for measuring and recording binary-gas adsorption isotherm is required. This section describes a method for measuring binary gas isotherm and thus should help to fill this gap in data information.

It is fairly straightforward to determine the pure-component adsorption isotherm for two compounds A and B. However, it is not straightforward to determine the binary adsorption isotherm for A and B because of interaction between compounds, also the adsorbed-phase concentration is unknown. For interacting systems one must simultaneously measure the amounts of A and B adsorbed over the entire range of compositions. The standard method of determining adsorption equilibrium is to determine the amount of each species present in the gas and solid at equilibrium by gravimetric, volumetric or other analytical means. This depends on measuring the

composition of the gas mixture and either the total amount of adsorbed gas (by weight) or the amount of non-adsorbed gas (by pressure and volume). As the total amount of gas mixture in the system is known, the amount, and composition, of the adsorbed gas can be determined from an overall mass balance. The method is slow and expensive.

In contrast to the static methods, dynamic (chromatographic) methods involve the mixture of interest flowing through a packed column, where the composition of the outlet is monitored. The methods have several advantages such as speed and the relative ease with which conditions can be changed.

The method is based on a GC (where a composition detection) and also a detection to flow-rate change in the outlet of the adsorption column (Mason and Buffham , 1996). A small perturbation flow, typically one of the two components, is added to (or removed from) a much larger stream of carrier gas mixture. The addition or removal of this perturbation stream is intended to change the mole fraction of the gas in the column and thus alter slightly the amount of adsorption of both components. The result is that there are short-term changes in the total flow-rate and in the composition of the gas leaving the column. The main change in concentration of the gases in the column is because of the change in mole fraction produced by adding or removing the perturbation stream. However, there is a secondary effect; the extra flow caused by adding the perturbation stream increases the pressure drop down the column. This will increase the mean pressure in the column and lead to an increase in the total amount adsorbed. This effect can be measured using differential pressure

transducer (DPT) for the flow rate change and thermal conductivity detector (TCD) for composition change as shown in Figure 4.10.

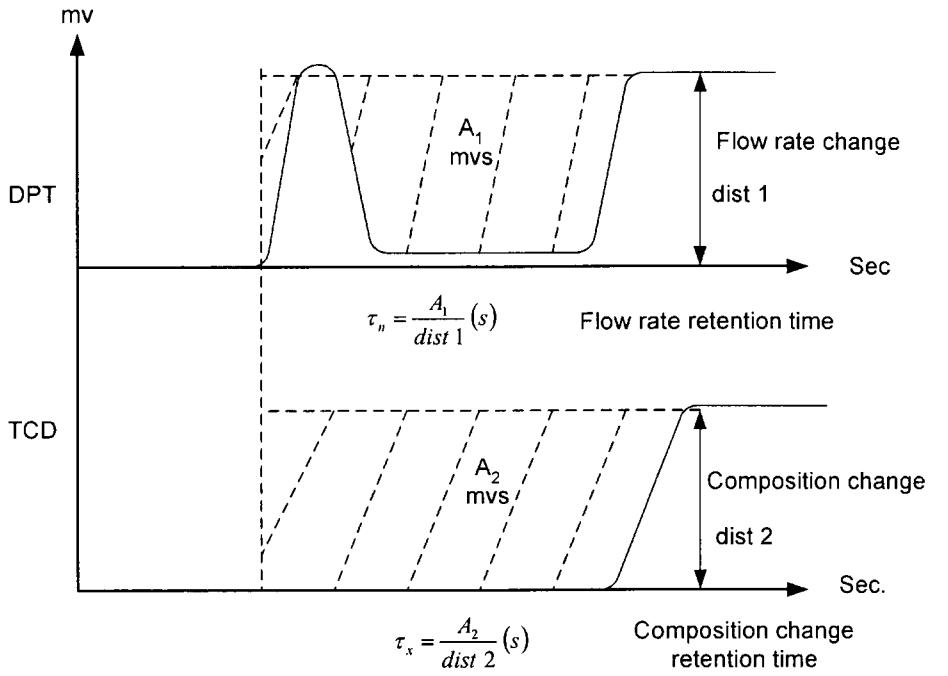

Figure 4.10 Typical flow rate and composition-time curves for binary systems when a small step change in composition is made

Now let us consider a chromatographic column which has volume V_c and is packed with an adsorbent having porosity ε. The volume of packing will be $(1-\varepsilon)V_c$ and the void volume will be (εV_c) as shown in Figure 4.11. The total amount of species i in the system (both adsorbed and free in any void space), is the holdup, (H_i) which can be calculated from the mass balance of the adsorbed column as in Equation (4.59).

$$\Delta H_i = \Delta C_i \varepsilon v_c + \Delta q_i w \tag{4.59}$$

This is leading to give the isotherm gradient

$$\frac{\delta q_i}{\delta C_i} = \frac{\Delta H_i / \Delta C_i - \varepsilon V_c}{W} \tag{4.60}$$

where ε is defined geometrically in terms of the superficial shape of the adsorbent particles, C is the concentration in the gas and q the concentration in the adsorbent, V_c is the sample column volume and W is the amount of the adsorbent

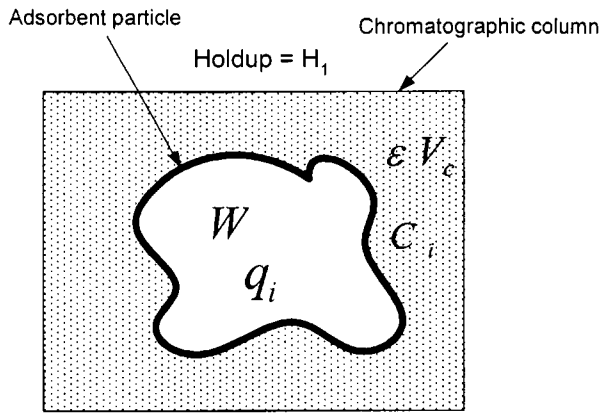

Figure 4.11 Schematic representation of a packed chromatographic column. There are two regions; the pore space and the adsorbent particles.

The value of $\frac{\Delta H_i}{\Delta C_i}$ can be calculated from the composition and flow rate transient time as follows.

$$\frac{\Delta H_i}{\Delta C_i} = Q_c \left[\tau_x + \frac{y_i^0}{y_i^p - y_i^0} \tau_n \right] \tag{4.61}$$

where τ_x is the retention time of the composition transient time, τ_n is the retention time of the flow-rate transient time, y_i^0 the composition of the component i in the main flow and y_i^p the composition of the component i in the perturbation flow. The term Q_C is the column flow rate which can be calculated from the ambient flow rate Q_{amb} as follows.

$$Q_C = Q_{amb} \frac{P_{amb}}{P_c} \frac{T_c}{T_{amb}} \tag{4.62}$$

where P_{amb} and P_c are the ambient and column pressures respectively and T_{amb} and T_c are the ambient and column temperatures.

The quantity $\delta q_i / \delta C_i$ of Equation (4.60) represents the gradient of the equilibrium hypersurface. By integration of $\delta q_i / \delta C_i$ from $C_i = 0$ gives q_i as a function of C_i which represents the binary adsorption isotherm. The basic theory of this method is described in detail in (Mason and Buffham, 1996).

4.3 Temperature-programmed desorption mass spectrometry (TPD-MS) technique for studying CO_2 desorption (regeneration) process

The experimental aspects of thermal desorption are based on the concepts of adsorption and desorption. If a solid with a surface free of adsorbed particles is placed in a gas medium, the process of adsorption will proceed. Under static conditions, this process will continue in static until an equilibrium concentration of adsorbed particles is reached. The material under study is then placed in decomposition glass-tube (TPD cell) and heated at a programmed linear rate in an inert atmosphere flow, while contained in a vacuum and simultaneously detecting the residual gas in the vacuum (the flux of desorbing molecules) by means of a mass analyzer. As the temperature rises and a particular species is able to desorb from the surface, the pressure will rise. As the temperature rises still further the amount of the species on the surface will reduce causing the pressure to drop again. This results in a peak in the pressure versus time plot. The temperature of the peak maximum provides information on the binding energy of the bound species. The data obtained

from such an experiment consists of the intensity variation of each recorded mass fragment as a function of time/temperature. Figure (4.12) shows the schematic diagram of the whole adsorption-desorption process during TPD analysis.

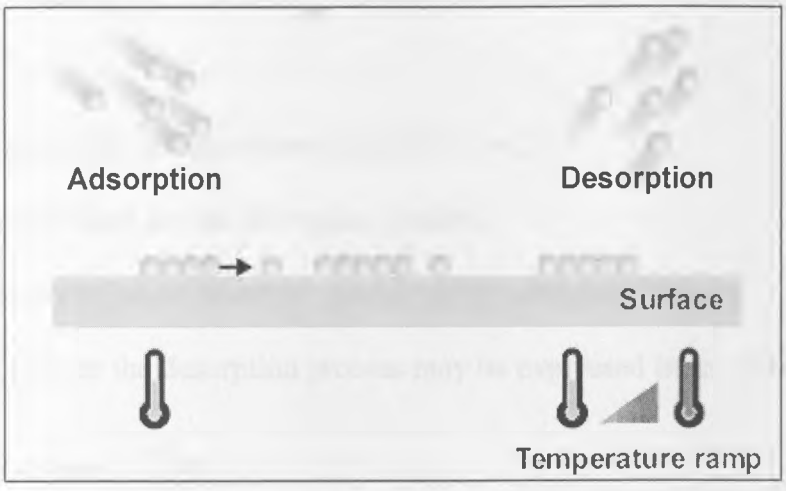

Figure 4.12 Illustration of processes during temperature programmed desorption. As shown on the left side, the exposure of the surface to a molecular beam of gases results in the formation of mono- and multilayers by physisorption or chemisorption. The desorption as shown on the right side, is carried out by heating the sample surface in a linear fashion and the desorbing molecules are monitored using a quadruple mass spectrometer.

A mass spectrometer measures the ionized molecules according to their mass-to-charge ratio. The sample is being bombarded by a stream of electrons. The electrons must have sufficient kinetic energy to break covalent bonds forming ionic fragments. The mass spectrometer is provided with an electrostatic field capable of accelerating charged fragments. The charged fragments are separated in a magnetic field (Ewing, 1997).

4.3.1 Redhead equation of first-order desorption.

The rate of desorption of an adsorbate from a surface can be expressed in the general form:

$$R_{des} = K_{des} \,.\, N^{X} \tag{4.61}$$

where

X- kinetic order of desorption (typical 0,1 or 2)

K- rate constant for the desorption process

N- concentration of adsorbed species on the adsorbent surface.

The rate constant for the desorption process may be expressed in an Arrhenius form,

$$K_{des} = A \exp\left(\frac{-E_{des}}{RT}\right) \tag{4.62}$$

where

E_{des} is the activation energy for desorption,

A is the pre-exponential factor

So, the rate of desorption of an adsorbate from a surface can be expressed in the general expression.

$$R_{des} = -\frac{dN}{dt} = A \,.\, N^{X} \,.\, \exp\left(\frac{-E_{des}}{RT}\right) \tag{4.63}$$

In a temperature programmed desorption experiment, the temperature is increased linearly with time from some initial temperature T_0 , then :

$$T = T_0 + \beta \,.\, t \quad \text{and} \quad dT = \beta \,.\, dt \Rightarrow \beta = \frac{dT}{dt} \tag{4.64}$$

Redheads assume that when adsorbed species desorbed from surface in a simple molecular manner; desorption will usually be a first order process (X=1). In the TPD

experiment the intensity of desorption signal (TPD spectra), (I (T)), is proportional to the rate at which the surface concentration of adsorbed species is decreasing (rate of desorption).

$$I(T) \quad \alpha \quad R_{des} \tag{4.65}$$

Therefore a combination of equations (4.64), (4.65) and (4.66) gives;

$$I(T)\ \alpha \quad - \quad \frac{dN}{dT} = \frac{A\,.\,N^{x}}{\beta}\,.\exp\left(\frac{-E_{des}}{R\,T}\right) \tag{4.66}$$

In the case where the desorption kinetics will usually be first order (i.e. x = 1). The maximum desorption signal in the I(T) trace will occur when (d I(T) / dT) = 0 , i.e. when.

$$\frac{d}{d\,T}\left[\frac{A\,.\,N}{\beta}\,.\exp\left(\frac{-E_{des}}{R\,T}\right)\right] = 0 \tag{4.67}$$

Hence, remembering that the surface coverage changes with temperature i.e. $N = N(T)$, so Equation (4.67) gives.

$$\frac{A\,.\,N}{\beta}\,.\frac{E_{des}}{R\,T^{2}}\exp\left(\frac{-E_{des}}{R\,T}\right) + \frac{A}{\beta}\exp\left(\frac{-E_{des}}{R\,T}\right).\frac{d\,N}{d\,T} \quad = \quad 0 \tag{4.68}$$

Substituting for dN/dT from Equation (4.66) gives.

$$\frac{A\,.\,N}{\beta}\left[\frac{E_{des}}{R\,T^{2}} + \frac{A}{\beta}\exp\left(\frac{-E_{des}}{R\,T}\right)\right]\exp\left(\frac{-E_{des}}{R\,T}\right) \quad = \quad 0 \tag{4.69}$$

The solution is given by setting the expression in square brackets to be equal to zero, i.e.

$$\frac{E_{des}}{R\,T_P^2} = \frac{A}{\beta}\exp\left(\frac{-E_{des}}{R\,T_p}\right) \tag{4.70}$$

where we have now defined the temperature at which the desorption maximum occurs to be $T = T_p$ (the *peak temperature*). Equation (4.70) relates the desorption parameters at the maximum rate of desorption which is known as Redhead equation, a theoretical model of TPD, which is used to interpret the TPD spectra with the goal of determining thermodynamic and kinetic parameters (E_{des} and A) . A normalized expression for the peak shape for first order desorption is given by Redhead (1963).

$$\ln\left(\frac{N_p}{N}\right) = \frac{E_{des}}{R}\left(\frac{1}{T}-\frac{1}{T_p}\right)+\left(\frac{T}{T_p}\right)^2\exp\left[-\frac{E_{des}}{R}\left(\frac{1}{T}-\frac{1}{T_p}\right)\right]-1 \tag{4.71}$$

Where N_p is the maximum desorption rate at peak temperature, T_p, and N is defined as the desorption rate at any temperature.

Chapter 5

Experimental Procedures

This chapter deals with the preparation and properties of resorcinol-formaldehyde (RF) carbon and activated carbon xerogels as a promising candidate for CO_2 capture and separation by adsorption, which could operate at high temperature. This set of experiments reveals very interesting features concerning the structural and performance characteristics. In addition, a description of the set of experiments that were conducted to quantify the factors that may affect the adsorption properties of the prepared carbons is also included.

The first part is associated with the initial solution recipe, the subsequent gelation and curing of the gel, pyrolysis and the activation process. The most important factors that affect the properties of the resulting carbon xerogels are experimentally described. However, as a part of the contribution of this study, a new basic medium was used for the polycondensation reaction of resorcinol with formaldehyde which we believe that it will lead to a new carbon surface chemistry. In addition, a detailed experimental procedure for a further step for surface chemistry modification of the produced carbons, by co-pyrolysis with nitrogen containing compound, is also described in this chapter.

The second part deals with the experimental procedure used for characterization, while the third part involves a modified GC to determine the binary-gas adsorption isotherm for CO_2-N_2 system at low and high temperature and 1.05 bar. This technique has not been used before for the CO_2-N_2 system. The experimental procedures carried out to study the effect of pressure on the CO_2 adsorption capacity are shown in part four.

Finally, the fifth part explains the regeneration and the desorption characteristics of the prepared carbon xerogels using temperature programming desorption mass spectrometry (TPD-MS) technique.

5.1 Preparation of the carbon and activated carbon xerogels procedure.

Figure 5.1 shows the basic experimental procedures steps used for the preparation of carbon and activated carbon xerogels. First, resorcinol (R) and formaldehyde (F) are mixed at the appropriate molar ratio in the presence of a basic catalyst. Then the solution is heated in a closed container to a predetermined temperature for a sufficient period of time to form a stable crosslinked gel. The gel is then washed with acetone to exchange the aqueous solvent. Next, the gel is dried with vacuum drying technique, which produces an RF-xerogels. To produce a carbon xerogel, the dried gel is carbonized in argon to form the highly porous carbon network. For studying the effect of the carbon surface chemistry on the CO_2 capture and separation, the dried gels may also mixed with nitrogen containing compound prior to the carbonization process. The samples are then activated with CO_2 following the carbonization, for the purpose of studying the effect of the pore structure on CO_2 capture and separation.

5.1.1 Resorcinol-Formaldehyde (RF) xerogel synthesis and initial solution formulation.

RF-xerogels were synthesized by the polycondensation of resorcinol (R) (1, 3-dihydroxybenzene $C_6H_4(OH)_2$) (reagent-grade 98%, Aldrich) and formaldehyde(F)

(HCHO)(37% in water, stabilized by 10-15% wt. methanol, Aldrich) using an initial R/F molar ratio of 1:2. Deionised water (W) was used as the diluent. Three common alkanolamines (monoethanolamine(MEA), diethanolamine(DEA), methyldiethanolamine (MDEA)) all shown in Figure 5.2 , potassium carbonate (K_2CO_3) (research grade, Aldrich) as well as sodium carbonate (Na_2CO_3) (research grade, Aldrich), were also used as catalysts. Each resin has been designated as (RF), followed by the catalytic species and resorcinol to catalyst ratio used.

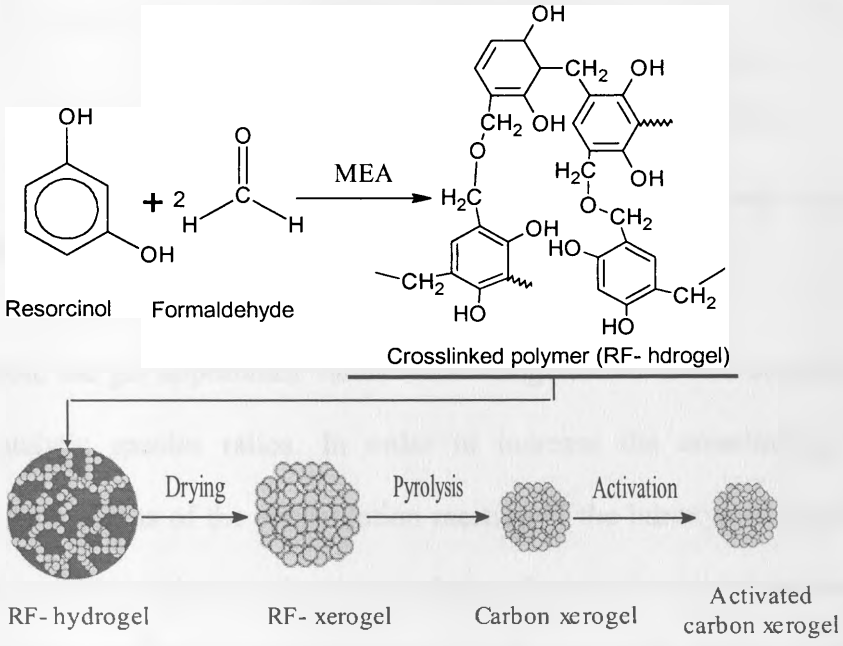

Figure 5.1 The basic experimental procedure for the preparation of organic and carbon xerogels.

After dissolution of the resorcinol/water mixture, formaldehyde was added and the pH value was then adjusted by addition of a dilute solution of HNO_3 (2N or 0.5N). The uses of different dilute solutions of various concentrations enables minimization the amount

of water added during pH adjustment. The mixture was then stirred for 15 minutes. The vials were sealed and gelation was performed at 85°C in an oven for three days. To study the influence of the synthesis conditions for sol-gel polycondensation using the new basic mediums on the porous structures of the carbon xerogels, the amount of catalyst, diluent and initial aqueous solution pH were varied in a series of experiments.

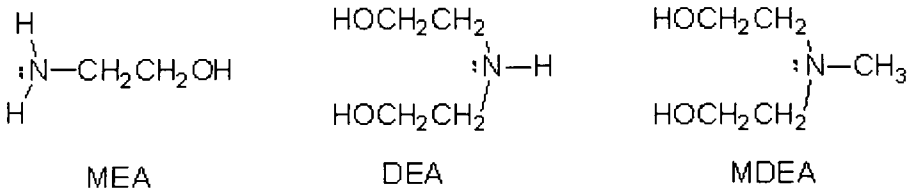

Figure 5.2 The chemical structures of the three common alkanolamine used as a catalyst in the polycondensation reaction of resorcinol with formaldehyde

After gelation, the gel appearance varies from orange to red brown according to initial pH and catalytic species ratios. In order to increase the crosslinking density by promoting the progress of the condensation reaction of the hdroxymethyl groups, 15 ml of 5% acetic acid was added to the solvent during the initial water to solvent exchange. The excess water was then removed from the gel by soaking in acetone for 24 hour and in cyclohexane for another 24 hour. In this case, the solvent exchange is used in order to reduce the capillary forces responsible for the pore texture destruction. The solvent was then removed from the pores of the gel slowly, first by evaporating at 60°C for two hours, and then further by exposing it to a vacuum at 120°C for 12 hours. After drying, the dried gels are crushed and sieved to 500 μ m < D < 1.18 mm particle size.

5.1.2 Preparation of RF carbon xerogel.

The RF-xerogels was placed in a ceramic boat, pyrolyzed at 850°C under argon flow (100 ml/min) in a tubular oven Figure 5.3. The pyrolysis conditions were determined previously by the thermogravimetric analysis. Figure 5.4 shows the pyrolysis program which was selected so that the heating rate was dwelled after a temperature of 110, 450 and 650°C.

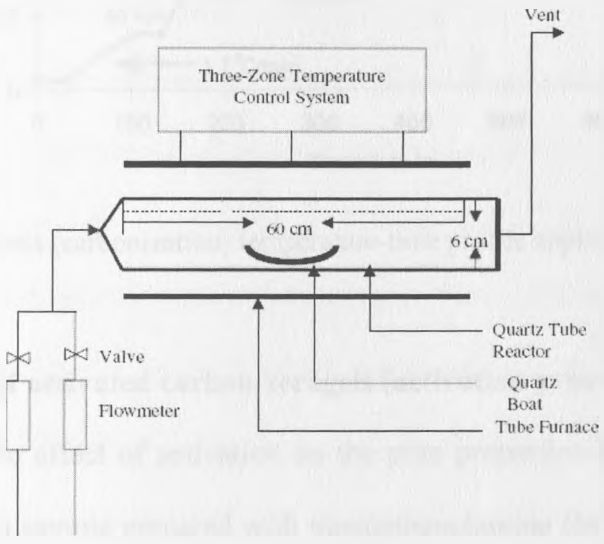

Figure 5.3 Schematic diagram of the tubular furnace used for the carbonization and activation process.

As, the high heating rate could cause a dramatic effect on the pore structure. Thereby, the heating program included the following seqential steps, 1) ramp at 0.5°C/min. to 110°C, and then dwells for 30 min., 2) ramp at 5°C /min to 450°C , and then dwell for 30 min., 3) ramp at 10°C/min. to 850°C and dwell for 180 min., 4) cool slowly to room temperature. All steps were performed under a flowing of argon 100 ml/min. After

pyrolysis step, each sample has been designated as RFC- followed by the catalytic species and resorcinol to catalyst ratio.

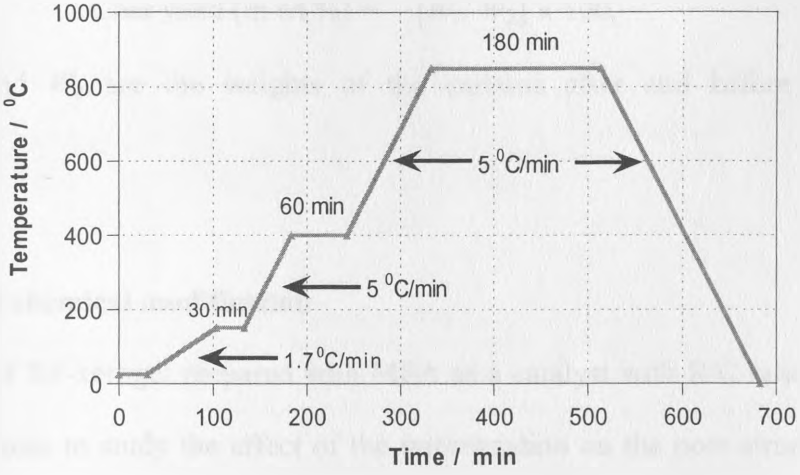

Figure 5.4 The pyrolysis (carbonization) temperature-time profile applied.

5.1.3 Preparation of activated carbon xerogels (activation process).

In order to study the effect of activation on the pore properties and subsequently CO_2 adsorption, the resin sample prepared with monoethanolamine (MEA) as a catalyst with a R/C ratio of 100 was selected for this study. After pyrolysis the sample is activated under flow of CO_2 100 ml/min. The activation temperature was varied from 850°C and 980°C with a heating rate 30°C/min. for a period of one to three hours. Argon flow was used during heating and cooling steps. The resultant activated samples for these series were labelled as RFAC-a-b-c where a is denoted for R/C ratio and b and c denote for the activation temperature and activation time, respectively.

To investigate the effect of the activation on the char yield, the yield was calculated by using Equation (5.1).

$$\text{Char yield (in wt \%)} = [W_1 / W_2] \times 100, \quad (5.1)$$

where W_1 and W_2 are the weights of the carbons after and before activation , respectively.

5.1.4 Surface chemical modification

The sample of RF-xerogel prepared with MEA as a catalyst with R/C ratio of 100 was selected, in order to study the effect of the impregnation on the pore structure, surface chemistry and consecutively the amount of CO_2 adsorption of the produced carbons xerogels. Figure 5.5 shows the schematic diagram of the different steps of the surface modification or impregnation process which has been done to fulfil this task. After synthesis of the RF-xerogel, the N-source (*m*-phenylenediamine (MPDA) or diphenylenimine (DPI)) was dissolved in acetone, followed by the addition of the cured RF-xerogel then the mixture was heated at a temperature of 100°C until evaporation of all the solvent. Figure 5.6 shows the chemical structure of the two nitrogen compounds selected for the impregnation. The typical physical properties of the two compounds are presented in Appendix C. The reason for using MPDA and DPI as the nitrogen source in the impregnation method is that they contain an aromatic ring that should easily get involved in the ring condensation structure during impregnation and subsequent carbonization process. The N-content of the RF-xerogel after impregnation was

controlled by adjusting the N-source addition at 10-50 wt. % of the original RF-xerogel weight.

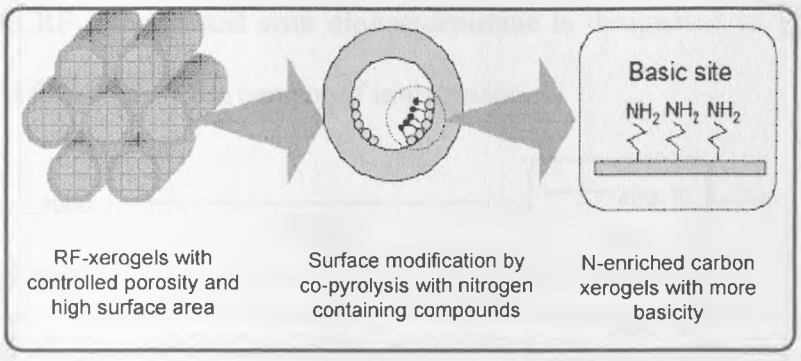

Figure 5.5 Schematic diagrams of the surface modification steps

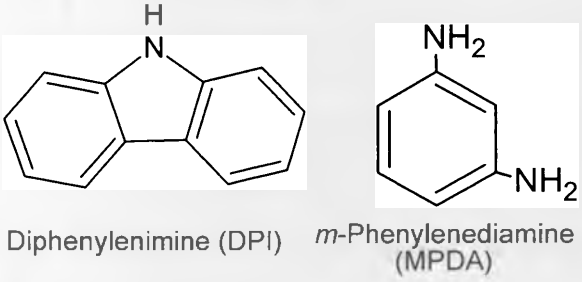

Figure 5.6 The chemical structure of the two nitrogen containing compounds used for RF-xerogel impregnation

After complete evaporation of the acetone out of the solution the impregnated RF-xerogels were dried for 2 h at 60°C and then 12 h at 100°C. The impregnated RF-xerogels were then placed in a ceramic boat, pyrolyzed at different temperature 400, 600, 700, 800 and 900°C under argon flow (100 ml/min) in a tubular oven for 2 hours Figure 5.7, and at 700°C for 0.5, 1, 2, 2.5 and 3 hr Figure 5.8. This is to study the effect

of co-pyrolysis temperature and time on the porous structure of the resulting carbons and chooses the optimum co-pyrolysis conditions. The carbon prepared from RF impregnated with *m*-phenylenediamine is designated as RFC-MPDA and carbon prepared from RF impregnated with diphenylenimine is designated as RFC-DPI, then each sample is followed by the percent of impregnation.

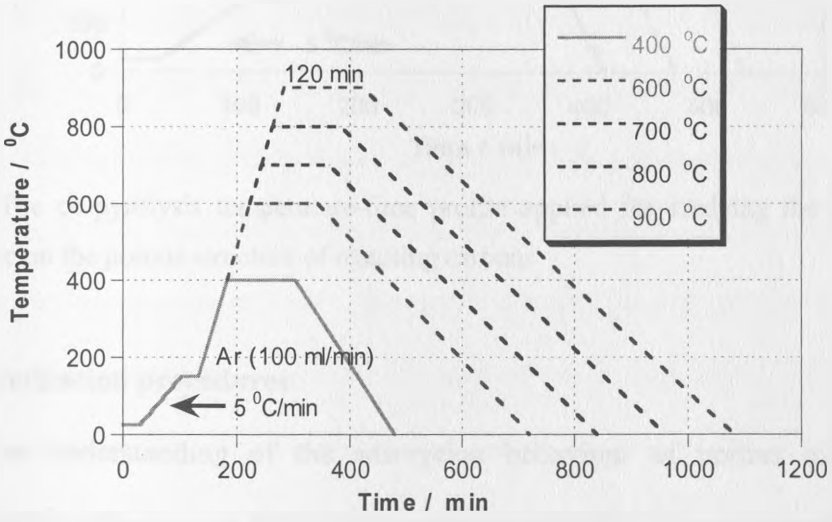

Figure 5.7 The co-pyrolysis temperature-time profile applied for studying the effect of co-pyrolysis temperature on the porous structure of resulting carbons

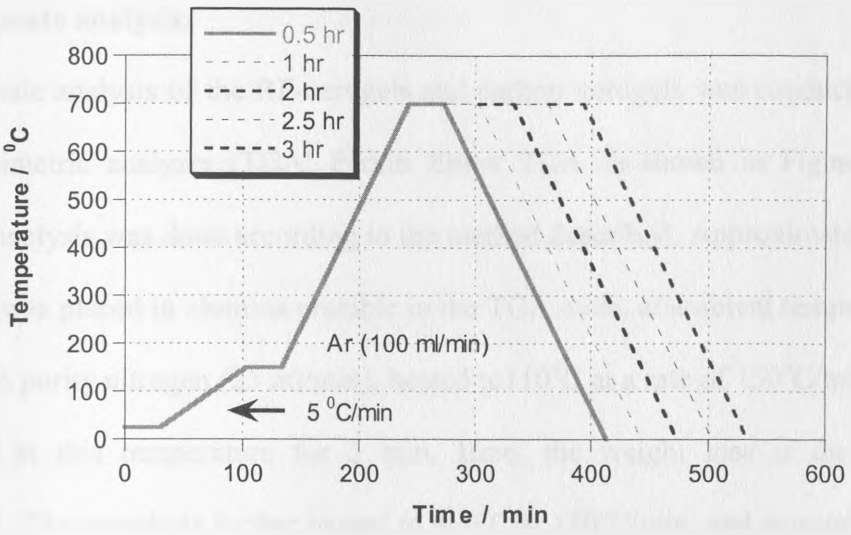

Figure 5.8 The co-pyrolysis temperature-time profile applied for studying the effect of co-pyrolysis time on the porous structure of resulting carbons

5.2 Characterization procedures.

For a proper understanding of the adsorption behaviour of porous materials, the characterization methods must take into consideration both the chemical and the porous structure, which includes the nature and the amounts of the surface chemical functional group, surface area, and pore size distribution as well as the chemical and physical characteristics of the adsorbate such as its chemical structure, polarity, and molecular dimensions. It is therefore essential to characterize the surface, pore size distribution, micropore volume, and surface area. This section deals with various techniques and experimental procedures, which have been used to characterize the prepared RF-xerogels and carbon xerogels.

5.2.1 Proximate analysis.

The proximate analysis of the RF-xerogels and carbon xerogels was conducted using a thermogravimetric analyzer (TGA; Perkin Elmer TGA 7) shown in Figure 5.9. The proximate analysis was done according to the method described. Approximately 3 mg of the sample was placed in alumina crucible in the TGA oven, at ambient temperature in a flow of high purity nitrogen (25 ml/min), heated to110°C at a rate of 150°C/min and then maintained at this temperature for 5 min. Here, the weight loss is due to water evaporation. The sample is further heated to 900°C at 150°C/min. and maintained at this temperature for 5 min. Here, the weight loss is due to volatile matter leaving the sample. Maintaining the temperature at 900°C the gas is changed to oxygen flowing at 25 ml/ min. The weight loss which now occurs is due to the carbon being burnt off in the oxygen atmosphere. The residual weight corresponds to the ash yield of the sample (Ottaway , 1982).

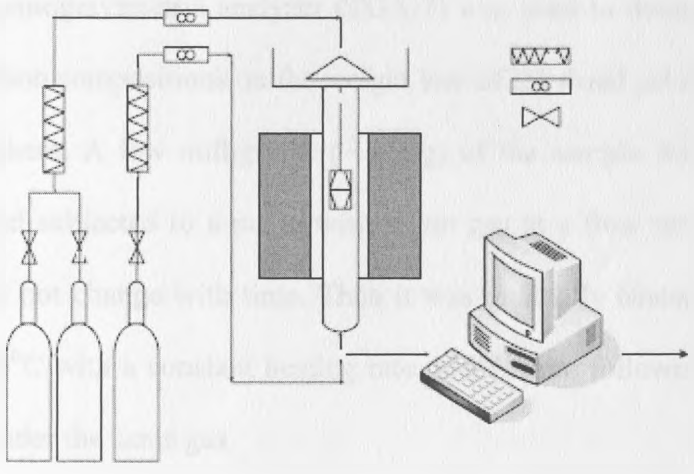

Figure 5.9 Schematic diagram of the TGA system

5.2.2 Infrared and CHN-O elemental analysis

This measurement was used for all RF-xerogels samples as well as carbon forms. Firstly, before the analysis, the samples were dried in an oven at 50–60°C (at atmospheric pressure) for 3–5 hours to guarantee complete removal of water. For IR analysis, the functional groups in the sample were qualitatively analyzed with a Fourier transform infrared spectrometer (Perkin-Elmer spectrometer spectrum 2000, USA). The FT-IR spectra of the samples were measured with a KBr pellet consists of mainly a sample of 1/200 KBr (w/w). Sample-KBr discs were prepared and scanned for IR transmittance in the range 4000 to 400 cm^{-1}. For CHN-O elemental analysis, about 30–50 mg of a sample was analysed and the data was recorded using a Perkin-Elmer Series II CHNS/O Analyser model 2400.

5.2.3 Thermogravimetric analysis.

A Perkin-Elmer thermogravimetric analyzer (TGA-7) was used to determine the effect of different preparation compositions on the weight loss of the dried gel during pyrolysis in an argon atmosphere. A few milligrams (~ 3 mg) of the sample was placed in the alumina crucible and subjected to a purge with argon gas at a flow rate of 20 ml/min until the weight did not change with time. Then it was gradually heated from ambient temperature to 1000°C with a constant heating rate of 5°C/min. followed by cooling to room temperature under the same gas.

5.2.4 Scanning Electron Microscope (SEM) analysis.

The morphology and particle size of some chosen samples were examined by the field – emission gun scanning electron microscope (FEGSEM, Sirion made by FEI of Eindhoven), which employs electron beams in the energy range 200V – 30 KV and has a field-emission tip. A magnification of 50000 was applied. A conventional (Everhart-Thornley) detector was used in the analysis.

5.2.5 Carbon porosity characterization by N_2 (77 K) adsorption.

The porous structures of the carbon xerogel were determined by nitrogen adsorption-desorption techniques, determined at the boiling temperature of liquid nitrogen (77K) using Micromeritics (Accelerated Surface Area and Porosimetry Analyzer, ASAP 2010) apparatus shown in Figure 5.10. RF carbon xerogels were first degassed at 110°C for 12 hours under vacuum, then the isotherm were measured for a relative pressure (p/p_0) range between 0.01 and 0.99. The partial pressure of nitrogen increases (adsorption direction) or decreases (desorption direction) in steps controlled by the instrument. After equilibrium had been attained for each step, the amount (volume) of nitrogen adsorbed was recorded. The porosity parameters of the sample (surface area, micropore surface area and pore volume and pore diameter) were then calculated.

The Brunauer-Emmett-Teller (BET) analysis was performed for a relative pressure (p/p_0) between 0.06 and 0.2. Total pore volume was calculated from the amount of vapour adsorbed at a relative pressure of (0.975). Following the IUPAC nomenclature,

the pore sizes 2 nm and 50 nm were taken as micro/meso and meso/macro - pores boundaries, respectively. The Horvath-Kawazoe and BJH models were used to investigate the micropore and mesopores size distributions respectively. The micropore volume was calculated from the amount of nitrogen adsorbed at relative pressure $(p/p_0)$of 0.2, and the mesopore volume was calculated by subtracting the amount adsorbed at a relative pressure of 0.2 from that adsorbed at relative pressure of 0.99.

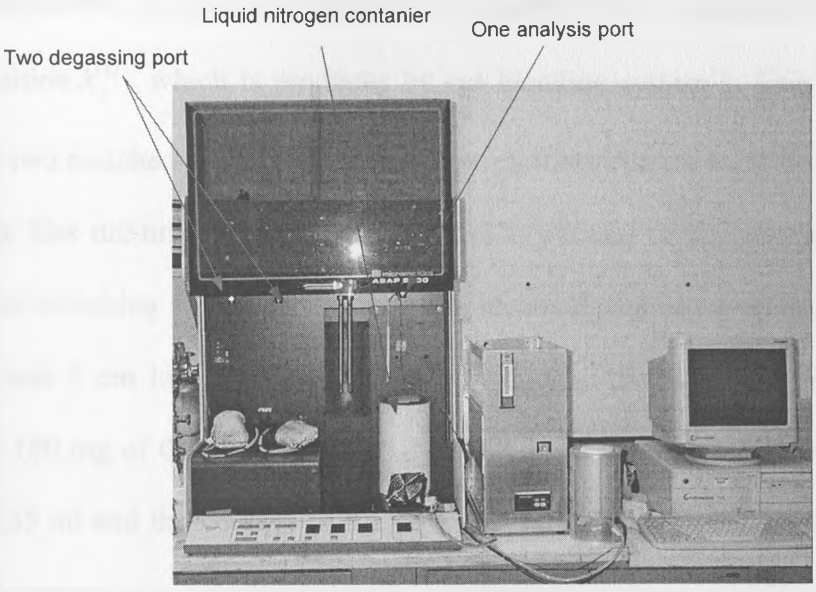

Figure 5.10 Accelerated Surface Area and Porosimetry Analyzer, ASAP 2010

5.3 Studying binary adsorption isotherm of CO_2–N_2 system by modified gas chromatograph technique.

An apparatus which was used to determine the binary gas adsorption isotherm for CO_2-N_2 system is shown diagrammatically in Figure 5.11. Before each experiment, the sample to be tested is subjected to purge with a N_2 flow of 20 ml/min while maintaining at a temperature of 100°C for 3 hr, and then allowed to cool slowly back to room temperature. This to flush any water vapour or any gas adsorbed which could interfere with the measurements. A typical experimental run starts with a main molar flow M of gas of composition X_i^O , which is produced by gas blending system 1. This mixture is then passed to two matched capillary chokes. These capillary chokes were the main flow setting devices. Gas mixture flowed from each capillary choke to opposite sides of the perturbation gas switching valve and on to the two identical packed adsorption columns. Each column was 5 cm long in length and 3 mm internal diameter and packed with approximately 160 mg of the carbons material to be tested. The volume of each packed column was 0.35 ml and the voidage of the packing estimated to be 0.376. The column outlets were connected to a standard thermal conductivity detector (TCD): the signal from this gives the composition transient time τ_x. After passing through the TCD, the gas mixture flowed to low-resistance capillary chokes. A sensitive differential pressure transducer (DPT) was connected between the upstream ends of these capillary chokes. The combination of the capillary, delay-lines and DPT acts as a differential flow meter and the differential pressure indicated by the transducer is exactly proportional to flow-rate leaving the column. The very small perturbation flows of CO_2 and N_2 were

produced by mass-flow controller. These regulators maintain a controlled pressure drop across a needle valve. Both the needle valve and pressure drop are adjustable. The regulators are stable enough to produce steady low flow-rates during the experiment. When the baselines on both the TCD and DPT were steady, the perturbation flow was switched from one-side to the other and the signals from the TCD and TPD were logged by data acquisition system. Eventually, after around 10 to 15 min., the concentration front emerged from the column and the meter recordings reached new equilibrium levels. The TCD response can be considered linear with composition for small changes in composition, and so the data could be produced to give the value of τ_x to be calculated. The TCD response is not linear with composition for large changes in composition, and so the TCD sensitivity will vary over the composition range. The DPT results were simultaneously recorded on the same DA system and can be integrated in the same way as the composition data to give the value of τ_n. The whole process was carried out for mixtures with approximate CO_2 mole fractions of 0, 0.25, 0.5, 0.75 and 1.0. The values of τ_x and τ_n were then used to calculate the isotherm gradient of CO_2-N_2 system according to the theory described in section.

For fitting the experimental results for CO_2-N_2 system adsorption on carbon xerogles samples with the isotherm models, we consider only Langmuir adsorption because it requires fewer parameters and because the isotherms are so nearly linear. For example, the binary–Langmuir equation can be written as (Buffham et al., 1999).

$$w_A = \frac{w_A^o \, y_A}{y_A + \frac{w_A^0}{R_{AB} w_B^0} y_B} \tag{5.2}$$

$$w_B = \frac{w_B^o \, y_B}{\frac{R_{AB} w_B^0}{w_A^0} y_A + y_B} \tag{5.3}$$

where;

y_A, y_B = mole fraction of species A and B in column gas phase (mol M^{-1}),

$(y_A + y_B = 1)$.

w_A, w_B = molar amounts of A and B adsorbed per unit mass of adsorbent (mol M^{-1})

w_A^0, w_B^0 = pure-component amounts adsorbed per unit mass of adsorbent (mol M^{-1})

R_{AB} = binary-Langmuir isotherm parameter for both component A and B

In equations (5.2) and (5.3) there are three parameters, namely, the pure-component amount adsorbed, w_A^0 and w_B^0, and R_{AB}, which need to be determined. However, when these three are grouped as $w_A^0 / R_{AB} w_B^0$, there are two parameters per component isotherm. Thus Equations (5.2) and (5.3) can be written as;

$$w_A = \frac{w_A^o \, y_A}{y_A + x y_B} \tag{5.4}$$

$$w_B = \frac{w_B^o \, y_B}{\frac{1}{x} y_A + y_B} \tag{5.5}$$

where $x = w_A^0 / R_{AB} w_B^0$

By differentiating equation 5.4 and 5.5 yields

$$\frac{dw_A}{dy_A} = \frac{w_A^o x}{[x + (1-x)\, y_A]^2} \tag{5.6}$$

$$\frac{dw_B}{dy_B} = \frac{w_B^o / x}{\left[1/x + \left(1 - 1/x\right) y_B\right]^2} \tag{5.7}$$

For best fitting a new term, $z = a\, y_A\, y_B$, added to Equation 5.4 and 5.5, where a, is constant (mol M^{-1}) and $y_A + y_B = 1$

Equation 5.6 and 5.7 can thus be expressed as shown in Equation 5.8 and 5.9

$$\frac{dw_A}{dy_A} = \frac{w_A^o x}{[x + (1-x)\, y_A]^2} + a\,(1 - 2\, y_A) \tag{5.8}$$

$$\frac{dw_B}{dy_B} = \frac{w_B^o / x}{\left[1/x + \left(1 - 1/x\right) y_B\right]^2} + a\,(1 - 2\, y_B) \tag{5.9}$$

The new added term will not affect the CO_2/N_2 pure amount adsorbed of the binary adsorption isotherm at the boundary conditions (i.e. $y_A = 0$ and $y_B = 1$ or vice versa). This is attributed to, the value of $a\,(1 - 2\, y_A) = 0$ when $y_A = 1/2$, it will has a *positive* value when $y_A = 0$ and it will has a *negative* value when $y_A = 1$. The same values are obtained for $a\,(1 - 2\, y_B) = 0$, *positive* and *negative* when $y_B = 1/2, 0$ and 1, respectively

The four gradient obtained from running the experiment at the boundary condition, i.e. pure CO_2 was used for the main gas and pure N_2 for the perturbation and vice versa, were then used to calculate the four unknown (w_A^o , w_B^o, x and a) in Equation (5.8) and (5.9).

Extended Langmuir equation was also considered for fitting however, we use equations 5.2 and 5.3 for its simplicity. In this equation the Langmuir isotherm for single-gas adsorption can readily be extended to $n-$ component mixture. For binary Langmuir isotherms, when expressed in terms of the amounts adsorbed and mole fractions, the Langmuir equations can be written as (Buffham et al., 1999).

$$w_A = \frac{H_A}{1 + L_A y_A + L_B y_B} \tag{5.10}$$

$$w_B = \frac{H_A}{1 + L_A y_A + L_B y_B} \tag{5.11}$$

where;

y_A, y_B, w_A and w_B have the same definition as in 5.2 and 5.3

H_A and H_B are the $w-y$ forms of the Henry's law constants for adsorption of A, B(mol M^{-1})

L_A and L_B are the $w-y$ forms of the Langmuir constants for adsorption of A, B.

By differentiating equation 5.10 and 5.11 yields

$$\frac{dw_A}{dy_A} = \frac{H_A(1+L_B)}{[(1+L_B)+(L_A-L_B)y_A]^2} \tag{5.12}$$

$$\frac{dw_B}{dy_A} = \frac{H_B(1+L_A)}{[(1+L_A)+(L_B-L_A)y_B]^2} \tag{5.13}$$

Note that L_A and L_B are shared between the two isotherms equations 5.10 and 5.11, so it was difficult to determine the four unknown L_A, L_B, H_A and H_B of equations 5.12 and 5.13 from the four gradient obtained from running the experiment at the boundary condition.

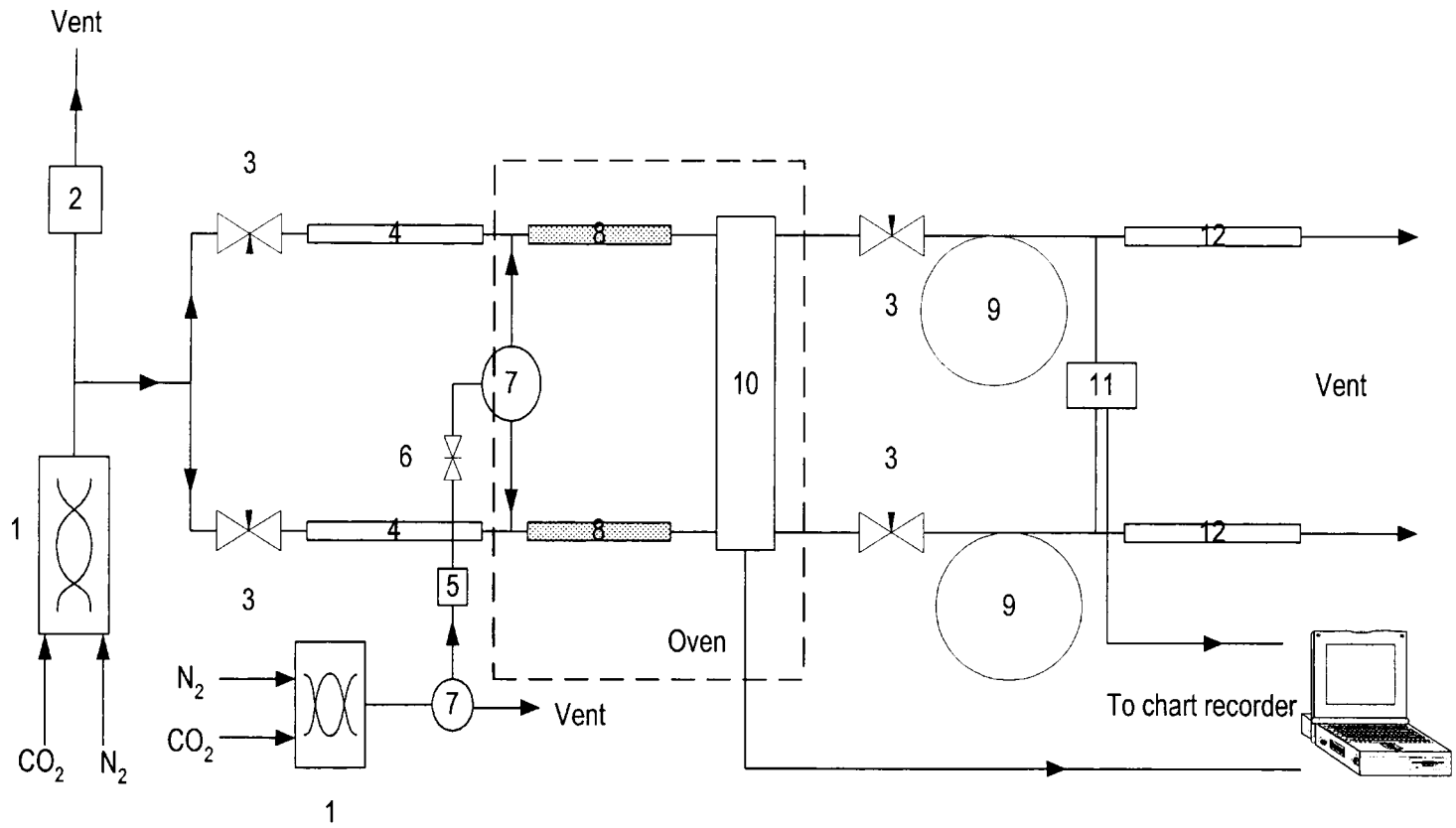

Figure 5.11 Schematic diagrams of the apparatus. The main gas mixture is split into two equal streams. Each stream passes through a column , katharometer and flow meter. 1, Gas blending system ; 2, back pressure regulator; 3, needle valve; 4, main capillary choke; 5, mass flow regulator; 6, perturbation gas on-off valve; 7, perturbation gas change over valve; 8, matched columns containing adsorbent; 9, delay lines ; 10, katharometer (TCD) ; 11, differential pressure transducer (DPT) ; 12, flow-sensing capillary

5.4 Effect of pressure on the CO_2 adsorption capacity

A 100 mg sample of the carbon xerogels was purged with a N_2 flow 20 ml/min. in a high-pressure cell shown in Figure 5.12, while heating at a heating rate of 20°C/min to a temperature of 120°C. Held at that temperature for 30 min, and then cooled to room temperature (25°C) at a rate of 10°C/min. After that, it was loaded with CO_2 to the desired pressure (10 or 20 bar). It was exposed to this CO_2 environment for 12 hr. After that, the CO_2 pressure was rapidly released. Then CO_2 desorption was carried out in TPD-MS system for the sample loaded with CO_2 at various pressure.

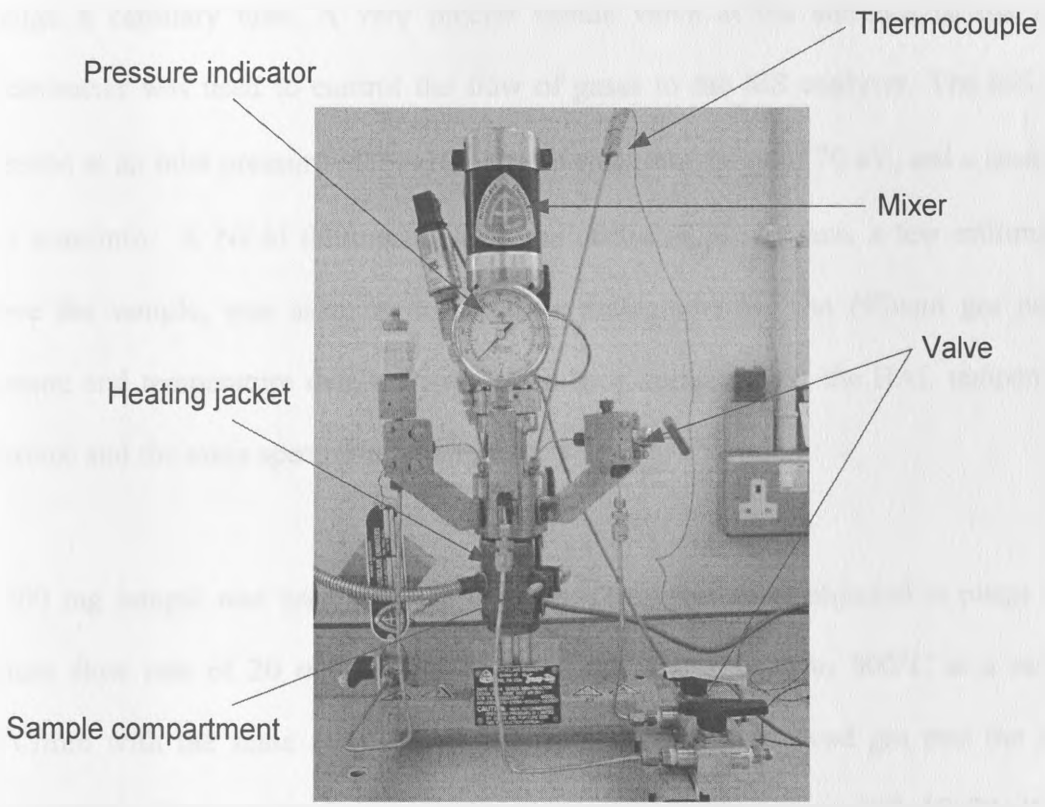

Figure 5.12 Micro-reactor (high-pressure cell) where the sample of carbons xerogels are loaded with CO_2

5.5 Studying of CO_2 desorption (regeneration process) using temperature programmed desorption/mass spectrometry (TPD-MS)

TPD-MS experiments were carried out using a temperature programming furnace coupled to an on-line Hiden Analytical HAL/HPR20 Quadruple Mass Spectrometer (QMS) shown in Figure 5.13. In the experiment, a sample was placed in the reactor (a quartz tube with an inside diameter of 4 mm). This was placed in a temperature programmed furnace and connected to the gas inlet system of the QMS via a stainless steel capillary tube. Sampling of effluent gas from the desorption chamber were taken through a capillary tube. A very precise needle valve at the entrance of the mass spectrometer was used to control the flow of gases to the MS analyzer. The MS was operated at an inlet pressure of 3×10^{-7} Pa, an electron energy of 70 eV, and a scan rate of 1 scan/min. A Ni/Al thermocouple in the centre of the furnace, a few millimetres above the sample, was used for temperature measurements. The effluent gas partial pressure and temperature data were collected by a computer via the HAL temperature interface and the mass spectrometer interface.

A 200 mg sample was used for each analysis. This was first subjected to purge with helium flow rate of 20 ml/min. for 30 min, and then heated to 900°C at a rate of 30°C/min with the same flow rate of helium to flush the evolved gas into the mass spectrometer. The mass spectrometer was adjusted to detect masses of 17, 18, 28, 30 and 44. These masses were chosen because of the CO_2 gases adsorbed and/or the decomposition product of the adsorbent.

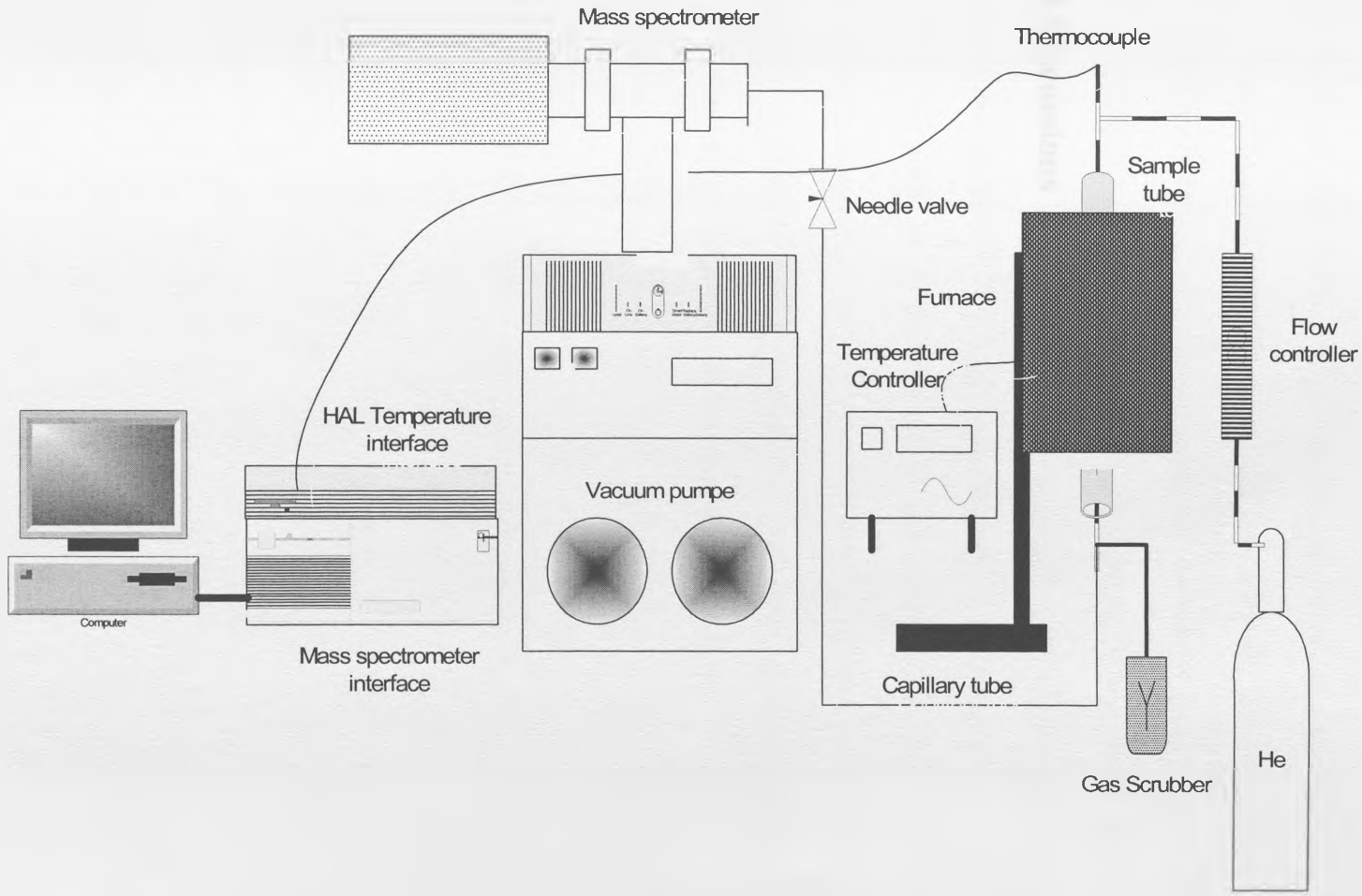

Figure 5.13 Schematic diagram of the TPD-MS system

Chapter 6

Results and Discussions

As described in Chapters 1, the main contribution of this investigation is to make high surface area nitrogen enriched carbon xerogel with a controlled pore structure, new surface chemistry and high yield, which could be regenerated and can be operated at high temperature for more efficient CO_2 separation by adsorption. This goal was pursued by experimentally develop and modify resorcinol-formaldehyde sol-gel synthesis procedure as described previously in Section 5.1. This chapter presents the results for the research tasks of this study. These results include the effect of different initial solution formulation on the evolution of the porous structure as well as surface chemistry; characterization, in addition to the results of activation and surface modification processes and their influence on the physical and chemical properties of the prepared carbons. Finally, a study of critical evaluation of the applicability of these carbons xerogels in the field of CO_2 adsorption and separations is presented.

6.1 Analysis of resorcinol-formaldehyde organic and carbon xerogels.

6.1.1 Ultimate and proximate analysis.

Table 6.1 shows the ultimate and proximate analysis of the cured dried resorcinol-formaldehyde (RF)-xerogel and its counter part carbon (RFC). All the samples were prepared under the same condition of pH=6 and R/W ratio = 0.25 cm^3/g, with different catalytic species and catalyst ratio.

From the proximate analysis we can concluded that the high fixed carbon and zero ash contents of the produced RF-xerogel make it a good starting materials for preparing activated carbons because this is can lead to formation of carbon with high yield and zero impurities. The amount of fixed carbon content is significantly decreased from 46 % sample prepared with Na_2CO_3 to 33% sample prepared with MEA, whilst the volatile content is increased from 49% to 61%. These trends were due to the release of increasing volatile matter which results from the nitrogen-containing cross-links introduced through the selection of alkanolamines compound as a catalyst in the polycondensation reaction. The increase of resorcinol to catalyst (R/C) ratio from 50 to 300 leads to decrease the volatile content from 64% to 59% , whilst the fixed carbon content increase from 32% to 37%. This would further indicate that the changing of the catalyst ratio leads to a change of the degree of the cross-linked structure which yields compounds with different degrees of polymerization. The moisture content might be due to insufficient drying but does not affect the subsequent carbon. The moisture content in the RF-xerogels did not exhibit any particular pattern with varying catalyst species or

catalyst ratio. As expected, all samples give zero ash percent indicating zero impurities. Pyrolysis increased the fixed carbon contents in the carbon xerogel samples whilst the volatile content decreased.

The ultimate analysis of the RF-xerogel shows that the selection of amine species as a catalyst during the polycondensation reaction leads to formation of nitrogen-containing cross-links introduced through RF-xerogels structure. This is obvious from the nitrogen percent in the samples prepared with amine. In addition, the selection of three different common alkanolamine MEA, DEA, and MDEA leads to the observed difference of the amount of nitrogen atom incorporated to the final RF-xerogels structure (MEA> DEA> MDEA).

Table 6.1 Analysis of resorcinol-formaldehyde (RF)-xerogel and carbon xerogels (RFC) prepared under the same condition of pH=6 and R/W= 0.25 g/cm^3 with different catalyst species and catalyst ratio.

Nomenclature	Ultimate (wt% dry-ash-free basis) (± 0.05)				Proximate (wt%) (± 0.05)			
	C	H	N	[1]O	Moisture content	Volatile content	Fixed carbon	Ash
[2]RF-MEA100	62.98	5.45	0.42	31.15	4.72	61.81	33.47	0.00
RF-DEA100	64.73	5.24	0.35	29.68	4.41	62.32	33.27	0.00
RF-MDEA100	64.67	5.63	0.31	29.40	2.54	63.73	33.73	0.00
RF-$K_2CO_3$100	73.04	6.12	0.00	20.84	2.35	50.42	47.23	0.00
RF-$Na_2CO_3$100	72.90	6.00	0.00	21.10	3.56	49.77	46.67	0.00
[3]RF-MEA50	60.54	5.32	0.56	33.58	3.72	63.72	32.56	0.00
RF-MEA100	62.98	5.45	0.42	31.15	4.74	61.81	33.45	0.00
RF-MEA200	64.12	5.98	0.34	29.56	4.02	59.12	36.86	0.00
RF-MEA300	64.89	5.78	0.27	29.06	4.21	58.64	37.15	0.00
RFC-MEA100	87.25	2.12	0.41	10.22	1.32	39.57	59.11	0.00
RFC-DEA100	88.24	2.65	0.34	8.77	1.51	40.42	58.07	0.00
RFC-MDEA100	89.69	3.24	0.31	6.76	0.93	38.71	60.36	0.00
RFC-$K_2CO_3$100	90.25	4.21	0.00	5.54	2.17	27.41	70.42	0.00
RFC-$Na_2CO_3$100	93.26	4.44	0.00	2.30	1.92	24.20	73.88	0.00

[1] The oxygen contents calculated by difference. [2]RF-xerogel samples followed by the catalyst species used during the polycondensation reaction and the resorcinol to catalyst ratio(R/C). [3]Carbon xerogel samples followed by the catalyst species and catalyst ratio. Note; the number of significant figures quoted in the table an indication of precision

The different R/C ratios lead to a slight change in the amount of nitrogen incorporated in the RF-xerogels structure. As expected, carbonization increased the carbon contents whilst the oxygen contents decreased. This is due to the removal of hydrogen and oxygen atoms which occurred through the breaking of the C-O and C-H bonds during pyrolysis process. However the nitrogen content was more stable and could withstand heat treatment.

6.1.2 Thermogravimetric analysis

Figures 6.1 and 6.2 show that all of the TG curves indicate a common behaviour; the catalyst species and the catalyst ratios in the synthesis of the RF xerogels do not lead to any great difference in the behaviour of RF xerogels during carbonization process. However, the carbon yield seems to be slightly varied according to catalytic species and catalyst ratio. The thermogram can be divided into four stages. The first stage is up to 200°C and the second stage up to 400°C, the weight losses in both stages being around 25 %. The third stage, in which the main degradation of RF-xerogels takes place, starts from approximately 450°C and the degradation components of around 35 % are released up to 850°C. In the fourth stage, T > 1000°C, the sample mass does not change.

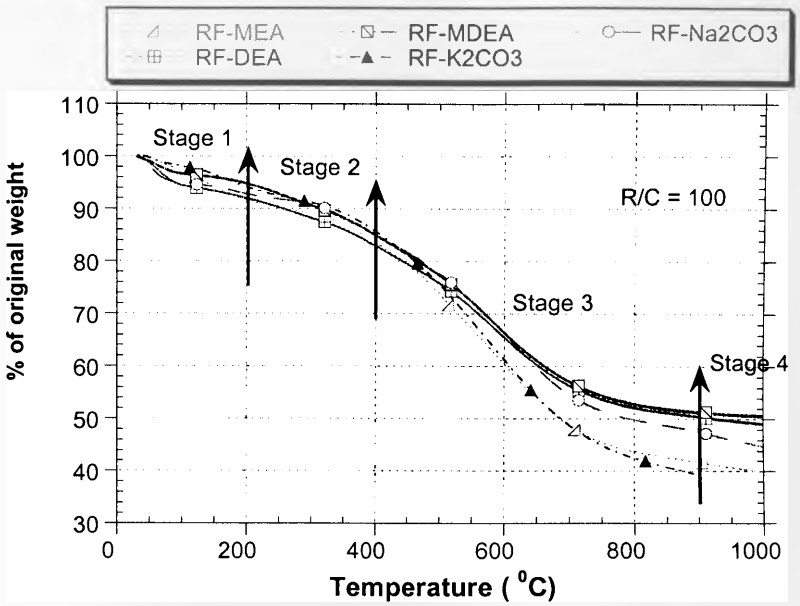

Figure 6.1 TG curves of a RF xerogels prepared with different catalyst species and the same R/C ratio, a heating rate of 5°C/min in argon flow 20 ml/min.

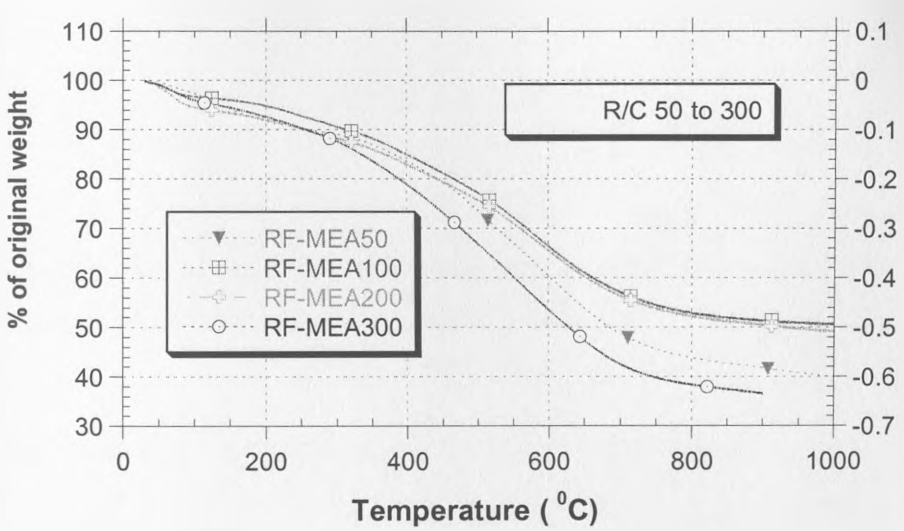

Figure 6.2 TG curves of a RF xerogels prepared with the same catalyst species and different R/C ratio, a heating rate of 5°C/min in argon flow 20 ml/min

The differential thermal gravimetric (DTG) curve Figure 6.3 shows two peaks around temperatures of 165 and 600°C and a shoulder at 400°C. The first peak around 165°C would be attributed to desorption of acetone, water, and residual organic precursor. The shoulder around 400°C may be related to the carbonization reaction of the organic xerogel, which involve the breaking of C-O bonds, while the peak around 600°C related to breaking of C-H bonds. All the DTG curves show the same behaviour so only one example is presented.

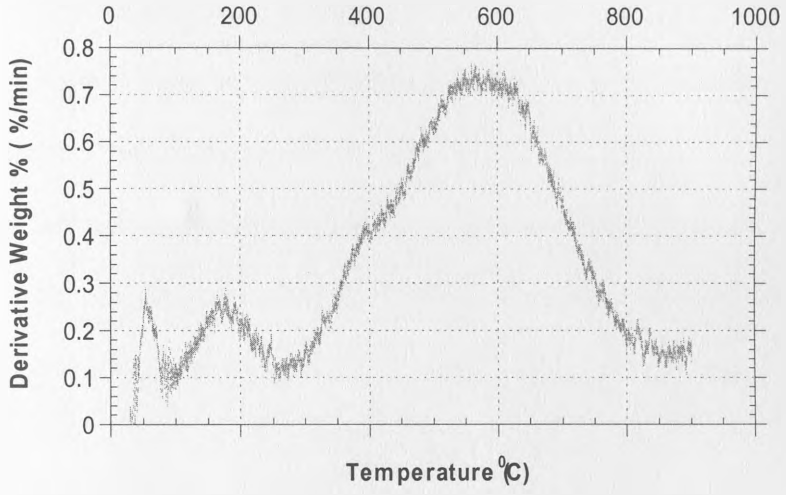

Figure 6.3 DTG curve for the RF-xerogels prepared with MEA as a catalyst with R/C ratio 100, a heating rate of 5^0C/min in argon flow 20 ml/min

6.1.3 FTIR analysis

Figure 6.4 a and b show the IR spectra for the synthesis RF xerogels with different type of catalytic species and the same R/C ratio = 100. The samples are classified into two groups according to their behaviour. The strong peak at ~ 3420 cm^{-1} arises from phenolic –OH stretching, indicating the existence of intermolecular OH···HO–

interactions (H-bonding). The peak at 1637 cm^{-1} and a doublet peak at 1612 and 1593 cm^{-1} arise due to the quadrant aromatic ring-stretching of the mixture of 1,2,4- and 1,2,6-trisubstituted and phenyl–alkyl ether type substituted aromatic ring structures. Peaks arising from 1,2,4- and 1,2,6-trisubstituted and 1,2,4,6-tetrasubstituted aromatic ring stretch and CH_2 asymmetric bending show up at 1506, 1474, and 1427 cm^{-1}, respectively. The strong intensity of the peak at 1506 cm^{-1} indicates that this RF-xerogels is abundant in 1,2,4,- or 1,2,6- trisubstituted aromatic ring units as might be expected from the resol type phenolic resin. Among several peaks in the region of 1300–1000 cm^{-1}, the peak at 1187 cm^{-1} characterize the alkyl–phenyl ether stretching is very strong as compared with various –C–O– ether stretching modes, which indicates that alkyl–phenyl ether linkages are predominant in these RF-xerogel. Based on the FT-IR spectrum analysis, the chemical structure of RF-xerogels is schematically sketched in Figure 6.5.

The main nitrogen functional groups introduced by the selection of amine species as a catalyst in the polycondensation reaction of resorcinol with formaldehyde are as follows, amides and amines mixed in the very large band around 3430 cm^{-1}. Nitrile (C≡N), lactame groups should be found at 2247 cm^{-1} and 1730 cm^{-1}, respectively. There were also peaks seen at 1360-1250 cm^{-1}, identified as originating from aromatic primary, secondary and tertiary amine, C-N stretch. Open–chain imino (-C=N-) at 1690 cm^{-1} and finally amide group at 1625 cm^{-1} (Coates, 2000; Garcia, 2000; Burg et. al., 2002) The selection of three different alkanolamine species during the polycondensation reaction

did not lead to a significant change either in peak width or peak shift in the IR spectrum. Figure 6.6 shows the possible structure of cured RF-xerogel, which contains chemically bound nitrogen in the form of ammine bridges.

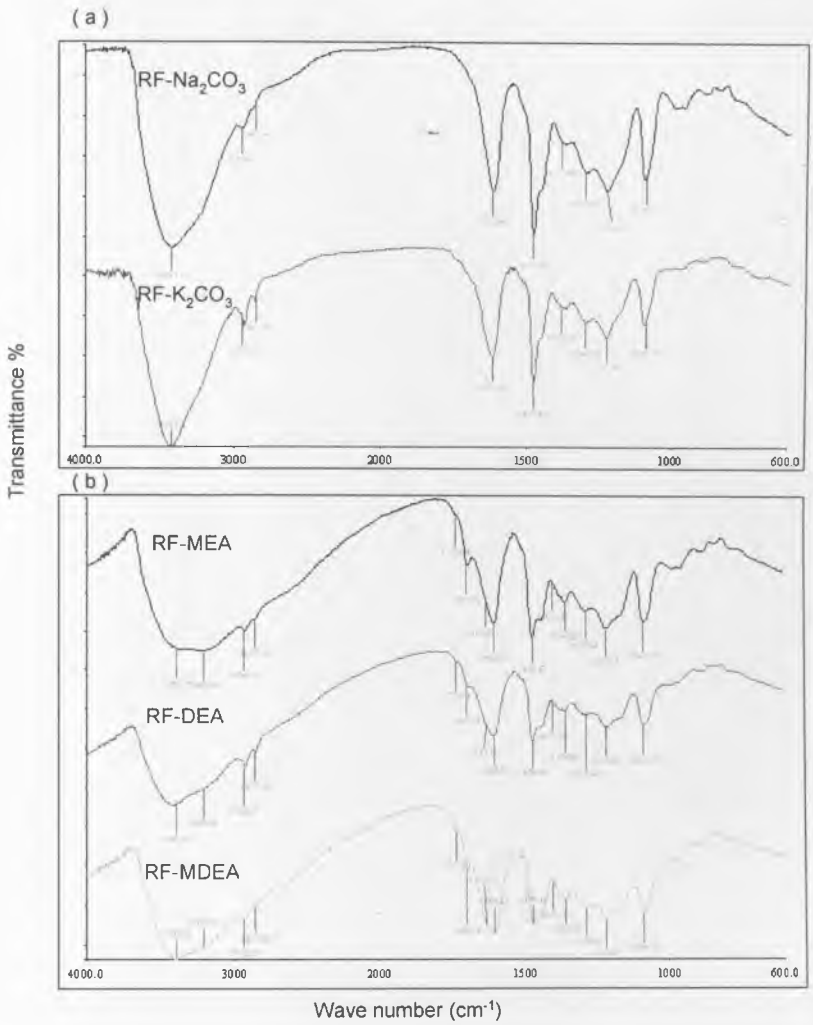

Figure 6.4 FTIR spectra for the synthesis RF-xerogel prepared with different type of catalytic species and the R/C = 100, R/W=0.25 g/cm^3 and pH=6. (a) K_2CO_3 and Na_2CO_3 are used as catalysts, while (b) MEA, DEA and MDEA are selected.

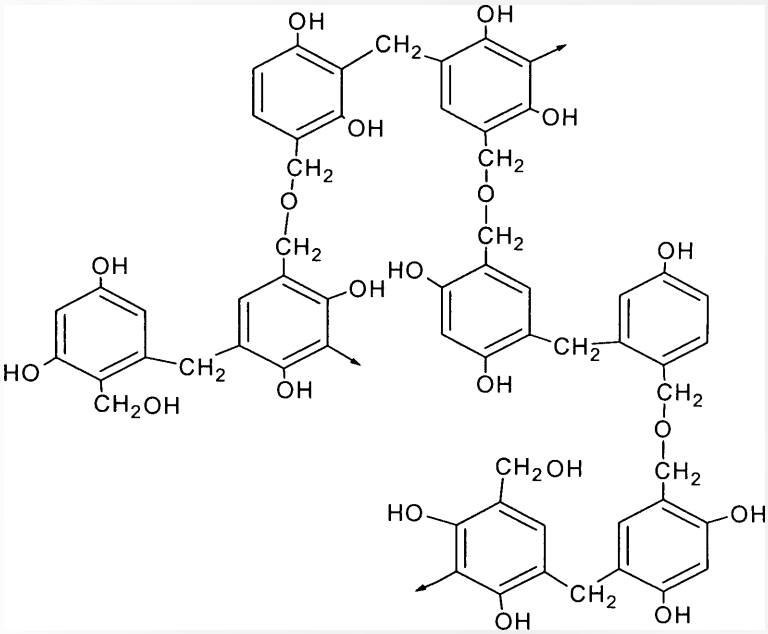

Figure 6.5 A possible chemical structures of RF-xerogels samples prepared with Na_2CO_3 or K_2CO_3 as a catalyst.

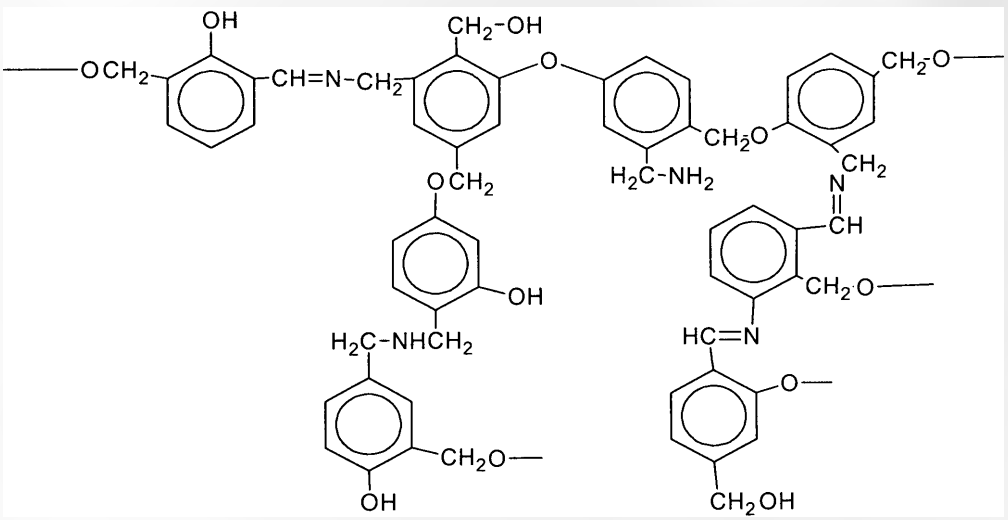

Figure 6.6 A possible chemical structures of RF-xerogels sample results from the selection of amine species as a catalyst, the proposed diagram shows the nitrogen-containing cross-link in the form of ammine bridges and the other possible positions for the nitrogen incorporation.

6.2 RF carbon xerogels pore structure.

6.2.1 Effect of changing catalyst species and the catalyst ratios on the pore structure.

In this study the influence of the type of basic catalyst and the resorcinol to catalyst ratio on the porosities of the produced RF carbon xerogels was investigated. The catalysts were classified into two families as a function of their behaviour: MEA, DEA and MDEA as the first group, while the second group are Na_2CO_3 and K_2CO_3. All samples were prepared under the conditions of R/W=0.25 g/cm^3 and pH=6 with subcritical drying conditions, followed by carbonization at 850°C for 180 min in argon flow 100 ml/min. The amount of N_2 adsorbed at 77 K is plotted against the relative pressure in Figures 6.7 - 6.11.

The samples vary from a micro-macroporous solid (RF-K_2CO_3: combination of type I and II isotherms) to micro-mesoporous solid (RF-Na_2CO_3: combination of types I and IV isotherms), and then to an exclusively microporous material (RF-MEA, DEA, MDEA: type I isotherm). The type IV isotherm originates from both non-porous and mesoporous solids. It describes a multilayer adsorption process where complete filling of the smallest capillaries has occurred. Whilst type I isotherm is typical of microporous solids where only monolayer adsorption occurs. In these micropores, filling occurs significantly at relatively low partial pressure $< 0{\cdot}1\ p/p_o$, the adsorption process being complete at $p/p_o \approx 0{\cdot}5$. The main feature of such isotherm is the long plateau which is indicative of a relatively small amount of multilayer adsorption on the open surface.

Micropore filling may take place either in pores of molecular dimensions (i.e. primary micropore filling) at very low p/p_o or in wider micropores (co-operative filling) over a range of high p/p_o. The isotherms for the samples prepared by MEA, DEA and MDEA exhibit low-pressure hysteresis, which could be attributed to irreversible up-take of adsorptive molecules in pores of about the same width as that of adsorbate molecules, and/or swelling of non-rigid pore walls (Lowell, 1991). Open hysteresis with increase in desorption branch was also observed in the isotherms which we did not have an explanation for such phenomena.

In Figures 6.7 - 6.11 it is worth states that the lowest relative pressure which have been achieved by the Accelerated Surface Area and Porosimetry Analyzer, ASAP 2010 for N_2 (77K) adsorption was in order of 10^{-2}. This level of relative pressure is considered to be acceptable for calculation of micropores volume by Horvath-Kawazoe model. This is attributed to at that level of relative pressure the micropores will most likely be filled. In general, at very low relative pressure and due to the high adsorption potential associated with micropores, coupled with the use of adsorbate substantially below their critical temperature (necessary for physical adsorption) lead to significantly hinder the N_2 diffusion, resulting in lengthy equilibration times. Most adsorption apparatus, using liquid nitrogen (77K) can operate for up to 48 hours on a single Dewar of liquid N_2. However, for high resolution, analysis of the adsorption within micropores can often take much longer than this, necessitating multiple runs using the same sample.

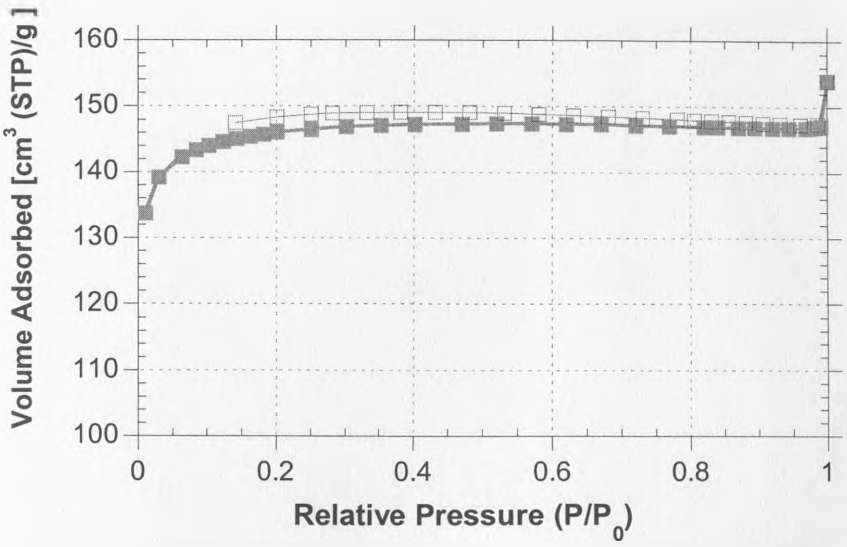

Figure 6.7 Adsorption profiles of N_2 at 77 K on the RF carbon xerogels generated with MEA as a catalyst with R/C=300. Open keys indicate adsorption, and closed keys indicate desorption.

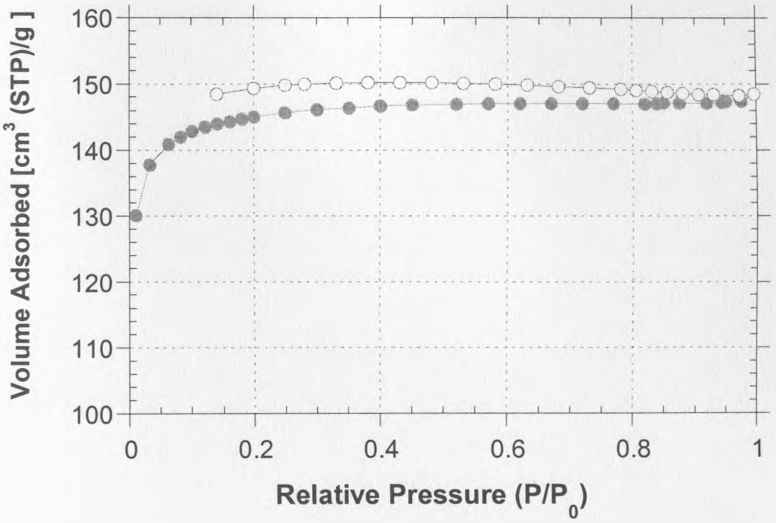

Figure 6.8 Adsorption profiles of N_2 at 77 K on the RF carbon xerogels generated with DEA as a catalyst with R/C=300, Open keys indicate adsorption, and closed keys indicate desorption

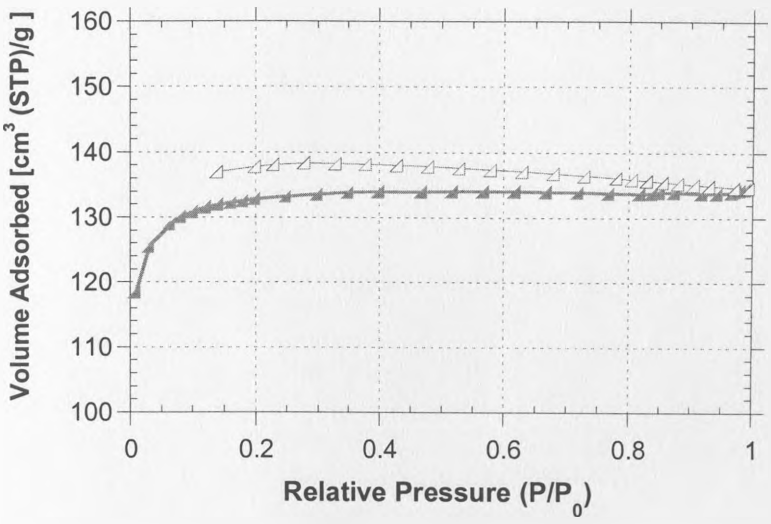

Figure 6.9 Adsorption profiles of N_2 at 77 K on the RF carbon xerogels generated with MDEA as a catalyst with R/C=300, Open keys indicate adsorption, and closed keys indicate desorption

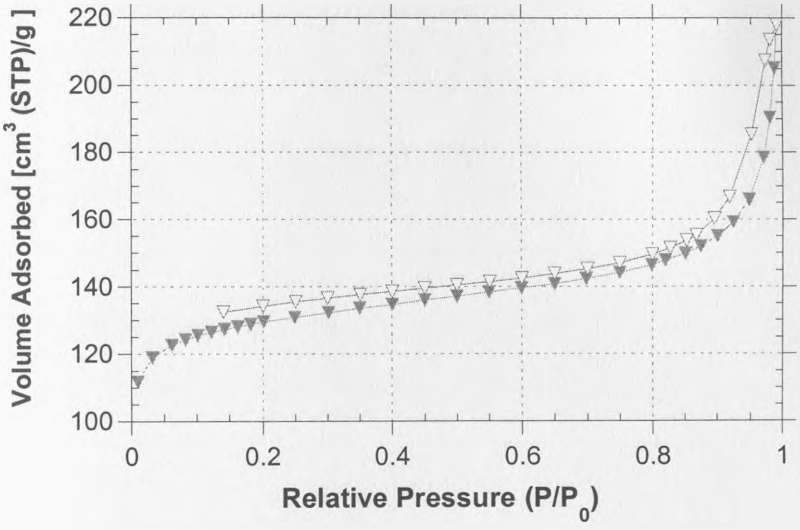

Figure 6.10 Adsorption profiles of N_2 at 77 K on the RF carbon xerogels generated with K_2CO_3 as a catalyst with R/C=300, Open keys indicate adsorption, and closed keys indicate desorption

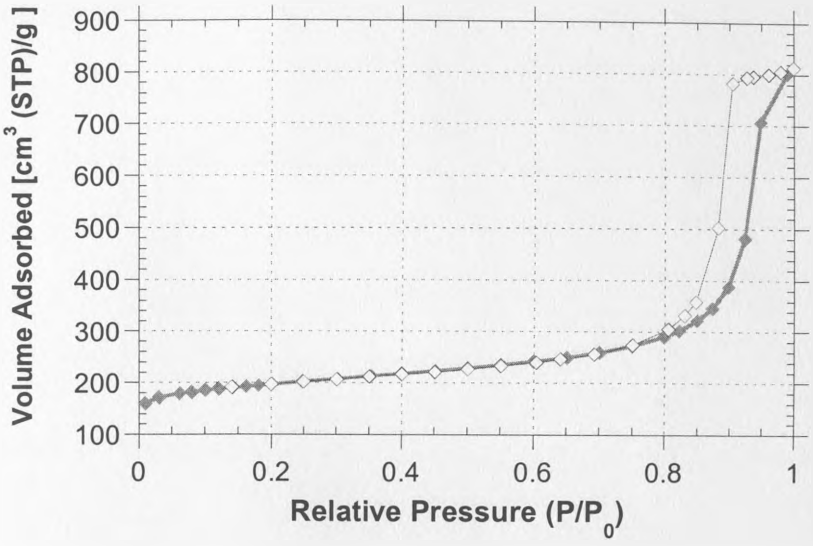

Figure 6.11 Adsorption profiles of N_2 at 77 K on the RF carbon xerogels generated with Na_2CO_3 as a catalyst with R/C=300, Open keys indicate adsorption, and closed keys indicate desorption

When K_2CO_3 and Na_2CO_3 were selected as a catalyst, the N_2 adsorption isotherms are different; they exhibit a significant increase in adsorption at higher relative pressure. The knee comes to be more open and rounder and the slope of the plateau increases. Also, the nitrogen uptake occurs mostly at (p/p_o >0.9). This indicates that the meso- or macropore structure in the sample significantly developed. Both isotherms are characterized by hysteresis loops, which appear in the multilayer rang of physisorption isotherms. This kind of loops is generally associated with capillary condensation. It is well known that most mesoporous adsorbents give distinctive and reproducible hysteresis loops (de Boer 1958; Sing et al., 1985).

The main difference when different catalysts are used is the aggregation of primary particles of the RF-xerogel. This leads to different gelation mechanisms in each sample. Polymerization of resorcinol with formaldehyde involves two reactions; addition of formaldehyde to resorcinol and condensation of the hydroxyl-methyl derivatives formed. The first reaction is catalyzed by bases, generally alkaline carbonates. Therefore, the chemistry of the process is highly dependent on the catalyst used. The primary role of the catalyst could be summarized as follows; the presence of the catalyst results in the creation of ionized resorcinol by hydrogen abstraction from one of the OH group to form an O. The formaldehyde molecules then attach themselves to the carbon ring at either two of the 2, 4, or 6 sites to form a hydroxyl-methyl derivative of resorcinol containing two CH_2OH functional groups (Lin et al., 1997). The use of catalyst is important because it is the creation of the ionized resorcinol by the catalyst that dramatically increases the chances of formaldehyde bonding, which creates the resorcinol derivative that undergoes condensation. So different type of catalyst could leads to different reaction mechanisms. The effect of the alkaline carbonate might be related with the different polarization power of Na^+ and K^+ ions due to their different size. Horikawa et al. (2004) reported that the employment of sodium or potassium carbonates or bicarbonates as catalysts in the preparation of RF carbon aerogel, with R/C ratio of 50, affected the mesopore volume and, in some cases, the mean pore width of the carbon aerogel obtained. On the other hand, they found that larger mesopore volumes were yielded by sodium than potassium salts. Moreover, as reported by Rojas et. al, 2004 when the intention is to incorporate certain metals (e.g., Pt, Pd, or Ag) in the final

structure of the RF carbon gels, various salts of theses metals are used as the catalyst. The addition of this metals and the use of their salts as a catalyst leads to increases of the meso- and macrospore volumes and results in increase in total pore volumes and surface area under certain conditions. Therefore, in this work the selection of different amine compounds as a catalyst were in purpose to incorporate nitrogen atom in the RF-xerogels structure and consequently this result in increasing basicity of the derived carbon.

Figure 6.12 shows the effect of the resorcinol to catalyst (R/C) ratio on the amount of nitrogen adsorbed. It can be seen that, as the R/C increases from 50 to 300 the isotherms are shifted from combination of type I and IV isotherms to type I isotherm with almost horizontal plateau, which extends up to p/p_o >0.9, indicating that the carbon xerogels prepared with ratio R/C ≥300 are mainly ultramicroporous, whilst the development of mesoporesity were significantly observed with R/C ratio of 50. According to the international union of pure and applied chemistry (IUPAC) classification of hystersis loops, the hystersis loops are shifted from type H1 (sample prepared with R/C ratio 50) to type H2 (sample prepared with R/C ratio 100) and then finally to type H3 (sample prepared with catalyst ratios 200 and 300). Type H1 is a fairly narrow loop with very steep and nearly parallel adsorption and desorption branches. In contrast, the Type H2 loop is broad with a long and almost flat plateau and a steep desorption branch. Type H1 loops are given by adsorbents with a narrow distribution of uniform pores (eg. open-ended tubular pores). Type H2 loops correspond to adsorbents with complex pore

structures and tend to be made up of interconnected networks of pores of different size and shape. Type H3 loops are usually given by the aggregates of platy particles or adsorbents containing slit-shaped pores (Sing et al., 1985).

The R/C ratio is an important element in determining the structure of the carbon xerogels. The catalyst assists in the formation of the RF xerogels by ionizing the resorcinol molecules. The ionization of the resorcinol increases its propensity to react with formaldehyde to create functional monomer groups. The functional monomer groups cross-link to create nanometer-size clusters.

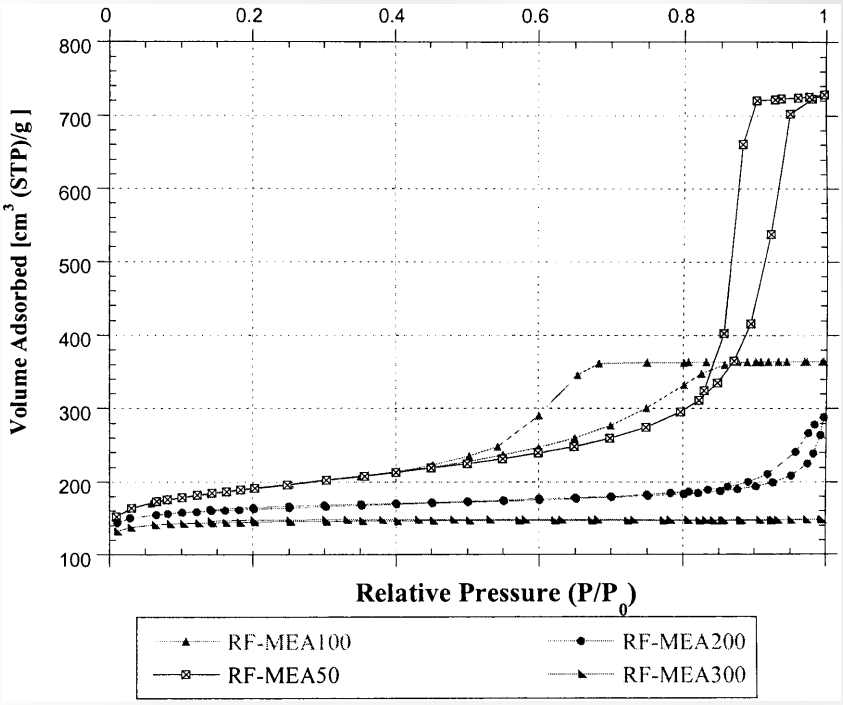

Figure 6.12 Adsorption profiles of N_2 at 77 K, on the RF carbon xerogels generated with MEA as a catalyst with different R/C ratios.

Once a cluster is created, additional monomer groups will attach to the cluster. As the clusters grow in size, the surface area of the cluster and thus the number of reaction sites increases. The result is exponential growth in cluster size. Some of the methylene ether bridges break down to methylene bridges and release formaldehyde. Consequently, excess formaldehyde is always present and the particle growth continues until all the resorcinol is consumed (Cook et al., 1997). The ratio of the resorcinol to the catalyst (R/C) determines the likelihood of a cluster being formed. When the ratio has a small value, such as 50, the amount of catalyst is very large. The initial result is a significant number of clusters. With a large number of clusters each attracting resorcinol monomers, the rate of particle growth is slowed. The end effect is that more clusters exist and each cluster has a small particle diameter. When the ratio is large, the amount of catalyst is fairly small. Fewer clusters are initially created, which results in less competition over resorcinol monomers. The clusters that do appear can easily grow in size. Due to how the number of reaction sites increases with volume, these clusters grow exponentially. The result is a small number of particles with large particle diameters (Yamatoto et al., 2001).

The characteristic pore properties of the RF carbon xerogels prepared with different catalyst species and different catalyst ratios are listed in Table 6.2, while Figure 6.13 shows the percent micro-mesopores volume fraction for different carbon xerogels prepared with different catalyst species and under the same condition of R/C ratio of 300 The specific surface area values varies from 430 m^2/g, (RFC-K_2CO_3), to 670 m^2/g, (RFC-Na_2CO_3). The mesopores volumes varies from 0.14 and 0.95 cm^3/g for samples RFC-

K_2CO_3 and RFC-Na_2CO_3, to $\approx$ 0.02 cm^3/g for samples RFC-DEA and RFC-MDEA respectively. The selection of two different alkaline carbonate leads to two different types of RF-xerogels texture and consequently different carbon porosity. This effect might be related with the different polarizing power of Na^+ and K^+ ions due to their different size. Moreover, the selection of three different alkanolamine leads to different reaction mechanism of polycondensation which result in producing carbons with different pore texture as well. The surface area is in the order MEA > DEA > MDEA.

Table 6.2 The characteristic pore properties of RF carbon xerogels (all the samples prepared at the same pH=6. R/W ratio = 0.25 g/cm^3)

*Nomenclature	R/C.	S_{BET}[a] ± 10 (m^2/g)	V_t[b] ± 0.02 (cm^3/g)	V_{mic}[c] ± 0.02 (cm^3/g)	V_{mes}[d] ± 0.02 (cm^3/g)	D_p[e] ± 0.02 (nm)
RFC-Na_2CO_3	300	670	1.26	0.30	0.95	7.48
RFC-K_2CO_3	300	430	0.34	0.20	0.14	3.09
RFC-MEA	300	480	0.24	0.23	0.01	1.95
RFC-MDEA	300	440	0.21	0.21	0.00	1.87
RFC-DEA	300	460	0.23	0.22	0.00	1.97
RFC-MEA	50	650	1.13	0.29	0.83	6.91
RFC-MEA	100	600	0.56	0.29	0.27	3.75
RFC-MEA	200	540	0.45	0.25	0.19	3.26
RFC-MEA	300	480	0.23	0.22	0.00	1.89

*Each sample followed by the catalyst used during the polycondensation reaction

[a] Specific surface area determined from the BET equation. [b] Total pore volume, calculated from the amount of vapour adsorbed at a relative pressure of (0.99). [c] Micropore volume determine by Horvath-Kawazoe model, calculated from the amount of nitrogen adsorbed at relative pressure (p/p_0) of 0.20. [d] Mesopore volume, calculated by subtracting the amount adsorbed at a relative pressure of 0.2 from that adsorbed at relative pressure of 0.99. [e] Mean pore diameter, calculated from (4 V_t/S_{BET}). Note; the number of significant figures quoted in the table an indication of precision

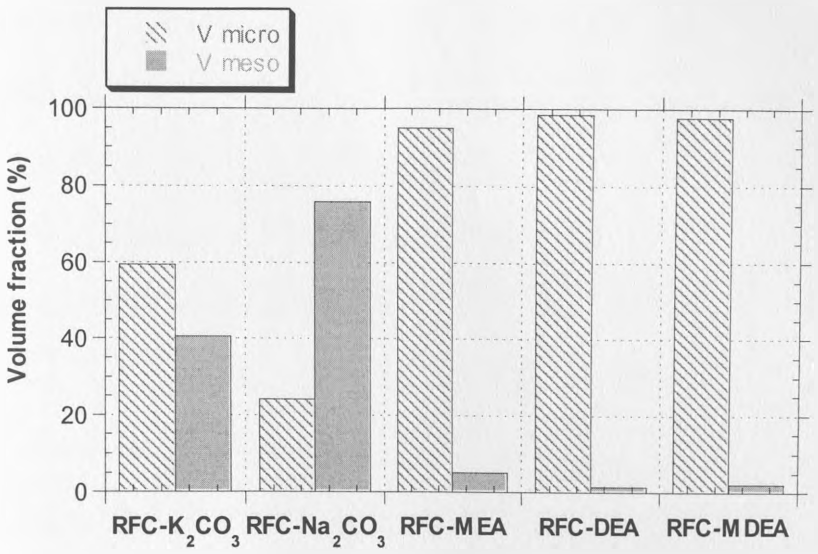

Figure 6.13 The percent micro-mesopores volume fraction for different carbon xerogels prepared with different catalyst species and under the same condition of R/C ratio of 300

The amount of catalyst plays indeed a major role in the formation mechanism of the RF precursor gels by changing the sizes of primary particles forming the cross-linked structure of RF xerogels and sequentially affects the porous properties of the RF carbon xerogels. As R/C decreased from 300 to 50 the total pore volume increase from 0.23 cm^3/g (RFC-MEA300), to 1.13 cm^3/g (RFC-MEA50). The same trend could be observed for the surface area and the mean pore diameter. On the other hand, the micropore volume fraction increases from 26% (RFC-MEA50), to 97 % (RFC-MEA300) as R/C decreases from 300 to 50. Moreover, the mean pore diameter is strongly affected by the R/C ratio, as one can observe an obvious decrease in the mean pore diameter due to the increase of R/C ratio. On conclusion, the RF carbon xerogels prepared by K_2CO_3 and Na_2CO_3 as a catalyst are mainly mesoporous, while those prepared by amine species are

mainly microporous. The volume fractions of micropores vary from 24% (RFC-Na_2CO_3), to 98% (RFC- DEA).

Figure 6.14 and 6.15 illustrate the BJH adsorption pore distribution of mesopores size for the RF carbon xerogels synthesized with different catalytic species. The results are divided into two groups according to the nature of the resulting carbons. The development of the mesoporosity is strongly dependent on the change of the catalyst applied. The results show that, an increase in mesopores is observed for the sample prepared by K_2CO_3 and Na_2CO_3. Sample prepared with Na_2CO_3 has a significant one peak around 30 nm while the sample prepared with K_2CO_3 has broad peaks in the meso- and macropore range. On the other hand, the samples prepared by amines compound have one sharp peak with maximum intensity at $\approx$3 nm. Figure 6.16 shows Horvath-Kawazoe micropore size distribution. All of the samples have a sharp peak around 1 nm. However, the micropore size distribution for the sample prepared with Na_2CO_3 is more open and rounder which indicates a broad pore size distribution. Despite the percent of the microporosity in the sample prepared with Na_2CO_3 is less than the others, the micropore volume of this sample is greater.

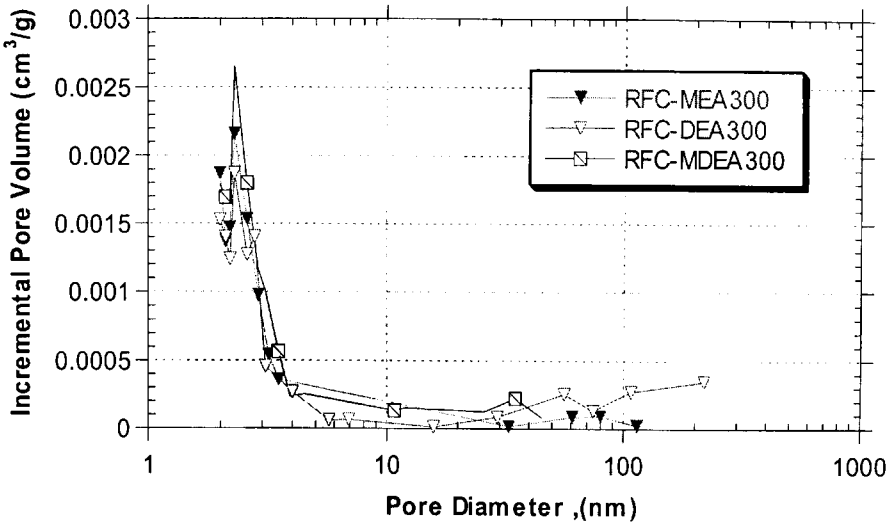

Figure 6.14 The BJH adsorption pore distribution of meso- size for the RF carbon xerogels synthesized with different amine catalytic species

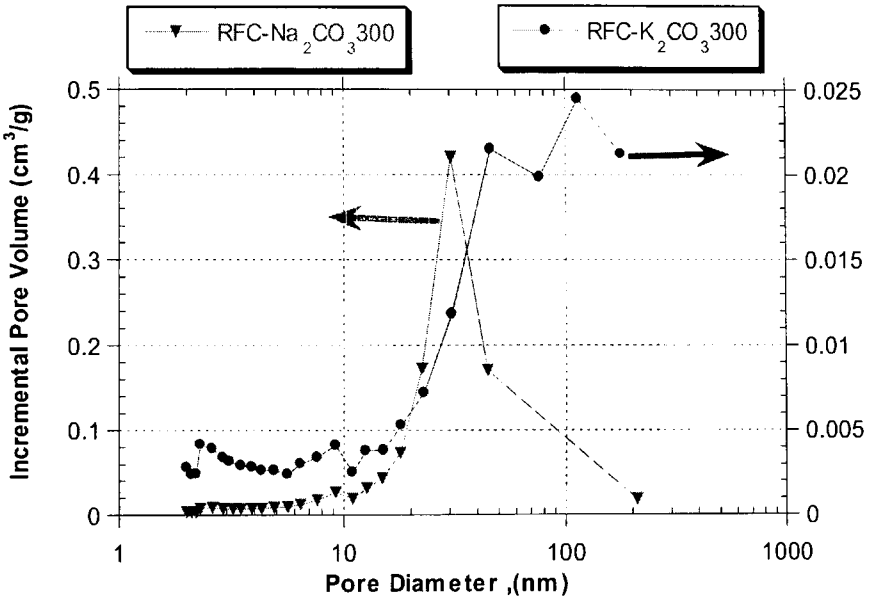

Figure 6.15 The BJH adsorption pore distribution of meso- size for the RF carbon xerogels synthesized with different carbonates catalytic species.

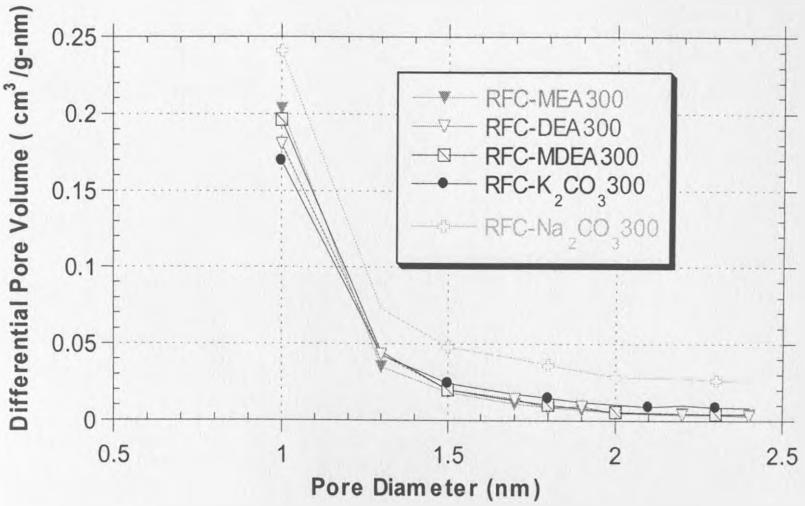

Figure 6.16 The Horvath-Kawazoe micropore size distribution for the RF carbon xerogels synthesized with different carbonates catalytic species.

6.2.2 Effect of resorcinol to water ratio (R/W) on the porous structure of RF carbon xerogels.

To elucidate the influence of R/W on the porous structure of RF carbon xerogels, the samples were prepared using R/C = 100, pH= 6 and MEA as a catalyst. The variations of pore characteristics with R/W for the RF carbon xerogels prepared are shown in Figures 6.17 and 6.18. The BET surface area (S_{BET}) vary from 540 m^2/g (R/W=0.05 g/cm^3), to 470 m^2/g (R/W= 0.35 g/cm^3), reach its maximum value 730 m^2/g at (R/W=0.2 g/cm^3). Choosing R/W values lower than 0.05 the sol did not allow the gel to dry. The micropore surface area does not vary significantly with R/W in the range of 0.05 to 0.2 g/cm^3 and then gradually decreased with further increase of R/W. This indicated that at higher R/W value more larger pore are formed which did not contribute much to the surface area.

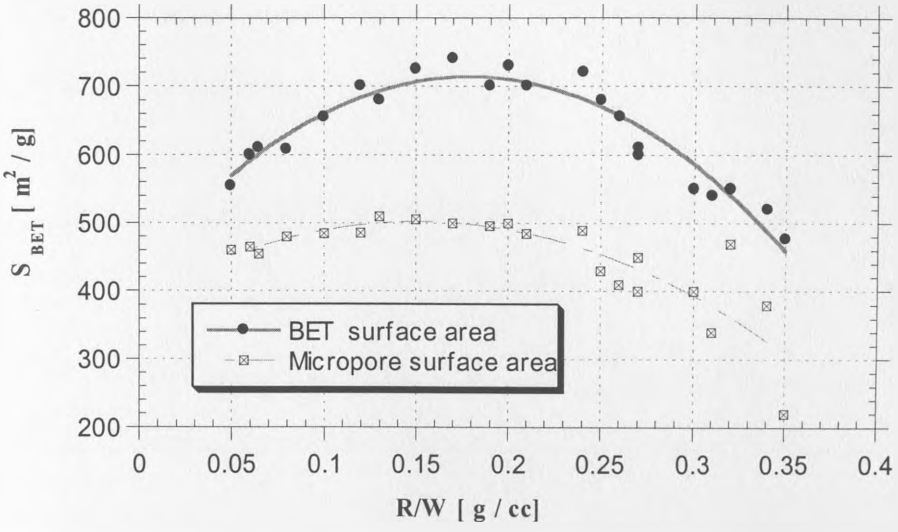

Figure 6.17 Influence of resorcinol to water ratio (R/W) on the BET surface area and micropore surface area of carbon xerogels

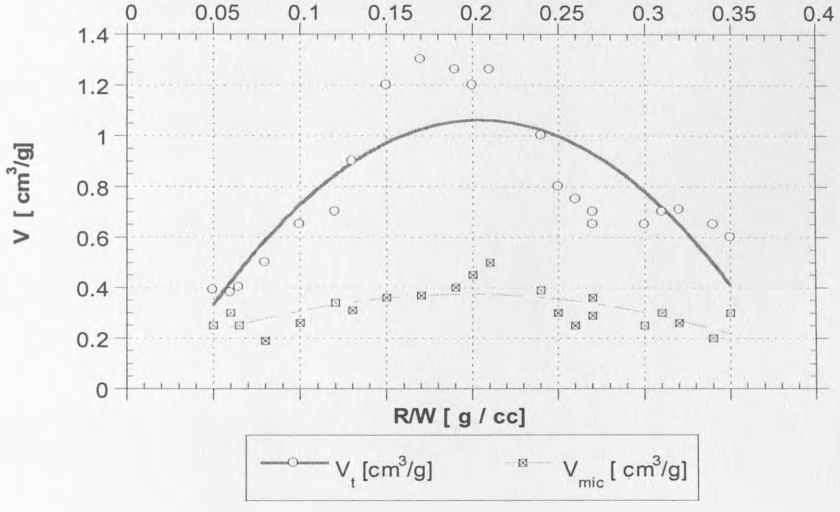

Figure 6.18 Influence of resorcinol to water ratio (R/W) on the total and micro-pore volume of carbon xerogels

Figure 6.18 shows that total pore volume V_t and the micropore volume V_{mic} have similar R/W dependence as S_{BET}. In general, these results show that R/W ratio plays a significant role in the final RF-xerogels pore structure and consequently the porous structure of the produced carbons. Tamon and Ishizaka (1998) previously investigated the gelation process of RF solution by SAXS measurements. They confirmed that the values of R/C and R/W can be related to the sizes of primary particles forming the cross-linked structure of RF hydrogel, and that the final sizes of primary particles influence the porous properties of the gels. Therefore it can be assumed that the ratio of R/W for the same R/C affect the ratio of catalyst to water (C/W). During the first stage of gelation process, each particle grows individually at the site of the catalyst. Subsequently, they aggregate to form the interconnected structure, and finally the cross-linked structure (RF-xerogel) is formed. If C/W is large, the starting points of the growth of the particles have a high density. Thus, a small amount of the reactant is consumed per particles and consequently the size of the particles becomes small. On the other hand, if the C/W is small the starting points exist sparsely. Hence, a large amount of the reactant is consumed per particle and consequently the particles can grow large.

6.2.3 Effect of RF initial solution pH on the on porous structure of the carbon xerogels

RF carbon xerogels were prepared with R/C=100 by mole, R/W= 0.25g/cm^3 and MEA as a catalyst. After gelation the gel appearance varied from orange to red brown according to initial pH and catalytic species. Figure 6.19 and 6.20 shows that, in general the surface

area and pore volume of RF carbon xerogels has a weak dependence on the initial solution pH in the acidic range, but as a pH higher than 7.3 the surface area tended to decrease and the material become non porous. When an initial pH greater than 7.3 was used the gelation was too fast, the polycondensation reaction was hindered and the gels were not easy to collect. On the other hand, lower pH value promoted the condensation reaction, thereby forming a highly cross-linked and thus very strong structure, where the majority of the pores could withstand the high temperature treatment. Therefore, typical pH values are in the approximate range of 4 to 6.

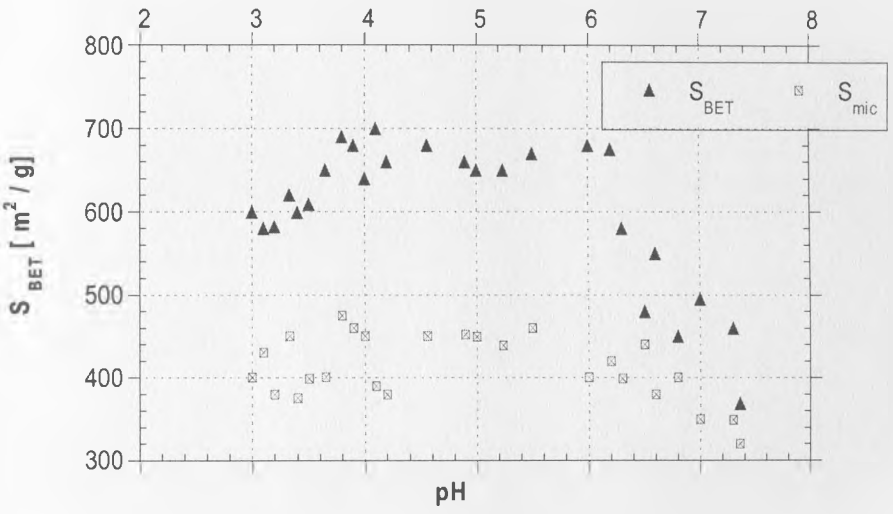

Figure 6.19 Effect of the RF initial solution pH on the BET surface area and micropore surface area of carbon xerogels

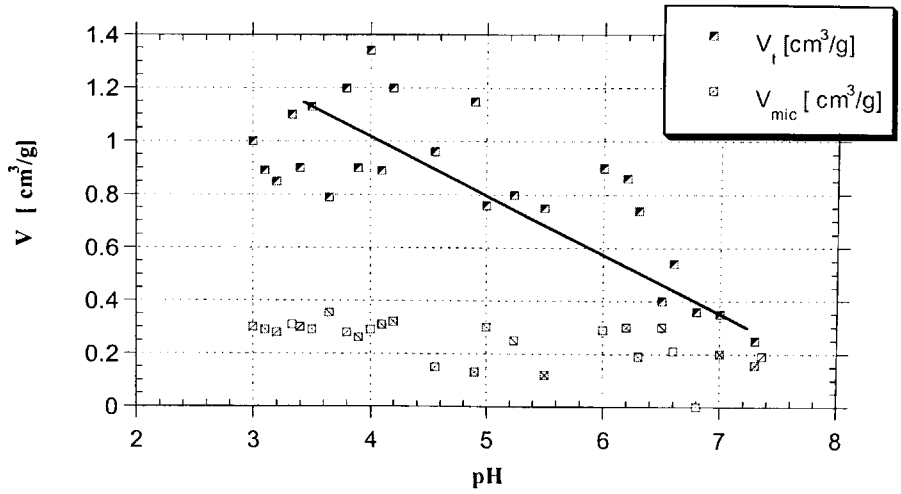

Figure 6.20 Effect of the RF initial solution pH on the total and micropore volume of carbon xerogels

The BET surface area S_{BET} varied from 580 m^2/g (pH=3.2) to 680 m^2/g (pH= 6) indicating that more pores and surface area were created in the RF xerogel and consequently in the carbon. However, as the pH increased > 6 the surface area decreased. It appears that the high pH value > 6 yielded gels with a weak chemical structure. This may be attributed to that the gelation reaction can be controlled remarkably by the pH. If the pH is low the particle growth stage may result in an incomplete aggregation reaction. This attributed to insufficient resorcinol anion formation during the addition reaction, which limits the RF cluster formation. Moreover, the solutions must not be too acidic or the basic catalyst will be consumed. It seems logical that the optimal pH for the solution would be mildly acidic. At such case, the basic salt would not be consumed and could activate the resorcinol molecules. Meanwhile, enough H^+ ions would be present to remove an OH^- from one of the

CH_2OH groups to allow for cross-linking. In case of a weak xerogel structure, the xerogels could not withstand the drying and pyrolysis conditions which cause the pores to collapse. This results in formation of RF carbon xerogels with no or very little surface area. Figure 6.20 shows that the total pore volume increased almost linearly as the pH decreased. Therefore, we can conclude that carbon xerogels evolve from macro-mesoporous solid at lower pH to micro-mesoporous solid at higher pH to completely non-porous material at pH over 7.5.

6.2.4 Structural characterization with scanning electron microscopy (SEM) analysis

The SEM photographs in Figure 6.21 a and b show the images of the samples synthesized at pH=6, R/C=300 and R/W=0.25 before and after pyrolysis. The small white particles in the RF-xerogels sample could be remaining portion of catalyst species which did not react.

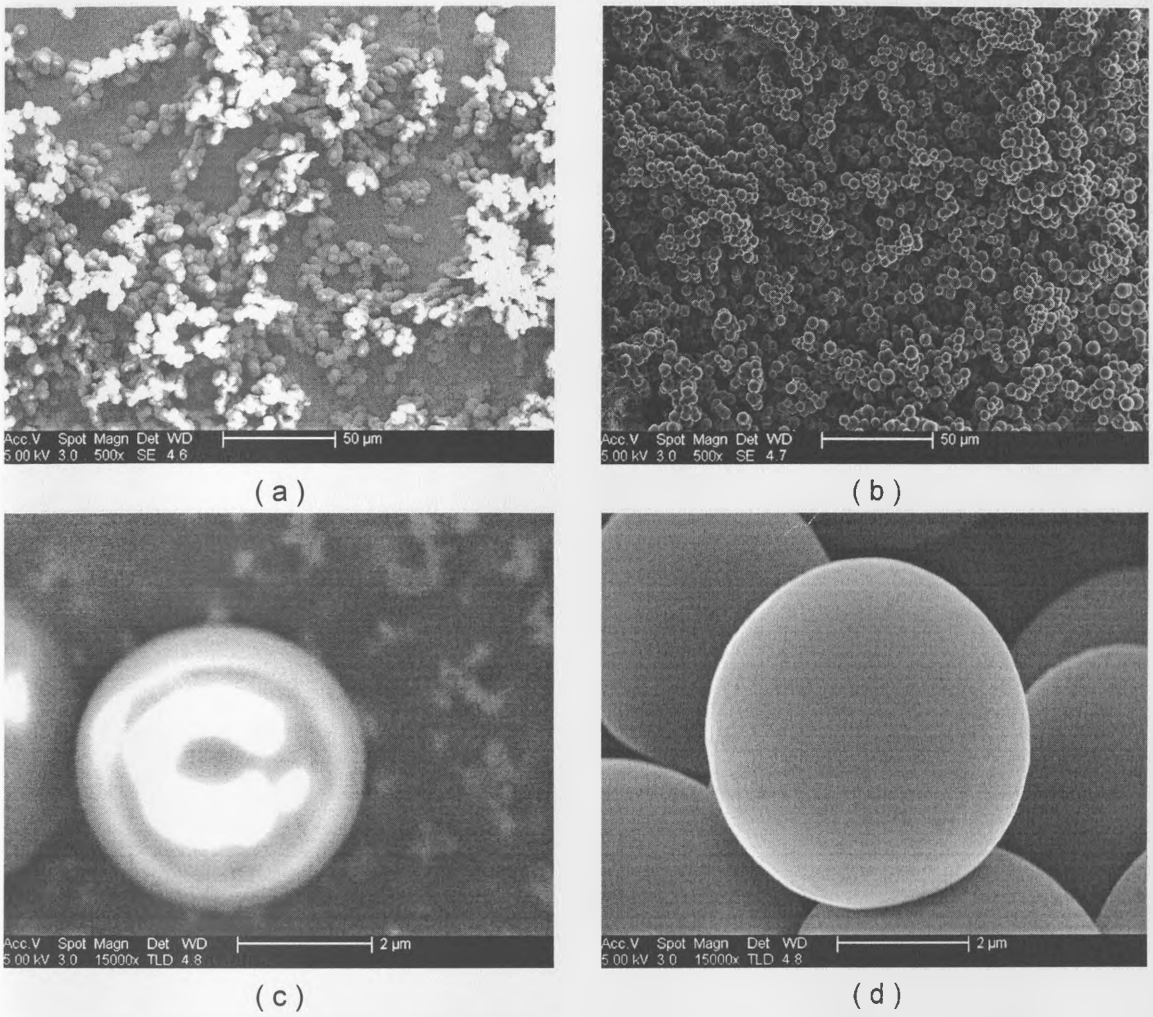

Figure 6.21 SEM images of samples synthesized with Na_2CO_3 as a catalyst under condition of pH=6, R/C=300 and R/W=0.25 (a) before and (b) after pyrolysis, both scale bar = 50 µm (c) and (d) higher magnification for both samples, respectively both scale bar = 2 µm,

There are few differences between the textures obtained before and after pyrolysis despite a mass loss between 35-50%. The SEM images suggest that both dried and pyrolyzed materials are made of interconnected spherical particles. Moreover, the particles seem to be more interconnected after pyrolysis and the size of the mesovoids formed between

these particles has also decreased. Figure 6.21 c and d show the pictures taken with a higher magnification which enabled measurement of an approximate particle diameter. In case of sample after pyrolysis, this diameter increase during pyrolysis from 3.5 μm (polymer before pyrolysis) to 6 μm (carbon particles). Figure 6.22 show the photographic images (magnification 15000X) for the samples of carbons synthesized with monoethanolamine MEA as a catalyst under condition of pH=6, and R/W=0.25 with different R/C ratios (300 and 50). As confirmed before from the N_2 adsorption measurements, the development of meso-and macroporosity are observed for the sample prepared with lower R/C ratio.

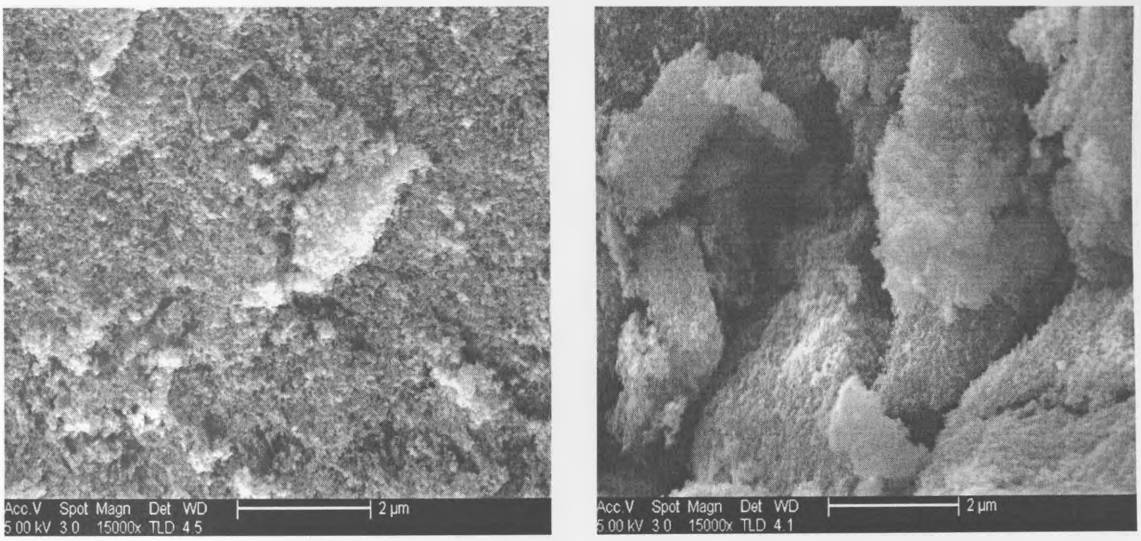

Figure 6.22 SEM images of samples synthesized monoethanolamine with MEA as a catalyst under condition of pH=6, and R/W=0.25 (a) R/C=300 and (b) R/C= 50, scale bar = 2 μm

6.3 Activation of RF-carbon xerogels

The main objectives of this section of the work are; firstly to undertake a rigorous analysis of the porous structure of activated carbon derived from resorcinol-formaldehyde (RF)-xerogel and the effect of activation conditions on the pore size distribution, surface area and surface chemistry of the resulting carbons; secondly to critically evaluate the applicability of these carbons as an adsorbent in the field of CO_2 capture and separation. A series of sub-objectives were defined in order to give a structure to the research and make it more manageable. They were as follows,

- Investigate the effect of activation conditions on the proximate and ultimate analysis of carbons.
- Investigate the effect of activation temperature on the pore structure by N_2 adsorption at 77 K.
- Investigate the effect of activation time on the pore structure by N_2 adsorption at 77 K.
- Investigate the effect of activation conditions on the carbon surface chemistry by FTIR.
- Investigate the effect of activation conditions on the particle morphology by SEM.

6.3.1 Proximate and ultimate analysis

The proximate and ultimate analyses of the RF-xerogel, carbon xerogel and its activated counterparts were measured using a thermogravimetric analyzer and CHN-elemental analyzer, respectively. The results of such analyses are shown in Table 6.3. All the samples were prepared under the same conditions of pH= 6, R/W ratio of 0.25 cm^3/g and MEA was used as a catalyst with R/C ratio of 100. The results show that, the nitrogen percent in the RF-xerogels structure indicating the developing of nitrogen functional groups in the RF-xerogels surface due to the selection of MEA as a catalyst. And it seems that these groups are not affected by the activation; this may be due the strong C-N bonds which are able to withstand high heat treatments.

The percent carbon increased from 63 % to 92 % upon activation. This could be attributing to the fact that activation caused breaking of more C-O and C-H bonds. Since activation is associated with weight loss, the volatile content is significantly decreased while the fixed carbons increase with increasing of the extent of activation; this resulted in samples with higher carbon contents. In general, during carbonization and activation of the RF xerogel, most of the non-carbon elements, hydrogen and oxygen are first removed in gaseous form by pyrolytic decomposition of the starting materials. The free atoms of elementary carbon are grouped into organized crystallographic formations known as elementary graphite crystallites. The arrangement of the crystallite is irregular, so that free interstices exist between them. Thus carbonization and activation processes involve thermal decomposition of carbonaceous material, eliminating non-carbon

species producing a fixed carbon mass ,rudimentary pore structure and finally creating more pore structure.

Table 6.3 Analysis of resorcinol-formaldehyde (RF)-xerogel, carbon xerogels and its activated counterpart forms.

Nomenclature	Ultimate (wt% dry-ash-free basis) (± 0.05)				Proximate (wt%) (± 0.05)			
	C	H	N	O	Moisture contents	Volatile contents	Fixed carbon	Ash
[1]RF-xerogel	62.98	5.45	0.43	31.15	4.92	61.79	33.29	0
[2]RFC	87.59	2.12	0.41	10.22	1.23	39.5	59.20	0
[3]RFAC-850-1	85.53	3.99	0.40	10.08	0.17	13.21	86.62	0
RFAC-850-2	86.78	3.35	0.40	9.47	0.10	8.94	90.96	0
RFAC-850-3	87.23	3.39	0.39	8.99	0.87	7.81	91.32	0
RFAC-900-1	91.23	2.39	0.39	5.99	0.87	7.80	91.33	0
RFAC-980-1	92.12	1.98	0.41	5.49	0.73	3.40	95.87	0

[1]RF xerogel sample, [2] RF carbon xerogel sample and [3] RF activated carbon xerogel sample followed by the activation temperature and activation holdup time. Note; the number of significant figures quoted in the table an indication of precision

6.3.2 Effect of activation on the surface chemistry by FT-IR analysis

Figure 6.23 shows the FTIR spectra for the synthesis RF xerogel, carbon xerogel and for the samples prepared under the same condition and activated with CO_2 at 850°C and 900°C for 1 hour. All the samples were prepared under the same conditions of pH= 6,

resorcinol to water ratio (R/W) of 0.25 cm^3/g and MEA was used as a catalyst with resorcinol to catalyst (R/C) ratio of 100. The pyrolysis and activations result in variation of the peak intensities of all the mentioned characteristic absorption bands in Section 6.1.3, together with peak shift and/or peak merge, this is due to transformation of the organic gel into a relatively pure carbon structure by removing any remaining oxide and hydrogen groups at an elevated temperature.

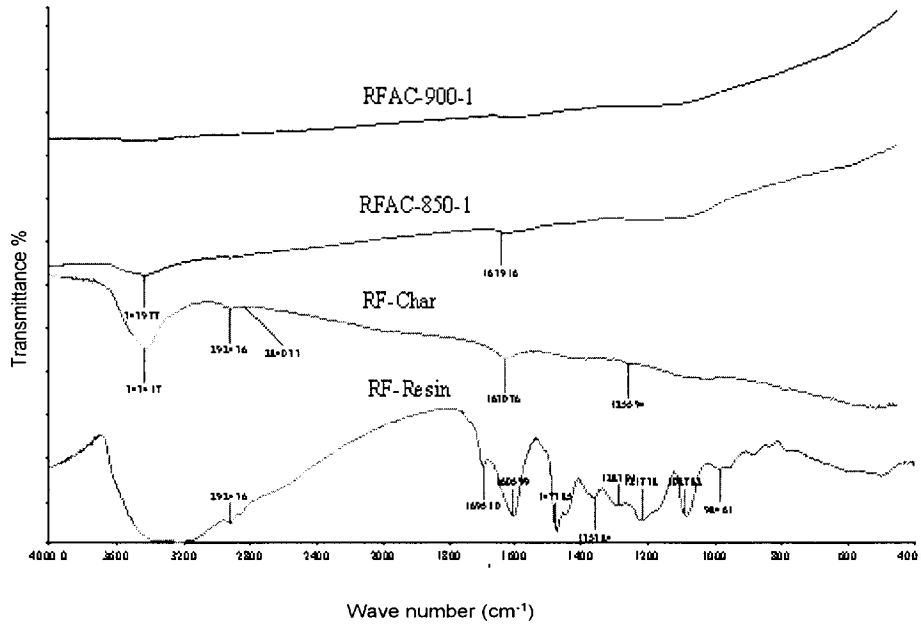

Figure 6.23 FTIR spectra for the synthesis RF xerogel, RF-carbon xerogel and for the samples prepared under the same condition and activated with CO_2 at temperature of 850°C and 900°C for 1 hour.

6.3.3 Effect of activation on the N_2 (77K) adsorption

It has been long recognize that the activation conditions, time and temperature, as well as the properties and structure of the precursor affect the porous structure of the resultant activated carbon. Accordingly, this study has been conducted to ascertain the effect of

time and temperature on the porous structure of activated carbons produced from resorcinol-formaldehyde RF-xerogel. For this series of samples the conditions of preparation were, pH= 6, R/W ratio of 0.25 cm^3/g and MEA was used as a catalyst with R/C ratio of 100. Figure 6.24 shows the N_2 adsorption isotherm of sample activated at 900°C for 1 and 2 hr. For comparison, the isotherm of the RF-xerogels and carbon xerogel is also presented. Comparing the isotherms of the samples before and after activation, the isotherm of the activated samples have significantly increased the adsorbed volume at low relative pressure, this observation indicates that the activation process developed micropores in the carbon xerogel. The isotherms of the activated samples are a combination of type I and IV, which corresponds to micro-mesoporous solid. The main feature of such an isotherm is the long plateau and a hysteresis loop at higher relative pressure (Lowell 1991). However, by increasing the activation time, the isotherm shows a more open and rounder knee at low relative pressure and the slope of the plateau increases, indicating a broader pore size distribution with larger micropores and increasing mesoporosity. Also, nitrogen uptake significantly occurs at high relative pressure. This indicates that the meso-or macropores structure in the sample are developed with an increase of extent of activation due to the widening of the micropores (Lin and Ritter 2000). In general most of activated carbons are produced by two–stage process, i.e. carbonization followed by activation. The purpose of the carbonization is to enrich the carbon content and create in the carbon xerogel an initial porosity and some ordering in the carbon structures. While the activation is carried out to enlarge the diameters of the pores which are created during the carbonization process and to create

some new porosity thus resulting in the formation of a well-developed and readily accessible pore structure with very large internal surface area. There are several parameters in the production of activated carbon that would affect its structure, one of which is the activation extent.

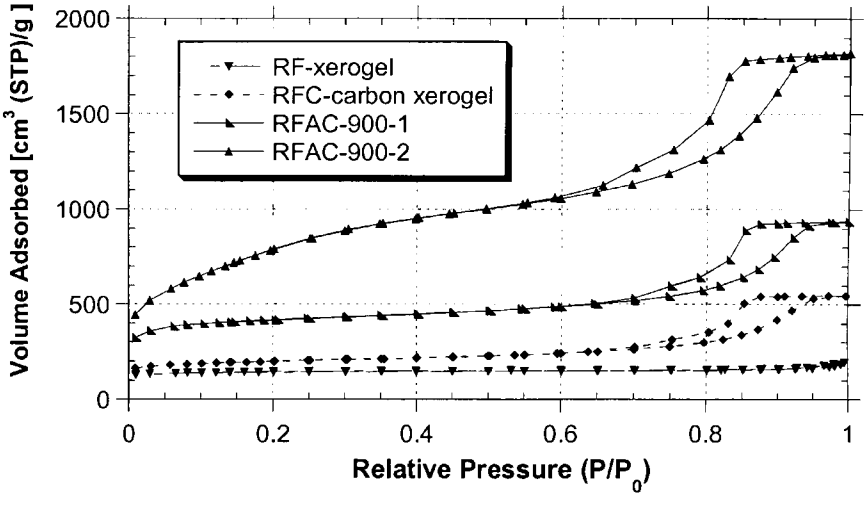

Figure 6.24 N_2 adsorption isotherms at 77 K of the resorcinol-formaldehyde RF-xerogel, carbon xerogel and its counterpart activated samples at 900^{0}C for 1 and 2 hr

Figure 6.25 shows the N_2 (77K) adsorption isotherms for the sample prepared under the same conditions with different R/C ratios and activated at the same conditions (activation with CO_2 at 850^{0}C for 1 h.). The resultant activated samples for these series were labelled as RFAC-a-b-c, where (a) is denoted for R/C ratio, (b) and (c) denote for the activation temperature and activation time, respectively.

The samples vary from a micro-mesoporous solid (samples prepared with R/C = 50 and 100) which is combination of types I and IV isotherm to approximately an exclusively

microporous material (samples prepared with R/C = 200 and 300) type I isotherm. The isotherm for the sample prepared under condition R/C = 300 exhibits low-pressure hysteresis. The main feature of such isotherm is the long plateau which is indicative of a relatively small amount of multilayer adsorption on the open surface. For the samples prepared at higher R/C, the N_2 adsorption isotherms are different; they exhibit a significant increase in adsorption at higher relative pressure. The knee becomes more open and rounder and the slope of the plateau increases. Also, the nitrogen uptake occurs mostly at (P/P_0 >0.9). This indicates that the presence of meso- or macropore structure in these samples.

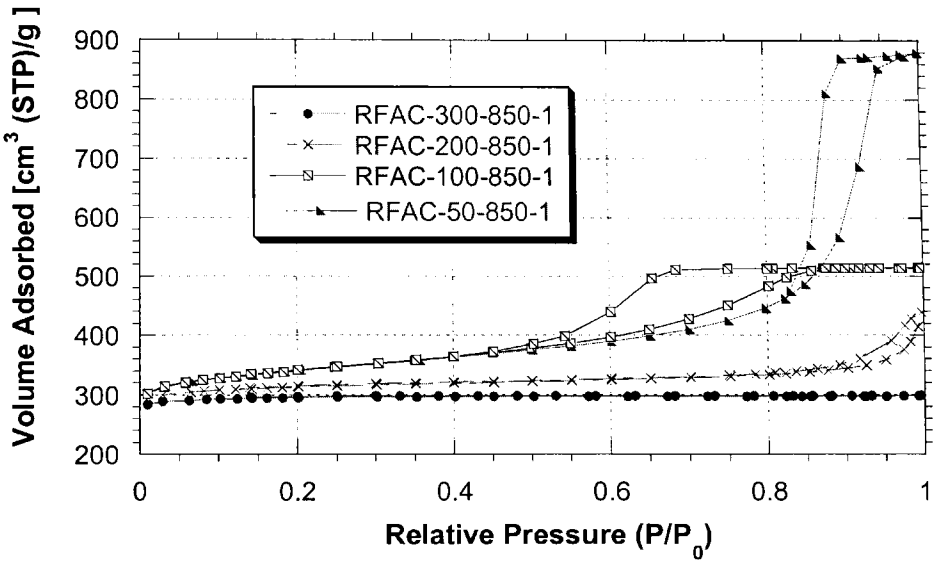

Figure 6.25 Adsorption profiles of N_2 at 77 K, on the RF carbon xerogels generated at different R/C molar ratio and activated with CO_2 at a temperature of 850 ^{o}C for 1 hour.

Table 6.4 shows the characteristic pore properties of the RF carbon xerogel prepared with different R/C molar ratio and activated at 850°C for 1 h. The influence of the R/C ratio is obviously marked in spite of activation, as R/C ratio increased from 50 to 300 the total pore volume and surface area decreased from 1.35cm^3/g and 970 m^2/g respectively, to 0.46 cm^3/g and 720 m^2/g. On the other hand, the micropore volume fraction increases from 26 %, (RF-50-850-1), to 96 %, (RF-300-850-1). Comparing these results with the results obtained in Section 6.2.1 Figure 6.12, it can be concluded that activation leads to increase the surface area, total pore volume and micropore volume, however it did not affect the shape of the N_2 adsorption-desorption profile.

Table 6.4 Characteristic pore properties of RF activated carbon xerogels prepared under the same conditions, with different R/C ratios and activated with CO_2 at a temperature of 850°C for 1 hr.

Nomenclature	R/C	S_{BET}[a] (m^2/g) (± 10)	V_t[b] (cm^3/g) (± 0.02)	V_{mic}[c] (cm^3/g) (± 0.02)	V_{mes}[d] (cm^3/g) (± 0.02)	D_p[e] (nm) (± 0.02)
RFAC-50-850-1	50	970	1.36	0.35	1.01	5.61
RFAC-100-850-1	100	900	0.73	0.37	0.36	3.22
RFAC-200-850-1	200	810	0.67	0.38	0.29	3.23
RFAC-300-850-1	300	720	0.46	0.45	0.02	2.54

[a] Specific surface area determined from the BET equation. [b] Total pore volume. [c]Micropore volume determine by Horvath-Kawazoe equation.[d] Mesopore volume.[e] Mean pore diameter. Note; the number of significant figures quoted in the table an indication of precision

6.3.4 Effect of activation on the pore size distribution (PSD)

Figure 6.26 shows the mesopore size distribution for the sample before and after activation as calculated by the BJH method. The conditions of preparation were, pH= 6, R/W ratio of 0.25 cm^3/g and MEA was used as a catalyst with R/C ratio of 100, the sample are then activated at 900°C for 1 and 2 hr. For comparison, the pore size distributions (PSDs) of the RF-xerogels and carbon xerogel are also presented. It is seen that the development of mesoporosity is strongly dependent on the activation process. It was observed that the sample before activation has one broad peak in the range of 30 nm while the activated forms have several peaks and as the activation time increase these peaks are shifted to the smaller pore diameter indicating the formation of more mesopores with the increase of activation time at that temperature. For better characterization of the change in the microporous structure during activation studies, the micropore size distributions were calculated by Horvath-Kawazoe method. Figure 6.27 shows the micropore size distribution as a function of activation time. It is shown that all samples have one main peak which is centred on 1 nm without any additional peak and as the activation time increase the micropore volume is significantly increased and pores size distribution becomes wider. As mentioned above, it is found that activation results in the enhancement of micropore volumes and distributions.

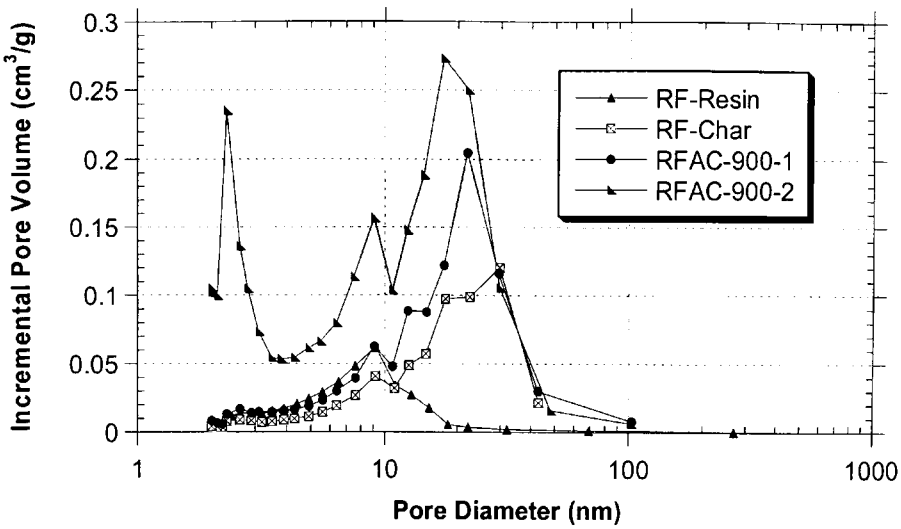

Figure 6.26 Mesopore size distributions of the resorcinol-formaldehyde (RF)-xerogel, carbon xerogel and its counterpart activated at 900°C for 1 and 2 hr.

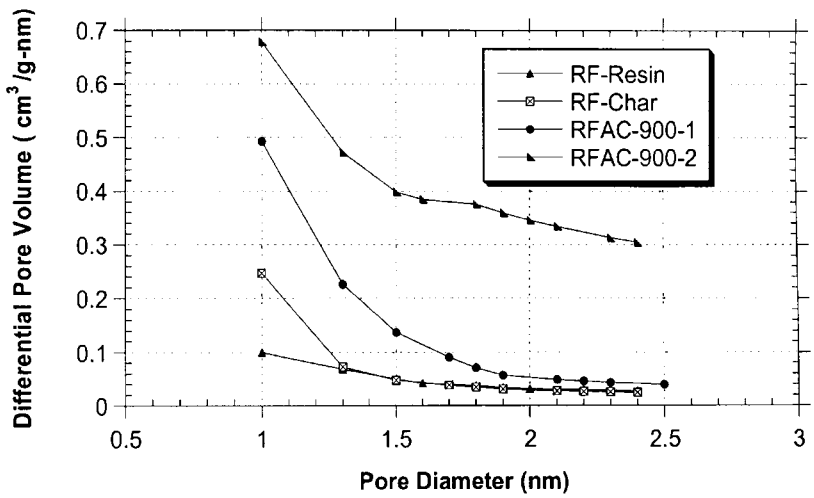

Figure 6.27 Micropore size distribution of the resorcinol-formaldehyde carbon xerogel and its counterparts activated at 900°C for 1and 2 hr.

Figure 6.28 and 6.29 show the variation of total, micro- and mesopores volume and surface area for a series of samples activated with CO_2 at 900°C for various times. The total pore volume and surface area of the activated samples are mainly due to micropores. This predominant microporosity will lead to applications in gas phase adsorption for the removal of gaseous pollutants. However, it should be noted that increasing the activation time at this temperature results in a continuous steady rise of the mesopores area and volume, while the micropore and total pore area and volume reached a maximum and then decreased.

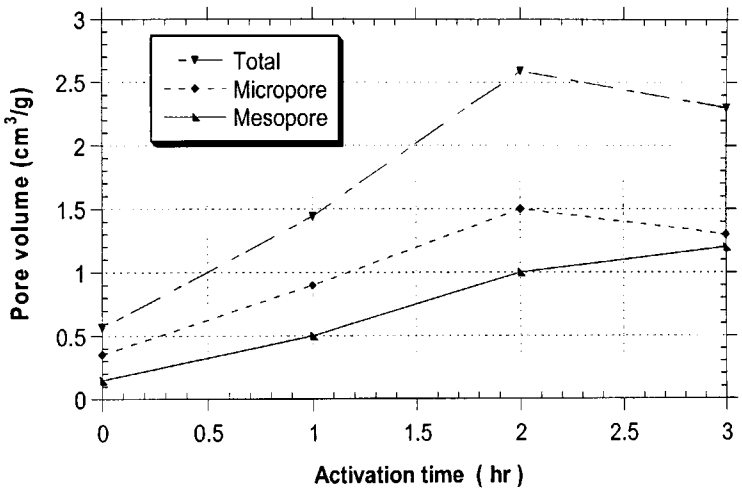

Figure 6.28 Variation of the total, micro, meso-pore volume with activation time for the sample activated at 900°C.

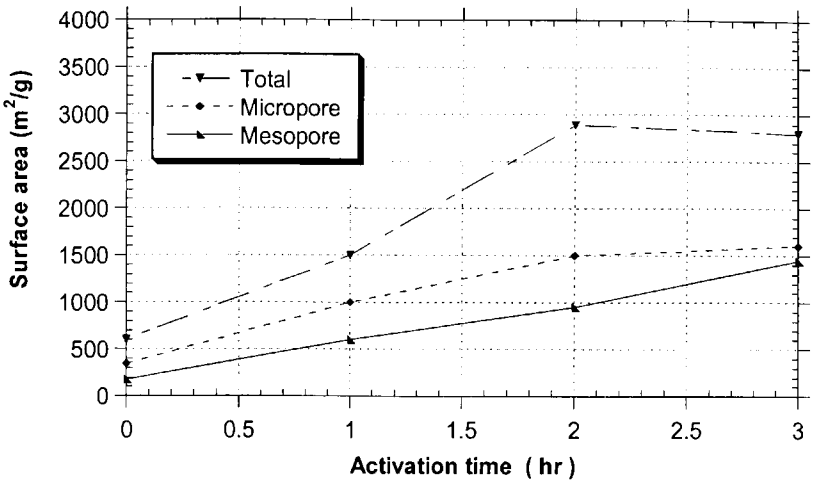

Figure 6.29 Variation of the BET, micro, meso-pore surface area with activation time for the sample activated at 900^{0}C.

This phenomenon could be attributed to the fact that during carbonization the free interstices present in the carbon become filled or at least partially blocked by disorganized carbon apparently as a result of deposition of tarry substances. At lower activation, the micropore was mainly developed due to opening of closed pores. The further increase in the micropore volume could be due to a pore-creating mechanism. In the latter phase, excessive activation reaction lead to elimination of the pore walls by the activating agent, which resulted in an increase in mesopores and macropores. Consequently, the volume of the micropores decreases and there is no significant increase in adsorption capacity or internal surface area (Manocha et al., 2002). Figure 6.30 illustrates the possible four propagation processes which occurred during the carbon activation. Theses processes are creating of new porosity, opening of closed porosity, widening of existing pores and finally burn-out of pore walls.

Another possible interpretation of this phenomenon of decreasing of micropore volume is that, at deep activation most of activation process occurs at the exterior of the surface that lead to the particle to shrink, at this case activation does not lead to any pore development, and pore widening occurs (Guo, 2002; Leboda, 2003).

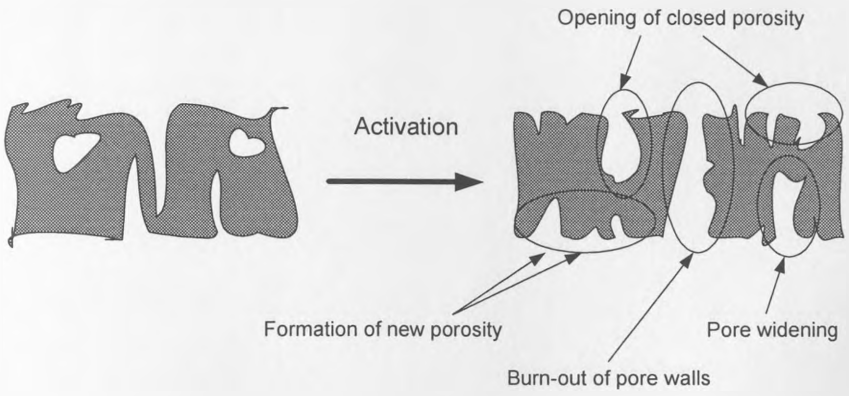

Figure 6.30 Porosity and surface area development process occurring during activation

A series of samples were activated at a temperature of 850, 900 and 980°C for periods of time 1-3 hr. The variation of total pore volume and surface area with different activation temperature and time are shown in Figures 6.31 and 6.32, respectively. The BET surface area and pore volume increased progressively with increasing activation temperature. This was attributed to the high activation energy of the C-CO_2 reaction. When keeping the activation time constant, both the pore volumes and surface area rise with increasing activation temperature. For a given activation temperature, the surface area and pore volume did not rise continuously with increasing activation time. The activation time needed to achieve the highest surface area and pore volume shifts to lower values as the

activation temperature increased. For example, for the activation studies conducted at 900 and 980°C, the surface area and pore volume decrease when the activation time is extended over 2.5 hr., while for the sample activated at 850°C, the surface area and pore volume seems that it is not decrease till the activation time is extended over 3 hr., and probably longer times are needed for this low temperature of activation before the surface area and pore volume start to decrease.

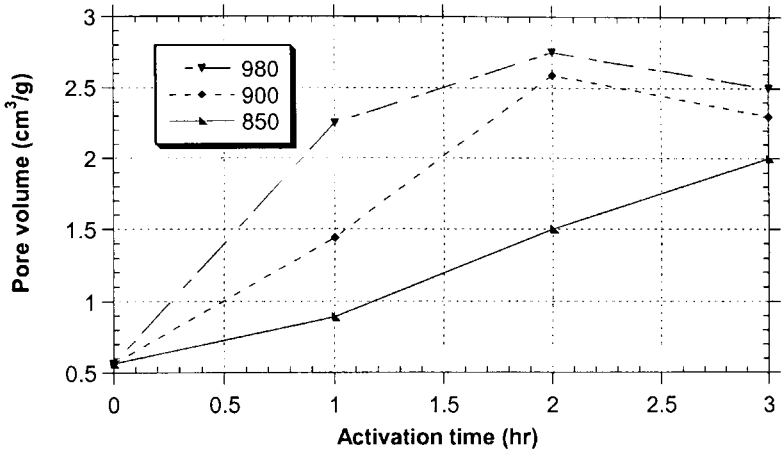

Figure 6.31 Variation of the total pore volume with activation time at different activation temperatures (850-980 °C)

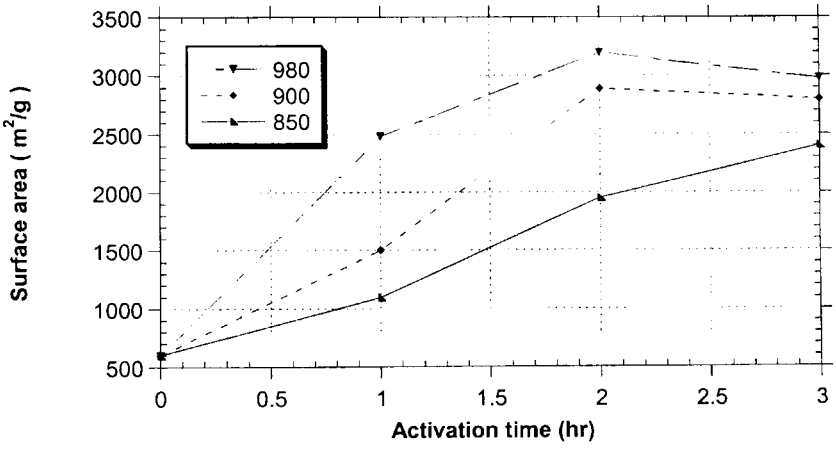

Figure 6.32 Variation of the BET surface area with activation time at different activation temperatures (850-980°C)

6.3.5 Effect of activation on the char yield

To investigate the effect of the activation on the activated char yield, the yield of the activated samples studied was calculated by using the following Equation 6.1.

$$\text{Char yield (in wt \%)} = [W_1/ W_2] \times 100, \quad (6.1)$$

where W_1 and W_2 are the weights of the activated carbons product and the parent carbon xerogels, respectively. Table 6.5 lists the solid yield of the samples activated under different conditions (time and temperature). As expected, the solid yields decreased with increasing activation time and temperature. For example, for the sample activated for 1 hr, the solid yield goes from 78% to 31% as the activation temperature increased from 850°C to 980°C. Similarly, for a given activation temperature, the solid yield decreases with activation time.

Table 6.5 Solid activated char yield (wt % ±1) of samples activated under different conditions (time and temperature)

	1h	2h	3h
850°C	78	57	42
900°C	63	40	17
980°C	38	21	5

Note; the number of significant figures quoted in the table an indication of precision

Carbon atoms differ from each other in their reactivity depending on their spatial arrangement. Activation eliminates the disorganized carbon, exposing the aromatic sheets to the action of activation agents and leads to development of a microporous structure. Since activation is associated with weight loss of the host carbon, the extent of burn-off (100 - %yield) of the carbon material is taken as a measure of the degree of activation (Manocha et al, 2002). At a particular temperature, weight loss increases linearly with activation time. Normally, in the first phase, the disorganized carbon is burnt preferentially when the burn-off is about 10%. This results in the opening of blocked pores. Subsequently, the carbon of the aromatic ring system starts burning, producing active sites and wider pores. In the latter phase, excessive activation reaction results in knocking down of the walls by the activated agents and a weight loss of more than 70%. This results in an increase in transitional pores and macropores. The volume of the micropores decreased and there is no significant increase in adsorption capacity or internal surface area. At higher burn-off (lower carbon yield), the difference in porosity created by activating agent (CO_2) become more pronounced. Figure 6.33 shows the variation of the BET surface area with the level of carbon yield at different activation temperatures. It is very clear that activation at lower activation temperature results in a linear relationship between the surface area and carbon yield so as the carbon yield decrease the BET surface area increase and vice verse. However, activation at higher temperature, the BET increase with the decrease of the carbon yield then passes through a maximum (around 40 % for activation at 900°C and 20 % for activation at 980°C) and then decreases again. This decrease of the overall surface area with further decrease of

carbon yield when activation has been done at higher temperature my result from the extensive gasification which cause the shrinkage of the carbon particles or the destruction of the porous framework at the external portion of the particles.

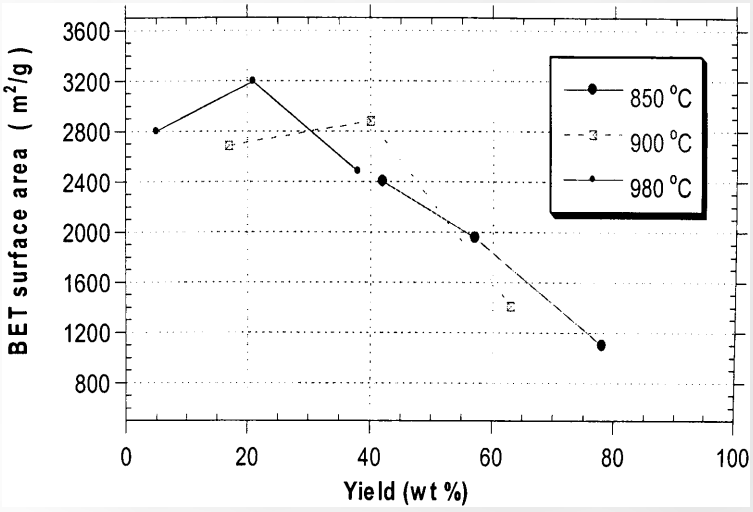

Figure 6.33 Variation of the BET surface area with the level of carbon yield at different activation temperatures

6.3.6 Effect of activation on the particle morphology by scanning electron microscope (SEM) analysis

Figure 6.34 a and b show the SEM image for the sample before and after activation at a temperature of 900°C for 1 hr. The activated sample has a compact structure, enlarging of the micropores and breaking of pore walls were observed, resulting in an increase in the number of mesopores and macropores. The large numbers of small pits distributed over the surface, indicating that most pore development occurs inside the particles.

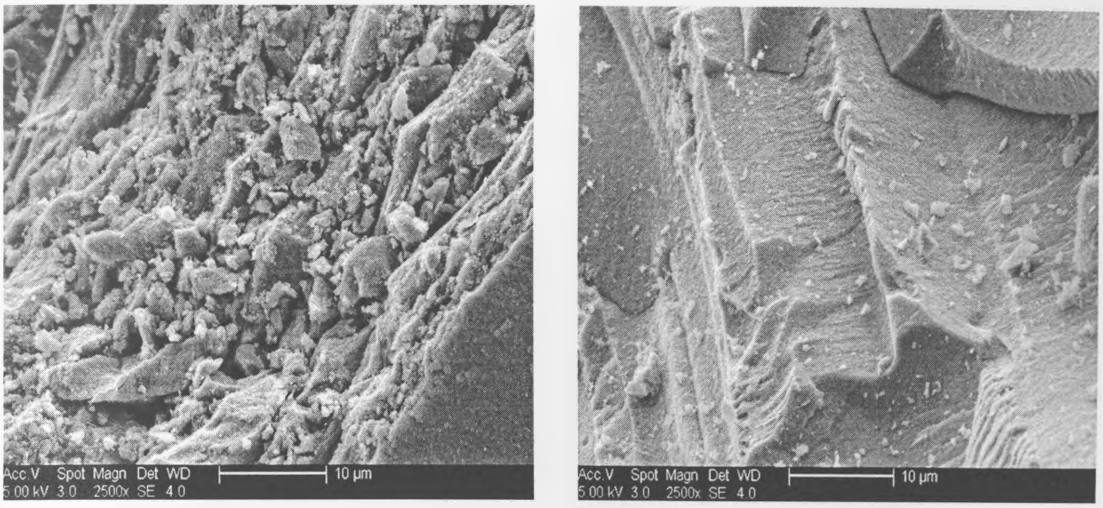

(a) (b)

Figure 6.34 SEM images of cross-section of (a) carbon xerogel sample (b) activated sample at a temperature of 900^{0}C for 1 hr.

6.4 Resorcinol-formaldehyde carbon xerogels surface modification

As discussed before in Section 3.3, the surface chemistry of carbon is governed by the presence of heteroatoms such as oxygen, nitrogen, etc. Their origin depends upon the chemical nature of the precursor and the method of carbon preparation and activation. So, in this section we will discuses the effect of the surface modification which has been carried out through co-pyrolysis of the RF-xerogels with nitrogen containing compounds. The RF-xerogels sample prepared with monoethanolamine (MEA) as a catalyst with resorcinol to catalyst ratio R/C = 100, resorcinol to water ratio R/W= 0.25 g/cm^3 and pH=6 was used for this series of preparations. The carbon prepared from RF-xerogels impregnated with *m*-phenylenediamine is designated as RFC-MPDA and carbon prepared from RF-xerogels impregnated with diphenylenimine is designated as RFC-DPI, then each sample is followed by the percent of impregnation.

6.4.1 Proximate and ultimate analysis

The proximate and ultimate analyses of the surface modified carbon xerogels samples prepared using different degrees of impregnation with the nitrogen-source (m-phenylenediamine (MPDA) and diphenylenimine (DPI)) are shown in Table 6.6. The surface modification may have hindered the pyrolysis of the RF-xerogels, since the proximate analysis shows an increase in volatile content with the degree of N-source addition. The ultimate analysis of the samples shows that the nitrogen content is low in the non-impregnated sample while it is a significant on the samples treated with MPDA and DPI. The low presence of nitrogen in the non-impregnated sample is attributed to the selection of monoethanolamine as a catalyst in the polycondensation reaction of resorcinol with formaldehyde. The presence of nitrogen in the surface modified samples indicates the existence of secondary reactions and interactions occurring during the carbonization process that lead to the incorporation of the nitrogen into the final structure. The nitrogen content is proportional to the amount of MPDA and DPI added, indicating the good distribution and incorporation of the nitrogen into the RF-xerogels matrix. However it is worth states that for the series of samples impregnated with MPDA, the nitrogen content almost fixed with further increase of MPDA addition from 40% to 50%. This may be attributed to the structures of the resin reaching a certain degree of saturation during the co-pyrolysis process where there are no available sites available for any-more nitrogen atoms to be incorporated. In contrast to the series of samples impregnated with DPI, the steady rise increase of the nitrogen content in the carbon with DPI addition up to 50% indicating that the RF-xerogel structures still has

more vacant positions for the incorporation of more nitrogen atoms during the co-pyrolysis process. In addition, the use of MPDA in the impregnation leads to a higher nitrogen presence than DPI. This is attributed to the higher initial nitrogen content of the MPDA than DPI.

Table 6.6 Analysis of resorcinol-formaldehyde carbon xerogels (RFC) prepared under condition of pH=6 and R/W= 0.25 g/cm^{3}and its counterparts samples co-pyrolyzed with two different nitrogen-sources at a temperature of 700°C for 2 hr.

Nomenclature	Ultimate (wt% dry-ash-free basis) (± 0.05)				Proximate (wt%) (± 0.05%)			
	C	H	N	O	Moisture content	Volatile content	Fixed carbon	Ash
RFC	87.25	2.12	0.40	10.22	1.25	39.53	59.22	0
*RFC-MPDA10%	87.06	1.46	3.00	8.48	1.15	45.61	53.23	0
RFC-MPDA20%	87.62	1.00	5.77	5.61	1.35	56.91	41.74	0
RFC-MPDA30%	84.41	1.52	6.24	7.83	1.45	60.94	37.61	0
RFC-MPDA40%	87.16	1.21	7.13	4.50	1.66	66.12	32.22	0
RFC-MPDA50%	87.94	0.81	6.84	4.41	1.85	70.23	27.93	0
RFC-DPI10%	91.23	1.16	1.01	6.60	1.30	22.90	75.82	0
RFC-DPI20%	93.23	1.14	2.46	3.17	1.14	48.32	50.54	0
RFC-DPI30%	88.41	1.50	2.84	7.25	1.55	56.63	41.85	0
RFC-DPI40%	91.13	1.08	2.91	4.88	1.85	60.64	37.51	0
RFC-DPI50%	91.21	0.98	3.60	4.21	2.02	65.95	32.03	0

*Each sample followed by the nitrogen compound used for surface modification and then the percent of impregnation to the original weight of RF xerogel. Note; the number of significant figures quoted in the table an indication of precision

6.4.2 Effect of impregnation on the mass loss profile of the RF-xerogels during pyrolysis by TGA

The mass loss during the pyrolysis process can be observed in Figures 6.35 and 6.36. The results of such analysis are classified into two groups according to the nitrogen compounds used during the co-pyrolysis. Figure 6.35 indicates the following: RF-xerogels (RF), RF-xerogels impregnated with 10 and 30 % DPI (RF-DPI10%, RF-DPI30%) and diphenylenimine (DPI) sample. While Figure 6.36 indicates: RF-xerogels(RF), RF-xerogels impregnated with 10 and 30 % MPDA (RF-MPDA10%; RF-MPDA30%) and m-phenylenediamine (MPDA) sample. In these tests, 3 mg of sample was weighed in the crucible of the TGA, and the temperature was increased to 900°C at a rate of 20°C/min in an argon flow of 20 ml/min. It can be observed from the Figures 6.35 and 6.36 that, at the end of the pyrolysis procedure the nitrogen compounds (DPI and MPDA samples) yield no carbon xerogel while the untreated RF-xerogels gives about 40 wt. % of carbon xerogel yield. The impregnation with nitrogen compounds leads to a small difference to the carbon xerogel yields, while leads to a great change of the temperature profile of the samples during pyrolysis which could be observed in the DTGA curves. The thermogram of the RF-xerogels sample (RF) can be divided into four stages. The first stage is up to 200°C and the second stage up to 400°C, the weight losses in both stages being around 25%. The third stage, in which the main degradation of RF-xerogels takes place, starts from approximately 450°C and the degradation components of around 35% are released up to 850°C. In the fourth stage, ranging from 850 to 1000°C, the sample mass does not change. Whilst, the thermogram of the impregnated RF-xerogels can be divide into three stages only.

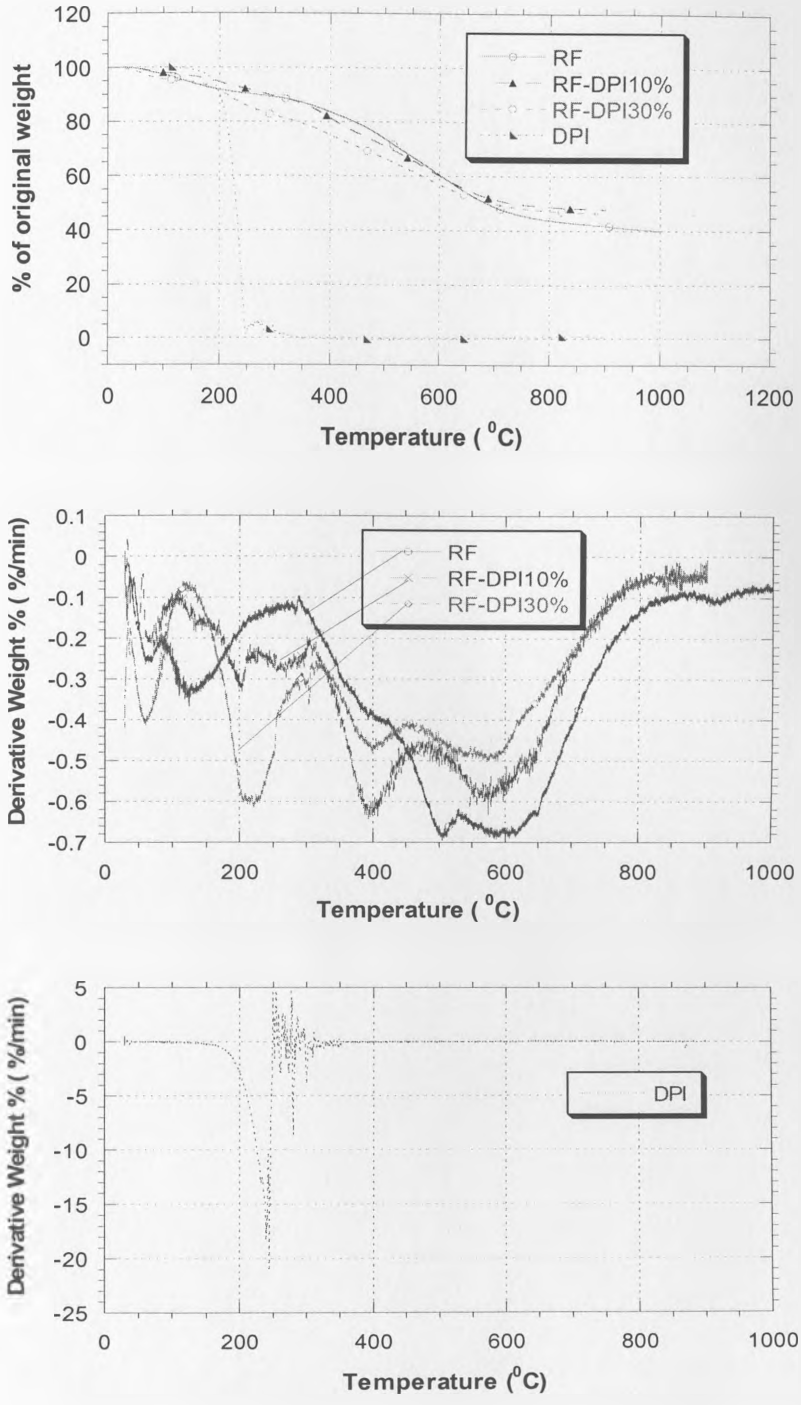

Figure 6.35 TGA and DTGA curves of: RF-xerogels (RF), RF-xerogels impregnated with 10 and 30 % DPI (RF-DPI10%; RF-DPI30%) and DPI sample. Argon flow is used as the heating medium with a heating rate of 20^0C/min.

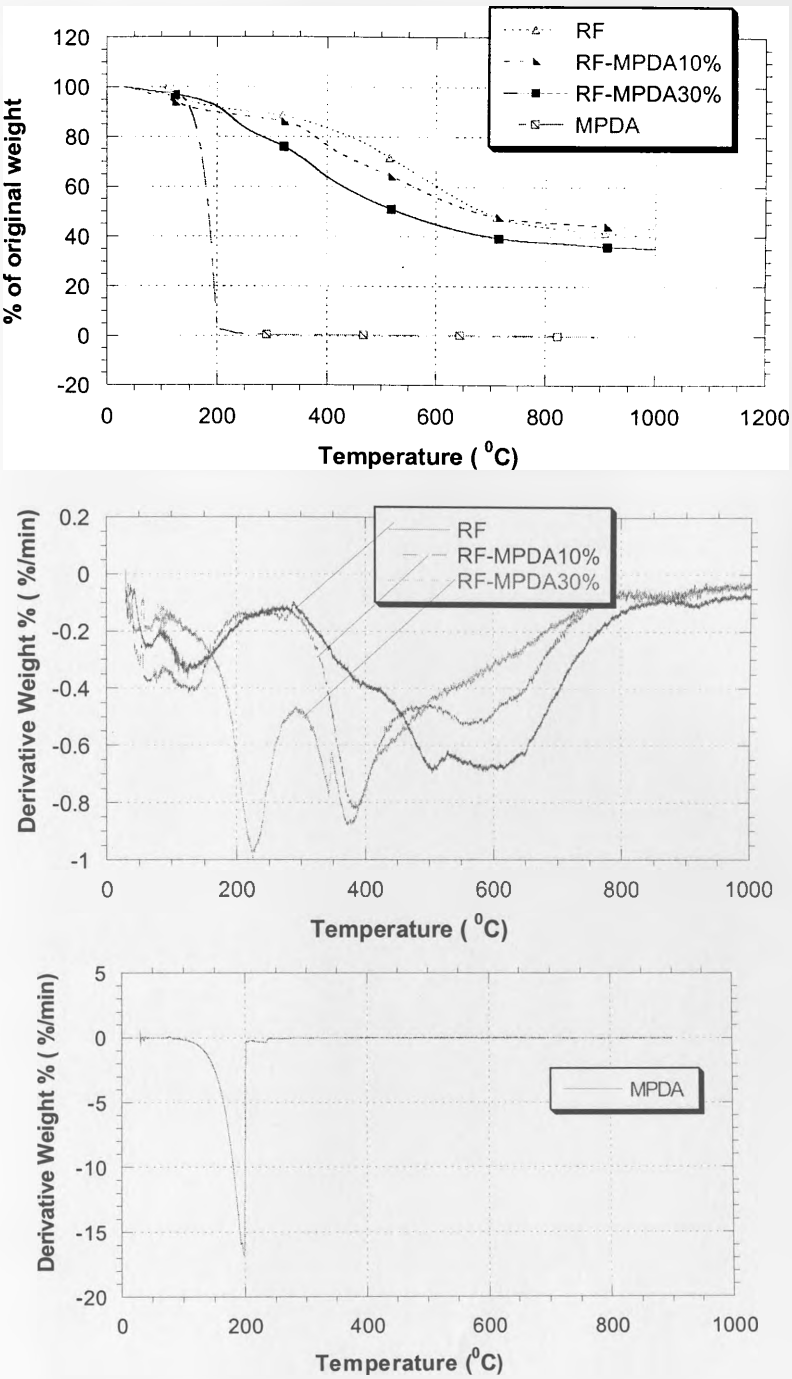

Figure 6.36 TGA and DTGA curves of: RF-xerogels (RF), RF-xerogels impregnated with 10 and 30 % MPDA (RF- MPDA 10%; RF- MPDA 30%) and MPDA sample. Argon flow is used as the heating medium with a heating rate of 20^{0}C/min.

The first stage is up to 100°C, where the weight loss associated around 5 –10%. The second stage, in which the main degradation takes place, starts from approximately 200°C and the weight loss associated around 45–55%. In the third stage, ranging from 900 to 1000°C, the sample mass does not change any more. So apparently, the co-pyrolysis with nitrogen compounds may have hindered the pyrolysis of the RF-xerogels, since the change in the mass loss profile can be clearly observed.

The DTG curve of the RF-xerogels sample shows three peaks around temperatures of 165, 400 and 600°C. The first peak around 165°C would be attributed to desorption of acetone, water, and residual organic precursor. The peak around 400°C would be related to the carbonization reaction of the organic aerogel, which involve the breaking of C-O bonds, while the peak around 600°C related to breaking of C-H bonds. Whilst, the DTG curves of the nitrogen source alone, DPI and MPDA samples, show one peak at a temperature of 250 and 200°C, respectively. The DPI and MPDA samples began to decompose above 150°C then a sharp weight loss appeared and finally both of the samples were completely decomposed and removed as volatiles.

The co-pyrolysis of the RF-xerogels with nitrogen compounds leads to a significant change in the intensity of the carbon characteristics peaks of the DTGA curves of the RF-xerogels sample. This change is accompanied by peaks shift towards the decomposition temperature of the nitrogen compounds. This is may be attributed to, the co-pyrolysis of the RF-xerogels with nitrogen compounds produces a series of

interactions that leads to a significant change in the mass loss profile of the RF-xerogels during pyrolysis.

6.4.3 Effect of impregnation on the surface chemistry of the RF-xerogel and carbon xerogel by FT-IR

Figure 6.37 shows the IR spectrum for the synthesis RF xerogels (RF) with MEA as a catalyst with R/C ratio = 100, R/W = 0. 25 g/cm^3 and pH = 6, compared with the prepared samples under the same conditioned and impregnated with MPDA 20% (RF-MPDA20%) and DPI 20% (RF-DPI20%). The evolution of FTIR spectra for RF xerogels with different percentage of surface modification by MPDA and DPI are presented in Appendix B.

The spectrum of the prepared non-impregnated RF-xerogel has been discussed previously in Section 6.1.3. The presence of nitrogen functional group in the non-impregnated sample can be attributed to the use of monoethanolamine (MEA) as a catalyst in the polycondensation reaction. The impregnation of the resulting RF-xerogels according to the method described in Section 5.1.5 leads to a great variation of the intensity of theses nitrogen functionality with/or peak shifts. The spectra of the two impregnated samples show many peaks and could be assigned as follows: amides and amines mixed in the very large band around 3430 cm^{-1}; nitrile (C≡N) and lactame groups should be found at 2247 cm^{-1} and 1730 cm^{-1} respectively (Burg et al., 2002). In connection with a presence of C=O groups (1787 cm^{-1}), the presence of both C-N (1190

cm^{-1}) and N-H (1480 cm^{-1}) bands may indicate the formation of (-CO-NH-) groups during impregnation (Przepiorski et al., 2004). The following bands can be easily recognized: N-H stretching vibration in secondary amide with a bonded hydrogen at 3079 cm^{-1}; coupling of C-N stretching and N-H deformation modes of C-N-H group (amide I band) at 1330 and 1306 cm^{-1}; aromatic C-N stretching vibrations at 1248 cm^{-1}; C-N stretching (amid III band) at 866, 784 and 688 cm^{-1}.

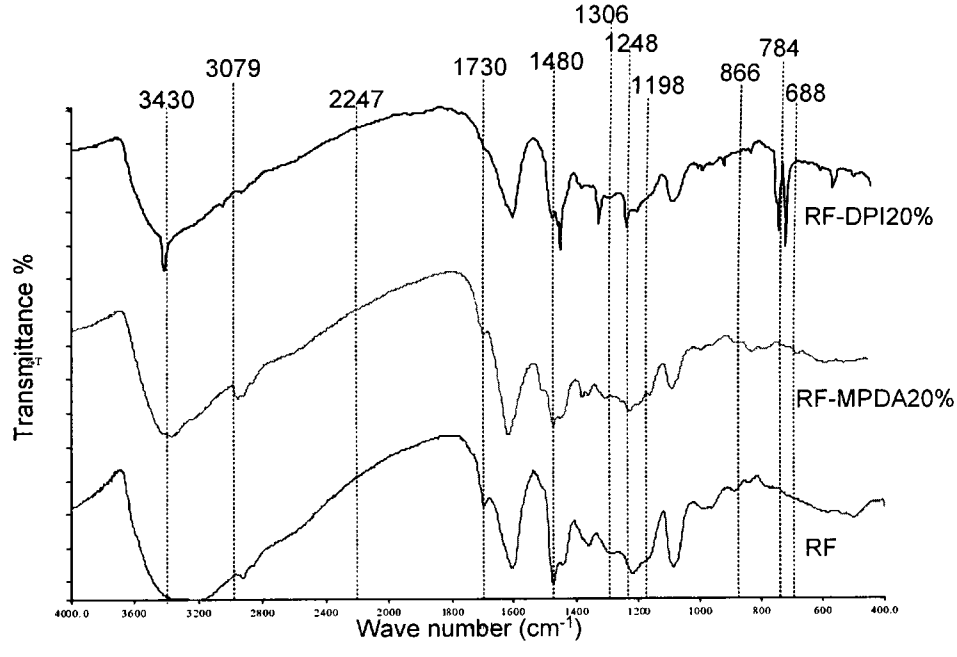

Figure 6.37 FTIR spectrum for the RF-xerogels prepared under condition of: MEA as a catalyst with the R/C = 100; R/W=0.25 g/cm^3 and pH=6 compared with its counterpart's surface modified with MPDA and DPI 20%.

Figure 6.38 shows a possible structure of RF-xerogels after impregnation with a N-source at a temperature of 100°C, the nitrogen atom incorporated into the benzene ring condensation structure.

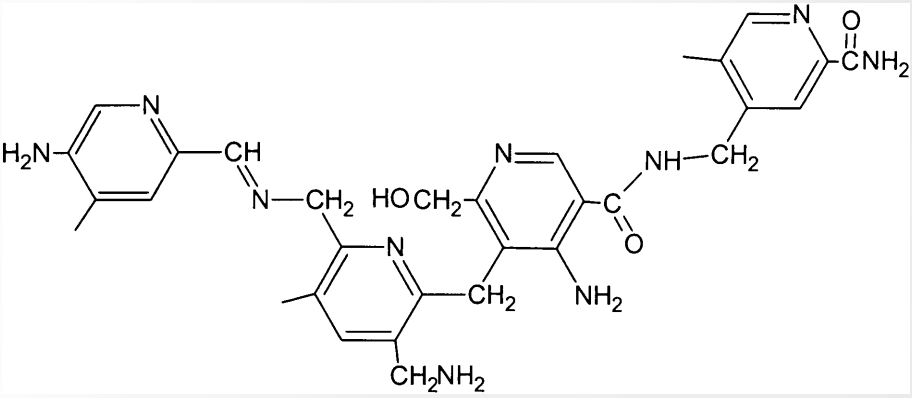

Figure 6.38 A possible structure of the nitrogen-containing compound resulting from the co-pyrolysis of RF-xerogel with N-containing compounds at a temperature of 400°C.

6.4.3.1 Effect of co-pyrolysis temperature on the surface chemistry

The FTIR spectra in the range from 400 to 4000 cm^{-1} of RF-MPDA20% and RF-DPI20% and its counterparts co-pyrolyzed at 400, 600, 700 and 800°C are shown in Figure 6.39. In general, carbonization of the prepared impregnated samples under argon results in the variation of the peak intensities of all the above-mentioned characteristics absorption bands together with peak shift and/or peak merge.

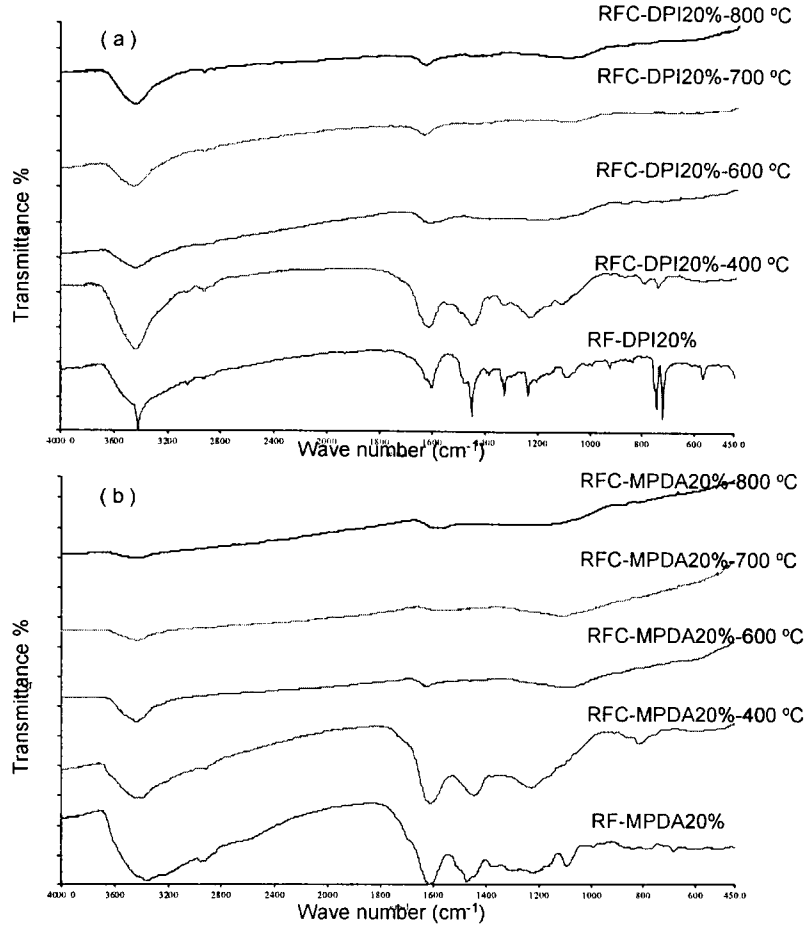

Figure 6.39 Evolution of FTIR spectra for RF carbon xerogel, which are impregnated with (a) DPI 20% (b) MPDA 20%, with co-pyrolysis temperatures at 400, 600, 700, and 700°C.

These changes are gradually increased with increasing of carbonization temperature. These changes could be summarized in brief as follows: O-H stretching vibration and O-H in plane deformation vibrations absorption bands become gradually smaller in transmittance with an increase of carbonization temperature, because the OH group participate in the reaction of dehydration and cyclodehydration during the carbonization. The aromatic ring C-O vibrations and aromatic C-H out-of-plane deformation vibrations

absorption bands becomes gradually smaller in transmittance with rising carbonization temperature, because the gases, CO, CO_2, and CH_4, are evolved from samples during the carbonization. In general, carbonization (pyrolysis) usually leads to breaking of more C-O and C-H bonds (Kim et al., 2004)

The temperature range up to 400°C covers the first and second stages of thermal degradation, as discussed in Section 6.1.2. In addition, it has been reported that the water retained from the production process is released up to 200°C and other volatiles such as unreacted components or degradation products of oligomers or side groups in RF-xerogels are driven off up to 400°C (Tennison, 1998). So these reactions may be responsible for approximately 8% weight loss during stages one and two, as shown in Figures 6.35 and 6.36.

It can however, be noticed from Figure 6.39 (a) and (b) that the peaks in the range 1300–1100 cm^{-1} due to various C–O–C linkages have rather strong intensity, as compared with those in original RF-xerogel sample before pyrolysis. This indicates that the crosslinking reaction between –OH groups and aromatic C–H or other –OH groups occurs with the evolution of water. Moreover, the significantly decreased relative intensity of the 1,2,4- and 1,2,6- trisubstituted aromatic ring stretching peak at 1506 cm^{-1} suggests that the crosslinking reaction occurred concurrently to some extent with the degradation reactions, leading to the formation of a disubstituted aromatic ring structure (Tennison , 1998).

The chemical structure change in the range of co-pyrolysis temperature 400 to 600°C is the peaks in the 1640–1590 cm^{-1} regions tend to merge to an apparently single symmetrical peak centered at 1593 cm^{-1} (which indicates that the environment of the ring structure has changed greatly in this temperature range). The pyrolysis of both impregnated samples in the range 600 to 800°C leads to a great chemical structure change in the surface functionality. The relative peak intensities of all characteristic bands decreased considerably compared to the samples carbonized at 400°C. No absorption peak can be distinguished after pyrolysis at 800°C. The pyrolyzed sample no longer contains IR-detectable oxygen or hydrogen and is primarily composed of pure carbon. This implies that polyaromatization is a predominant reaction occurring at this temperature level (Kim et al., 2004). Figure 6.40 shows a possible structure of the carbon xerogels after co-pyrolysis with nitrogen-compounds at a temperature up to 800°C.

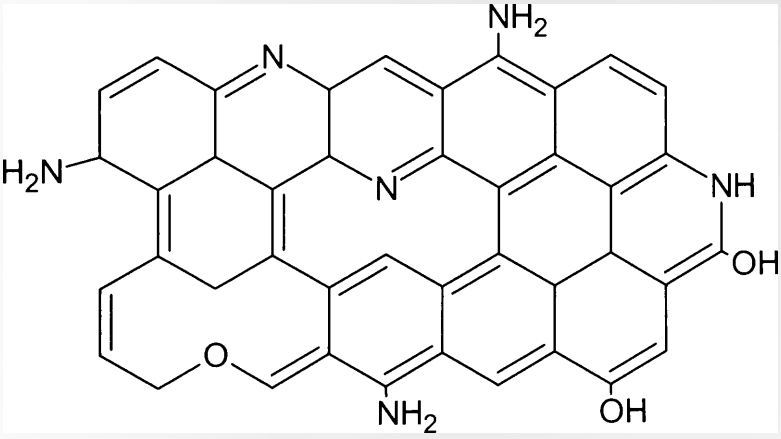

Figure 6.40 A possible structure of the nitrogen-containing carbon xerogel resulting from the co-pyrolysis of RF-xerogel with N-containing compounds at a temperature of 700 – 800°C

6.4.4 Effect of impregnation on the pore structure by N_2 (77K) adsorption

For these series of experiments the RF-xerogel prepared with MEA as a catalyst (R/C ratio = 100, R/W = 0. 25 g/cm^3 and pH = 6) was chosen. Then the sample was impregnated with different percentages of *m*-phenylenediamine (MPDA) and diphenylenimine (DPI) according to the method described in Section 5.1.5. For the purpose of obtaining optimum pore structure after impregnation, the co-pyrolysis conditions (co-pyrolysis temperature and hold time) were first studied for the samples impregnated with 20% MPDA and DPI. Figures 6.41 and 6.42 show the effect of the co-pyrolysis temperature on the BET surface area, micropore area and micropore volume for the two impregnated samples (MPDA 20% and DPI 20%). For both samples, theses three textural properties (BET surface area and micropore area and volume) of the prepared carbons increased with increases co-pyrolysis temperature from 400 to 700°C, but decreased with further increases in temperature. The BET surface area decreased from 510 to 400 m^2/g (for sample DPI20%) and from 420 to 170 m^2/g (for sample MPDA20%) as the co-pyrolysis temperature was increased from 700 to 900°C.

The two distinct temperature regimes (the increase in surface area and then further decrease with respect to temperature) for both samples are consistent with the TGA and DTGA results discussed in Section 6.4.2 for the emission of the low and high molecular weight volatiles. In the low temperature regime (the first increase in surface area), increasing the co-pyrolysis temperature from 400 to 700°C increases the release of low molecular-weight volatiles from the sample matrix structure, resulting in increasing

rudimentary pores in the carbon. This leads to the production of carbon with high BET and micropore surface areas and volume. At this case, as the co-pyrolysis temperature increases the BET and micropore surface areas and volume also increase. However, when the co-pyrolysis temperature was increased too much (800–900°C), softening and sintering of the high-molecular weight volatiles occurred, resulting in the depolymerisation of the melt and shrinkage of the total volume of the carbon sample. Hence, for increasing co-pyrolysis temperature from 800 to 900°C, the co-pyrolysis yields carbon with both a low BET surface area and a low micropore surface areas and volume.

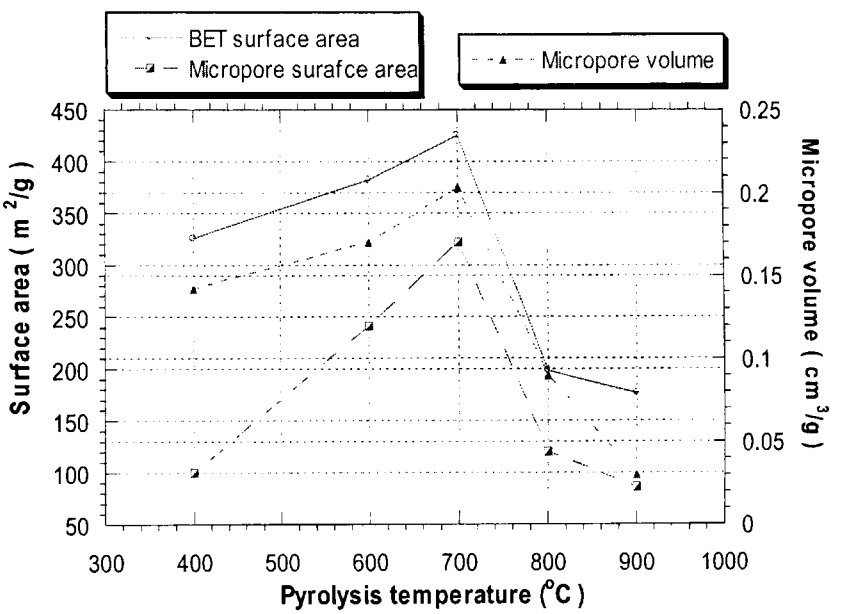

Figure 6.41 Effect of co-pyrolysis temperature on the BET surface area, micropore area and volume of the sample of surface modified carbon xerogel with MPDA 20%. Hold time = 2hr; argon flow = 100 ml/min., and heating rate = 5°C /min.

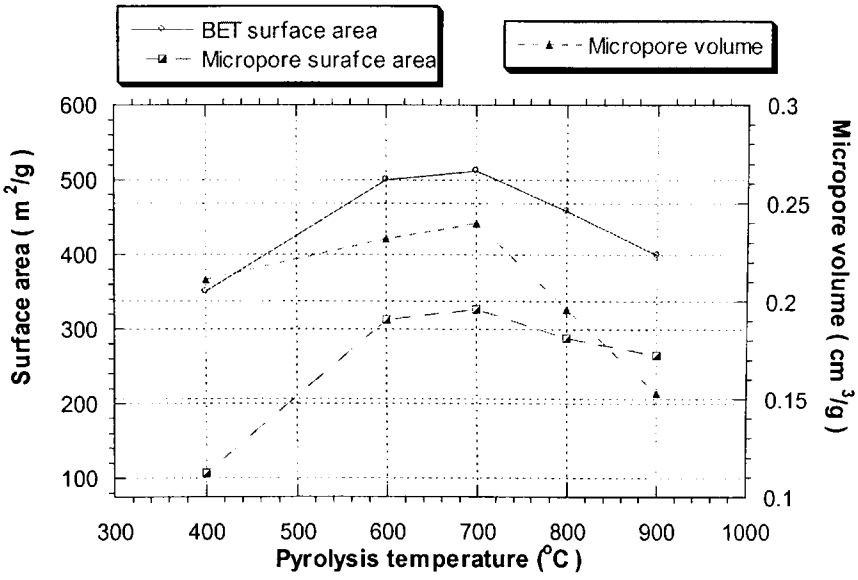

Figure 6.42 Effect of co-pyrolysis temperature on the BET surface area, micropore area and volume of the sample of surface modified carbon xerogel with DPI 20%. Hold time = 2hr; argon flow = 100 ml/min., and heating rate = 5°C /min.

Within the experimental conditions studied, the best co-pyrolysis temperature to derive the best textural characteristics for the resulting carbons was 700°C. At this condition, the co-pyrolysis involves thermal decomposition of both the carbonaceous material and the nitrogen compounds, eliminating non-carbon species producing a fixed carbon mass and rudimentary pore structure. The process involves various important stages that markedly determine the properties of the final carbons to be obtained. For a low degree of co-pyrolysis, the basic pore structure is formed. Some of these pores are blocked by the tarry products evolved during co-pyrolysis and these pores are only available when further heat treatment to about 700°C is carried out. Further heat treatment to 800°C or above, leads to hardening of the carbon structure (due to partial alignment of the graphitic planes) accompanied with a decrease in porosity.

Figures 6.43 and 6.44 show the influence of the co-pyrolysis hold time on the BET surface area, micropore area and volume of the resulting carbons. As the co-pyrolysis hold-time increased, the rudimentary development of pores in the carbon improved. These could be attributed to the increasing release rate of volatile matters from the carbon structure. However, an increasing prolonged heat treatment at 700°C during co-pyrolysis lead to an increased softening and sintering of the low-molecular-weight volatiles, forming an intermediate melt. This melt could seal off some of the pores in the char. So, according to the experimental conditions studied, the maximum BET surface area, micropore area and volume were obtained for carbons co-pyrolyzed at a hold time of 2 hr.

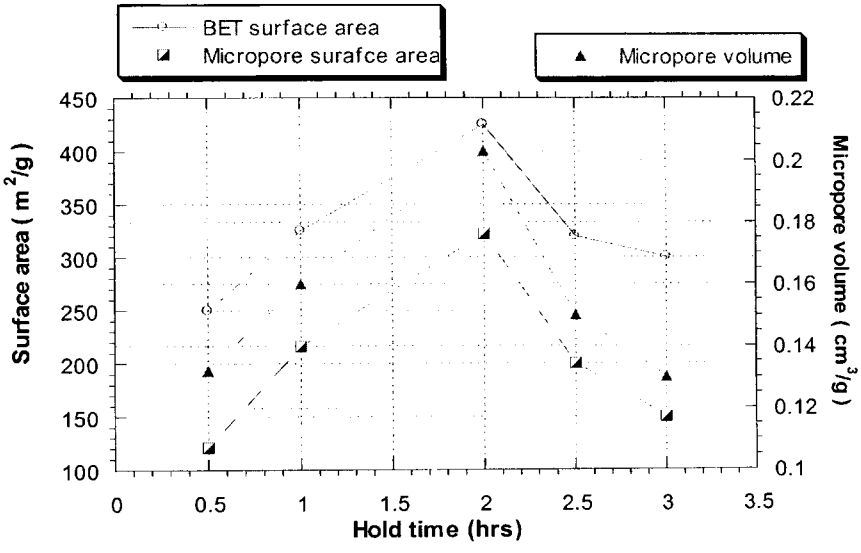

Figure 6.43 Effect of co-pyrolysis hold time on the BET surface area, micropore area and micropore volume of surface modified carbon xerogels with MPDA 20%. Co-pyrolysis temperature = 700°C, argon flow = 100 ml/min., and heating rate = 5°C /min.

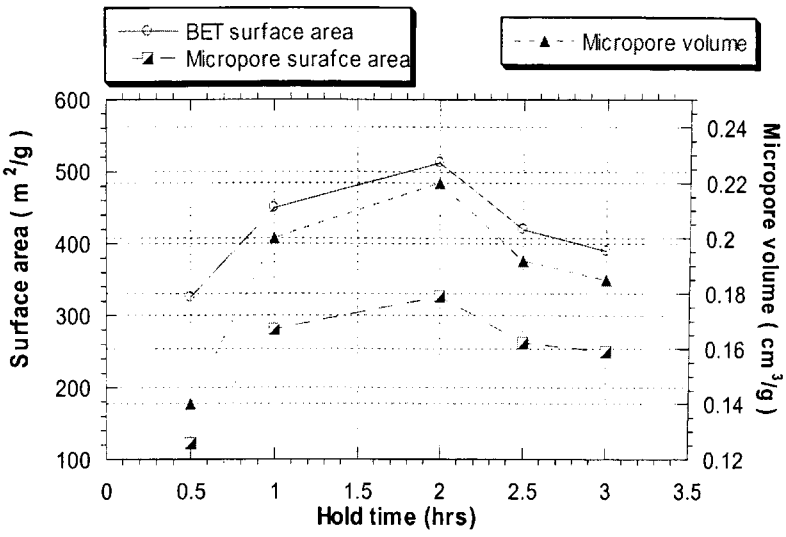

Figure 6.44 Effect of co-pyrolysis hold time on the BET surface area, micropore area and micropore volume of surface modified carbon xerogels with DPI 20%. Co-pyrolysis temperature = 700°C, argon flow = 100 ml/min., and heating rate = 5°C /min

Table 6.7 shows the characteristic pore properties for the surface modified carbon xerogels with MPDA and DPI (pyrolyzed under argon flow 100 ml/min at a temperature of 700°C for 2 hr heating rate = 5°C /min). The co-pyrolysis of the RF-xerogel with nitrogen compounds resulted in a dramatic decrease in the surface area, total pore volume and micropore volume. This is probably due to pore blockage and surface coverage by *m*-phenylenediamine (MPDA) and diphenylenimine (DPI) during pyrolysis of the RF-resins. In addition, the selection of DPI for the co-pyrolysis leads to a great decrease of the micropore volume and surface area than MPDA: this is obvious from the slope of the curves as shown in Figure 6.45. This could be attributed to the molecular weight difference between the two compounds.

Apparently, co-pyrolysis of the RF-xerogel with nitrogen compounds produces a series of interactions that, although having the positive effect of incorporating nitrogen into the carbon xerogels structure have the disadvantage of markedly diminishing the textural properties of the resulting carbons

Table 6.7 Characteristic pore properties of RF carbon xerogels and its counterparts surface modified carbon xerogels with different percentage MPDA and DPI. Pyrolysis conditions: argon flow 100 ml/min, pyrolysis temperature of 700°C for 2 hr and heating rate = 5°C /min.

Nomenclature	S_{BET} [a] (m^2/g) ±10	S_{mic} [b] (m^2/g) ±10	V_t [c] (cm^3/g) ±0.02	V_{mes} [d] (cm^3/g) ±0.02	V_{mic} [e] (cm^3/g) ±0.02	D_p [f] (nm) ±0.02
RFC-700°C	760	410	0.73	0.35	0.38	3.81
*RFC-MPDA10%-700°C	520	320	0.46	0.23	0.24	3.55
RFC-MPDA20%-700°C	420	320	0.62	0.42	0.20	5.84
RFC-MPDA30%-700°C	180	130	0.14	0.06	0.08	3.01
RFC-MPDA40%-700°C	3.94	-	0.01	0.01	0.01	-
RFC-MPDA50%-700°C	-	-	0.01	0.01	-	-
RFC-DPI10%-700°C	560	340	0.42	0.16	0.26	2.97
RFC-DPI20%-700°C	510	320	0.30	0.09	0.21	2.38
RFC-DPI30%-700°C	460	310	0.32	0.13	0.19	2.76
RFC-DPI40%-700°C	120	80	0.10	0.03	0.07	3.29
RFC-DPI50%-700°C	20	10	0.02	0.01	0.01	4.20

* Each sample followed by the nitrogen compound used for surface modification and the percent of impregnation and then finally the co-pyrolysis temperature. [a] Specific surface area determined from the BET equation. [b] Micro pore surface area. [c] Total pore volume. [d] Mesopore volume. [e] Micropore volume determine by Horvath-Kawazoe equation [e] Mean pore diameter. Note; the number of significant figures quoted in the table an indication of precision

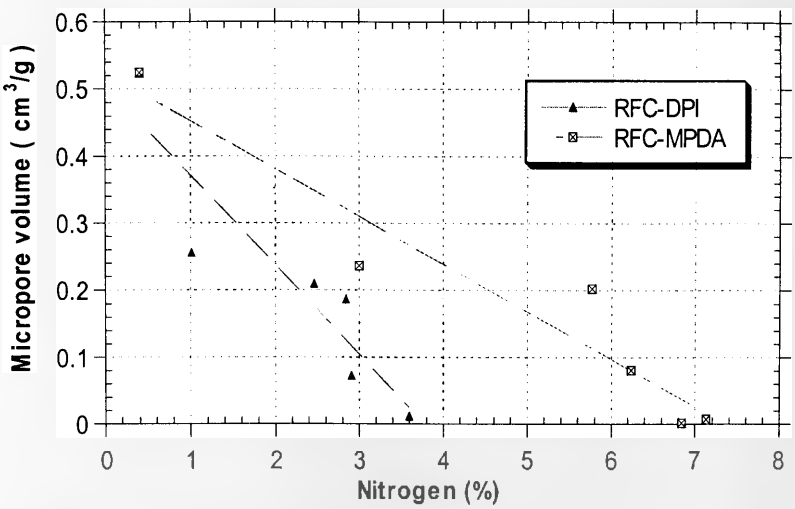

Figure 6.45 The dependence of the micropore volume on the nitrogen percent for the two series of surface modified carbon xerogels

6.5 Binary adsorption of CO_2-N_2 system by modified GC technique

The flow-rate and composition records of the experiment described in Section 6.3, for the sample of carbon xerogel prepared with MEA as a catalyst with R/C ratio = 100, R/W = 0. 25 g/cm^3 and pH = 6, and pyrolyzed at a temperature of 700°C for 2 hr., are shown in Figures 6.46 and 6.47 respectively. The differential pressure transducer (DPT) flow-rate records are shown for the addition of each perturbation gas to the carrier mixture. The times τ_x and τ_n for the TCD and DPT were determined by measuring the areas and the offsets on the chart records.

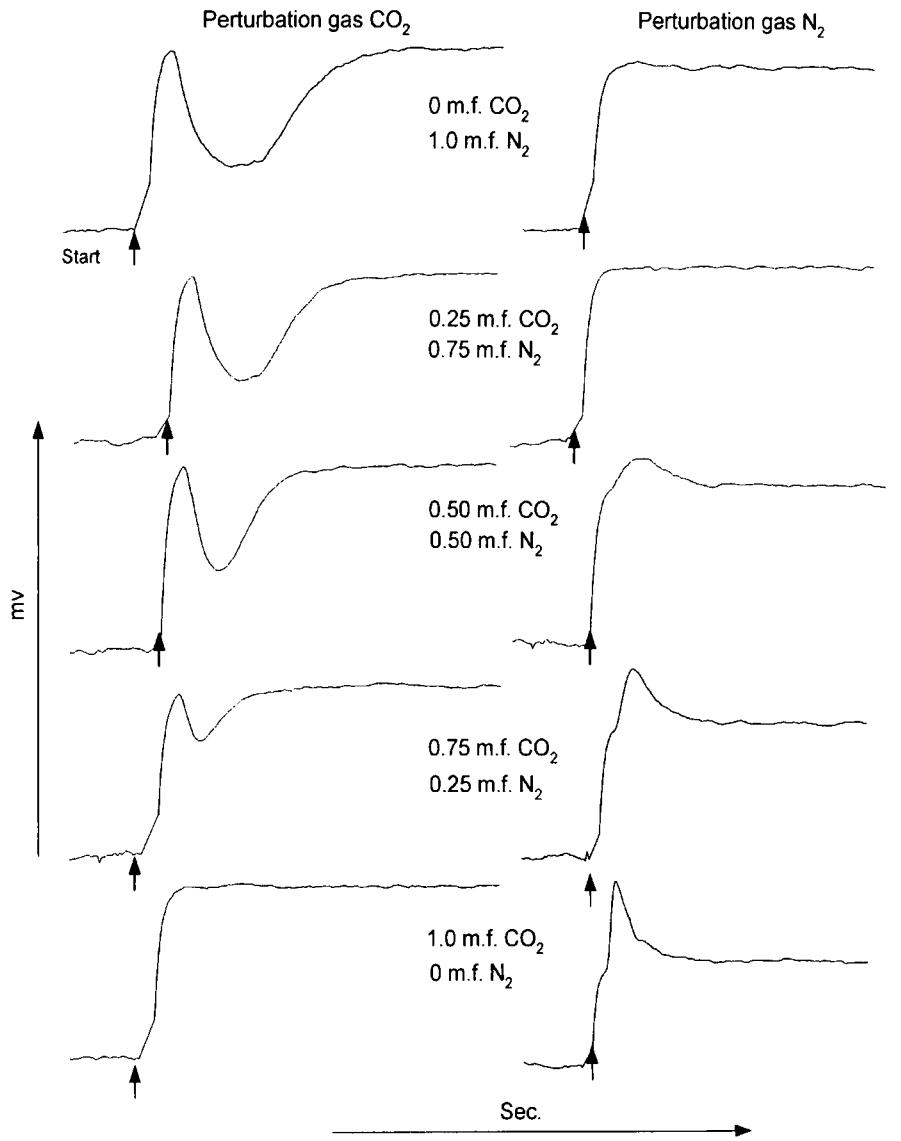

Figure 6.46 The flow-rate records (of DPT) due to addition of a perturbation flow, showing a net increase in flow when N_2 perturbation gas is added (net desorption) and a decrease when CO_2 perturbation gas is added (net adsorption).

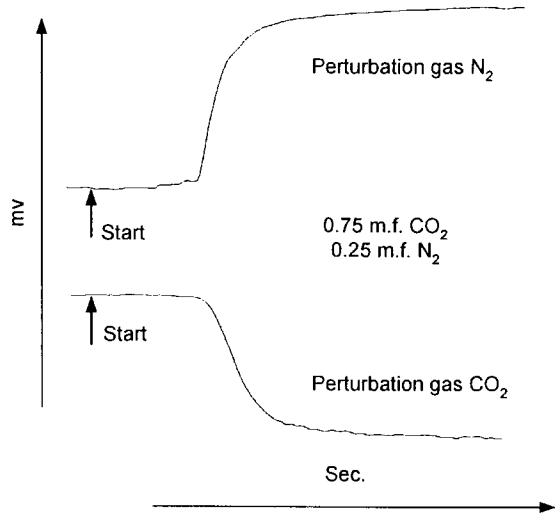

Figure 6.47 The composition records of TCD, they are straight forward and of well-known type and so only one example is shown

The results of the illustrative experiment in Section 5.3 are shown in Table 6.8. It can be seen from a cursory inspection of the results that, the time for the composition transient to pass (τ_x) is independent of which perturbation gas is used. The flow-rate retention times (τ_n) however, show considerable variation, being positive when CO_2 is added and generally negative when N_2 is added. The flow-rate of the main flow varies considerably with composition; this is due to the flow being set by a fixed pressure drop across a length of capillary tube and hence varying with the viscosity of the gas mixture. The viscosities of CO_2 and N_2 are different, and the mixture viscosity varies slightly with composition.

Table 6.8 Typical experimental results from the apparatus described in Section 5.3 for the sample of carbon xerogel prepared with MEA as a catalyst with R/C ratio = 100, R/W = 0. 25 g/cm^3 and pH = 6

Main flow mole fraction CO_2	Flow-rate Q_{at}(ml/s)	Perturbation gas	τ_x / s ±5	τ_n / s ±5
0	0.38	N_2	-	2
		CO_2	80	38
0.25	0.39	N_2	53	-2
		CO_2	60	30
0.50	0.42	N_2	48	-4
		CO_2	47	19
0.75	0.49	N_2	23	-4
		CO_2	22	11
1.0	0.52	N_2	12	-9
		CO_2	-	3

Note; the number of significant figures quoted in the table an indication of precision

Figure 6.48 shows the experimental and Langmuir fitting binary adsorption isotherm of CO_2-N_2 system for the sample RFC. All others binary adsorption isotherms are presented in Appendix A. The isotherm describes the amount adsorbed of CO_2 and N_2 via the mole fraction of CO_2 at 25°C and 1.05 bar. The isotherm was used to calculate the adsorption capacity of the activated carbon xerogels via CO_2 and N_2. The isotherm shows that the CO_2 adsorption isotherm increases with CO_2 mole fraction in the main gas flow. The adsorption isotherm also shows that the uptake of CO_2 was higher than that of nitrogen; this may be attributed to specific functional groups on the carbon

surface which are created due to the usage of MEA as a catalyst in the polycondensation reaction of resorcinol with formaldehyde. This preferential uptake of CO_2 indicates that this sorbent is promising for the separation of CO_2 from gaseous mixtures.

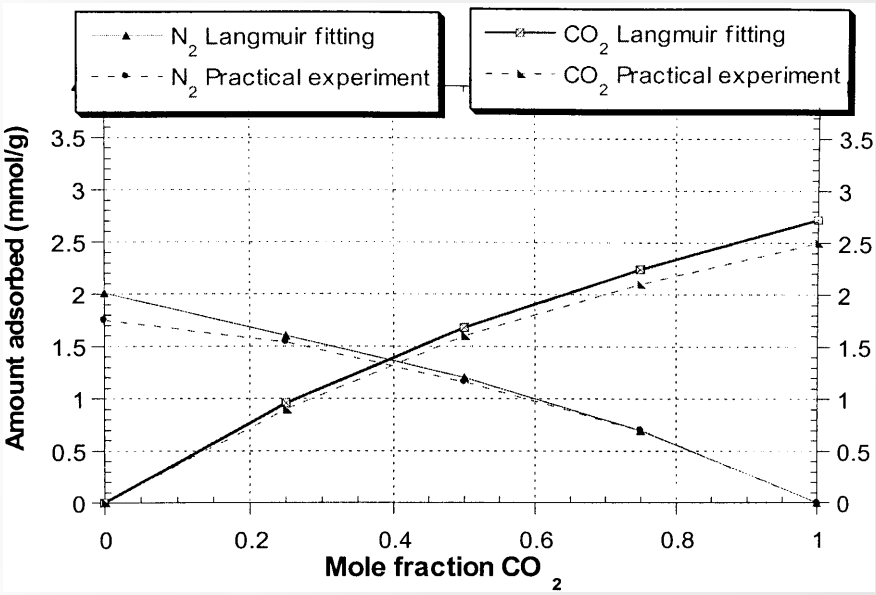

Figure 6.48 Experimental and Langmuir fitting binary isotherm for CO_2-N_2 gas mixture at 25°C and 1.05 bar for resorcinol-formaldehyde RF carbon xerogel (RFC) sample.

6.5.1 Effect of pore structure and activation conditions on CO_2 adsorption capacity and separation factor

Table 6.9 shows the CO_2 capture capacity and CO_2/N_2 uptake ratio (the ratio of pure-component adsorbed) at 25°C and 1.05 bar of activated carbon xerogel prepared at different R/C ratio and under different activation condition. The results show that, as the R/C ratio is increased from 50 (RFAC-50-850-1) to 300 (RFAC-300-850-1), the CO_2 adsorption capacities increase from 110 to 130 mg/g. This could be attributed to the

increase of the micropore volume of the resulting carbon due to changing R/C as described in the results of Section 6.3.3, where the microporė volume of sample RFAC-50-850-1 is 0.35 cm^3/g, while it equals 0.45 cm^3/g for RFAC-300-850-1. There is no clear relationship between surface area and CO_2 capacity and selectivity. For example, the activated carbon xerogel with surface area 970 m^2/g (sample RFAC-50-850-1) has a CO_2 capture capacity and CO_2/N_2 selectivity of only 110 mg-CO_2/g-adsorbent and 2 respectively, while the activated carbon xerogel with surface area of only 720 m^2/g (sample RFAC-300-850-1), has CO_2 capture capacity and CO_2/N_2 selectivity 130 mg-CO_2/g-adsorbent and 2.9 respectively. In general, the adsorption capacity of an activated carbon highly depends on the presence of micropores. So, with regard to activated carbon adsorption capacity, it is of interest to investigate how it depends on the micropore volume.

Table 6.9 Effect of the activation conditions on the CO_2 adsorption capacity and CO_2/N_2 uptake ratio at 25°C and 1.05 bars.

Sample name	Adsorption capacity (mg /g adsorbent ±1.0) at 25°C and 1.05 bar		$CO_2/N_2 \pm 0.1$ ratio
	CO_2	N_2	
RFAC-50-850-1*	110	55	2.0
RFAC-100-850-1	115	54	2.1
RFAC-200-850-1	125	48	2.6
RFAC-300-850-1	130	45	2.9
RFAC-100-850-2	135	43	3.1
RFAC-100-850-3	156	42	3.7
RFAC-100-900-1	139	43	3.2
RFAC-100-980-1	146	40	3.6

*RFAC refer to resorcinol-formaldehyde activated carbon xerogel sample followed by the R/C ratio used during the preparation then the activation temperature and activation holdup time. Note; the number of significant figures quoted in the table an indication of precision

Figure 6.49 shows the relationship between the CO_2 adsorption capacity and the CO_2/N_2 uptake ratio (the ratio of pure-component adsorbed) versus the micropore volume at 25°C and 1.05 bar. It seems that the samples with the highest micropore volume have the highest CO_2 adsorption capacity and CO_2/N_2 pure uptake ratio. Previous studies have shown that only pore sizes less than 5 times the molecular size of the adsorbate are effective for gas adsorption at atmospheric pressure (Martin-Martinez et al., 1995). So,

accordingly to this only pore less than 1.0 nm are effective for CO_2 capture at atmospheric pressure. In addition, Pradhan and Sandle (1999) found that 70% of the adsorption capacity in CMS is due to the micropores present .

Since the molecular size of CO_2 is 0.209 nm and that of N_2 is 0.364 nm, it is easier for the CO_2 molecule to diffuse through the micropores than the N_2 molecules. So as the micropore volume increases the selectivity towards CO_2 adsorption will also increase. Therefore, it is desirable to tailor the pore size distribution of the activated carbons, especially in order to maximize the pores less than 1.0 nm, to optimize the physical adsorption of CO_2 onto the carbon surface.

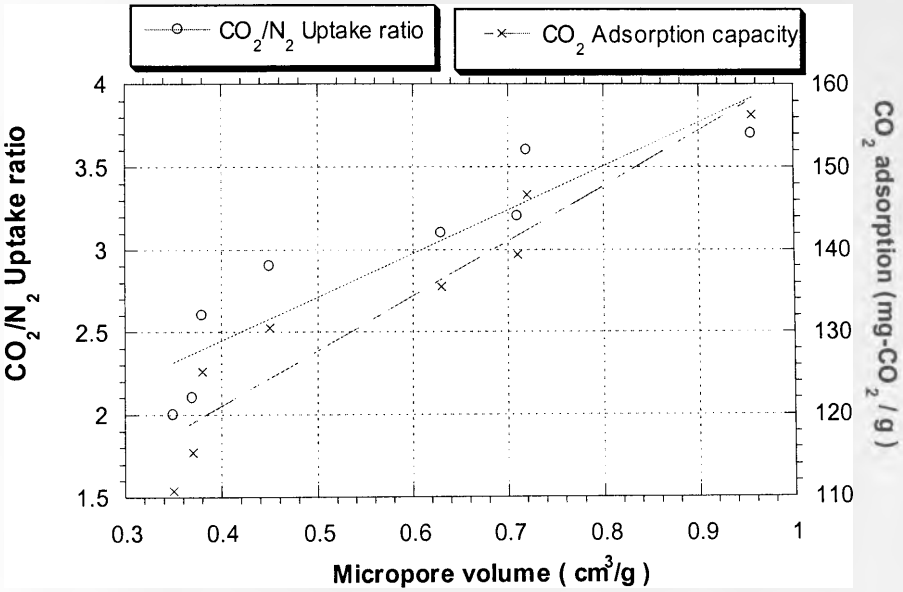

Figure 6.49 Variation of CO_2 adsorption capacities and CO_2/N_2 uptake ratio at 25^0C via micropore volume

6.5.2 Effect of adsorption temperature on CO_2 adsorption capacity.

Figure 6.50 shows the CO_2 adsorption capacities for the sample of carbon xerogel prepared with MEA as a catalyst (R/C ratio = 100, R/W = 0. 25 g/cm^3 and pH = 6, and pyrolyzed at a temperature of 700°C for 2 hr) measured at different adsorption temperatures (25, 50 and 100°C). It can be seen that the adsorption capacity decreases rapidly with increasing adsorption temperature. This behavior is typical of a physical adsorption process which is the dominant type in these series of adsorption study. In this process, both the surface adsorption energy and the molecule diffusion rate increase with increasing temperature. As a consequence, the adsorbed gas on the surface of activated carbon xerogel becomes unstable, resulting in desorption of adsorbed CO_2 molecules. In the present study, the CO_2 capture capacity of the activated carbon xerogel at 25°C is about 7-8 times higher than that at 100°C (120 mg-CO_2/g-adsorbent vs. 15.3 mg-CO_2/g-adsorbent). Since the CO_2 and N_2 are both physically adsorbed in the carbon surface. Both the pure components adsorbed amounts of CO_2 and N_2 reduce with increasing temperature.

6.5.3 Effect of surface chemical modification on CO_2 adsorption capacity

For these series of experiments the sample of RF-xerogel prepared with MEA as a catalyst with R/C ratio = 100, R/W = 0. 25 g/cm^3 and pH = 6 was chosen. Then the sample is impregnated with different percentage of *m*-phenylenediamine (MPDA) and diphenylenimine (DPI) according to the method described in Section 5.1.5 All the samples were the pyrolyzed under pyrolysis conditions; argon flow 100 ml/min.,

pyrolysis temperature 700°C for 2 hr and heating rate = 5°C /min. Table 6.10 shows the amount of CO_2 adsorbed and CO_2/ N_2 uptake ratio at 25 and 100°C for these series of samples. For simplicity and ease of comparison the corresponding results of the nitrogen percentage and micropore volume are also presented in the same table.

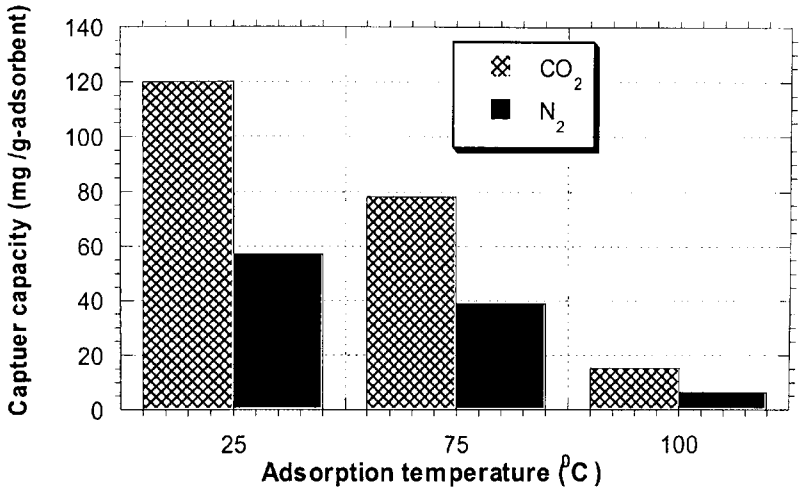

Figure 6.50 CO_2 and N_2 adsorption capacities of the carbons xerogel as a function of adsorption temperature

For lower temperature, the amount of CO_2 adsorbed and the CO_2/N_2 uptake ratio is reduced by the impregnation. Figure 6.51 shows the variation of CO_2 adsorption capacities measured at 25°C, with the % loading MPDA and DPI to the resin during pyrolysis for the both prepared series RFC-MPDA and RFC-DPI of carbons. Again as confirmed before, the results shows that the samples that have high micropore volume also have the higher CO_2 adsorption capacity. Figure 6.52 shows the relationship between CO_2 adsorption capacity and the micropore volume for the two impregnated

series of samples. The CO_2/N_2 uptake ratio is low at low temperature. However, it seems this ratio increased due to impregnation.

Table 6.10 The effect of surface chemical modification of the prepared carbon xerogels on CO_2 adsorption capacity and CO_2/N_2 uptake ratio at 25 and 100°C compared with the corresponding amount of the nitrogen percent and micropore volume of each sample

Sample name	N % ±0.05	V_{mic} (cm^3/g) ±0.02	Adsorption capacity ± 1.0(mg /g) 25 °C CO_2	N_2	CO_2/N_2 ratio ± 0.1	100 °C CO_2	N_2	CO_2/N_2 ratio ± 0.1
RFC-	0.40	0.38	120	57	2.1	15	6	2.5
RFC-MPDA10%	3.00	0.24	60	24	2.4	25	8	3.0
RFC-MPDA20%	5.77	0.20	49	19	2.6	35	8	4.4
RFC-MPDA30%	6.24	0.08	34	34	3.0	46	8	5.6
RFC-MPDA40%	7.13	0.01	25	11	3.0	37	7	5.2
RFC-MPDA50%	6.84	-	19	6	3.0	27	5	5.4
RFC-DPI10%	1.01	0.26	66	28	2.3	20	7	2.7
RFC-DPI20%	2.46	0.21	52	20	2.6	32	7	4.6
RFC-DPI30%	2.84	0.19	46	16	2.8	42	8	5.1
RFC-DPI40%	2.91	0.07	35	12	2.9	50	8	7.1
RFC-DPI50%	3.60	0.01	29	9	3.0	47	7	6.6

RFC refers to resorcinol formaldehyde carbon xerogels followed by the nitrogen compounds used for surface modification and the percentage of impregnation. Note; the number of significant figures quoted in the table an indication of precision

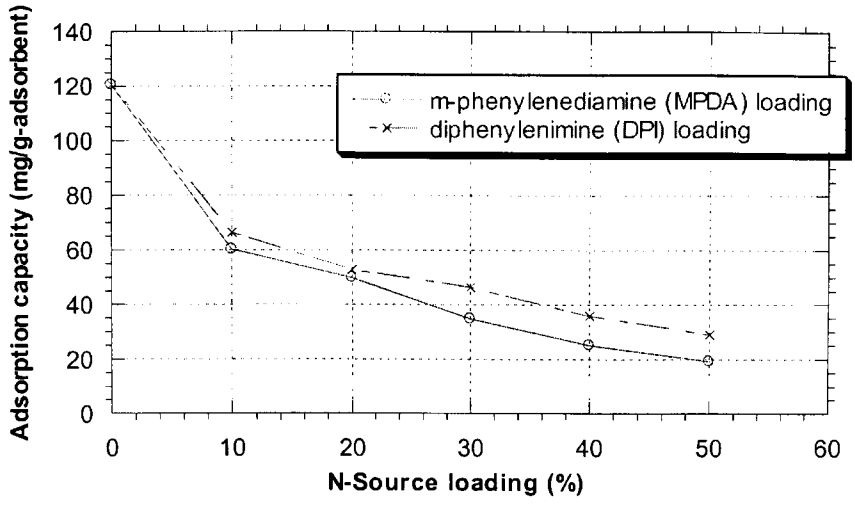

Figure 6.51 The variation of CO_2 adsorption capacities measured at 25°C, with the % loading MPDA and DPI to the RF xerogel during co-pyrolysis for the both prepared series RFC-MPDA and RFC-DPI of carbons

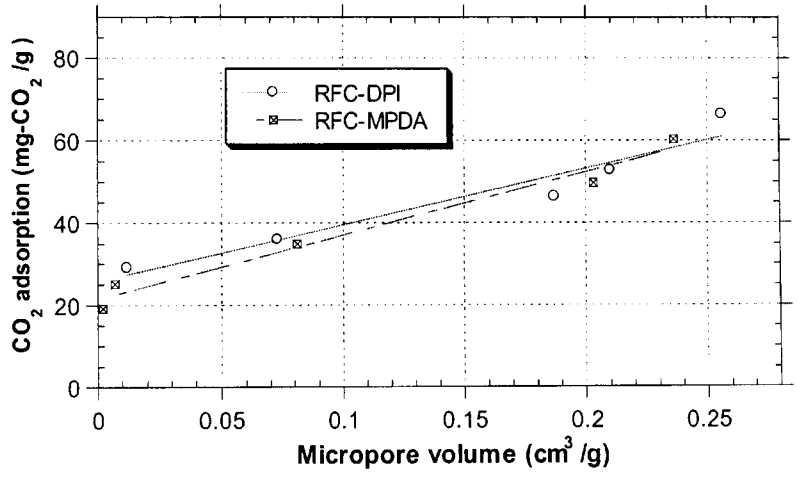

Figure 6.52 Variation of CO_2 adsorption capacities measured at a temperature of 25°C via micropore volume for the prepared carbon series RFC-MPDA and RFC-DPI

For adsorption studied at higher temperature, the amount of CO_2 adsorbed and CO_2/ N_2 uptake ratio for impregnated sample are significantly higher than that of non impregnated one. In addition to, as the % impregnation increase the amount of CO_2 adsorbed and CO_2/ N_2 uptake ratio increase, reach to a maximum (30% sample impregnated with MPDA and 40% sample impregnated DPI) and then decrease. Figure 6.53 shows the variation of CO_2 adsorption capacities measured at 100°C with the % loading MPDA and DPI to the resin during pyrolysis, for the both prepared series RFC-MPDA and RFC-DPI of carbons. This decrease of adsorption capacity observed may be attributed to lose of the porous structure of the sample due to excessive impregnation.

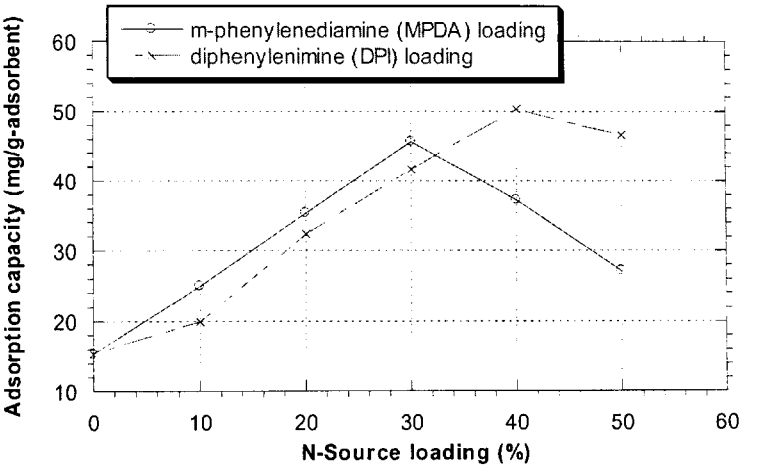

Figure 6.53 The variation of CO_2 adsorption capacities measured at 100°C, with the % loading MPDA and DPI to the RF xerogel during co-pyrolysis for the both prepared series RFC-MPDA and RFC-DPI of carbons

The impregnated samples show higher affinity to adsorb CO_2 than N_2, and as the % of impregnation increase this affinity increase. This affinity might be due to the presence of nitrogen functional groups produced in accordance of using N-containing compounds as impregnant before the pyrolysis process. This N-functionality makes chemisorptions to take a part in the adsorption process. For practical applications, selective adsorbents with high capacity are desired, as many of the separations should preferably be operated at elevated temperature, e.g., higher than room temperature and up to ~ 100 ^{o}C. Figure 6.54 shows the dependence of the CO_2 adsorption capacity on the percent nitrogen in the samples. It seems like the sample with the highest nitrogen percent has higher adsorption capacity. In general, there are many factors that influence CO_2 adsorption some of them are physical and some chemical. The porous structure will be the overriding factor for any adsorption process, but in the case of CO_2 adsorption the surface chemistry of the adsorbent is also relevant.

Since, CO_2 is an acidic gas, alkaline surface functional groups introduced by the impregnation favor chemisorptions of CO_2. Among the surface functional groups studied before on the activated carbon surface, only some nitrogen functional groups are alkaline (Cagniant et al., 1998). This is also why surface impregnation was applied to improve the adsorption capacity of activated carbon especially at higher temperature, and the incorporation of nitrogen atoms gives a prior a basic character to the activated carbon surface and thus promotes the CO_2 adsorption. It worth to say that , the samples impregnated with impregnation percent over 30% , the CO_2 adsorption capacity

increased with temperature, as expected from a chemical adsorption process. Mercedes et al.,(2005) reported that the CO_2 adsorption capacity increased with temperature for the sample of anthracites impregnated with PEI (polyethylenimine). The same phenomena reported by many researchers (Xiaochun et al., 2002, 2003).

According to Equations 6.1 to 6.3 the formation of carbamate is favored for the majority of the CO_2 capture systems. Two moles of amine groups react with one mol of CO_2 molecule. Prepared carbon xerogels should have similar reactions with gaseous CO_2 and amine sites on its surface as shown in Figure 6.55.

$$CO_2 + 2RNH_2 \Leftrightarrow NH_4^+ + R_2NCOO^- \quad (6.1)$$

$$CO_2 + 2R_2NH \Leftrightarrow R_2NH_2^+ + R_2NCOO^- \quad (6.2)$$

$$CO_2 + 2R_3NH \Leftrightarrow R_4N^+ + R_2NCOO^- \quad (6.3)$$

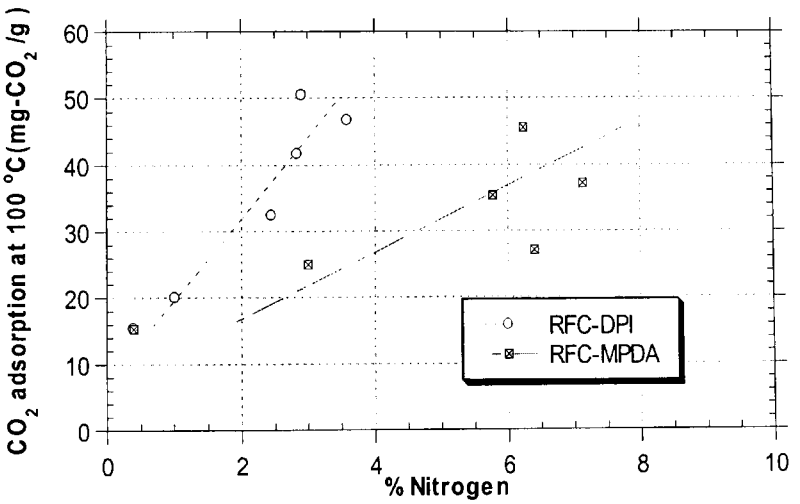

Figure 6.54 The variation of CO_2 adsorption capacities measured at 100°C, with the nitrogen content for the both prepared carbon series RFC-MPDA and RFC-DPI

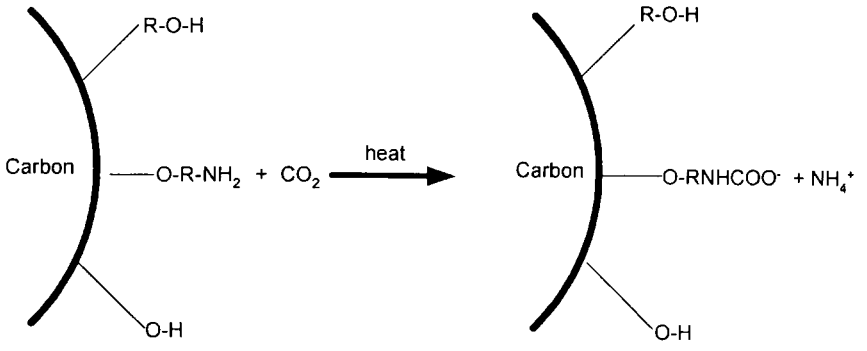

Figure 6.55 Proposed reaction of the nitrogen functionality on the prepared carbon with CO_2

In addition, the presence of –OH functional groups in the carbon surface may promote CO_2 adsorption. In a previous CO_2 adsorption study Delaney and co-workers (2002) reported that the ratio of CO_2 molecular per available nitrogen atom in the presence of hydroxyl group is approximately twice that without the hydroxyl group. They suggest that the CO_2 chemical adsorption mechanism of the amine changed in the presence of hydroxyl group. In the presence of hydroxyl groups, the formation of carbamate type zwitterions is stabilized by the presence of –OH groups, so that one molar amine groups react with one mole CO_2 molecule. Therefore the presence of -OH may influence the chemical adsorption mechanism that leads the adsorption capacity to be increased.

Finally it is worth stating that the samples obtained by impregnation with DPI40-50%, despite the low amount of nitrogen incorporated compared with those impregnated with MPDA40-50% show a high CO_2 adsorption capacity. This phenomena could be because of not only the amount of nitrogen in the adsorbent is going to be the only important factor for adsorption of CO_2 at higher temperature, but there are also another important

factors which are the nitrogen functionalities and the pore structure, as it has reported that nitrogen functionalities can have different basicity (Burg et al., 2002). Thus, the micropore volume, accessibility, distribution and orientation of the available amine sites all have the potential of playing an important role in the performance of this solid CO_2 capture sorbent.

Compared with conventional adsorbents, the prepared carbon xerogels samples in this study showed better CO_2 adsorption performance at low and relatively high temperature. Table 6.11 lists the CO_2 adsorption performance of zeolite, activated carbon, PEI/polymer composite and molecular basket (Si/Al-MCM-41) adsorbents. The prepared carbon xerogel sample (RFAC-100-850-3) shows a good CO_2 adsorption capacity compared to zeolite 4A and activated carbon, 156 mg/g vs 135 and 110 mg/g respectively. Sample RFC-DPI40% in this study shows superior CO_2/N_2 ratio (7 vs 2.9 for Si-MCM-41) at relatively high temperature.

Table 6.11 Comparison of CO_2 adsorption performance of the prepared carbon xerogels adsorbents and other adsorbents

Adsorbents	Temp (°C)	Pressure (atm)	Ads. capacity (mg/g)	CO_2/N_2 ratio	Ref.
Si-MCM-41	25	1	27.3	-	Xu et al., 2003
Si-MCM-41-PEI-50	25	1	32.9	-	Xu et al., 2003
Zeolite 13 X	25	1	168	-	Siriwardane et al., 2001
Zeolite 4A	25	1	135	-	Siriwardane et al., 2001
Activated carbon	25	1	110	-	Siriwardane et al., 2001
Norit RBI activated carbon	21.5	1	108	~2(CO_2/CH_4)	Vaart et al.,2000
Activated carbon	20	1	88	~2(CO_2/CH_4)	Berlier et al., 1997
Norit RBI activated carbon	25	1	140.8	~1.9(CO_2/CH_4)	Dreisbach et al., 1999
APT(Carbon sphere)	30	1	87.8	-	Przepiorski et al., 2002
GP30(Carbon sphere)	30	1	59.2	-	Przepiorski et al., 2002
RFAC-100-850-3	25	1.05	156	3.7	This study
RFAC-300-850-1	25	1.05	130	2.9	This study
Si-MCM-41	75	1	8.6	-	Xu et al., 2003
Si-MCM-41	75	0.149	6.3	2.9	Xu et al., 2002
Si-MCM-41-PEI-50	75	1	112	-	Xu et al., 2003
Al-MCM-100-PEI-50	75	1	127	-	Xu et al., 2003
Norit RBI activated carbon	75	1	40	~2(CO_2/CH_4)	Vaart et al.,2000
Activated anthracite	75	1	28	-	Mercedes et al., 2005
PEI- Activated anthracite	75	1	26.3	-	Mercedes et al., 2005
Ammonia-treated-Ac. anthracite	75	1	23.7	-	Mercedes et al., 2005
PEI-silica gel	75	1	78.1	-	Xu et al., 2003
PEI-polymer	50	0.02	40	-	Satyapal et al.,2001
Ammonia-treated-active carbon	36.5	1	75	-	Przepiorski et al.,2004
RFC-MPDA30%	100	1.05	45.56	5.6	This study
RFC-DPI40%	100	1.05	50.32	7.0	This study

6.6 Effect of pressure on the CO_2 adsorption capacity by TPD-MS

In this part, the results of temperature programmed desorption mass spectrometry experiments on carbons samples loaded with high pressure CO_2 are discussed. Carbons were initially loaded with CO_2 at high pressure for a certain time, and then the pressure was reduced to atmospheric pressure. TPD-MS was used to monitor desorption of reversibly sorbed CO_2 as a function of temperature. More detailed of the experimental conditions found in Sections 5.4 and 5.5.

Firstly for better understanding of the CO_2 desorption profile characteristics, the sample loaded with CO_2 at 25°C and 1.05 bar where chosen, in which the adsorbed amount of CO_2 was 120 mg/g as measured according to the method described in Section 6.3 and the results of the adsorption experiment of that sample were discussed in section 5.5.3. Figure 6.56 shows the rates of CO_2 desorption as a function of temperature before and after loading with CO_2. The thermo desorption spectrum for CO_2 desorption from the fresh sample is almost at the baseline. A small difference between the TPD spectrum of the fresh sample and the baseline might be due to the presence of small amount of CO_2 in the sample tubes or adsorbed on carbon sample when it was exposed to the atmosphere before performing TPD. The figure shows that the intensity of desorption signal is quite high. The shape of the spectrum shows that as the temperature increases CO_2 is desorbed from carbon, the rate of desorption increases then goes through a maximum and drops to zero as further increases of temperature. This shows that the desorbing molecules must pass through an activated state and CO_2 desorption from

carbon is an activated process. At low temperature the surface coverage is high, but the rate constant is low so that desorption of adsorbed molecules is difficult and desorption rate is low. As the temperature is increased, the rate constant increases and thus the desorption rate increases. At medium temperature, both the surface coverage and the rate constant are high therefore desorption rate reaches a maximum. At higher temperatures most of the adsorbed molecules have desorbed so that the coverage is almost zero and although the rate constant is in its maximum the desorption rate goes to zero.

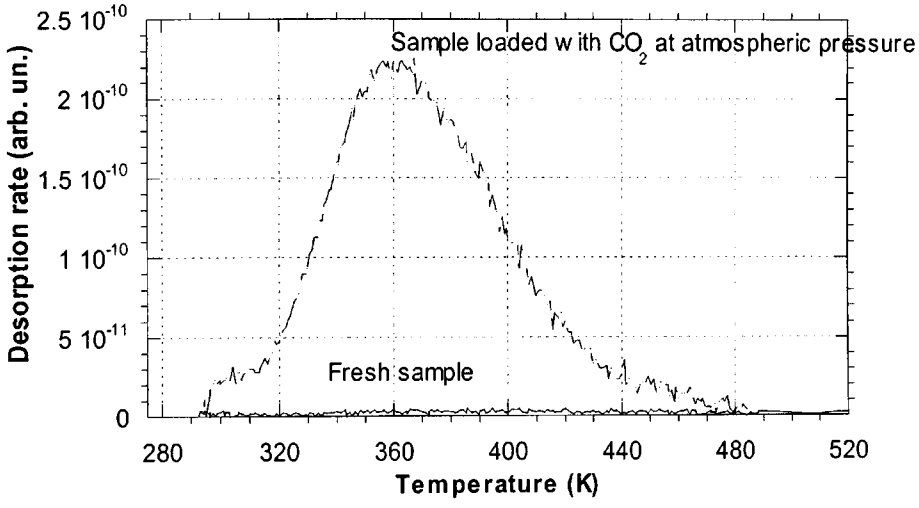

Figure 6.56 TPD spectra of CO_2 desorption of carbon xerogel (RFC) sample without surface modification, the sample loaded with CO_2 at 25°C and 1.05 bar

TPD-MS spectra of CO_2 adsorbed on sample of carbon xerogels at various pressures are shown in Figures 6.57 and 6.58. The spectra have two regions of interest. The first one at low temperatures in the region of (250-400 K) and the second one after the peak temperature, T_p (the temperature of maximum rate of desorption), where desorption rates decrease with increasing temperature. To analyze the desorption data, the TPD-MS

spectra have been modeled using The Redhead equation 6.4, the assumption of a first order desorption process with a single activation energy for desorption (Redhead, 1962),

$$\ln\left(\frac{N_p}{N}\right) = \frac{E_{des}}{R}\left(\frac{1}{T}-\frac{1}{T_p}\right)+\left(\frac{T}{T_p}\right)^2 \exp\left[-\frac{E_{des}}{R}\left(\frac{1}{T}-\frac{1}{T_p}\right)\right]-1 \qquad (6.4)$$

where N_p is the maximum desorption rate at peak temperature, T_p, and N is defined as the desorption rate at any temperature. The equation has been used to describe the desorption kinetics of desorbed CO_2. The fitting curve shows that the Redhead equation provides a good fit to the experimental data in the range of (250-400 K). As can be seen, the CO_2 desorption from the sample of interest follows the first order desorption model at low temperature and the low temperature part of the spectra is well represented by equation.

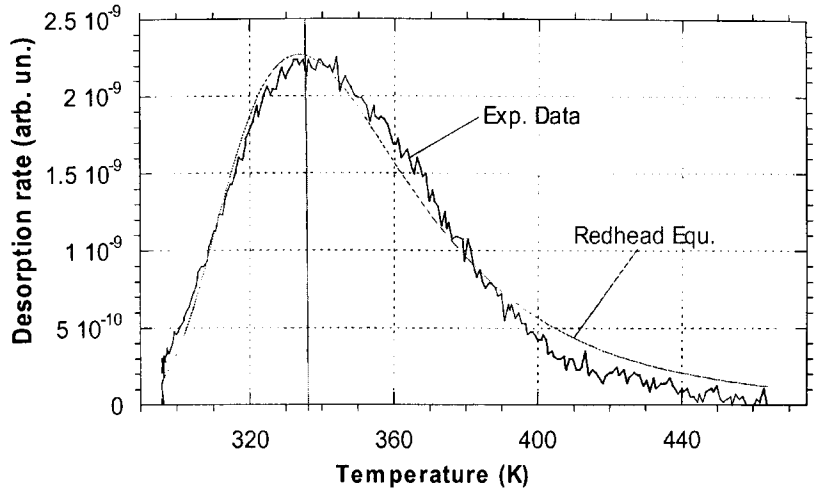

Figure 6.57 TPD spectra of CO_2 desorption of carbon xerogel (RFC) sample without surface modification, the sample loaded with CO_2 at 25°C and 10 bar

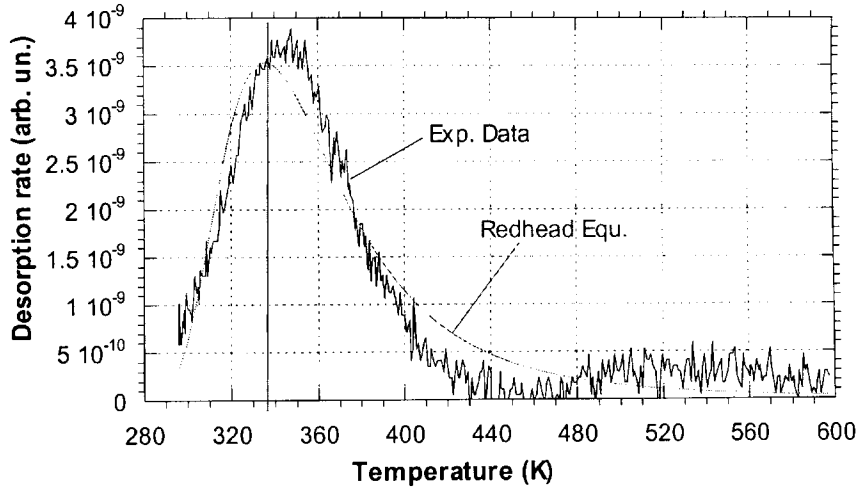

Figure 6.58 TPD spectra of CO_2 desorption of carbon xerogel (RFC) sample without surface modification, the sample loaded with CO_2 at 25°C and 20 bar

However, the high temperature part of the spectra do not follow the fist order desorption model. The rate of desorption after the peak temperature obtained from TPD-MS experiment is differ than that predicted by the first order desorption model. This comparison shows that desorption kinetics are changed and the change might be due to the diffusion resistance to desorption of CO_2 form the carbon surface as the result of the nitrogen functional groups. The sample of the prepared carbon xerogels is containing some nitrogen functional group as confirmed before from FT-IR study. These nitrogen functionality may hindered desorption of CO_2 due to the chemisorptions process.

The process of CO_2 desorption is a mass transfer process involving several elementary process. These processes may include diffusion through macropores, diffusion through micropores. In small micropores, diffusional resistance limits mass transfer process. The mass exchange can also be limited due to the large energy barrier for desorption due to the effect of the surface functional groups. At higher surface coverage's, the diffusivity is high and the rate of desorption reaches a maximum. The reason for this increase in rate is that desorption occurs from the most occupied sites in the microporous structure leading to the release of the low energetic physisosorbed sites. As temperature increases and desorption process proceeds, high energetic sites in the microporous structure, which are occupied by strong interactions with CO_2, are released. However due to the large energy barrier the rate of desorption from these sites is very low. As further increase of temperature the CO_2 molecules which is chemisorbed on the carbon surface start to get enough energy to break the strong chemical bond, and energy barrier for

desorption at that stage reach a maximum value and the deviation from first order assumption becomes more significant. Therefore the deviation of desorption spectra from redhead equation may be due to the contributions of activated diffusion effects, micropore diffusional resistance, barrier resistance of high energetic sites and experimental error in the instrument.

Comparing the CO_2 desorption profile which the CO_2 loaded at 10 and 20 bar, we could conclude that the deviation from fitting first-order desorption kinetics increases with increasing pressure. This might be due the high adsorbate adsorbent interactions which increase with increasing the pressure of adsorbate and consequently leads to formation more strong bonds with the adsorbent functionality. At that stage the barrier for desorption increase and deviation from first order assumption increase. Table 6.12 shows the desorption kinetics of trapped CO_2. The values of the activation energy for desorption, E_{des} are calculated from the fitting of the desorption spectra with Redhead equation. The data shows that, the total area under TPD-MS spectrum is proportional to the amount of CO_2 adsorbed and that energy of desorption increase with the increase of pressure.

Table 6.12 The desorption kinetics of trapped CO_2 at different pressure.

Pressure Bar	E_{des}(cal/mol)	N_p (arb. unit)	T_p (K)	Integrated area	Correlation factor
1	8308 ± 159	2.116×10^{-10}	375	1.68×10^{-8}	0.960
10	9609 ±78	2.240×10^{-9}	337	1.563×10^{-7}	0.989
20	1040 ± 118	3.48×10^{-9}	340	2.926×10^{-7}	0.958

E_{de} activation energy for desorption, Np desorption rate at peak temperature, T_p peak temperature. Note; the number of significant figures quoted in the table an indication of precision

TPD-MS spectra of CO_2 adsorbed on carbon xerogels sample at various pressures are compared in Figure 6.59. It can be noted that the desorption intensities increases with pressure, which indicate that the amount adsorbed in the sample is grater at high pressure, consequently this adsorbent could be ideal for pressure swing adsorption (PSA) applications.

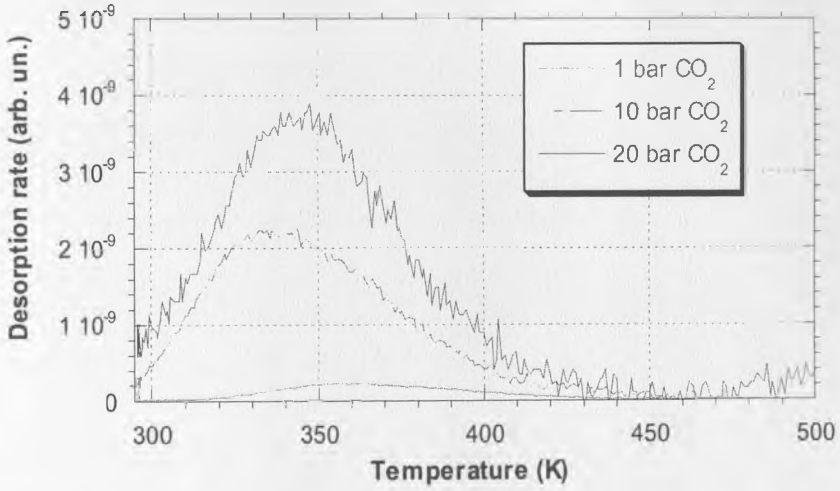

Figure 6.59 TPD spectra of CO_2 desorption of carbon sample, where the sample loaded with CO_2 at 25°C and 1, 10 and 20 bar.

6.7 CO_2 desorption measurements and carbon xerogels regeneration and by TPD-MS

The regeneration of any adsorbent consists of removing the adsorbed substances from its surface and restoring, as far as possible, the initial adsorptive properties. In industrial practice there are two concerns: the recovery of any valuable materials adsorbed on the carbon surface and use of the same adsorbent many times for removing toxic substances. The regenerated adsorbent should therefore recover as much as possible the initial adsorptive capacity. The difficulty in achieving this aim depends on whether we are dealing with physical or chemical sorption. Physical adsorption is a reversible process and removal of the adsorbate is fairly straightforward and may be realised, for instances, simply by increasing the temperature (TSA) or reducing the pressure (PSA).

6.7.1 Effect of surface chemical modification on the CO_2 desorption profile

In this part we will discuss the results of temperature programmed desorption mass spectrometry experiments of two surface modified RF carbon xerogels samples (RFC-MPDA30% and RFC-DPI30%). The samples were loaded with CO_2 at 100°C and 1.05 bar using the apparatus described in Section 5.2. The amounts of CO_2 adsorbed were 46 and 42 mg/g respectively, as measured according to the method described in Section 5.3. The results of the adsorption experiment of these samples were discussed in Section 6.5.3. After CO_2 adsorption experiments, TPD-MS was used to monitor desorption of reversibly sorbed CO_2 as a function of temperature. In TPD-MS analysis, approximately 200 mg of carbon sample was used in each analysis then the temperature increased to

900°C with a heating rate of 30°C/min under a helium flow of 100 ml/min to flush evolved gas into the mass spectrometer. The mass spectrometer was adjusted to detect the mass of CO_2 (44).

Figures 6.60 and 6.61 show the TPD profiles of RFC-MPDA30% and RFC-DPI30% respectively. The shape of the spectra show that as the temperature is increased CO_2 is desorbed from carbon and the rate of desorption increases to a maximum and then drops to zero as the temperature is increases further. However, compared to Figure 6.56, it is worth stating that the samples need more time or reach to higher temperatures for all the CO_2 to be desorbed. As it could recognize that the samples reach to about 900 K without desorbed all the adsorbed amount of CO_2. This can be attributed to, in contrast to physical adsorption which could be recognize in Figure 6.56 regeneration in the case of chemisorption Figures 6.60 and 6.61 is a much more complex problem, due to the much stronger forces bonding the adsorbate (CO_2) molecules to the adsorbent surface (surface modified carbon xerogels). Or this is probably due to the experimental conditions of desorption, where the heating rate was 30°C/min. This high heating rate did not give sufficient time for all the CO_2 to be desorbed. In general, the optimal conditions of the regeneration or reactivation process ensure minimal losses of carbon and good recovery of the adsorbate should be determined. There are three factors playing a major role in the regeneration process: (1) the maximum temperature of regeneration, (2) the time or rate of regeneration or reactivation (heating rate in case of thermal regeneration), (3) the

degree of saturation of the carbon with the adsorbed substance. This leads to a potential work which could be investigated in the future.

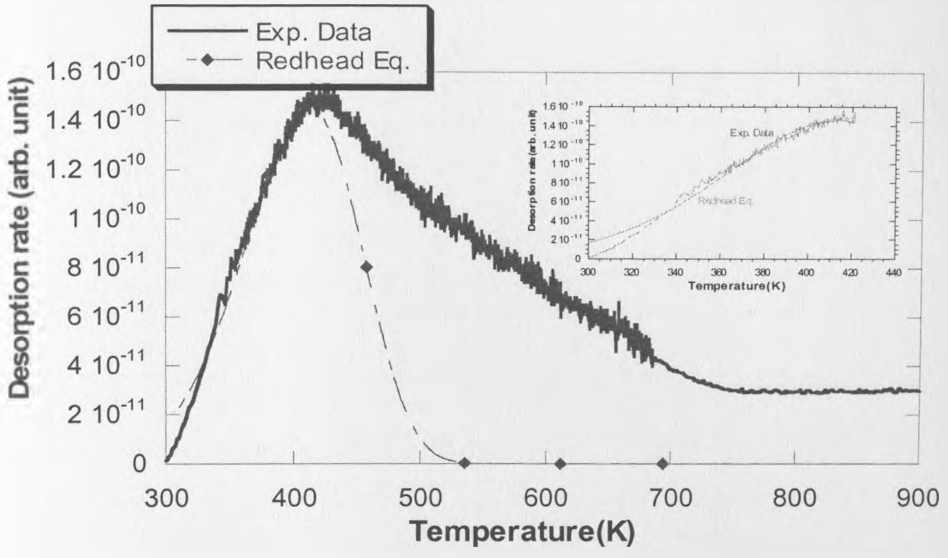

Figure 6.60 TPD spectra of CO_2 desorption of carbon sample RFC-MPDA30%, where the sample was originally loaded with CO_2 at 100°C and 1.05 bar. The sample heated to 900°C at a rate of 30°C/min with a flow rate of helium 20 ml/min to flush the evolved gas into the mass spectrometer. The embedded graphs shows the fitting of the low temperature part of the curve with Redhead equation

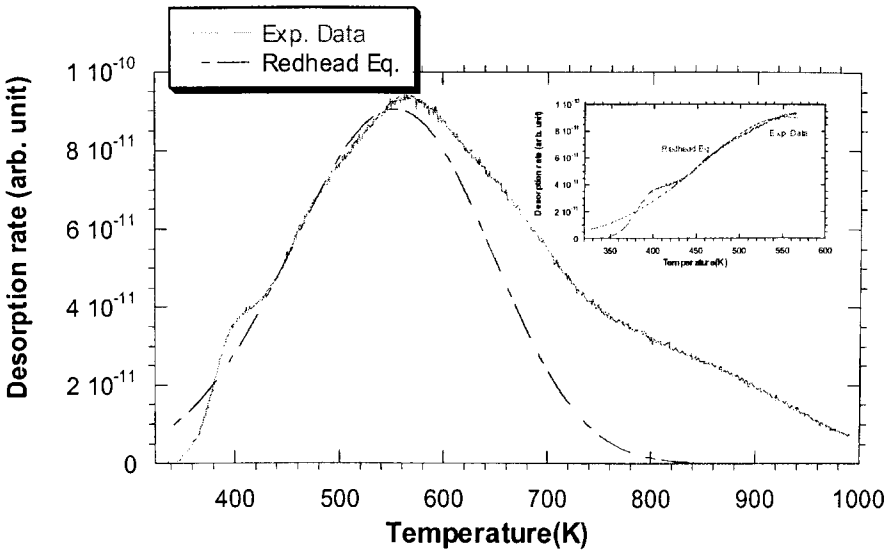

Figure 6.61 TPD spectra of CO_2 desorption of carbon sample RFC-DPI30%, where the sample was originally loaded with CO_2 at 100°C and 1.05 bar. The sample heated to 900°C at a rate of 30°C/min with a flow rate of helium 20 ml/min to flush the evolved gas into the mass spectrometer.The embedded graphs shows the fitting of the low temperature part of the curve with Redhead equation

6.7.2 Desorption kinetics calculation

As discussed before the TPD-MS spectra have been fitted with Redhead equation to enable determination of the desorption kinetics. The embedded graphs in Figures 6.60 and 6.61 show that the Redheads equation and the first order desorption assumption provides a good fit to the experimental data in the low temperature part of the curve where physical adsorption dominates the adsorption process. However, in the high temperature range Redhead equation provides a poor fit where chemisorptions is the dominate process. In contrast to physical adsorption, which it easily to be recognize in the TPD results discussed before in Section 6.6, regeneration in the case of

chemisorptions is much more complex problem, due to the much stronger forces bonding the adsorbate molecules to the adsorbent surface. In case of the physical process the attachment of the adsorbate is due to Van der Vaals forces, hydrogen bonds, etc., whereas in chemisorptions we are dealing with ionic or covalent bonding. When the adsorbate molecules are weakly bonded to the adsorbent surface (physical adsorption), it is sufficient to lower the partial pressure of the adsorbate in the gas phase and hence shift the adsorption equilibrium towards desorption simply by lowering the overall pressure. If these energies are somewhat higher, desorption is affected by heating. This, however, may sometimes lead to the destruction of the adsorbate molecules and such a possibility should be taken into account. In the case of chemisorption the reversibility between the adsorption and desorption processes is incomplete. Supply of energy equal to desorption energy does not lead to complete regeneration of the adsorbent surface. So, after desorbing or release of CO_2 from the low energetic physisosorbed sites, it becomes very hard to overcome the high energy barrier in the high energey chemisorbed sites and as a result the deviation from the first order (Redhead equation) increases. These deviations are very obvious in the high temperature part of the Figures 6.60 and 6.61. Table 6.13 shows the desorption kinetics of the trapped CO_2. The values of the activation energy for desorption, E_{des} are calculated from the fitting of the low temperature part of the desorption spectra. It is worth noting that the peak temperature which is define the temperature at the maximum desorption rate is different for each sample. This temperature could be an indication about the strength of the adsorbate-

adsorbent bond, where the more weakly bound state has the lower activation energy for desorption and will therefore undergo desorption at a lower temperature

Table 6.13 The desorption kinetics of trapped CO_2, where the samples loaded with CO_2 at 100 °C and 1.05 bar.

Sample	E_{des}(cal/mol)	N_p	T_p (K)	Integrated area	Correlation factor
RFC-MPDA30%	6386.3 ±111.46	1.427×10^{-10}	423	4.083×10^{-8}	0.990
RFC-DPI30%	5236 ± 101.59	8.599×10^{-11}	590	3.016×10^{-8}	0.988

E_{de} activation energy for desorption, Np desorption rate at peak temperature, T_p peak temperature. Note; the number of significant figures quoted in the table an indication of precision

6.7.3 Effect of thermal treatment during desorption (regeneration) on the carbon xerogels structure stability

In this part of result we discussed the thermal stability of the prepared carbon structure during heat treatment of the desorption (regeneration) process. So, thermal gravimetric (TGA) and temperature programming desorption (TPD-MS) techniques were applied to measurer the weight losses profile as well as the evolving gases of carbons decomposition products during regeneration process. Two fresh (not originally loaded with CO_2) surface modified carbon xerogels samples (RFC-MPDA30% and RFC-DPI30%) have been chosen for this study. Where, we expect some instability in the structure or redistributions of the functional groups on the carbon surface and/or other

factors which consequently may lead to degradation of the carbon structure during regeneration.

For TGA analysis, 3 mg of sample was weighed in the crucible of the TGA, and the temperate was increased to 900°C at 30°C/min in argon flow of 20 ml/min. In this test we tried to match the same conditions of regeneration applied which are mainly the heating rate and the maximum temperature. Figure 6.62 and 6.63 show the thermal gravimetric analysis (TGA) and derivative thermal gravimetric analysis (DTGA) curves of RFC-MPDA30% and RFC-DPI 30% samples respectively.

The thermogram of the carbon samples can be clearly divided into three stages. Here, the first stage is up to 150°C and the second stage up to 750°C, the weight losses in both stages being around 9 % for (RFC-MPDA30%) and 3% for (RFC-DPI30%). The third stage, in which the main degradation of carbons takes place, starts from approximately 750°C and the degradation components of around 5-10 % are released. The DTGA curve of the carbons sample shows only two peaks. The first peak around a temperature of 100°C (RFC-MPDA30%) and 50°C (RFC-DPI30%), while the second peak around a temperature of 750°C (RFC-MPDA30%) and 820°C (RFC-DPI30%). The first peak can be attributed to desorption of water vapour or any atmospheric adsorbed gases. Whilst the second one could be related to the destruction of the surface functional groups, which it involve the breaking of C-H, C-O or C-N bonds. So, from the thermogravimetric analysis we could conclude that the prepared carbon xerogels material are quite stable during thermal

heating of regeneration process up to a temperature of 750-800°C . Heating above this temperature may leads to some degradation of the carbon structure. Sample RFC-DPI30% seems to be more stable for regeneration than RFC-MPDA30%, as the total weight losses in the later is 20% while for the RFC-DPI30% is 5% only. This might be due to the total percent nitrogen exist in the sample, the nitrogen percent in RFC-MPDA30% is 6.2 and that of RFC-DPI30% is 2.84 only

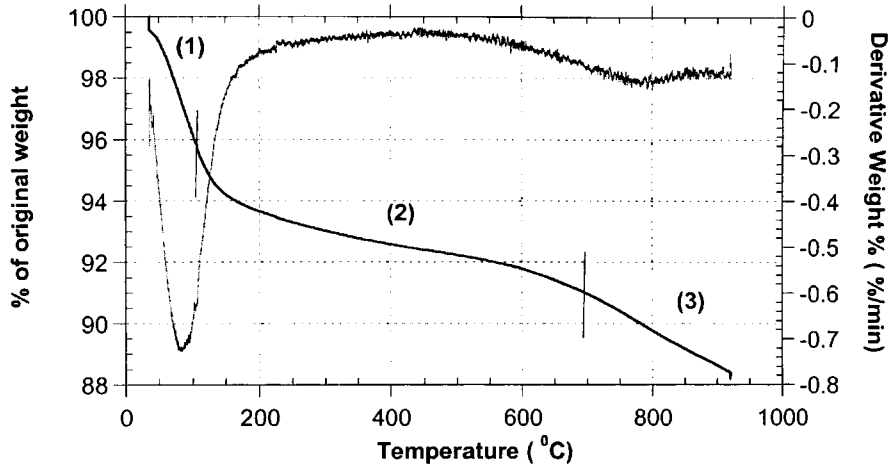

Figure 6.62 TGA and DTGA curves of RFC-MPDA 30% sample at the same regeneration conditions, (argon flow 20 ml/min and heating rate: 30 °C/min)

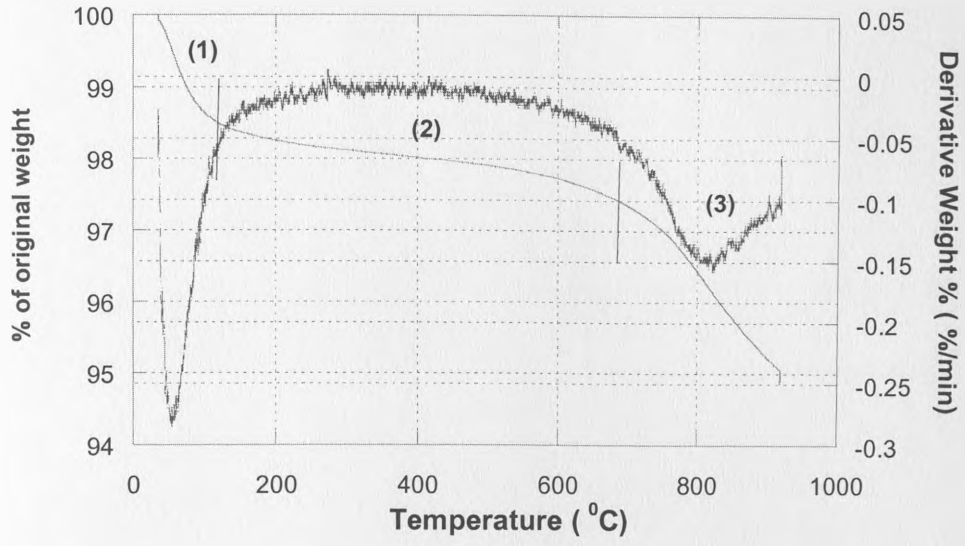

Figure 6.63 TGA and DTGA curves of RFC-DPI 30% sample at the same regeneration conditions, (argon flow 20 ml/min and heating rate: 30 ^{0}C/min)

For TPD-MS analysis, approximately 200 mg of carbon sample was used in each analysis then it is heated up to 900°C with a heating rate of 30°C/min under a helium flow of 20 ml/min to flush evolved gas into the mass spectrometer. The mass spectrometer was adjusted to detect masses of 17, 18, 28, 30 and 44. These masses were chosen regarding the decomposition product which may be evolved during regeneration. The experimental details are found in Section 5.5. Figures 6.64 and 6.65 show the TPD spectra of fresh carbon sample RFC-MPDA30%, and RFC-DPI30% where it show the possible decomposition products during regeneration process. As confirmed from the TGA study both samples start to decompose around a temperature of 750°C which could be observed from the peak of mass 28. This peak could be related to the release of CO gas which result from the destruction of the carbon structure

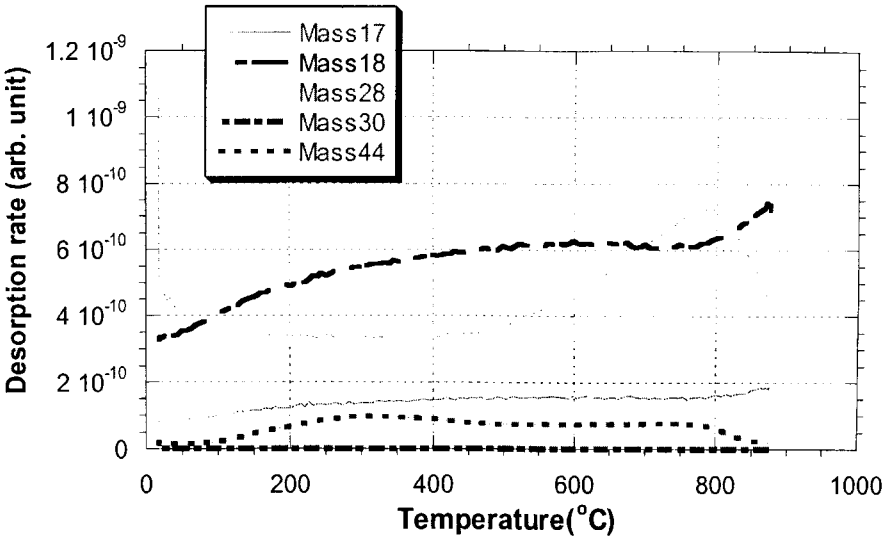

Figure 6.64 TPD spectra of fresh carbon sample RFC-MPDA30%, where it shows all possible composition products during regeneration process, heating rate of 30°C/min under a helium flow of 20 ml/min

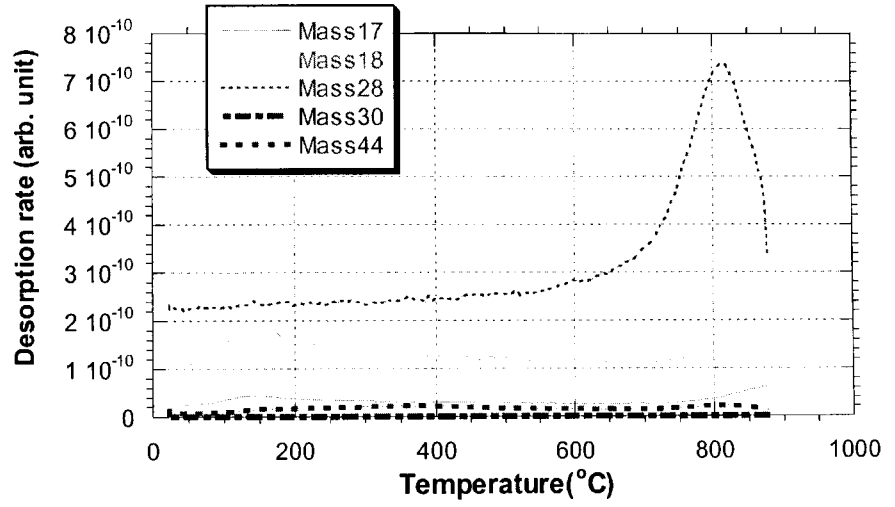

Figure 6.65 TPD spectra of fresh carbon sample RFC-DPI30%, where it shows all possible composition products during regeneration process, heating rate of 30°C/min under a helium flow of 20 ml/min

6.8 CO_2 adsorption measurements on regenerated carbon xerogels samples

Table 6.14 shows the CO_2 adsorption CO_2/N_2 uptake ratio after two regeneration cycle. The decrease in the CO_2 capture capacities upon regeneration was observed. And the impregnated samples show a higher decrease than the non impregnated one. This may be attributed to instability in the structure or that desorption of the CO_2 was incomplete. In addition, redistribution of the surface functional groups on the surface of the carbon and /or other factors could affect the adsorption and separation efficiency of CO_2 on the regenerated samples.

Table 6.14 The amount of CO_2 adsorbed and CO_2/N_2 uptake ratio at 100°C for fresh and regenerated samples

Sample name	Adsorption capacity ± 1.0 (mg/g) at 100°C		
	CO_2	N_2	CO_2/N_2 ratio ± 0.1
RFC-fresh	15	6	2.5
RFC-1st regeneration	14	6	2.3
RFC-2nd regeneration	14	6	2.3
RFC-MPDA30%-fresh	46	8	5.6
RFC-MPDA30%-1st regeneration	41	8	5.1
RFC-MPDA30%-2nd regeneration	40	8	5.0
RFC-DPI30%-fresh	42	8	5.2
RFC-DPI30%-1st regeneration	40	8	5.0
RFC-DPI30%-2nd regeneration	38	7	5.4

Note; the number of significant figures quoted in the table an indication of precision

In general, complete desorption of substances from carbons surface proceeds with great difficulty. This primarily due to the fact that the heat of adsorption and hence the heat of desorption is the greatest for small degrees of coverage of the adsorbent surface. In other words, the degree of desorption increases with temperature. However, since heating of the adsorbent layer to a high temperature is often undesirable, there always remains in the carbons a certain amount of adsorbate which reduces in successive cycles the adsorptive capacity of the carbon. Apart from normal reversible adsorption controlled by the adsorptive properties of the carbon, irreversible adsorption occurs consisting of the accumulation in the pores of in-volatile products of polycondensation of the adsorbate. These products are difficult to remove even if the active carbon is heated to 900°C. Usually good results are obtained by the action of steam heated to 700-900°C on the carbon. However, in all cases of regeneration and reactivation those process conditions should be established which exclude significant destruction of the carbon structure. Therefore when designing a new adsorbent, it is very important to measure the structure stability after or during regeneration.

Chapter 7

Critical appraisal and recommendation for future work

In this chapter we tried to collect all the critical appraisal of resorcinol-formaldehyde resin derived carbons preparations and its applicability as adsorbents for CO_2 capture and separation.

7.1 General

From the research presented and discussed in the preceding chapters, it was confirmed that resorcinol-formaldehyde xerogels catalyzed with amine could be successfully converted to activated carbon with high pore volume and surface area up to 2.58 cm^3/g and 3200 m^2/g, respectively with carbon yield 40% (Section 6.3). Furthermore the analyses revealed that high percent of this surface area and pore volume are mainly due to micropores (Figure 6.28). These features of high total surface area, pore volume, microporosity and carbon yields are good indicators that the carbon prepared from resorcinol-formaldehyde resins have promising features for application in the adsorption field. In addition, we have investigated the effect of loading different substances during the RF-xerogels pyrolysis stage which leads to new materials with different pore structures and a different surface chemistry. This changes the adsorption properties of the resulting carbons towards CO_2. This can be used to develop a new family of adsorbents with high selectivity and high adsorption capacity. In this a comprehensive review should be undertaken regarding all the synthesis parameter.

7.2 Carbon xerogels preparations critical appraisals.

In terms of the carbon xerogels preparation procedures and techniques discussed in Sections 6.1 and 6.2 it was concluded that the surface area and porosity of the resulting carbons prepared from the sol-gel polycondensation reaction of resorcinol with formaldehyde could be controlled through different parameters. The surface area of carbon xerogels can be controlled by controlling the resorcinol to catalyst ratio (R/C), while the micropore fraction depends on the selection of the catalyst. An alkanolamine basic medium produces a carbon with predominating micropore structure, while the carbonate basic medium yields carbon with meso- and macropore structure. It is possible to tailor the porosity of these materials by varying the initial pH of the precursor's solution in a narrow range. The selection of different catalyst species leads to RF xerogels with different surface chemistry. Selection of alkanolamine compounds as a catalyst leads to formation of some nitrogen surface functional groups, which we believe that it could enhance the CO_2 adsorptions. However, as a result of carbonization process of the resin most of these surface functionalities tend to be diminished. So, further research is required to choose the suitable carbonization conditions (carbonization temperature, hold up time, inert gas flow rate,..., etc) to produce carbons with similar porosity and maintain its inherent surface chemistry.

Activation of the resulting char is very important to enhance its surface area and pore volume. This increase of surface area and pore volume is usually achieved through a series of possible propagation processes which occurred during the carbon activation.

These processes are creating of new porosity, opening of closed porosity and widening of existing pores. However, excessive activation usually leads to burn-out of pore walls and most of activation process occurs at the exterior of the surface that lead to the particle to shrink, at this case activation does not lead to any pore development, and pore widening occurs. The evolutions of porosity with degree of activation were highlighted in Section 6.3. However more work should be conducted in this area to increase the carbon yields, as it was confirmed in the discussion of this section that the carbon yield is significantly decreased with degree of activation. This yield could be enhanced through selection of different treatments of the carbon xerogels samples (for example; treatment with HNO_3) before activation.

7.3 Surface modification critical appraisal.

The chemical nature of active carbons significantly influences their adsorptive, electrochemical, catalytic, acid-base, redox, hydrophilic-hydrophobic, and other properties. The great significance of this problem, both as regards its purely cognitive and practical aspects, has made it the subject of much research. So, in this study we give a proposal of a method for producing nitrogen enriched carbon xerogels. This has been done through the co-pyrolysis of the resulting resin with nitrogen compounds. However, many problems associated with this process are still not entirely explained. Due to different parameters that should be studied, further research is needed in the area. The surface modification research undertaken in this study revealed that the co-pyrolysis parameters such as temperature and holdup time have a significant influence in the

resulting carbon. The co-pyrolysis process involves various important stages that markedly determine the properties of the final carbons to be obtained. So, if suitable co-pyrolysis conditions were selected, high surface area and porosity nitrogen enriched carbons could be produced. The N-content of the resulting carbon was controlled by adjusting the N-source (*m*-phenylenediamine (MPDA) and diphenylenimine (DPI)) addition at 10-50 wt. %. The increasing of the nitrogen content resulted in a dramatic decrease of the surface area, total pore volume and micropore volume. Apparently, the co-pyrolysis of the RF-xerogel with nitrogen compounds produce a series of interactions that, although having the positive effect of incorporating nitrogen into the char, as mentioned before in Section 6.4.1 , have the disadvantage of markedly diminishing the textural properties of resulting carbons. So, it is the recommendation of this research that, if nitrogen enriched carbons to be produced from RF-xerogel, potential work should be done in the field of increasing the carbon basicity without affecting the porous structure such as: using different nitrogen sources with small molecular weight (e.g. urea, monoethanolamine); increasing basicity of RF carbon xerogels by incorporation of different nitrogen containing compounds (e.g. urea , melamine,....etc) in the polycondensation reaction of resorcinol with formaldehyde.

7.4 CO_2 adsorption by carbon xerogels critical appraisal

The binary gas adsorption isotherms for CO_2-N_2 system obtained from this research show a higher CO_2 uptake by the prepared surface modified carbon xerogels over N_2. This preferential uptake of CO_2 indicates that this sorbent is promising for the separation

of CO_2 from gaseous mixture. For the adsorption measurements research studied at ambient temperature and pressure, it revealed that, the samples with the highest micropore volume have the highest CO_2 adsorption capacity and CO_2/N_2 pure uptake ratio. Therefore, it is desirable to tailor the pore size distribution of the activated carbons, especially in order to maximize the pores less than 1.0 nm, to optimize the physical adsorption of CO_2 onto the carbon surface. This could lead to a potential work in the future and can be achieved by carbon deposition from the high-temperature cracking of gases such as methane.

The adsorption capacity decreases rapidly with increasing adsorption temperature. This behavior is typical of a physical adsorption process. For adsorption studied at higher temperatures, the amount of CO_2 adsorbed and CO_2/N_2 uptake ratios for the surface modified samples are significantly higher than those of non-impregnated one. In addition, as the % impregnation increase the amount of CO_2 adsorbed and CO_2/N_2 uptake ratio increase as a result of the chemisorptions reaction. Finally, the micropore volume, accessibility, distribution and orientation of the available amine sites all have the potential of playing an important role in the performance of this solid CO_2 capture sorbent. In conclusion, this study also demonstrates the potential of the surface chemistry of N-enriched RF-carbon xerogels for the generation of efficient CO_2 adsorbents, if this beneficial surface chemistry could be combined with advantageous pore structure. However, future work are required in this field, particularly the study of the nature of the nitrogen functionality by x-ray photoelectron spectroscopy (XPS), the

study of the effect of presence of water vapour in the gas mixture and study of their relevant effects on the CO_2 adsorption capacity by carbon.

TPD-MS spectra of CO_2 adsorbed on carbon xerogels sample at various pressures revealed that desorption intensities peak increases with pressure, which indicate that the amount adsorbed in the sample is greater at high pressure. Consequently, it is proposed that this adsorbent could be ideal for pressure swing adsorption (PSA) applications. However, development work on this proposal is required to evaluate the amount of CO_2 adsorbed, and study the effect of the applied pressure on the mechanical properties of carbons.

7.5 Carbon xerogels regeneration critical appraisal

The difficulty in regeneration of prepared carbons xerogels depends on whether we are dealing with physical or chemical sorption. Physical adsorption is a reversible process and the removal of the adsorbate from the surface may be realized, simply by heating. As we could realize from the work conducted that approximately all the amount of CO_2 adsorbed by physical adsorption could be desorbed by heating the sample up to temperature of 172°C. In the case of chemisorption, the reversibility between the adsorption and desorption processes is incomplete. So, for the surface modified samples, where the chemisorptions reactions takes place in the CO_2 adsorption, the samples need more time or reach to higher temperature for all CO_2 to be desorbed. In addition, the decrease in the CO_2 capture capacities upon regeneration was observed.

Further research in this field is required to accomplish the following; study the optimal conditions of the regeneration or reactivation process ensuring minimal losses of carbon and good recovery of the adsorbate such as (1) the maximum temperature of regeneration, (2) the time or rate of regeneration or reactivation (3) the degree of saturation of the carbon with the adsorbed substance., study the effect of high temperature of regeneration on the stability of recovered adsorbate structure. Evaluate the possibility of thermal regeneration with steam or regeneration by extraction.

Chapter 8

Conclusions

8.1 General

In this work we investigated the fascinating and remarkably flexible properties of resorcinol-formaldehyde (RF) carbon xerogels as a candidate adsorbent for CO_2 capture and separation and how these properties are related to the synthesis and processing conditions. These properties can be easily tailored by rigidly controlling the conditions. However, slight variations in the conditions may result in drastic variations in the structural characteristics and hence properties. Therefore, the effects of different conditions must be understood carefully before attempting to a specific application. This thesis should assist in this endeavor with understanding that the particular properties and trends reported in this study may be difficult to generalize because they are very much dependent on the specific conditions utilized.

8.2 Carbon xerogels preparation and characterization

Overall, in this study we prepared the RF carbon xerogels by changing the catalyst species and the catalyst ratios of the polycondensation reaction of resorcinol (R) with formaldehyde (F). The pore characteristics of the RF carbon xerogels varied with the catalyst species and the catalyst ratios. This study has demonstrated that monoethanolamine (MEA), diethanolamine (DEA), and methyldiethanolamine (MDEA) as well as the common catalysts potassium carbonate (K_2CO_3) and sodium carbonate (Na_2CO_3) can be used as catalysts in the preparation of RF carbon xerogels. The selection of Na_2CO_3 as a catalyst produced porous carbons having surface area and pore volumes as high as 672 m^2/g and 1.26 cm^3/g; respectively, with a micropore fraction of

24.2%. However, a sample of carbon xerogels with surface area of 488 m^2/g, pore volume of 0.24 cm^3/g and micropore fraction 95% can be achieved by the selection of MEA as a catalyst. The mean pore size varied from 1.97 nm (RFC-MEA) to 7.48 nm (RFC-Na_2CO_3). The initial gelation pH has an affects on the final properties of RF carbon xerogels. Using a high pH > 7.1 yielded xerogels with a weak structure while lower pH< 6 promoted the condensation reaction, thereby forming a highly cross-linked and thus very strong structure. Between an initial pH of 4 and 6, the carbon xerogels exhibited the highest surface area of about 680 m^2/g, with a corresponding pore volume of 0.856 cm^3/g. Therefore typical pH values are in the approximate range of 4 to 6. Resorcinol to water (R/W) ratio plays a role in the final RF xerogels pore structure and consequently the porous texture of the produced carbons. In addition, the ratio of R/W for the same R/C affects the ratio of catalyst to water (C/W).

The FTIR study shows that samples prepared by MEA, DEA and MDEA contain nitrogenated functional groups. Amides and amines groups are mixed in the very large band around 3430 cm^{-1}, nitrile and lactame groups at 2247 cm^{-1} and 1730 cm^{-1}, respectively. While the ultimate analysis shows that, the selection of three different common alkanolamine MEA, DEA, and MDEA leads to slight differences in the amount of nitrogen atom incorporated to the final RF-xerogel structure (MEA> DEA> MDEA).

Activation of the prepared carbon xerogels in CO_2 atmosphere leads to significant increase of the surface area and pore volume. Under certain conditions, an activated

carbon xerogels sample has been successfully prepared with high pore volume and surface area up to 2.58 cm^3/g and 3200 m^2/g, respectively with carbon yield 40 %. These surface area and pore volume are considered high values compared to the commercial available activated carbons prepared from coconut-shell and used for gas adsorption. According to this study we could conclude that, with the increase of activation temperature, the total pore volume and surface area increased, indicating further evolution of pore structures, particularly microporosity. With increasing the activation time at higher temperature > 850°C the total pore volume and surface area go through a maximum and then decreased. The initial increase in surface area is probably due to opening of porosity and formation of micropores, while the further decrease in surface area is due to the enlargement of micropores and pore wall removal. The carbon yield analysis shows that, as the activation temperature increased from 850°C to 980°C during the CO_2 activation process, the sample lost weight is significantly due to a combination of release of volatile matters in a continual carbonization process and carbon burn-off through carbon and CO_2 weak oxidation.

In addition, in this work we successfully investigated that the surface chemistry of the prepared carbon xerogels can be significantly modified by co-pyrolysis of the prepared RF-xerogel with different substances (*m*-phenylenediamine (MPDA) and diphenylenimine (DPI)). This process leads to produce a new material with different pore structure and surface chemistry. The co-pyrolysis conditions (co-pyrolysis temperature and hold time) were experimentally studied to choose the best co-pyrolysis

condition leads to a high surface area and pore volume. Within the experimental conditions studied, the best co-pyrolysis temperature and hold-up time to derive the best surface modified carbon xerogels textural characteristics were 700°C and two hours.

In general, the co-pyrolysis of the RF-xerogel with nitrogen compounds resulted in a dramatic decrease of the surface area, total pore volume and micropore volume. This is probably due to pore blockage and surface coverage by this material during the pyrolysis of the RF-xerogel. The surface area decreased from 765 m^2/g (for sample without impregnation) to 0.11 m^2/g (for sample impregnated with MPDA50%) and 20 m^2/g (for sample impregnated with DPI50%). While the nitrogen content of the sample increased from 0.4 (for sample without impregnation) to 6.8 (for sample impregnated with MPDA50%) and 3.6 (for sample impregnated with DPI50%). Apparently, the co-pyrolysis of the RF-xerogel with nitrogen compounds produces a series of interactions that although having the positive effect of incorporating nitrogen into the char have the disadvantage of markedly diminishing the textural properties of resulting carbons.

8.3 Binary gas adsorption isotherm for CO_2-N_2 system

A modified gas chromatograph technique was used to study the binary gas adsorption isotherms for the CO_2-N_2 system. This technique is fast and reliable compared to the static method. In which, the results of adsorption of the CO_2-N_2 system could be validate by adding or take-away a perturbation gas to the main gas flow. The isotherms obtained by that technique were used to calculate the adsorption capacity of the prepared samples

via CO_2 and N_2. The adsorption isotherms for all tested samples show that the uptake of CO_2 was higher than nitrogen. This is attributed to specific functional groups on the carbon xerogels which are created due to the usage of MEA as a catalyst in the polycondensation reaction of resorcinol with formaldehyde, in addition to the basic sites created in surface due to the co-pyrolysis of RF-xerogels with the nitrogen containing compounds. This preferential uptake of CO_2 indicates that this sorbent is promising for the separation of CO_2 from gaseous mixtures.

In general, at ambient temperature, the CO_2 adsorption capacity highly depends on the micropores volume and CO_2/N_2 uptake ratio is varied in a very narrow range, this attributed to the physical adsorption which is overriding the adsorption process at that condition. However, at high temperature there are many factors that influence CO_2 adsorption and CO_2/N_2 uptake ratio. On the other hand, the impregnated samples show higher affinity to adsorb CO_2 than N_2 lead to increase CO_2/N_2 uptake ratio up to 7 and CO_2 adsorption capacity 3.5 times greater than non impregnate sample. The samples obtained by impregnation with DPI- 40 and 50%, despite the low amount of nitrogen (2.9 and 3.6%) incorporated compared with those impregnated with MPDA- 40 and 50% (7.1 and 6.8%) show a high CO_2 adsorption capacity (50.3 and 46.6 mg/g compared to 37.2 and 27.1 mg/g, respectively). This could be because of not only the amount of nitrogen in the adsorbent is going to be the only important factor for adsorption of CO_2 at higher temperature, but there are also another important factors which are the nitrogen

functionalities. As it has reported that nitrogen functionalities can have different basicity which affects its affinity to capture CO_2.

Compared with conventional adsorbents, the prepared carbon xerogels samples in this study showed better CO_2 adsorption performance at low and relatively high temperature. The prepared carbon xerogel sample (RFAC-100-850-3) shows a good CO_2 adsorption capacity compared to zeolite 4A and activated carbon, 156 mg/g vs 135 and 110 mg/g respectively. Sample RFC-DPI40% in this study shows superior CO_2/N_2 ratio (7 vs 2.9 for Si-MCM-41) at relatively high temperature (100°C).

8.4 Carbon xerogel regeneration

The regeneration of the prepared samples was carried out using a TPD-MS technique. All the prepared samples of carbon and surface modified carbon xerogels show applicability for regeneration. For the non-modified carbon xerogels approximately all the amount of CO_2 adsorbed was desorbed by heating the sample up to temperature of 172°C. However, for the surface modified samples it seems that the carbon xerogels samples need to be heated to a temperature above 600°C for complete CO_2 desorption.

The thermogravimetric analysis of the carbon xerogels and surface modified carbon xerogels at the same conditions of regeneration was carried out to study the thermal stability of the prepared samples during regeneration. From this we concluded that the prepared carbon xerogels material are quite stable during thermal heating of regeneration

process up to a temperature of 750-800°C. Heating above this temperature may leads to some degradation of the carbon structure. Sample RFC-DPI30% seems to be more stable for regeneration than RFC-MPDA30%, as the total weight losses in the later is 20% while for the RFC-DPI30% is 5% only. This might be due to the total percent nitrogen exist in the sample, the nitrogen percent in RFC-MPDA30% is 6.2 and that of RFC-DPI30% is 2.84 only

The decrease in the CO_2 capture capacities upon regeneration was observed for all prepared samples. This may be attributed to instability in the structure or that desorption of the CO_2 was incomplete. In addition to, redistributions of the surface functional groups on the surface of the carbon and /or other factors could affect the adsorption and separation efficiency of CO_2 on the regenerated samples.

The regenerated carbon xerogel CO_2 capture capacity was approximately 93% of fresh one after two cycles of regeneration. While the CO_2 capture capacities for the surface modified carbon xerogels RFC-MPDA30% (second regeneration) and RFC-DPI30% (second regeneration) were 88% and 92% compared to fresh samples.

In conclusion, this study shows the potential of the surface chemistry of surface modified RF-carbon xerogels for the generation of efficient CO_2 adsorbents, if their beneficial surface chemistry could be combined with advantageous pore structure. *m*-phenylenediamine (DPI) shows a better results than diphenylenimine (MPDA) as an

impregnant for the surface modification of RF-xerogels. This is attributed to, the surface modified RF carbon xerogel samples prepared with DPI shows better CO_2 capture capacity and CO_2/N_2 uptake ratio at higher degree of impregnation (40 and 50%) than its counterparts prepared with MPDA. In addition, the stability of the produced carbon xerogel with this nitrogen containing compound during regeneration

Chapter 9

Appendices

Appendix A

Langmuir fitting binary adsorption isotherms for CO_2-N_2 gas mixture system at 25°C, 100°C and 1.05 bar.

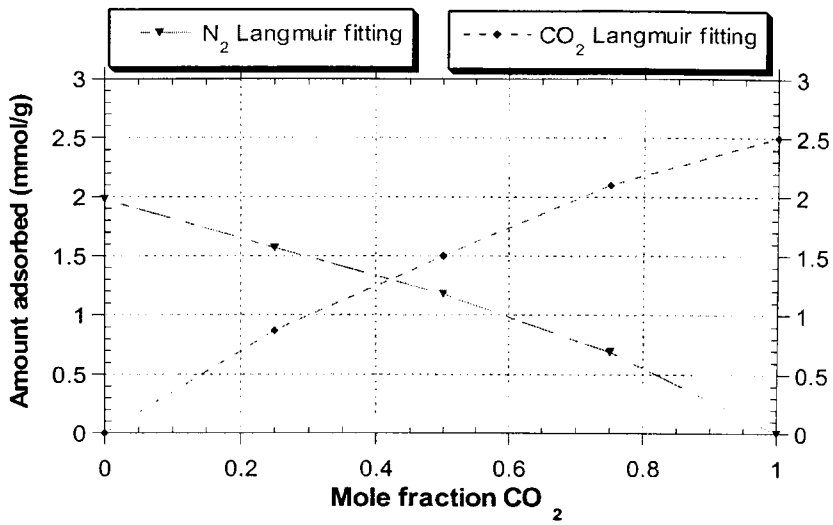

Figure 9.1 Langmuir fitting binary adsorption isotherm for CO_2-N_2 gas mixture system at 25°C and 1.05 bar for RF activated carbon xerogel (RFAC-50-850-1) sample, where the sample of RF xerogel prepared with R/C ratio = 50 and the carbon activated at a temperature of 850°C for one hour.

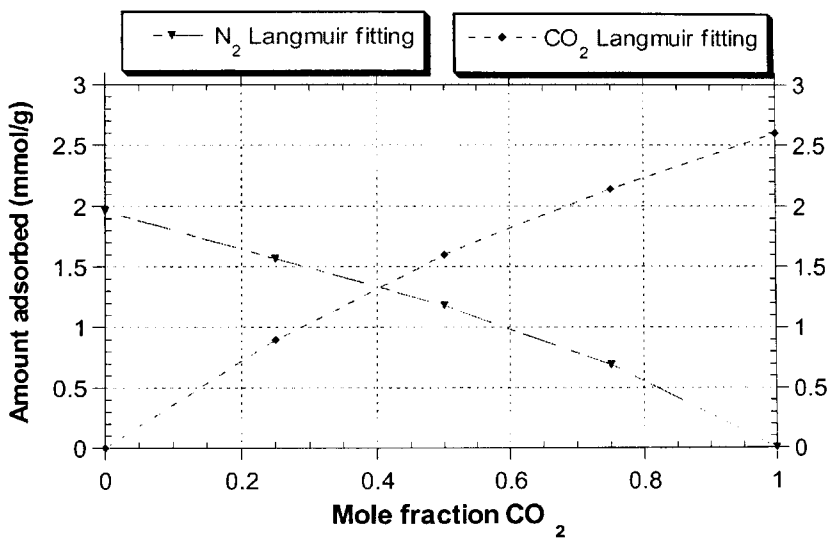

Figure 9.2 Langmuir fitting binary adsorption isotherm for CO_2-N_2 gas mixture system at 25°C and 1.05 bar for RF activated carbon xerogel (RFAC-100-850-1) sample, where the sample of RF xerogel prepared with R/C ratio = 100 and the carbon activated at a temperature of 850°C for one hour.

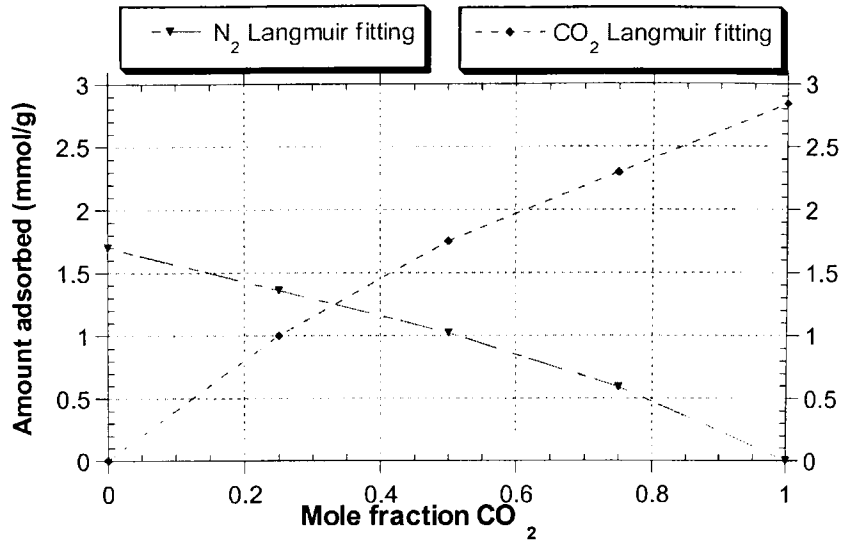

Figure 9.3 Langmuir fitting binary adsorption isotherm for CO_2-N_2 gas mixture system at 25°C and 1.05 bar for RF activated carbon xerogel (RFAC-200-850-1) sample, where the sample of RF xerogel prepared with R/C ratio = 200 and the carbon activated at a temperature of 850°C for one hour.

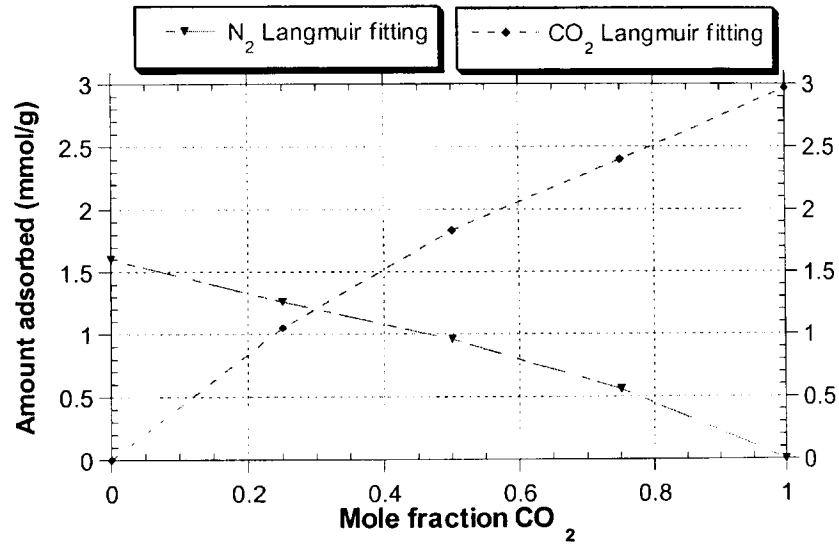

Figure 9.4 Langmuir fitting binary adsorption isotherm for CO_2-N_2 gas mixture system at 25°C and 1.05 bar for RF activated carbon xerogel (RFAC-300-850-1) sample, where the sample of RF xerogel prepared with R/C ratio = 300 and the carbon activated at a temperature of 850°C for one hour.

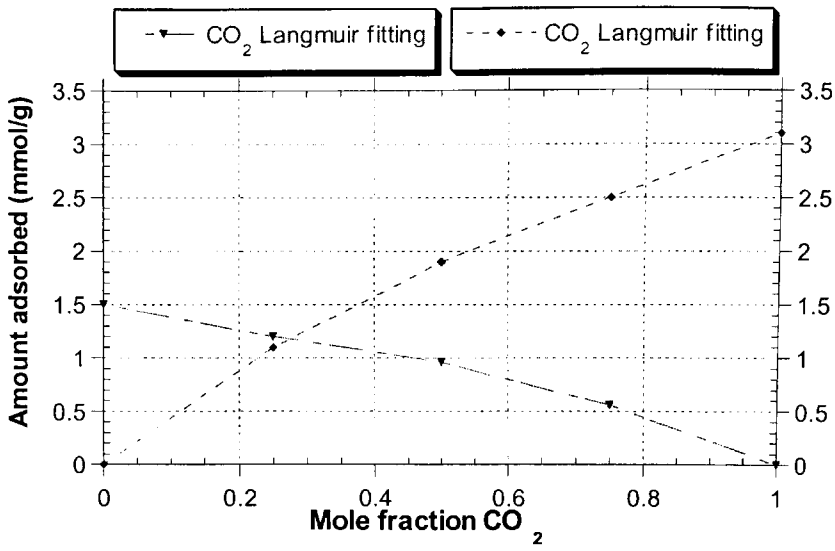

Figure 9.5 Langmuir fitting binary adsorption isotherm for CO_2-N_2 gas mixture system at 25°C and 1.05 bar for RF activated carbon xerogel (RFAC-100-850-2) sample, where the sample of RF xerogel prepared with R/C ratio = 100 and the carbon activated at a temperature of 850°C for two hours

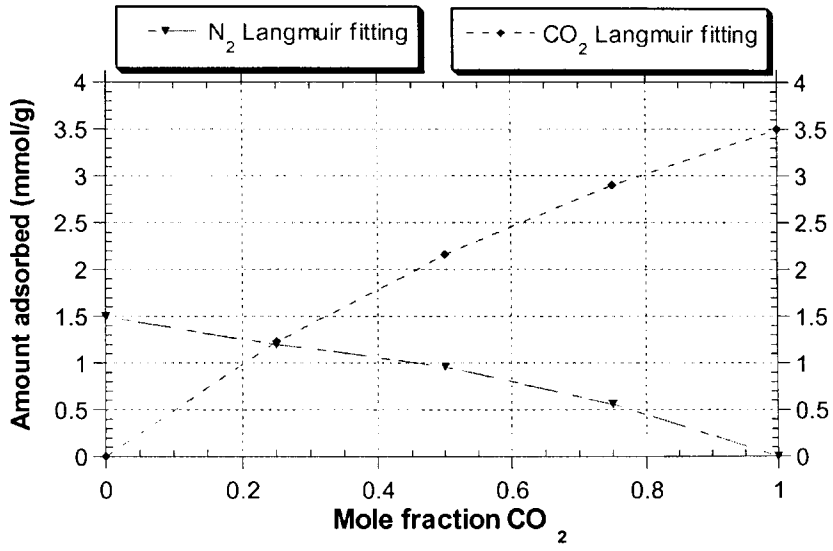

Figure 9.6 Langmuir fitting binary adsorption isotherm for CO_2-N_2 gas mixture system at 25°C and 1.05 bar for RF activated carbon xerogel (RFAC-100-850-3) sample, where the sample of RF xerogel prepared with R/C ratio = 100 and the carbon activated at a temperature of 850°C for three hours

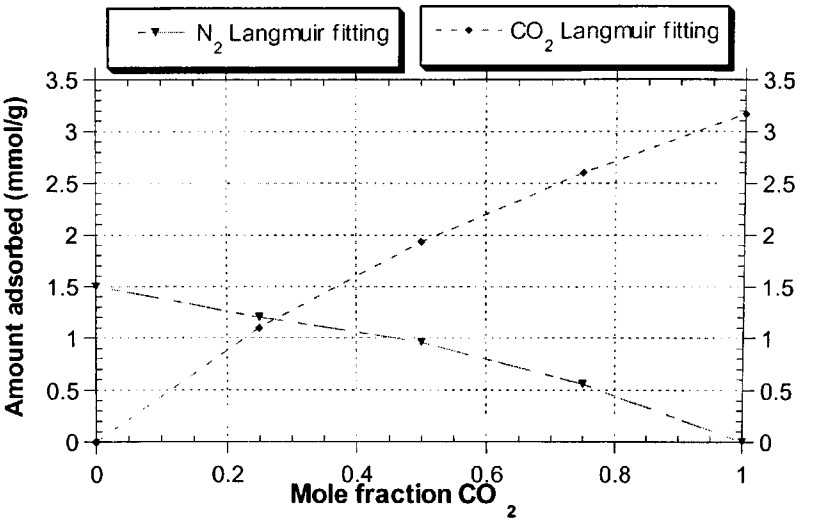

Figure 9.7 Langmuir fitting binary adsorption isotherm for CO_2-N_2 gas mixture system at 25°C and 1.05 bar for RF activated carbon xerogel (RFAC-100-900-1) sample, where the sample of RF xerogel prepared with R/C ratio = 100 and the carbon activated at a temperature of 900°C for one hour

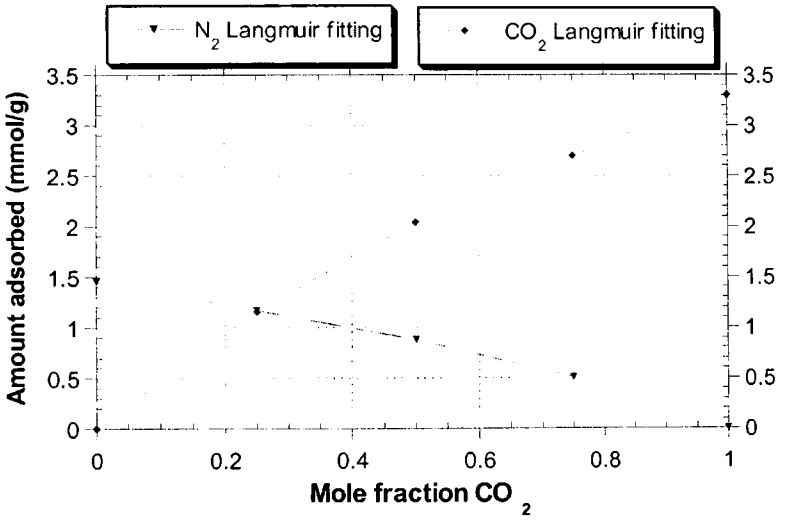

Figure 9.8 Langmuir fitting binary adsorption isotherm for CO_2-N_2 gas mixture system at 25°C and 1.05 bar for RF activated carbon xerogel (RFAC-100-980-1) sample, where the sample of RF xerogel prepared with R/C ratio = 100 and the carbon activated at a temperature of 980°C for one hour

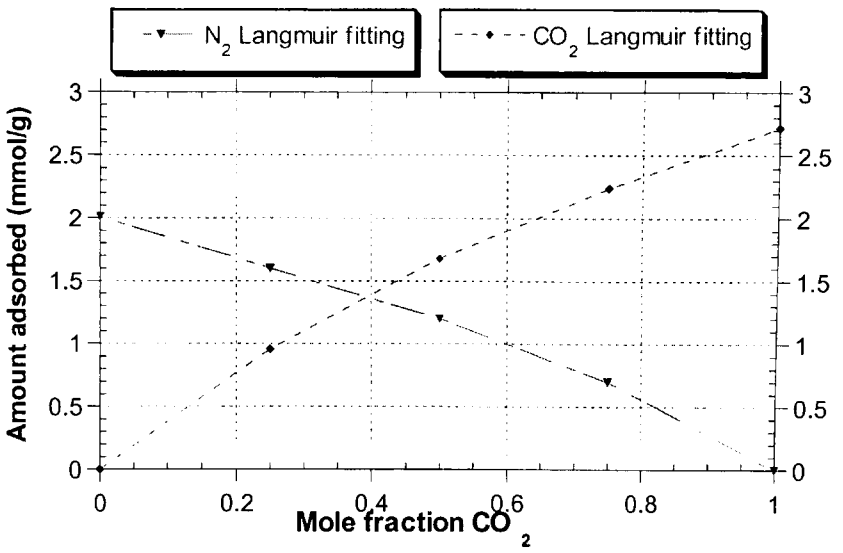

Figure 9.9 Langmuir fitting binary adsorption isotherm for CO_2-N_2 gas mixture system at 25°C and 1.05 bar for RF carbon xerogel (RFC) sample, where the sample of RF xerogel pyrolyzed at a temperature of 700°C for two hours.

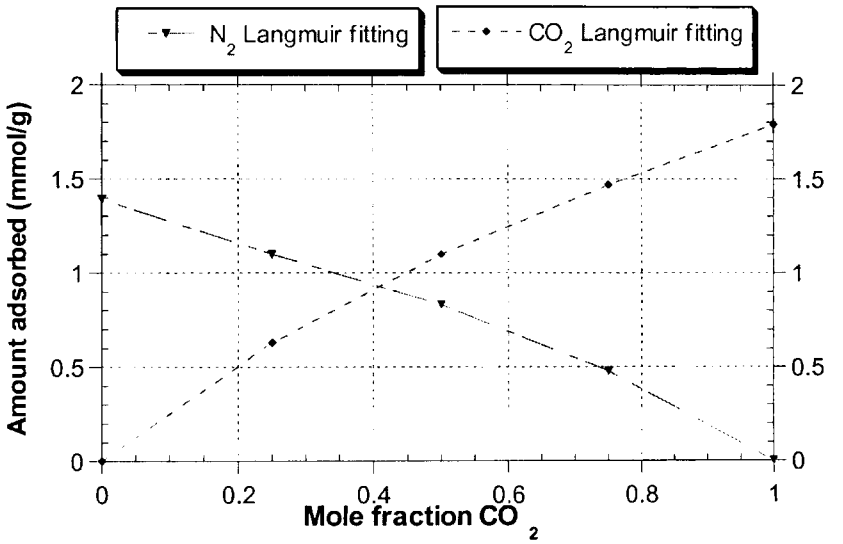

Figure 9.10 Langmuir fitting binary adsorption isotherm for CO_2-N_2 gas mixture system at 75°C and 1.05 bar for RF carbon xerogel (RFC) sample, where the sample of RF xerogel pyrolyzed at a temperature of 700°C for two hours

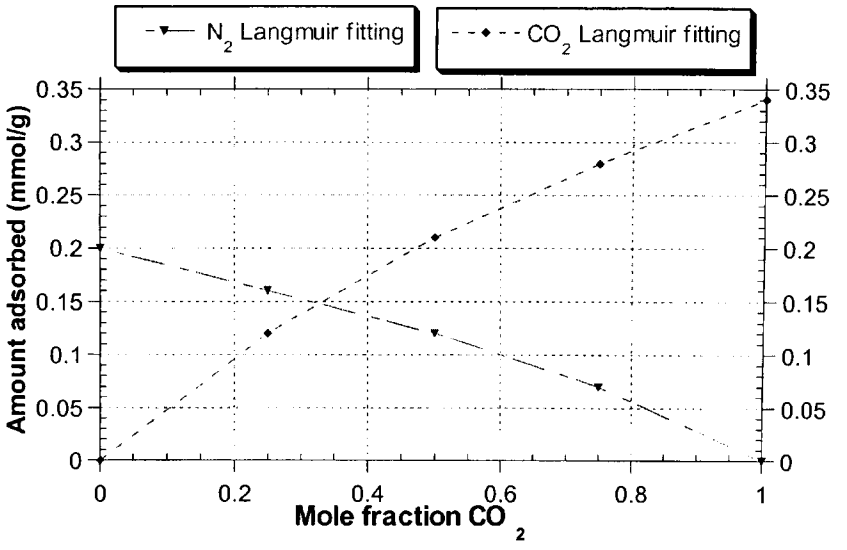

Figure 9.11 Langmuir fitting binary adsorption isotherm for CO_2-N_2 gas mixture system at 100°C and 1.05 bar for RF carbon xerogel (RFC) sample, where the sample of RF xerogel pyrolyzed at a temperature of 700°C for two hours

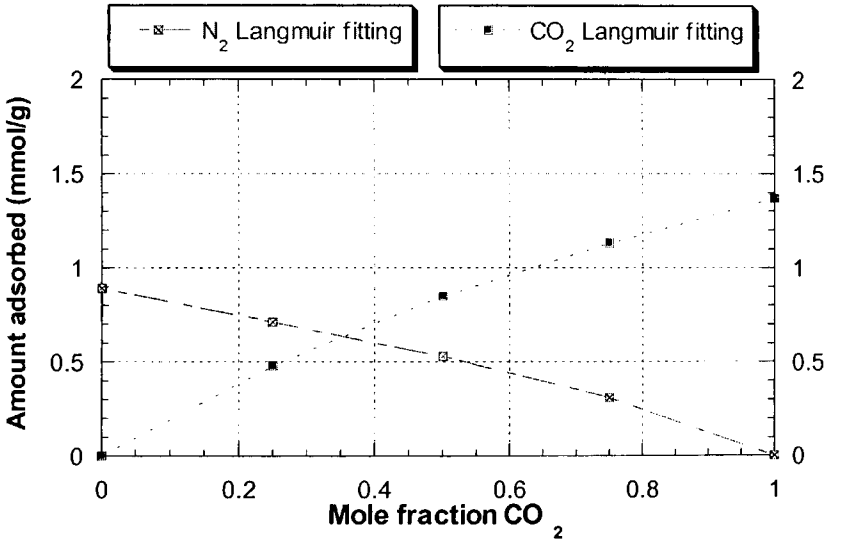

Figure 9.12 Langmuir fitting binary adsorption isotherm for CO_2-N_2 gas mixture system at 25°C and 1.05 bar for surface modified RF carbon xerogel (RFC-MPDA-10) sample, where the sample of RF xerogel co-pyrolyzed with 10 % MPDA at a temperature of 700°C for two hours.

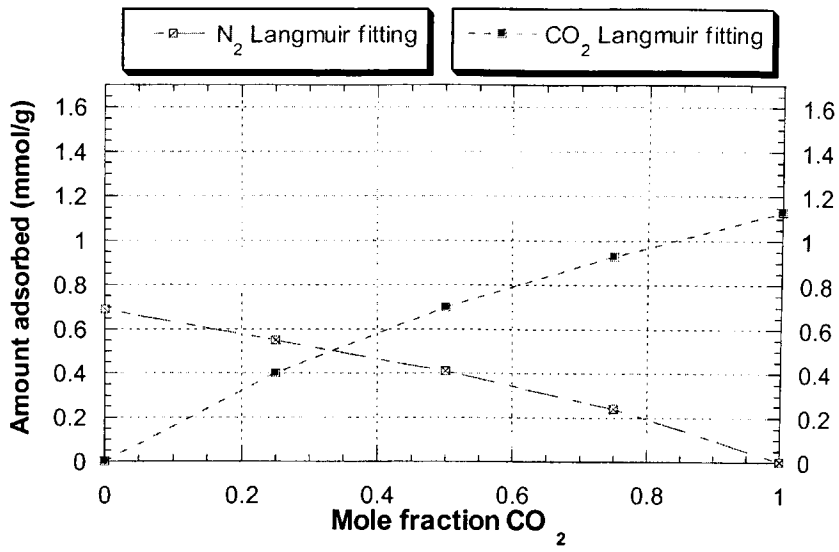

Figure 9.13 Langmuir fitting binary adsorption isotherm for CO_2-N_2 gas mixture system at 25°C and 1.05 bar for surface modified RF carbon xerogel (RFC-MPDA-20) sample, where the sample of RF xerogel co-pyrolyzed with 20 % MPDA at a temperature of 700°C for two hours.

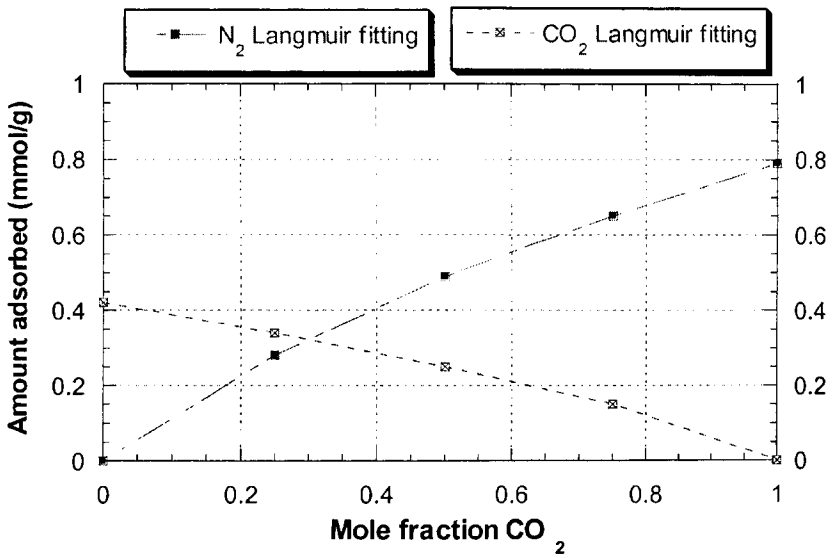

Figure 9.14 Langmuir fitting binary adsorption isotherm for CO_2-N_2 gas mixture system at 25°C and 1.05 bar for surface modified RF carbon xerogel (RFC-MPDA-30) sample, where the sample of RF xerogel co-pyrolyzed with 30 % MPDA at a temperature of 700°C for two hours

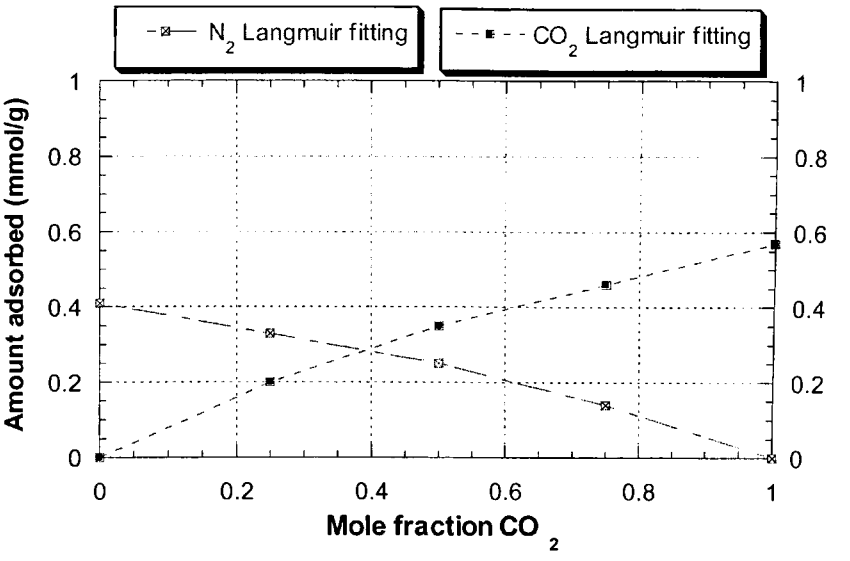

Figure 9.15 Langmuir fitting binary adsorption isotherm for CO_2-N_2 gas mixture system at 25°C and 1.05 bar for surface modified RF carbon xerogel (RFC-MPDA-40) sample, where the sample of RF xerogel co-pyrolyzed with 40 % MPDA at a temperature of 700°C for two hours

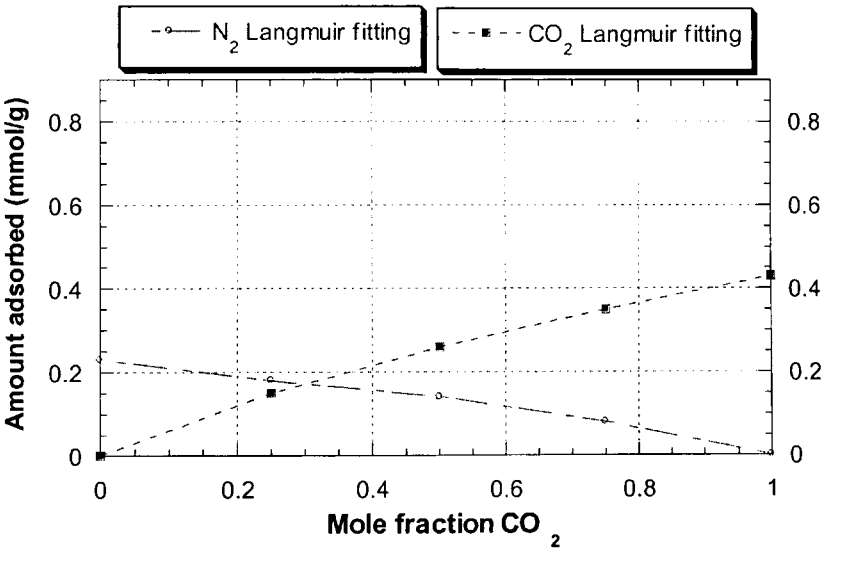

Figure 9.16 Langmuir fitting binary adsorption isotherm for CO_2-N_2 gas mixture system at 25°C and 1.05 bar for surface modified RF carbon xerogel (RFC-MPDA-50) sample, where the sample of RF xerogel co-pyrolyzed with 50 % MPDA at a temperature of 700°C for two hours

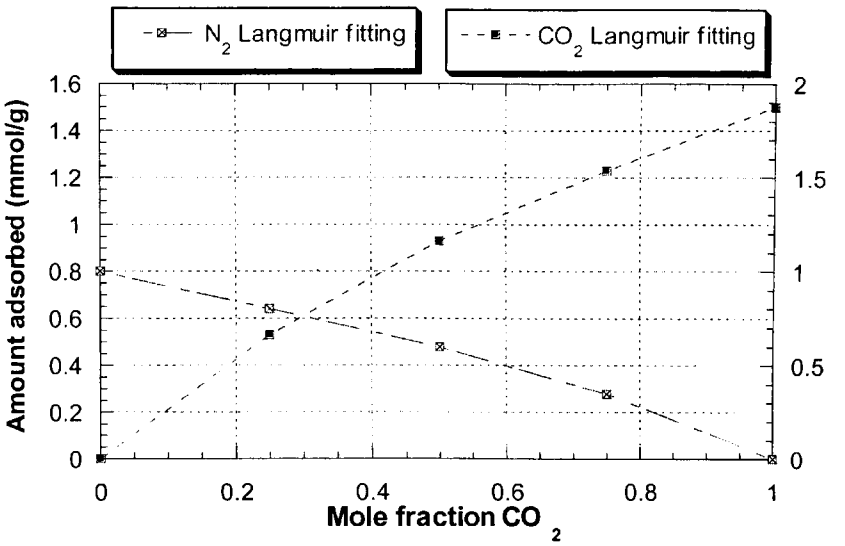

Figure 9.17 Langmuir fitting binary adsorption isotherm for CO_2-N_2 gas mixture system at 25°C and 1.05 bar for surface modified RF carbon xerogel (RFC-DPI-10) sample, where the sample of RF xerogel co-pyrolyzed with 10 % DPI at a temperature of 700°C for two hours

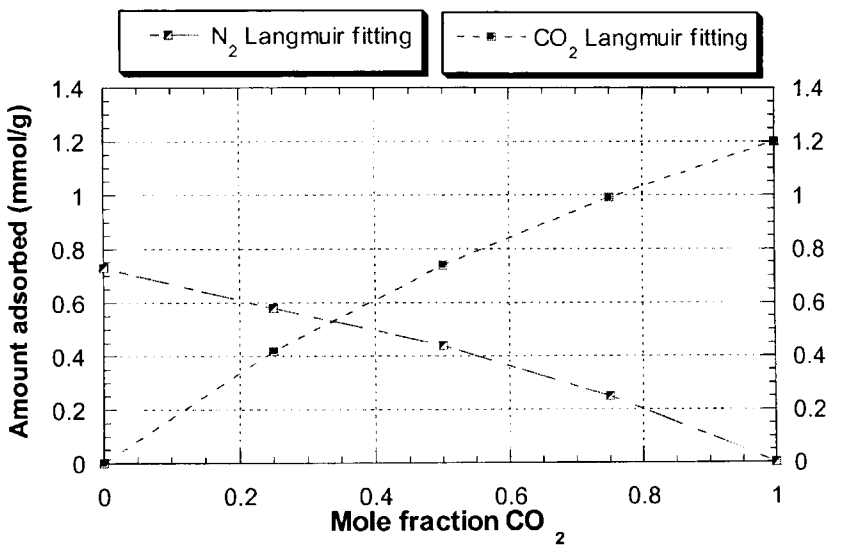

Figure 9.18 Langmuir fitting binary adsorption isotherm for CO_2-N_2 gas mixture system at 25°C and 1.05 bar for surface modified RF carbon xerogel (RFC-DPI-20) sample, where the sample of RF xerogel co-pyrolyzed with 20 % DPI at a temperature of 700°C for two hours

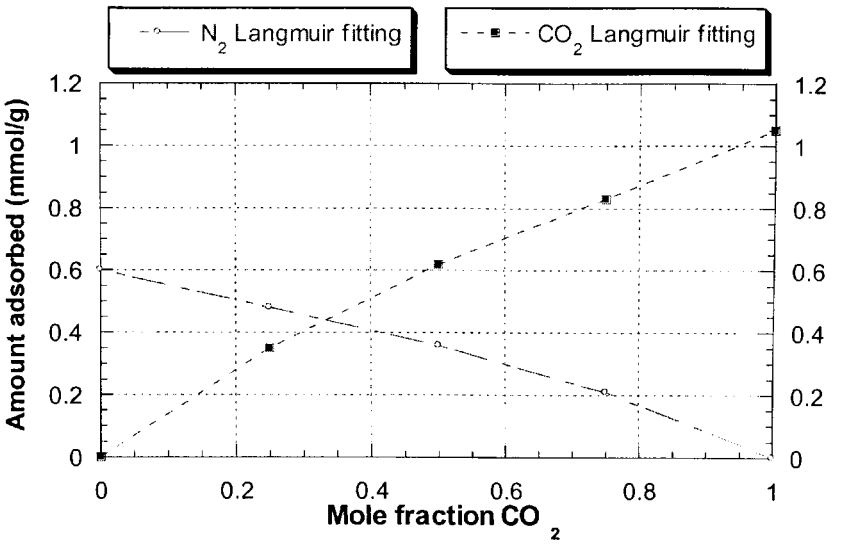

Figure 9.19 Langmuir fitting binary adsorption isotherm for CO_2-N_2 gas mixture system at 25°C and 1.05 bar for surface modified RF carbon xerogel (RFC-DPI-30) sample, where the sample of RF xerogel co-pyrolyzed with 30 % DPI at a temperature of 700°C for two hours

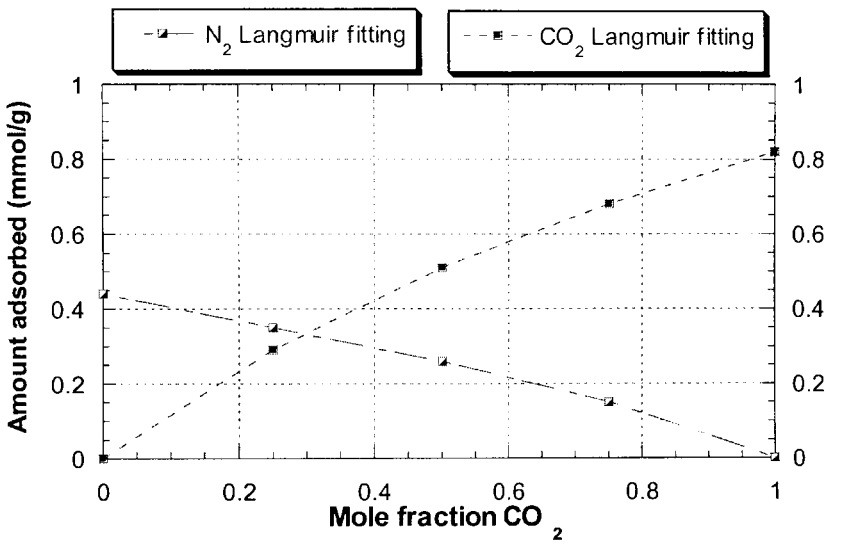

Figure 9.20 Langmuir fitting binary adsorption isotherm for CO_2-N_2 gas mixture system at 25°C and 1.05 bar for surface modified RF carbon xerogel (RFC-DPI-40) sample, where the sample of RF xerogel co-pyrolyzed with 40 % DPI at a temperature of 700°C for two hours

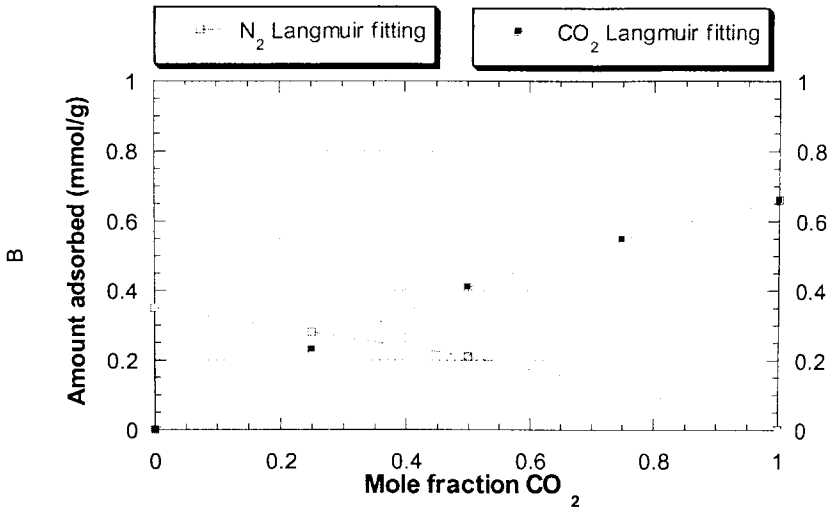

Figure 9.21 Langmuir fitting binary adsorption isotherm for CO_2-N_2 gas mixture system at 25°C and 1.05 bar for surface modified RF carbon xerogel (RFC-DPI-50) sample, where the sample of RF xerogel co-pyrolyzed with 50 % DPI at a temperature of 700°C for two hours

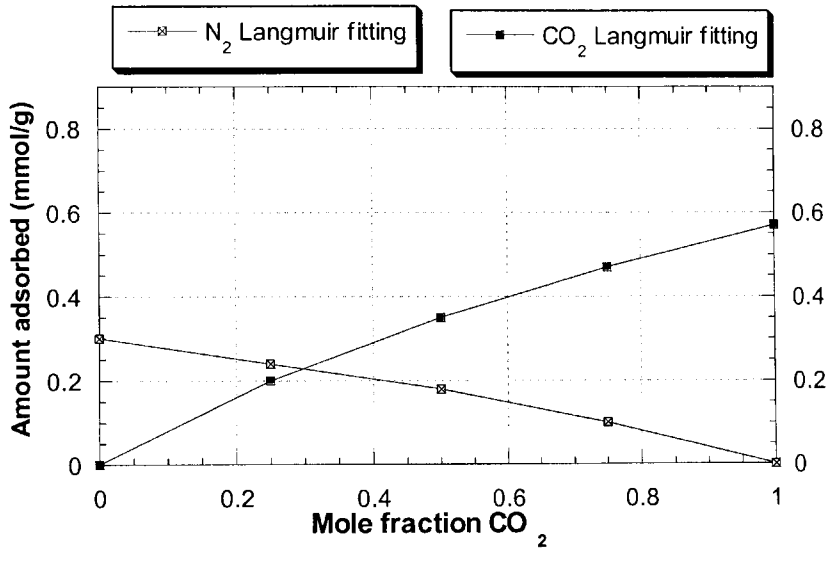

Figure 9.22 Langmuir fitting binary adsorption isotherm for CO_2-N_2 gas mixture system at 100°C and 1.05 bar for surface modified RF carbon xerogel (RFC-MPDA-10) sample, where the sample of RF xerogel co-pyrolyzed with 10 % MPDA at a temperature of 700°C for two hours

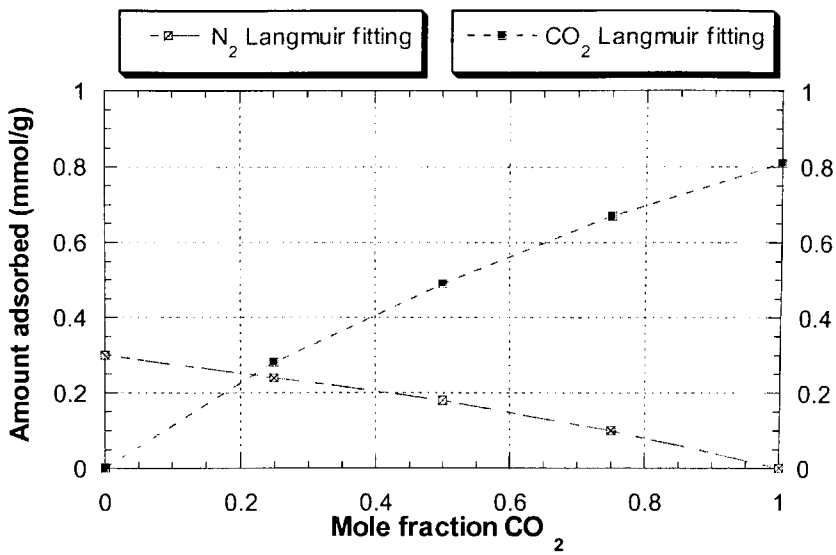

Figure 9.23 Langmuir fitting binary adsorption isotherm for CO_2-N_2 gas mixture system at 100°C and 1.05 bar for surface modified RF carbon xerogel (RFC-MPDA-20) sample, where the sample of RF xerogel co-pyrolyzed with 20 % MPDA at a temperature of 700°C for two hours

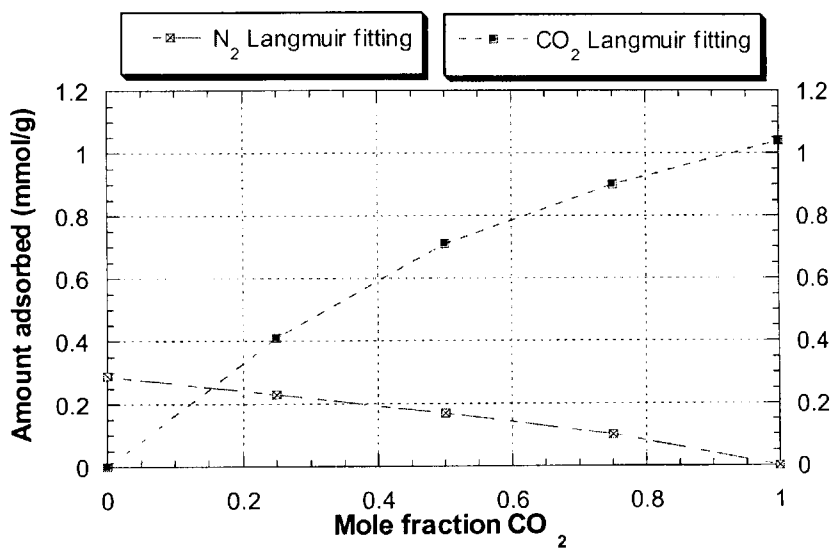

Figure 9.24 Langmuir fitting binary adsorption isotherm for CO_2-N_2 gas mixture system at 100°C and 1.05 bar for surface modified RF carbon xerogel (RFC-MPDA-30) sample, where the sample of RF xerogel co-pyrolyzed with 30 % MPDA at a temperature of 700°C for two hours

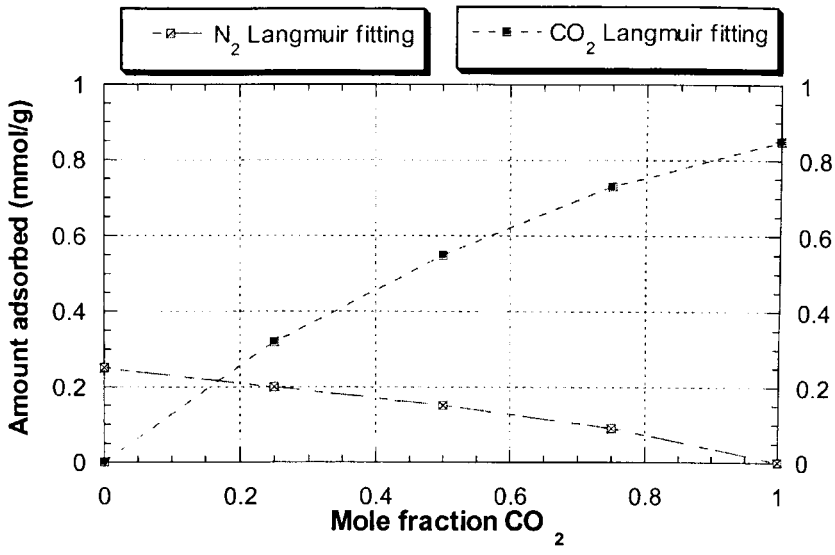

Figure 9.25 Langmuir fitting binary adsorption isotherm for CO_2-N_2 gas mixture system at 100°C and 1.05 bar for surface modified RF carbon xerogel (RFC-MPDA-40) sample, where the sample of RF xerogel co-pyrolyzed with 40 % MPDA at a temperature of 700°C for two hours

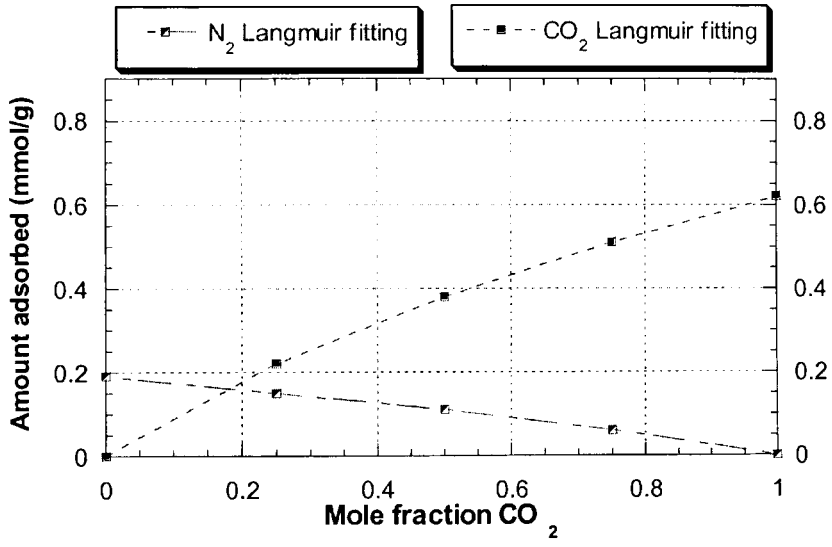

Figure 9.26 Langmuir fitting binary adsorption isotherm for CO_2-N_2 gas mixture system at 100°C and 1.05 bar for surface modified RF carbon xerogel (RFC-MPDA-50) sample, where the sample of RF xerogel co-pyrolyzed with 50 % MPDA at a temperature of 700°C for two hours

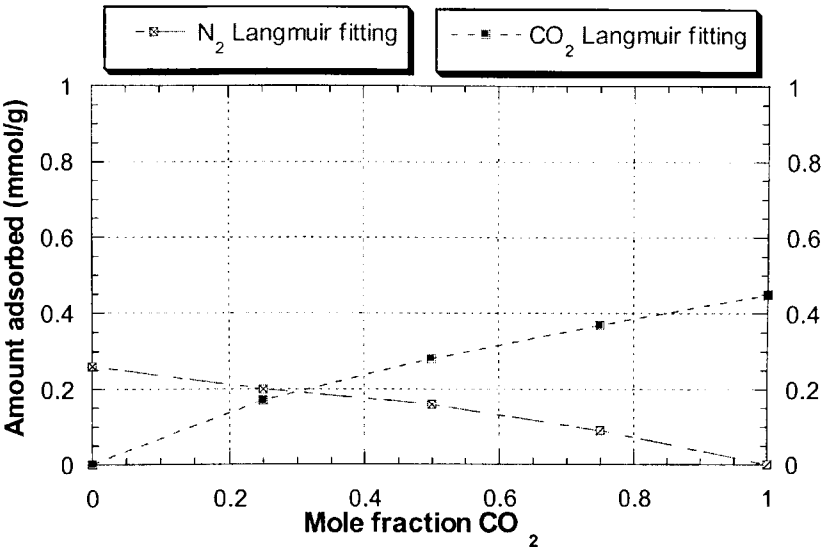

Figure 9.27 Langmuir fitting binary adsorption isotherm for CO_2-N_2 gas mixture system at 100°C and 1.05 bar for surface modified RF carbon xerogel (RFC-DPI-10) sample, where the sample of RF xerogel co-pyrolyzed with 10 % DPI at a temperature of 700°C for two hours

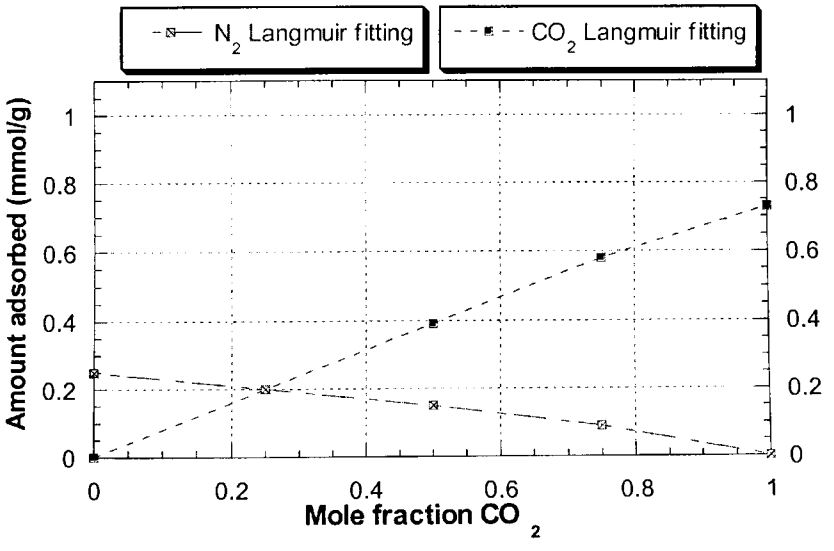

Figure 9.28 Langmuir fitting binary adsorption isotherm for CO_2-N_2 gas mixture system at 100°C and 1.05 bar for surface modified RF carbon xerogel (RFC-DPI-20) sample, where the sample of RF xerogel co-pyrolyzed with 20 % DPI at a temperature of 700°C for two hours

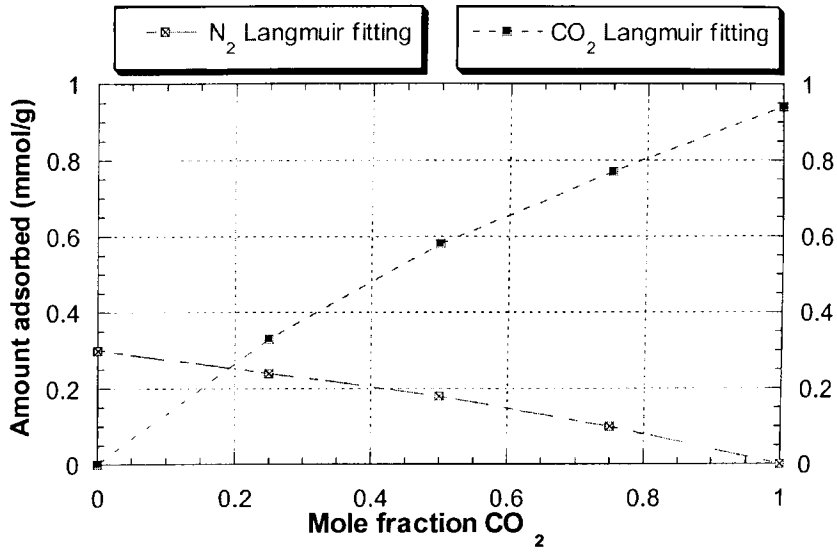

Figure 9.29 Langmuir fitting binary adsorption isotherm for CO_2-N_2 gas mixture system at 100°C and 1.05 bar for surface modified RF carbon xerogel (RFC-DPI-30) sample, where the sample of RF xerogel co-pyrolyzed with 30 % DPI at a temperature of 700°C for two hours

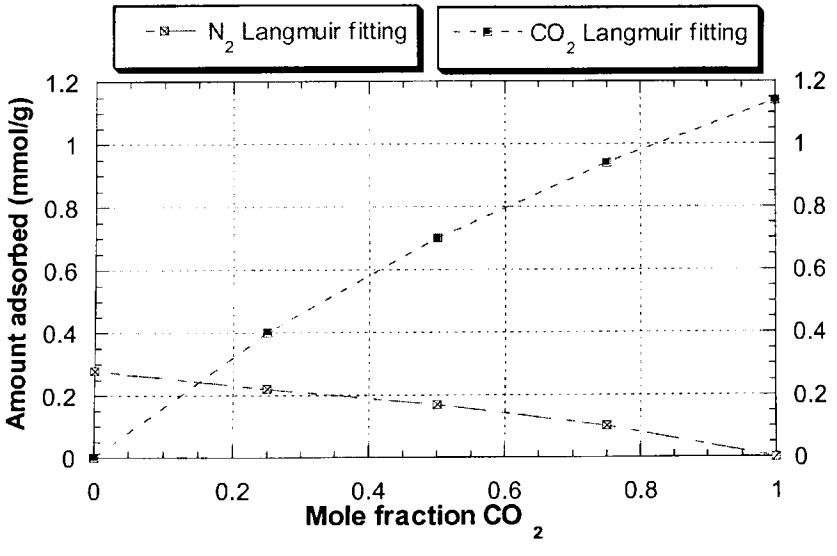

Figure 9.30 Langmuir fitting binary adsorption isotherm for CO_2-N_2 gas mixture system at 100°C and 1.05 bar for surface modified RF carbon xerogel (RFC-DPI-40) sample, where the sample of RF xerogel co-pyrolyzed with 40 % DPI at a temperature of 700°C for two hours

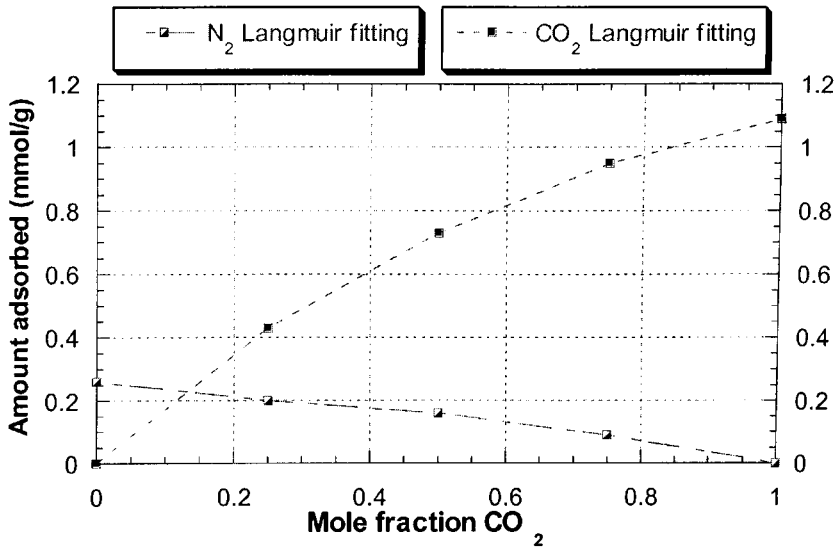

Figure 9.31 Langmuir fitting binary adsorption isotherm for CO_2-N_2 gas mixture system at 100°C and 1.05 bar for surface modified RF carbon xerogel (RFC-DPI-50) sample, where the sample of RF xerogel co-pyrolyzed with 50 % DPI at a temperature of 700°C for two hours

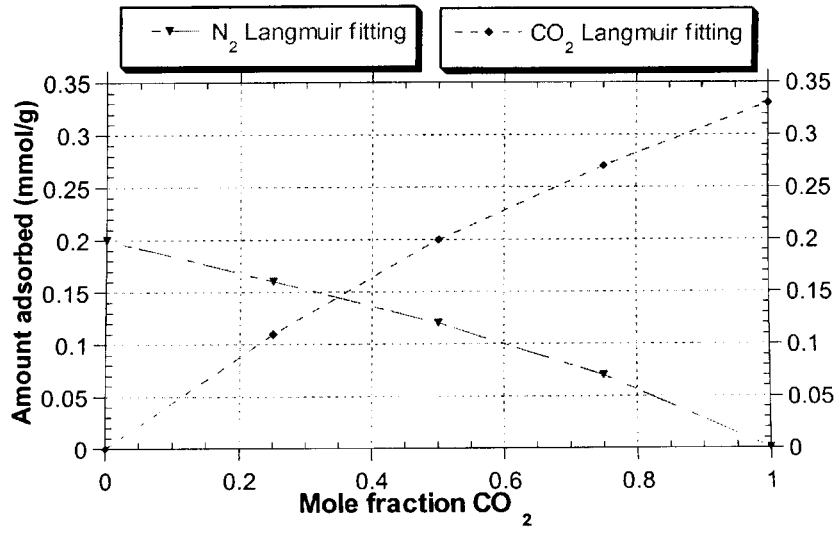

Figure 9.32 Langmuir fitting binary adsorption isotherm for CO_2-N_2 gas mixture system at 100°C and 1.05 bar for RF carbon xerogel (RFC) sample after first cycle of regeneration.

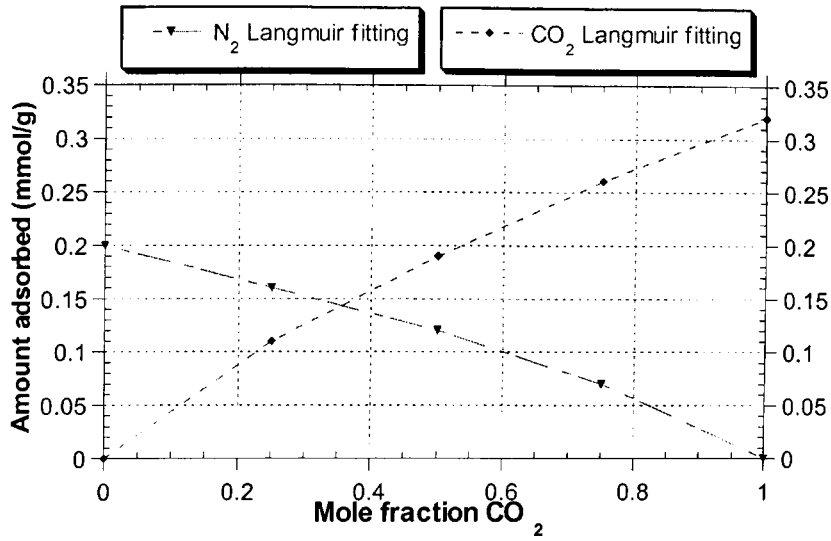

Figure 9.33 Langmuir fitting binary adsorption isotherm for CO_2-N_2 gas mixture system at 100°C and 1.05 bar for RF carbon xerogel (RFC) sample after second cycle of regeneration.

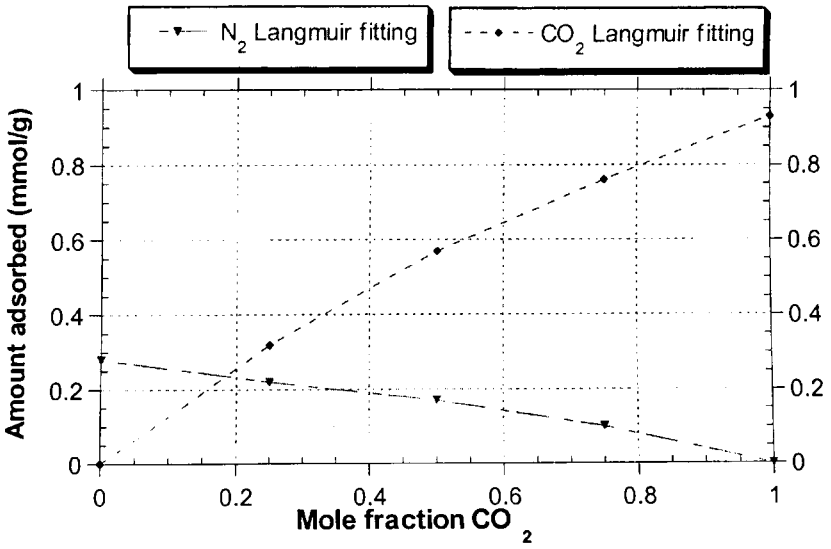

Figure 9.34 Langmuir fitting binary adsorption isotherm for CO_2-N_2 gas mixture system at 100°C and 1.05 bar for surface modified RF carbon xerogel (RFC-MPDA-30) sample after first cycle of regeneration

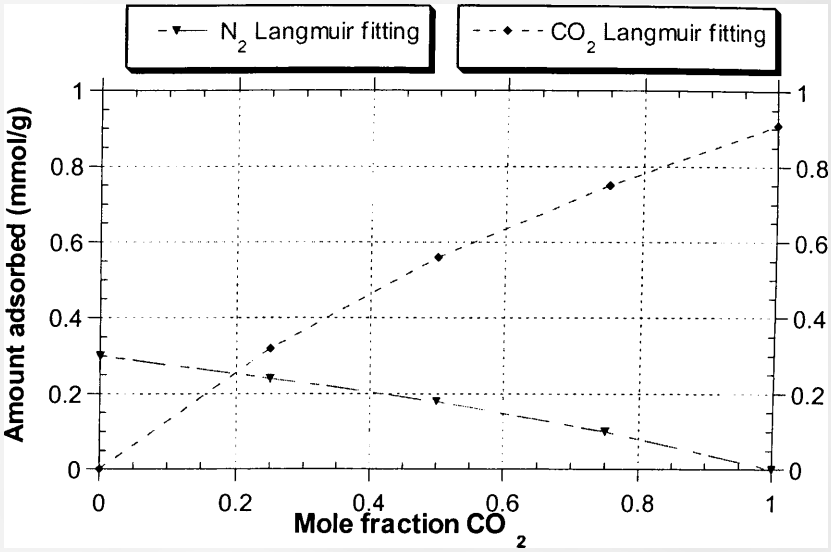

Figure 9.35 Langmuir fitting binary adsorption isotherm for CO_2-N_2 gas mixture system at 100°C and 1.05 bar for surface modified RF carbon xerogel (RFC-MPDA-30) sample after second cycle of regeneration

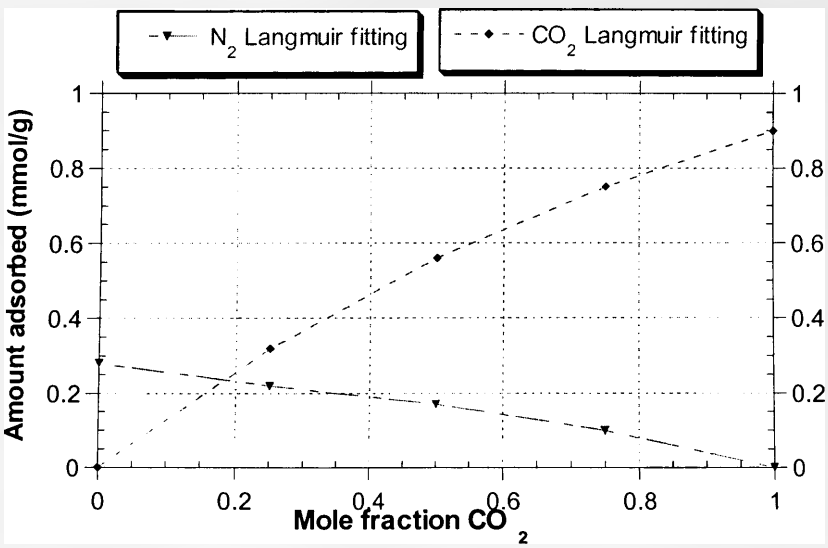

Figure 9.36 Langmuir fitting binary adsorption isotherm for CO_2-N_2 gas mixture system at 100°C and 1.05 bar for surface modified RF carbon xerogel (RFC-DPI-30) sample after first cycle of regeneration

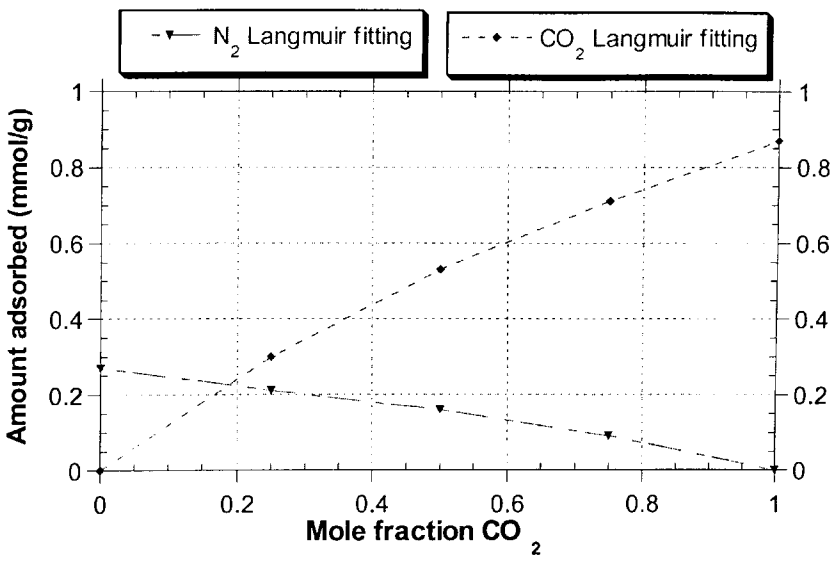

Figure 9.37 Langmuir fitting binary adsorption isotherm for CO_2-N_2 gas mixture system at 100°C and 1.05 bar for surface modified RF carbon xerogel (RFC-DPI-30) sample after second cycle of regeneration

Appendix B

Evolution of FTIR spectra for RF xerogels with different percentage of surface modification by MPDA and DPI.

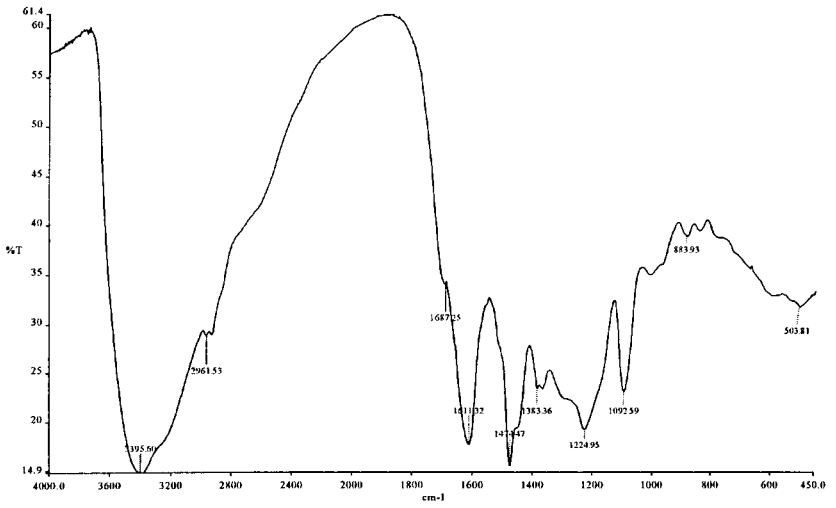

Figure 9.38 FTIR spectrum for the RF-xerogels prepared under condition of: MEA as a catalyst with the R/C = 100; R/W=0.25 g/cm^3 and pH=6 and then surface modified with MPDA 10%.

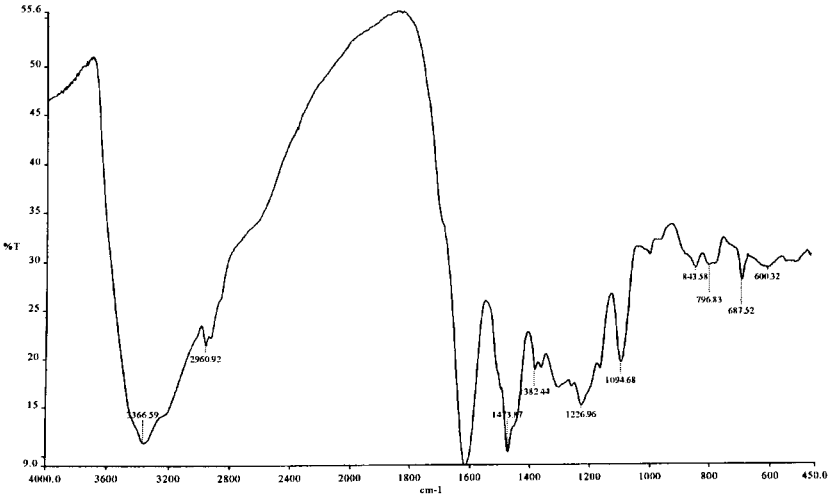

Figure 9.39 FTIR spectrum for the RF-xerogels prepared under condition of: MEA as a catalyst with the R/C = 100; R/W=0.25 g/cm^3 and pH=6 and then surface modified with MPDA 20%

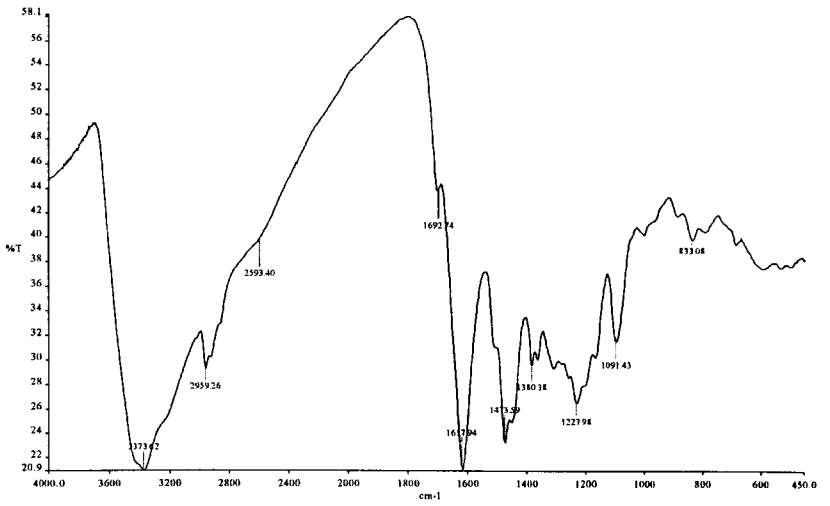

Figure 9.40 FTIR spectrum for the RF-xerogels prepared under condition of: MEA as a catalyst with the R/C = 100; R/W=0.25 g/cm^3 and pH=6 and then surface modified with MPDA 30%

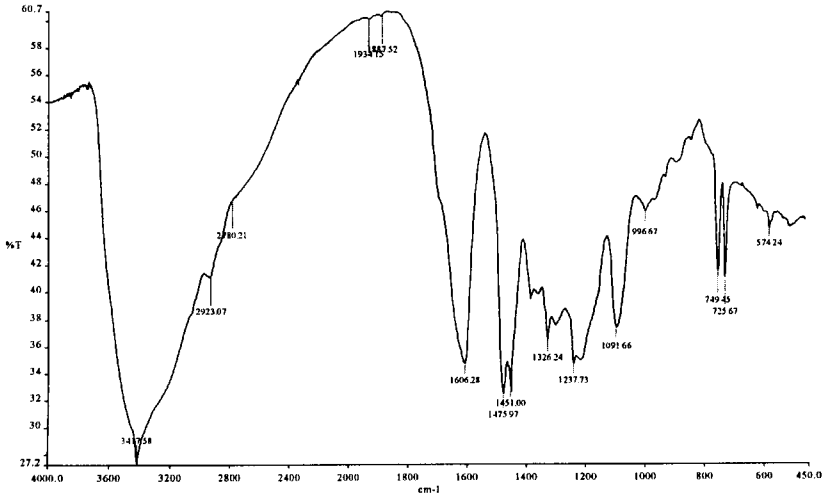

Figure 9.41 FTIR spectrum for the RF-xerogels prepared under condition of: MEA as a catalyst with the R/C = 100; R/W=0.25 g/cm^3 and pH=6 and then surface modified with DPI 10%

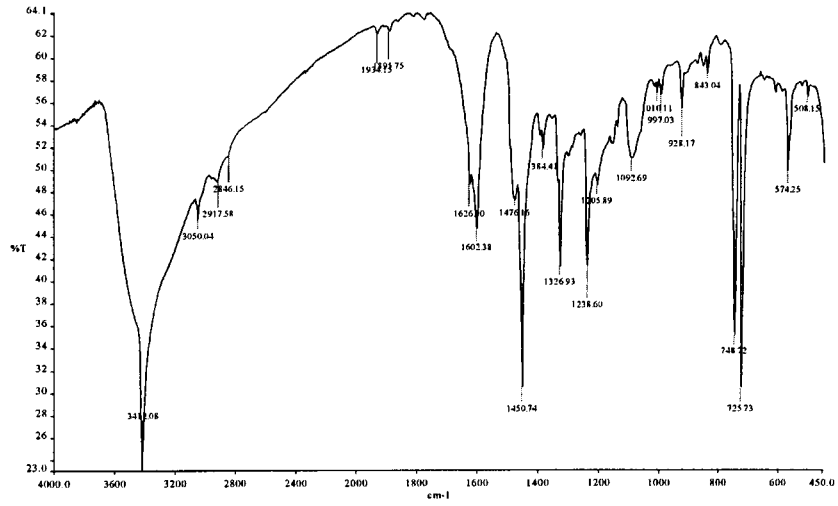

Figure 9.41 FTIR spectrum for the RF-xerogels prepared under condition of: MEA as a catalyst with the R/C = 100; R/W=0.25 g/cm^3 and pH=6 and then surface modified with DPI 20%

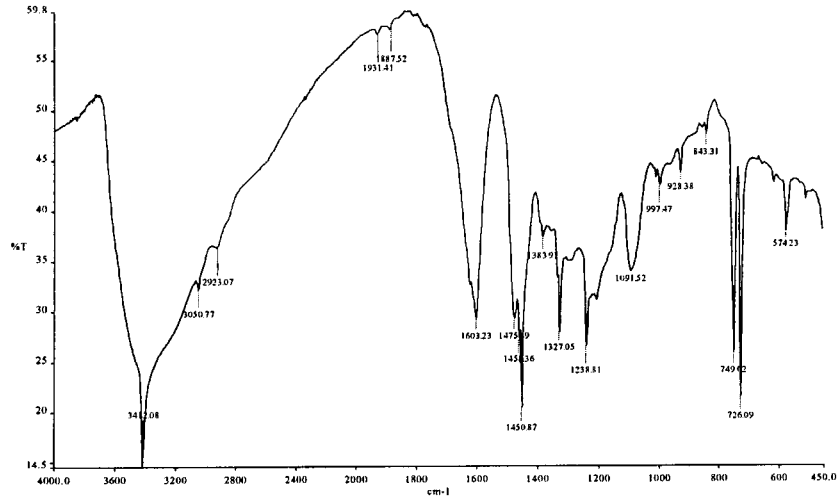

Figure 9.42 FTIR spectrum for the RF-xerogels prepared under condition of: MEA as a catalyst with the R/C = 100; R/W=0.25 g/cm^3 and pH=6 and then surface modified with DPI 30%

Appendix C

MPDA and DPI typical physical properties

m-Phenylenediamine Technical
1,3-Benzenediamine
1,3-Diaminobenzene

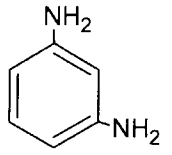

Formula	$C_6H_4 (NH_2)_2$
Property	**Typical Value**
Molecular Weight	108.1
Specific Gravity at 15°C (59°F) at 75°C (167°F)	1.14 1.10
Melting Point, °C (°F),	63 (145)
Boiling Point (760 mm Hg), °C (°F)	283 (541)
Vapor Pressure, mm Hg @ 25°C (77°F) @ 100°C (212°F) 1.0	0.002
Solubility in Water, wt% at 25°C (77°F) at 40°C (212°F)	35.1 90.0
Vapor Density	3.7 (Air = 1)
Flash Point, TOC, °C (°F)	138 (280)
pH Information	9.2 (Water Extract)
Odor	Slight Aromatic
Autoignition Temperature, °C (F°)	560 (1040)

Application

MPD is used an intermediate in the synthesis of engineering polymers, aramid fibers, and thermoplastics, and in the production of dyes for textiles, leather, and other materials. MPD is also a key component in hair dyes, epoxy coatings, and urethane foams. Benefits MPD imparts include fire resistance, fast cure, and excellent chemical and electrical resistance.

Diphenylenimine Technical
; 9H-Carbazole; 9-Azafluorene; Dibenzopyrrole; dibenzo[b,d]pyrrole; Diphenyleneimine; Diphenylenimide

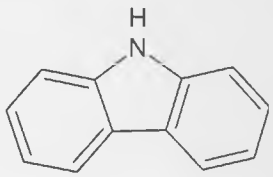

Formula	$C_{12}H_9N$
Property	**Typical Value**
Molecular Weight	167.21
Specific Gravity at 15°C	1.1
Melting Point, °C (°F),	244
Boiling Point (760 mm Hg), °C	355
Vapor Pressure, mm Hg @ 25°C	N/A
Solubility in Water, wt% at 25°C	insoluble
Vapor Density	N/A
Flash Point, TOC, °C	220
pH Information	N/A
Odor	N/A
Autoignition Temperature, °C (F°)	N/A

Application

Carbazole, azafluorene, is a group of organic heterocyclic compounds containing nitrogen atom in dibenzopyrrole system; white crystalline solid, insoluble in water, melts at 244 C. Carbazole and its derivatives are widely used as an intermediate in synthesis of pharmaceuticals, agrochemicals, dyes, pigments and other organic compounds

References

Aboudheir A., Tontiwachwuthikul P., and Chakma A., "CO_2-MEA Absorption in Packed Columns: Comprehensive Experimental Data and Modeling Results", *Proceedings of the Fifth International Conference on Greenhouse Gas Control Technologies*, Cairns, Australia, 217-222(2001).

Ahmadpour A. and Duong D.D., "The preparation of active carbons from coal by chemical and physical activation", *Carbon*, 34, 471-479(1996).

Al-Muhtaseb S. and Ritter J.A., "Preperation and properties of resorcinol-formaldehyde organic and carbon gels", *Advanced Materials*, 15, 101-114(2003).

Arrhenius, Svante. "On the Influence of Carbonic Acid in the Air Upon the Temperature of the Ground." *Philosophical Magazine* 41: 237-76(1896).

Bagreev A., Menendez J.A, Duknno I., Tarasenko Y and Bandosz T.J., "Bituminous coal-based activated carbons modified with nitrogen as adsorbents of hydrogen sulfide" *Carbon,* 42, 469-476(2004).

Baksh M , Yang R. AIChE 923,(1991).

Bansal R.C, Donnet J.B, Stoeckli F., "Active carbon", New York: Marcel Dekker, Inc., (1988).

Barbier O., Ehrburger F., Pieker T.P., Pajonk G.M., Pinto N and Rao A.V., "Small-angle X-ray scattering of a new series of organic aerogels", *Journal of Non-Crystalline Solids*, 285, 109-115(2001).

Barchas R. and Davis R., "The Kerr-McGee/ABB lummus crest technology for the recovery of CO_2 from stack gases", *Energy Converse. Mgmt.*, 33(5-8), 333-340(1992).

Barrett E.P. , Joyner L.G., Halenda P.P., Journal of American Chemical Society 73,373-380 (1951).

Barton S., Evans M., Halliop E. and MacDonald J., "Acidic and basic sites on the surface of porous carbon". *Carbon*, 35(9), 1361-1366(1997).

Beering B. P., Dubinin M.M., Serpinkii V.V., Journal of Colloid Interface Science , 39, 185 (1972).

Berlier K., Frere M., "Adsorption of CO_2 on microporous materials ; 1 on activated carbon and silica gel ", *Journal of Chemical Engineering Data*, 42, 533-537(1997).

Berthon S., Barbieri O. and Ehrbuger F., "DLS and SAXS investigation of organic gels and aerogels", *Journal of Non-Crystalline Solids*, 285,154-161(2001).

Biniak B., Szymanski G., Sieldlewski J., Swiatkowski A., "The characterization of activated carbons with oxygen and nitrogen surface groups", *Carbon* 35(12), 1799-1810(1997).

Blanco Lopez, M. C., Martinez-Alonso, A. & Tascon, J. M. D., "Microporous texture of activated carbon fibres prepared from Nomex aramid fibres. *Microporous and Mesoporous Material* , 34, 171-179(2000).

Boehm A.M., and Ouellette F.A., "Chamber testing of CO_2 removal system using solid amines", *25th international conference on environmental system*, San Diego,CA,July 10-13(1995).

Boudou J.P., "Surface chemistry of a viscose-based activated carbon cloth modified by treatment with ammonia and steam", Carbon, 41(10),1955-1963(2003).

Brunauer S. Deming L.S., Deming W.E. Teller E., Journal of American Chemical Society , 62,1723-1732(1940).

Brunauer, P. H. Emmett and E. Teller, J. Am. Chem. Soc., , 60, 309(1938).

Buffham, B.A., Mason G., Heslop. M.J., "Binary adsorption isotherm from chromatographic retention times. " *Industrial Engineering Chemical Research* , 38,1114-1124 (1999)

Burchell T.D., Judkins R.R., Rogers M.R. and Williams A.M., "A novel process and material for the separation of carbon dioxide and hydrogen sulfide gas mixtures", *Carbon*, 35(9), 1279-1294(1997).

Burg P., Fydrych P., Cagniant D., Nanse G., Bimer J. and Jankowska A., "The characterization of nitrogen-enriched activated carbons by IR, XPS and LSER methods", *Carbon*; 40, 1521-1531(2002).

Canizares, P., Carmona, M., Baraza, O., Delgado, A. & Rodrigo, M. A. "Adsorption equilibrium of phenol onto chemically modified activated carbon F400". *Journal of Hazardous Materials*, B131, 243 - 248(2006).

Carrott P.J.M., Nabais J.M.V., Ribeiro C.M.L. and Pajares J.A., "Preparation of activated carbon fibres from acrylic textile fibres". *Carbon* 39, 1543-1555(2001).

Chakma, A. and Tontiwachwuthikul, P., "Economics and cost studies of designer solvents for energy efficient CO_2 separation from flue gas streams", *Fifth*

International Conference on Greenhouse Gas Control Technologies, Cairns, Australia (2001).

Chapel D., Ernst J. and Mariz C., "Recovery of CO_2 from flue gases: commercial trends", *Presented at the Canadian Society of Chemical Engineers Annual Meeting*, Saskatoon, Saskatchewan, Canada, October 4-6, (1999).

Cheol-Min Y. and Katsumi K., "Adsorption properties of nitrogen-alloyed activated carbon fiber", *Carbon,* 39, 1075-1082(2001).

Choma J., *Polish Journal of Chemistry*. 57, 507 (1983)

Coates J., "Interpretation of infrared spectra, a practical approach". *Encyclopedia of analytical chemistry*, 10815-10837(2000).

Croiset E. and Thambimuthu K.V., "Coal combustion with flue gas recirculation for CO_2 recovery", *Proceeding of the 4th International Conference on Greenhouse Gas Control Technologies*, Interlaken, Switzerland, Reimer, P., Eliasson, B. and Wokaun, A., editors, (1999).

Czakkel O., Marthi K., Geissler E. and Laszlo K.," Influence of drying on the morphology of resorcinol-formaldehyde-based carbon gels", *Microporous and Mesoporous Materials,* 86,124-133(2005).

Daley M.A., Mangun C.L., DeBarrb J.A., Riha S., Lizzio A.A., Dunnals C.L. and Economy J. "Adsorption of SO_2 onto oxidized and heat treated active carbon fibers". *Carbon*, 35(3), 411–417(1997).

Daud W.M.A.W., Ali W.S.W. and Sulaiman M.Z.," Effect of activation temperature on pore development in activated carbon produced from palm shells." *Journal of Chemical Technology and Biotechnology,* 78, 1-5, (2002).

De Boer J. H., "The structure and properties of porous materials" D. H. Everett and F.S. Stone, eds, Butterworts, London, p. 68(1958).

Delaney W.S., Knowles G.P. and Chaffee A.L. *Preprints of symposia –American Chemical Society,* Division of Fuel Chemistry 47(1), 65-66(2002)

Derbyshier F., "Porosity in carbons; characterization and applications", J W Patrick, London: Edward Arnold, p. 227(1995).

Ding Y. and Alpay E., "Equlibria and kinetics of CO_2 adsorption on hydrotacite adsorbent" *Chemical Engineering Science*, 55(17), 3461-3471(2000).

Dreisbach F. Staudt R. and Keller J.U. , " High pressure adsorption data of methane, nitrogen, carbon dioxide and their binary and ternary mixtures on activated carbon " *Adsorption* 5(3) (1999).

Dubinin M.M., *Izv. Akad. Nauk SSSR*, Ser. Khim. 9 (1981).

Ewing. G. W., "Analytical instrumentation handbook", New York, (1997).

Garcia F., Alonso A. and Tascon J., "Nomex polyaramid as a precursor for activated carbon fibres by phosphoric acid activation. Temperature and time effects", *Microporous and Mesoporous Materials*, 75, 73-80(2004).

Glora M. Wiener M., Petricevic R., Probstle H. and Fricke J., "Integration of carbon aerogels in PEM fuel cells", *Journal of Non-Crystalline Solids*, 285, 283-287(2001).

Gray M. L., soong y., Champagne K.J., Baltus J., Stevens R. W., Toochinda P. and Chung S. S. C., "CO_2 Capture by amine enriched fly ash carbon sorbents", *Separation and Purification Technology*, 35, 31–36 (2004).

Guo J. and Lua A. C., "Textural and chemical characterization of adsorbent prepared from palm shell by potassium hydroxide impregnation at different stages," *Journal of Colloid and Interface Science*, 254, 227–233 (2002).

Guo J. and Lua A. C., "Textural and chemical properties of adsorbent prepared from palm shell by phosphoric acid activation," *Materials Chemistry and Physics*, 80, 114–119 (2003).

Guo, J. and Lua, A. C., "Characterization of adsorbent prepared from oil-pal shell by CO_2 activation for removal of gaseous pollutants" *Materials letters*, 55,334-339(2002).

Haefeli S., Bosi M. and Philiber C., " Carbon dioxide capture and storage issues – accounting and baslines under the united nations framework convention on climate change (UNFCC) " *Report for International Energy Agency*, Paris (2004).

Harlick P. J. E and Tezel F. H., "Adsorption of carbon dioxide, methane and nitrogen; pure and binary mixture adsorption for ZSM-5 with SiO_2/Al_2O_3 ratio of 280," *Separation and Purification Technology*, 33, 199–210 (2003).

Hippe Z., Debska B., Kerste A.," Exercieses in ohysical chemistry with program for computar calculations" PWN, Warsaw (1979)

Horikawa T., Hayashi J. and Muroyama K., "Controllability of pore characteristics of resorcinol-formaldehyde carbon aerogel", *Carbon*, 42, 1625-1633(2004).

Horvath G., Kawazoe K., Journal of Chemical Engineering Japan 16,470,(1983).

Hu, Z., Srinivasn, M. P. & Ni, Y., "Novel activation process for preparing highly microporous and mesoporous activated carbons". *Carbon*, 39, 877-886(2001).

Huang M.C. and Teng H., "Nitrogen-containing carbons from phenol-formaldehyde resins and their activity in NO reduction with NH_3", *Carbon*, 41, 951-957(2003).

Huang, Z., Kang, F., Yang, J., Liang, K., Fu, R. & Huang, A., "Effect of CO in activating gas on the pore structure of activated carbon fiber with CO_2 activation". *Journal of Material Science*, 22, 293-295(2003).

Jankowska H., "Active carbon" Ellis hardwood series in physical chemistry, Warsaw ,Poland (1991).

Job N., Pirard R., Marien J. and Pirard J.P., "Porous carbon xerogels with texture tailored by pH control during sol-gel process", *Carbon,* 42, 619-628(2004).

Job N., Thery A., Pirard R., Marien J., Kocon L., Rouzaud J. N., Beguin F. and Pirarad J.," Carbon aerogels, cryogels and xerogels: influnces of the drying method on the textural properties of porous carbon materials". *Carbon* 43, 2481-2494(2005).

Judkins R.R. and Burchell T.D., "CO_2 removal from gas streams using a carbon fiber composite molecular sieve", *First National Conference on Carbon Sequestration*, Washington, DC, May 15-17, (2001).

Keeling, Charles D.. "The Concentration and Isotopic Abundances of Carbon Dioxide in the Atmosphere." *Tellus* 12: 200-203(1960).

Kim Y.J. , Kim M., Yun C. H., Chang J.Y. Park C.R. and Inagaki M., " Comparative study of carbon dioxide and nitrogen atmospheric effects on the chemical structure changes during pyrolysis of phenol-formaldehyde spheres" *Journal of Colloid and Interface Science* ,724 ,555-562(2004).

Langmuir, *Journal of American Chemical Society*, 40, 1368 (1918)

Leon y.C.A., Solar J.M., Calemma V. and Radovic LR., "Evidence for the protonation of basal plane sites on carbon". *Carbon,* 30(5), 797-811(1992).

Leonard A., Job N., Blacher S., Pirard J. P. Crine M., and Jomaa W., " Suitability of convective air drying for the production of porous resorcinol-formaldehyde and carbon xerogels", *Carbon*, (2005).

Lin C. and Ritter A., "Carbonization and activation of sol-gel derived carbon xerogels" *Carbon*, 38, 849-861(2000).

Lin C. and Ritter J. A., "Effect of synthesis pH on the structure of carbon xerogels", *Carbon*, 25(90), 1272-1275(1997).

Lopez M., Alonso B.M. and Tascon J.M.D., "Microporous texture of activated carbon fibers prepared from nomex aramid fibres," *Microporous and Mesoporous Materials*, 34,171-179, (2000).

Loustalot M. F. G., Larroque S., Grand D., Grenier P. and Bedel D., " Phenolic resins:2 Influence of catalyst type on reaction mechanisms and kinetics", *Polymer*, 37(8), 1363-1369(1996).

Lowell S. "Powder surface area and porosity". London, Chapman and Hall, (1991).

Lozano-Castelló D., Lillo-Ródenas M. A., Cazorla-Amorós D. and Linares-Solano A. "Preparation of activated carbons from Spanish anthracite I. Activation by KOH" , *Carbon*, 39 ,741-749(2001).

Lu A X., Caps A. R., Fricke A.J. , Alviso B C.T. and Pekala R.W., "Correlation between structure and thermal conductivity aerogels of organic", *Journal of Non-Crystalline Solids* , 188 ,226-234(1995).

Lude k., Miroslav Z.. "Carbon-supported Mo catalysts prepared by a new impregnation method using a MoO / water slurry: saturated loading, hydrodesulfurization activity and promotion by Co", *Carbon* 39, 2023–2034(2001).

Maldonado F. J., Ferro M. A., Rivera J. and Moreno C. "Synthesis and textural characteristics of organic aerogels, transition-metal-containing organic aerogels and their carbonized derivatives", *Carbon*, 37, 1199–1205(1999).

Mangun C. L., Benak K. R., James Economy and Kenneth L., "Surface chemistry, pore sizes and adsorption properties of activated carbon fibers and precursors treated with ammonia" , *Carbon* , 39, 1809-1820(2001).

Mangun C.L., Benak K.R., Daley M.A., Economy J., "Oxidation of activated carbon fibers: effect on pore size, surface chemistry, and adsorption properties". *Chem. Mater.*, 11, 3476-3483(1999).

Manocha S., "Porous carbons," *Sadhana*, 28, 335-348(2003).

Manocha S., "Studies on development of porosity in carbons from different types of bio-wastes," *Korean Carbon Society*, 3(1), 1-5(2002).

Mariz C.L., "Carbon Dioxide Recovery: Large Scale Design Trends", *Journal of Canadian Petroleum Technology*, 37, 7, (1998).

Martin-Gullon, I., Andrews, R., Jagtoyen, M. & Derbyshire, F. "PAN-based activated carbon fiber composites for sulfur dioxide conversion: influence of fiber activation method". *Fuel*, 80, 969-977(2001).

Martin-Martinez J.M., Torregrosa-Macia R., and Mittelmeijer M.C, "Mechanisms of adsorption of CO_2 in the micropores of activated anthracite," *Fuel*, 74,111-114(1995).

Mathews J., "Seven steps to curb global warming" *Energy policy*, 35, 8, 4247-4259(2007).

Matsumoto A, Zhao JX, and Tsutsumi K., "Adsorption behavior of hydrocarbons on slit-shaped micropores". *Langmuir*, 13, 496-501(1997).

Megson N. J. L. "Phenolic resin chemistry", London, Butterworths scientific publications (1958).

Mercedes M. M., Tang Z. and Zhang Y. "CO_2 capture by activated and impregnated anthracites" *Fuel Processing Technology*, 86 (14-15), 1487-1502(2005)

Merzbacher C.I., Meier S.R., Pierece J.R., Korwin M.L., Carbon aerogels as broadband nonreflective materials, *Journal of Non-Crystalline Solids*, 285 (2001) 210-215.

Metz B. et al., "Climate change 2001: mitigation : contribution of Working Group III to the third assessment report of the Intergovernmental Panel on Climate Change" Cambridge ; New York : Cambridge University Press, (2001)

Mimura T., Matsumoto K., Iijuma M., and Mitsuoka S., "Development and application of flue gas carbon dioxide recovery technology", *Proceedings of the Fifth International Conference on Greenhouse Gas Control Technologies*, , Cairns, Australia, pp.138-142 (2001).

Molina-Sabio M., Pérez V. and Rodríguez-Reinoso F., "Impregnation of activated carbon with chromium and copper salts: Effect of porosity and metal content", *Carbon*, 32(7), 1259-1265(1994).

Molina-Sabio, M., Gonzalez, M. T., Rodriguez-Reinoso, F. & Sepulveda-Escribano, A. "Effect of steam and carbon dioxide activation in the micropore size distribution of activated carbon". *Carbon*, 34(4), 505-509(1996).

Moon S.H. and Shim J.W. " A novel process for CO_2/CH_4 gas separation on activated carbon fibers—electric swing adsorption" *Journal of Colloid and Interface Science* 298, 523–528(2006).

Newcombe G, Drikas M and Hayes R., "Influence of characterized natural organic matter on activated carbon adsorption: II. Effect on pore volume distribution and adsorption of 2-methylisoborneol", *Water Research*, 31(5), 1065-1073(1997).

Nowak K.O., Cannon F.S. and Mazyck D.W., "Enhancing activated carbon adsorption of 2-methylisoborneol: methane and steam treatments". *Environmental Science and Technology*: 38(1), 276-284(2004).

Ottaway M., "Use of thermogravimetric for proximate analysis of coals and cokes" *Fuel,* 61,713-716(1982).

Park, S. & Kim, K., "Influence of activation temperature on adsorption characteristics of activated carbon fiber composites". *Carbon*, 39, 1741-1746(2001).

Pekala R. Low density resorcinol-formaldehyde aero-gel. US patent 4873218, (1989). US patent 4997804, (1991).

Pekala R.W., Farmer J.C., Alviso C.T, Tran T.D., Mayer S.T., Miller J.M. and Dunn B., "Carbon aerogels for electrochemical applications", *Journal of Non-Crystalline Solids* , 225,74–80(1998).

Petricevic R., Glora M. and Fricke J., "Planar fibre reinforced carbon aerogels for application in PEM fuel cells", *Carbon*, 39, 857–867(2001).

Polovina M., Babic B., Kaluderovic B., Dekanski A., "Surface characterization of oxidized activated carbon cloth", *Carbon* , 35(8),1047-1052(1997).

Pradhan B.K. and Sandle N.K., "Effect of different oxidizing agent treatment on the surface properties of activated carbons", *Carbon*, 37, 1323-1332(1999).

Pradhan B.K. and Sandle N.K., "Preparation and characterization of rice-straw-based porous carbons with high adsorption capacity" *Fuel*, 81, 327 (2002).

Przepiorski J., Skrodzewicz M. and Morawski A. W., "High temperature ammonia treatment of activated carbon for enhancement of CO_2 adsorption" *Applied Surface Science* , 225 , 235-242(2004).

Przepiorski J., Tryba B. and Morawski M.A. "Adsorption of carbon dioxide on phenolic resin-based carbon spheres" *Applied Surface Science*, 196, 295-300(2002).

Radovic LR. "Surface Chemistry of Activated Carbon Materials". Surfactant Science Series, Surfaces of Nanoparticles and Porous Materials 78 (Chapter 20), New York, Marcel Dekker, Inc. 1999.

Raymundo-Pinero E., Cazorla-Amoro´s D., Salinas-Martinez de Lecea C., Linares-Solano A., " Factors controlling the SO_2 removal by porous carbons: relevance of the SO_2 oxidation step" *Carbon*, 38, 335-344(2000).

Ritzkowski M., and Stegmann R., "Controlling greenhouse gas emissions through landfill in situ aeration", *International Journal of Greenhouse Gas Control*, 1, 3, 281-288(2007).

Robinson A.B., Baliunas S.L, Soon W. and Robinson Z.W. "Environmental effect of increased atmospheric carbon dioxide" *Report for Oregon Institute of Science and Medicine* (1998) .

Robinson J.W, Skelly E.M. and George M., "Undergraduate instrumental analysis ", 6th ed, New York : M. Dekker, (2005).

Rojas M., Alonso L., Diaz J., Lopez A., Martin R. and Gomez V., "Basic metal-carbons catalysts prepared by sol-gel method". *Carbon*, 42, 1575-1582(2004).

Rouquerol F., Rouquerol J., Sing K., "Adsorption by powders and porous solids; Principles, methodology and applications" Academic press, (1999).

Ruthven D.M., "Principles of adsorption and adsorption processes", Wiley, New York, (1984).

Ryu, Z., Rong, H., Zheng, J., Wang, M. & Zhang, B. "Microstructure and chemical analysis of PAN-based activated caron fibers prepared by different activation methods". *Carbon*, 40, 1131-1150(2002).

Ryu, Z., Zheng, J., Wang, M. & Zhang, B. "Nitrogen adsorption studies of PAN-based activated carbon fibers prepared by different activation methods". *Journal of Colloidal Interface Science*, 230, 312-319(2000).

Saito A., Foly H. , AIChE 37,429(1991).

Saliger R., Bock V., Petricevic R., Tillostant T., Geic S. and Fricke J. , "Carbon aerogels from dilute catalysis of resorcinol with formaldehyde", *Journal of Non-Crystalline Solids*, 22,1144-150(1997).

Saliger R., Fischer U., Herta C., Fricke J., "High surface area carbon aerogels for supercapacitors" , *Journal of Non-Crystalline Solids* , 225, 81–85(1998).

Sarmeo D. , Blazewicz S. , Mermoux M. and Touzain P., "Intercalation of manganese chloride into mesophase pitch-based graphite fibers via gaseous complexes". *Carbon* 39, 2049-2058(2001).

Satyapal S. Filburn T. Trela J and Strange J., "Performance and properties of solid amine sorbent for carbon dioxide removal in space life support applications " *Energy & Fuels*, 15, 250-255(2001).

Schaefer D.W., Pekala R., Beaucage G., "Origin of porosity in resorcinol-formaldehyde aerogels" *Journal of Non-Crystalline Solids*, 186,159-167(1995).

Schellnhuber H.J., Cramer W., "Avoiding dangerous climate change" Cambridge University press (2006).

Schnitzer H., Brunner C., Gwehenberger G., " Minimizing greenhouse gas emission through the application of solar thermal energy in industrial processes" *Journal of Cleaner Production* , 15, 1271-1286(2007).

Service R. F., "Choosing a CO_2 separation technology", *Science*, 305(5686), 963-967(2004).

Severini F, Formaro L., Pegoraro M. and Posca L. "Chemical modification of carbon fiber surfaces", *Carbon*, 40, 735-741(2002).

Sing K. S. W. D. H. Everett, J. M. Haynes, N. Pernicone, J. D. F. Ramsay, and K. K. Unger, G. P., *Pure and Applied Chemistry* Vol. 62, No. 7 (1990).

Sing K. S. W., Everett D.H., Haul RA.W., Moscou L., Pierotti R.A., Rouquerol J. and Siemieniew T. *Pure Applied Chemistry*, 57(4), 603(1985).

Siriwardane R.V., Shen M.S., Fisher E.P. and Poston J.A. "Adsorption of CO_2 on molecular sieves and activated carbon" *Energy Fuels*, 15, 279-284(2001).

Snoeyink V.L. and Summers R.S. "Water Quality and Treatment", American Water Works Association, New York, McGraw-Hill, Inc., 1999

Stoeckli F. , Centeno T. A., Fuertes A. B. and Muñiz J. , "Porous structure of polyarylamide-based activated carbon fibres" , *Carbon* , 34 ,1201-1206(1996).

Streat, M., Patrick, J. W. & Perez, M. J. C., "Sorption of phenol and para-chlorophenol from water using conventional and novel activated carbons". *Water Research,* 29(2), 467-472(1995).

Suzuki M. "Adsorption engineering" New York, Elsevier, (1990).

Tamon H, Ishizaka H, Mikami M. and Okazaki M., "Porous structure of organic and carbon aerogels synthesized by sol-gel polycondensation of resorcinol with formaldehyde", *Carbon*, 35(6),791-796(1997).

Tamon H. and Ishizaka H., "SAXS study on gelation process in preparation of resorcinol-formaldehyde aerogel" *Journal of Colloidal Interface Science* 206, 577(1998)

Tamon H., Ishizaka H., Yamamoto T. and Suzuki T., "Influence of freeze-drying conditions on the mesoporosity of organic gels as carbon precursors", *Carbon*, 38 1099–1105(2000).

Tamon T., Ishizaka H., Yamamoto T. and Suzuki T., "Preparation of mesoporous carbon by freeze drying", *Carbon*, 37, 2049–2055(1999).

Tchobanoglous, G., Burton, F. L. & Stenset, H. D. "*Wastewater Eng, Treatment and Reuse*". *4th Edition ed.* McGraw-Hill Edition, New York, NY, USA (2003).

Teng H.. Wang S.C., "Preparation of porous carbons from phenol-formaldehyde resins with chemical and physical activation", *Carbon*, 38,817-824(2000).

Tennison S.R., "Phenolic-resin-derived activated carbons" *Applied Catalysis A: General* 173 , 289-311(1998).

Vaart R.V., Huiskes C., Bosch H. and Reith T., " Single and mixed gas adsorption eqilibria of carbon dioxide/methane on activated carbon" *Adsorption*, 6,311-323(2000).

Veawab A., Aroonwilas A., Chakma A. and Tontiwachwuthikul P., "Solvent formulation for CO_2 separation from flue gas streams". *First National Conference on Carbon Sequestration*, Washington, DC, May 15-17, (2001).

Wigmans T., "Industrial aspects of production and use of activated carbon," *Carbon*, 1, 13-22(1989).

Wong, S. and Bioletti, R. "Carbon dioxide separation technologies", *Carbon & Energy Management*, Alberta Research Council, Edmonton, Alberta, T6N 1E4, Canada (2002).

Xiaochun X , Song C., M.Andresen J., Miller B.G. and Scaroni A.W., " Preparation and characterization of novel CO_2 molecular basket adsorbents on polymer-modified mesoporous molecular sieve MCM-41" *Microporous and Mesoporous Material,* 62, 29–45 (2003).

Xiaochun Xu., Song C.,.Andresen J.M, Miller B.G. and Scaroni A.W., "Novel polyethylenimine modified mesoporous molecular sieve of MCM-41 type as high-capacity adsorbent for CO_2 capture," *Energy & Fuels,* 16,1463–1469 (2002).

Xu X., Song C., Andresen J.M, Miller B.G. and Scaroni A.W., " Preparation and characterization of novel CO_2 molecular basket adsorbents on polymer-modified mesoporous molecular sieve MCM-41" *Microporous and Mesoporous Material*, 62, 29–45 (2003).

Yamamoto T., Nishimura T., Suzuki T and Tamon H., "Control of mesoporosity of carbon gels prepared by sol-gel polycondensation and freeze drying". *Journal of Non-Crystalline Solids* , 288, 46-55(2001).

Yang, M. C. & Yu, D. G. "Influence of activation temperature on the properties of polyacrylonitrile-based activated carbon hollow fiber". *Journal of Applied Polymer Science*, 68(8), 1331-1336(1998).

Zabaniotou A., Madau P., Oudenne P.D., Jung C.G., Delplancke M.P., Fontana A., " Active carbon production from used tire in two-stage procedure: industrial pyrolysis and bench scale activation with H_2O-CO_2 mixture", *Journal of Analytical and Applied Pyrolysis* , 72, 289-297, (2004).

Zeebe R. E. and Gladrow-Wolf D., "CO_2 in Seawater: Equilibrium, kinetics, isotopes", *Elsevier Oceanography Series*, Volume 65 (2001).